CHARLES UNIVERSITY IN PRAGUE

Faculty of Science

Department of Genetics and Microbiology

Increasing affinity of Interferon gamma receptor 1 to Interferon gamma by combining molecular modeling and experimental methods

PhD Thesis

Mgr. Pavel Mikulecký

Supervisor:

doc. Ing. Bohdan Schneider, CSc.

Institute of Biotechnology CAS, v. v. i.

Laboratory of Biomolecular Recognition

Prague, 2015

Declaration

I hereby declare that I have completed this PhD thesis independently, and all publications and other sources used have been properly cited. This thesis has not been submitted previously in order to obtain the same or any other academic degree.

In Prague, August 24, 2015

Pavel Mikulecký

Acknowledgement

First and foremost I would like to express my sincere gratitude to my supervisor doc. Ing. Bohdan Schneider, CSc., for the scientific and financial support, and also to prof. Ing. Peter Šebo, CSc., for advices in the beginning of my PhD studies.

I am also very grateful to all the friends and colleagues in the laboratory for creating the supporting and exciting atmosphere.

Special thanks belong to my wife Zuzka for her enormous support and understanding.

Abstract

Protein-protein interactions play an important role in nearly all processes of the living cells and the function of many proteins is dependent on their specific interactions with other biomolecules. A reliable tool to modulate these interactions would be invaluable for the development of molecules suitable for diagnostics, medicine, and biotechnology. In this work, we aimed to study the specificity of interactions in the model system of Interferon gamma receptor 1 (IFNgR1) and its natural ligand Interferon gamma (IFNg), important in innate immunity.

We searched for mutations within the interferon receptor molecule IFNgR1 to modulate (increase as well as decrease) its affinity to IFNg by *in silico* analysis of the existing crystal structures of the complex between IFNgR1 and IFNg. We modeled amino acid substitutions and gauged how they influenced the interaction using empirical force field implemented in software FoldX. All selected promising IFNgR1 variants were expressed in *Escherichia coli*, purified to homogeneity, characterized, and kinetics of their interactions with IFNg was measured by Surface Plasmon Resonance (SPR).

The first set of IFNgR1 variants included mutations on the interface of the IFNg/IFNgR1 complex. According to our SPR measurements, the affinity of most of these receptor variants had virtually the same affinity as the wild-type receptor, a few had affinity slightly decreased, but a few variants bound IFNg with significantly higher affinity. The second, less orthodox approach comprised single mutations within the cavities of the IFNgR1 molecule. The results of these calculations suggested that they influenced the receptor affinity to IFNg very little. However, two cavity mutations increased the IFNgR1 affinity significantly in combination with the interface mutations.

Our results demonstrated that the combination of a computer-aided design using a relatively simple and accessible computational protocol together with experimental approaches was capable of predicting IFNgR1 variants with significantly increased affinity to IFNg. These new high-affinity binders help in better understanding of forces governing protein-protein interactions and could be developed into a new diagnostic tool.

Table of Contents

1 Introduction

Protein-protein interactions play an essential role in many biological processes, and proteins with artificially and specifically modified binding affinities to other molecules have become a helpful tool in research, biotechnology, and biomedicine. Computer-aided "rational design" of proteins with specifically targeted modifications is becoming a standard tool of protein engineering (Karanicolas and Kuhlman, 2009; Kortemme and Baker, 2004; Kraemer-Pecore *et al.*, 2001; Mandell and Kortemme, 2009; Reichmann *et al.*, 2007), although we still face some limitations in precision and reliability of computer predictions, which arise from our still incomplete comprehension of the structural and energetic aspects of protein-protein interactions. In this work, we aimed at testing power of combining an advanced structure-based yet affordable computer techniques with experimental confirmation of the computationally designed modifications. As a model system, we choose to study the interactions between Interferon gamma receptor 1 (IFNgR1) and its natural ligand, Interferon gamma (IFNg). The main goal of the project was to enhance the affinity of IFNgR1 to IFNg, as this approach could help to better understand the principles that govern the specificity and affinity of biomolecular recognition between these medically important proteins.

Interferon gamma is a cytokine of innate and adaptive immune responses but it also maintains immune homeostasis (Lin and Young, 2013). The IFNg signaling pathway begins with its binding to the cellular receptor 1 and further to receptor 2 (IFNgR2). The formation of the ternary complex subsequently activates the JAK/STAT signaling pathway leading to the establishment of immune response. The detection of IFNg has been used for the diagnosis of tuberculosis, for example in commercial kits such as QuantiFERON-TB Gold or T-SPOT.*TB*. Newer techniques in cytokine detection, including IFNg detection, comprise biosensors (Battaglia *et al.*, 2005; Chou *et al.*, 2010; Stigter *et al.*, 2005; Stybayeva *et al.*, 2010) utilizing different types of recognition elements – either engineered natural binding partners or *ad hoc* developed constructs such as antibodies or their components.

The goal of this work was development of high affinity IFNg binders based on IFNg natural binding partner, IFNgR1. This task was tackled by computer-aided design of IFNg variants with increased affinity using protocol based on analysis of crystal structures, molecular modeling, and subsequent validation of the predictions by biophysical measurements of expressed and purified model proteins. The modulation of the binding affinity of receptor 1 to

IFNg was based on two complementary structure-based strategies. In the first one, we searched for mutable residues at the IFNgR1 interface with IFNg, in the second strategy we searched for cavities inside the receptor structure and for amino acid replacements filling these cavities. Our computer analysis revealed several residues amenable to mutations, and all the designed variants were expressed, purified, and their affinities to IFNg were experimentally determined by Surface Plasmon Resonance (SPR). The predicted and measured affinities were compared and discussed, and the resulting process of design and testing of the receptor variants was formalized into an accessible protocol describing how to predict mutations increasing recognition between IFNg and its receptor 1.

2 Literature review

2.1 Model system – Interferon gamma and its receptors

2.1.1 Interferons

Interferons (IFNs) belong to a multigene family of inducible cytokines (Blatt *et al.*, 1996; Diaz *et al.*, 1996; Roberts *et al.*, 1998; Stark *et al.*, 1998; Young, 1996) that play key roles in mediating innate and acquired host immune responses against viral infections or intracellular bacteria. They exhibit antiproliferative and tumoricidal activity (Schindler and Brutsaert, 1999; Stark *et al.*, 1998). Following pathogen detection and subsequent IFN production, IFN molecules bind to cell surface receptors and initiate a signaling cascade via the JAK/STAT (Janus Kinase/Signal Transducer and Activator of Transcription) pathway, leading to the transcriptional regulation of hundreds of IFN-regulated genes (IRGs) (Stark and Darnell, 2012). The IFNs may be classified into three distinct types (Figure 1) that differ in their primary protein sequences, cognate receptors, genetic loci, and cell types responsible for their production (Pollard *et al.*, 2013).

2.1.1.1 Type I

Type I IFN genes encode IFNα (13 subtypes) and the structurally related IFNβ, IFNδ, IFNε, IFNκ, IFNω, and IFNτ. All exist in humans except for IFNδ and IFNτ that were described only in pigs and cattle, respectively. All human type I IFN genes are clustered on chromosome 9 (Pestka *et al.*, 1987) and the proteins signal through the type I IFN heterodimeric receptor complex comprising IFNα receptor 1 (IFNAR1) and receptor 2 (IFNAR2) subunits. The receptor subunits are associated with JAK1 and Tyrosine Kinase 2 (TYK2). Their interaction leads to the phosphorylation of STAT1 and STAT2 proteins. In specific cell types, STAT3, -4, -5, and -6 can also be phosphorylated (Fasler-Kan *et al.*, 1998; Matikainen *et al.*, 1999; Sadler and Williams, 2008).

Nearly all cells are capable of producing IFNα/β but the various type I IFNs display differential tissue expression and binding affinities for IFNAR1/2 receptor complex (Pestka, 2007), and consequently, the distinct subtypes give rise to various outcomes with respect to antiviral, antiproliferative, and immunomodulatory activity (Jaitin *et al.*, 2006; Kalie *et al.*, 2008; Moraga *et al.*, 2009).

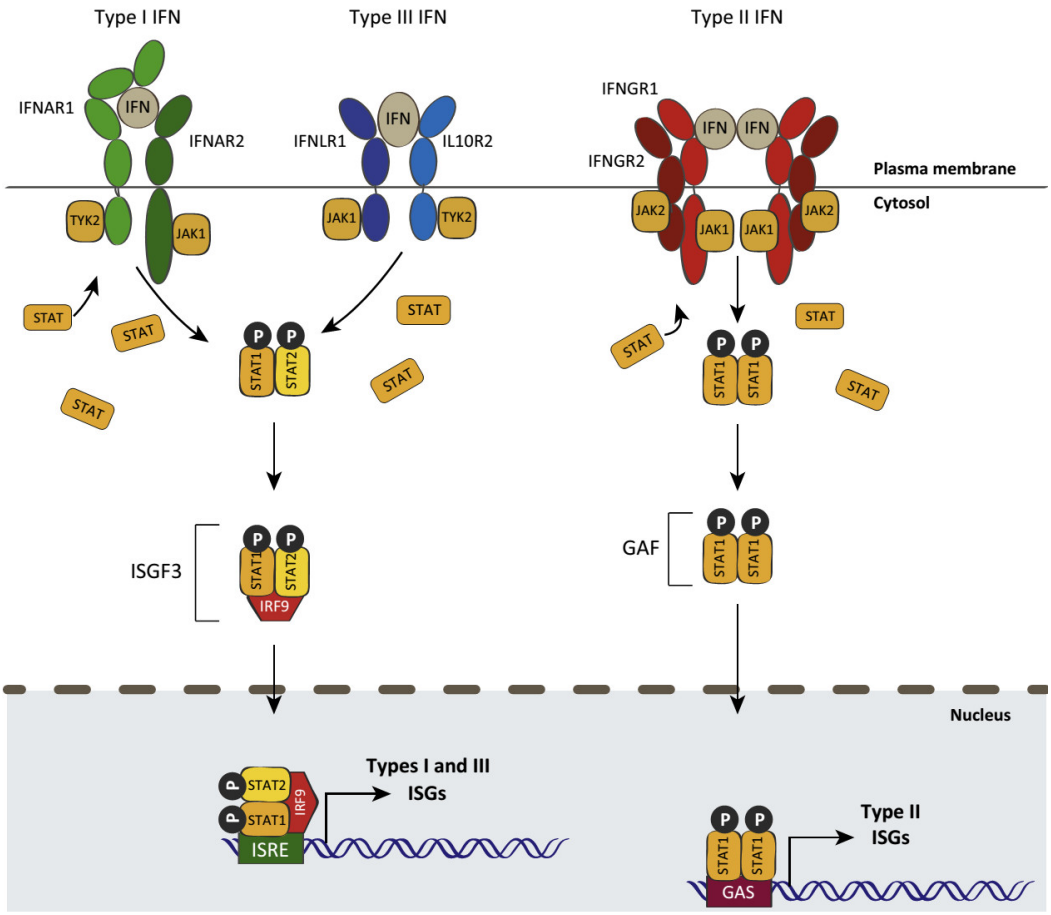

Figure 1
The interferon (IFN) signaling cascade via JAK/STAT pathway. The three different classes of IFNs signal through distinct receptor complexes on the cell surface. Binding of IFNs to their cognate receptors bring intracellular receptor-associated Tyrosine Kinases of Janus Kinase (JAK) family into close proximity leading to their activation by phosphorylation. Activated JAK proteins then phosphorylate the receptors at specific intracellular tyrosine residues, causing recruitment and subsequent phosphorylation of the STAT family proteins. This leads to STAT dimerization (and association with IFN-Regulatory Factor 9, IRF9, in case of type I and III IFN), translocation to the nucleus, binding to a DNA sequence and ultimately transcriptional regulation of hundreds of IFN-Stimulated Genes (ISGs). (Source: Hoffmann *et al.*, 2015).

2.1.1.2 Type II

There is only one representative of the type II IFNs – IFNγ (IFNg), and it is structurally different from type I IFNs. The gene encoding IFNg cytokine is located on chromosome 12 in humans and the protein signals through the formation of IFNg-receptor complex, initiated by the interaction of IFNg with two IFNgR1 subunits. This leads to additional binding of IFNgR2 subunit resulting in receptor activation (Walter *et al.*, 1995).

Although the IFNg cytokine is produced only by certain cells of the immune system, including natural killer (NK) cells, CD4 T helper 1 (Th1) cells, and CD8 cytotoxic suppressor cells (Bach *et al.*, 1997; Young, 1996), IFNgR1/2 receptors are widely expressed and therefore nearly all cell types are capable of responding to IFNg (Valente *et al.*, 1992).

IFNg and its receptors are described in more detail in further chapters.

2.1.1.3 Type III

Type III IFNs are the most recently discovered group of IFNs or IFN-like molecules (Pestka *et al.*, 2004), comprising four homologous members: IFNλ1 (synonymous name IL-29), IFNλ2 (IL-28A), IFNλ3 (IL-28B) (Kotenko *et al.*, 2003; Sheppard *et al.*, 2003), and the recently described IFNλ4 (Hamming *et al.*, 2013; Prokunina-Olsson *et al.*, 2013). All are encoded on chromosome 19. They also have antiviral properties (Kotenko *et al.*, 2003) and share structural features with members of IL-10 cytokine family. They are distinct from the type I and type II IFNs, and bind a different cell-surface receptor, which is composed of two chains, high-affinity IFNLR1 (also known as IL-28R1) and low-affinity IL-10R2 (Kotenko *et al.*, 2003). This receptor complex signals through a similar JAK/STAT pathway as the type I IFN receptor complex (Bolen *et al.*, 2014; Marcello *et al.*, 2006) (Figure 1).

2.1.2 Interferon gamma

As stated before, IFNg belongs to the type II interferon and it is the only member of this group. IFNg is a secreted glycoprotein that is encoded by a gene located on chromosome 12 (Naylor *et al.*, 1983). The gene consists of 4 exons, a repetitive DNA element, and a low order of polymorphism (Gray and Goeddel, 1982). Hereafter, we refer to the human IFNg homologue with UniProt entry code P01579. The mature protein consists of 143 amino acids (including C-terminal propeptide) and has predicted molecular mass of 16.7 kDa. In solution, it forms non-covalent homodimer (Figure 2) through the association of two monomeric subunits (Gray and Goeddel, 1983; Gray *et al.*, 1982). Each monomer has 6 alpha helices and no beta sheets (Ealick *et al.*, 1991). IFNg has two glycosylation sites (Asn48, Asn120) that are variably N-glycosylated during biosynthesis, increasing the molecular mass to 25 kDa (Kelker *et al.*, 1984). Another process producing heterogeneity of IFNg is its C-terminal partial proteolytic cleavage that causes alternative ending at Gly150, Gly157, and Gly161. The most predominant variant is 5 residues shorter (end at Gly157) than the full-length IFNg (Pan *et al.*, 1987).

IFNg represents an extraordinarily pleiotropic cytokine that can not only heighten both the innate and adaptive immune response against pathogens and tumors, but also has the ability to maintain immune homeostasis (Lin and Young, 2013). IFNg is secreted predominantly by T cells, natural killer cells (NK) and natural killer T cells (NKT) (Schoenborn and Wilson, 2007), and, to a lesser extent, by other cell types as macrophages, dendritic cells (DC), and B cells (Meyer, 2009). The broad array of IFNg responses are mediated by the cell-specific expression of many hundreds of IFNg-regulated genes (Hertzog *et al.*, 2011), for which the functional classification encompasses inflammatory mediators, signaling molecules, transcriptional activators, mediators of apoptosis and immune modulators (de Veer *et al.*, 2001). In addition to the pleiotropic nature of the IFNg response, there is a variety of cell types that possess the IFNg receptors and the molecular events that constitute IFNg-dependent signaling pathways (Hu and Ivashkiv, 2009; Stark *et al.*, 1998).

Binding of IFNg to its receptors triggers the JAK/STAT pathway. STAT1 is phosphorylated, subsequently dimerizes and then translocates into the nucleus to initiate the transcription of target genes. IFNg can induce both pro- and anti-inflammatory responses, and its ability to induce these two responses is critical for a balanced immune response. In addition to its function in activating innate immune cells, IFNg signaling also facilitates Th1 development, suppress Th2 differentiation, and inhibits development of Th17 cells. This complex yet delicate signaling network allows IFNg to tailor the immune response either for defense against infection or towards maintaining the homeostasis of the host (Lin and Young, 2013).

Aberrant IFNg expression has been associated with a number of autoinflammatory and autoimmune diseases. The most notable diseases associated with IFNg are systemic lupus erythematous (SLE), multiple sclerosis (MS) and rheumatoid arthritis (RA) (Lin and Young, 2013). IFNg also plays an important role against viral and intracellular bacterial infections, such as mycobacteria (Filipe-Santos *et al.*, 2006), Salmonella (John *et al.*, 2002), Listeria (Harty and Bevan, 1995), intracellular protozoans (including Toxoplasma and Leishmania), and certain viruses (Dalton *et al.*, 1993; Huang *et al.*, 1993; Jouanguy *et al.*, 1999). IFNg is also involved in tumor control (Ikeda *et al.*, 2002; Rosenzweig and Holland, 2005) as it directly enhances the immunogenicity of tumor cells and stimulates the immune response against transformed cells. Unfortunately, human tumors can evade this form of control by becoming unresponsive to IFNg (Kaplan *et al.*, 1998).

Due to the pleiotropic effects of IFNg on the immune system, it is believed to have a great potential as an immunomodulatory drug. IFNg clinical trials have been conducted using recombinant derived protein (Actimmune), adenovirus vectors which express IFNg cDNA (Adeno-IFNg), and neutralizing antibodies against IFNg (HuZaf). Actimmune has been used to treat a wide variety of diseases, including cancer, tuberculosis, hepatitis, chronic granulamotous disease, osteopetrosis, and scleroderma, among others. Adeno-IFNg has been used to treat cutaneous lymphoma and malignant melanoma. HuZaf has been used against autoimmune diseases, including rheumatoid arthritis and multiple sclerosis (Miller *et al.*, 2009). Because IFNg is critically important in immunity, its clinical use will depend upon a more precise understanding of its basic biology, complexity of its function, and localized effects in order to find better ways to use this molecule in the context of the disease setting.

2.2 Interferon gamma receptor complex

The actions of IFNg are mediated by a specific cell-surface heterodimeric receptor complex comprised of two IFNgR1 chains (Figure 2) and two IFNgR2 chains (Boehm *et al.*, 1997; Pestka *et al.*, 1997). IFNgR1 mediates IFNg binding, its trafficking through the cell, and signal transduction. IFNgR2 plays only a minor role in IFNg binding but it is required for signaling (Schroder *et al.*, 2004).

2.2.1 Interferon gamma receptor 1

IFNgR1 (Uniprot entry code P15260), also known as IFNg receptor α chain or CD119, belongs to the class 2 receptor family, which also includes the two chains of IFNα/β, the IL-10 receptor, the tissue factor, and the receptor-like molecule CRF2-4. The distinction of class 2 family from class 1 family (which includes e.g. IL-2 receptor gamma chain or IL-23 receptor (Liongue and Ward, 2007)) is made on the basis of differences within their extracellular domains, where the class 2 receptors lack the sequence WSXWS (in single-letter amino acid code) found in the C-terminal domain of the extracellular portion of class 1 receptors (Bazan, 1990).

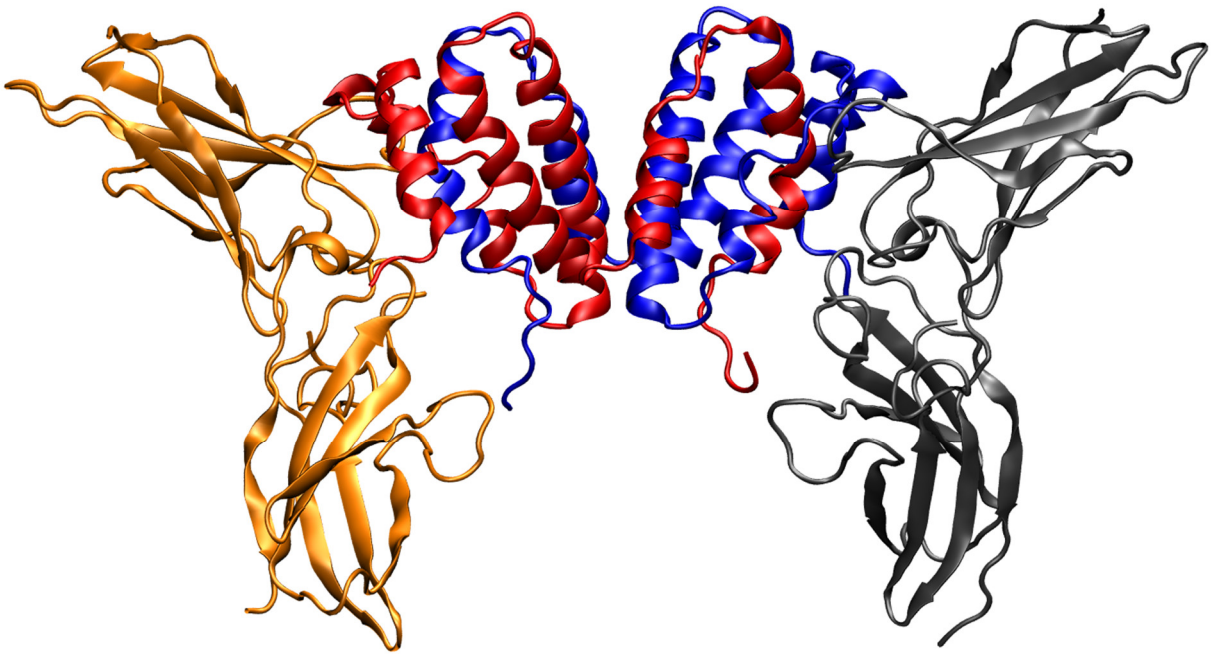

Figure 2
Interferon gamma receptor binary complex. Dimeric IFNg (red/blue) acts as a ligand for two IFNg receptor 1 molecules (gold and black) forming together the binary IFNg/IFNgR1 complex (Walter *et al.*, 1995) that further interacts with IFNg receptor 2 (Kotenko *et al.*, 1995; Pestka *et al.*, 1997). Assembly of the ternary complex IFNg/IFNgR1/IFNgR2 serves as a starting point of signal transduction ending with transcriptional regulation of IFN-Stimulated Genes (ISGs).

The IFNgR1 is a cell-surface glycoprotein that is encoded by a 30-kb gene located on the long arm of chromosome 6 (Aguet *et al.*, 1988; Le Coniat *et al.*, 1989). The gene consists of 7 exons of which exons 1-5 encode the receptor extracellular domain, exon 6 encodes a small portion of the membrane proximal region of extracellular domain and the transmembrane domain, and exon 7 encodes the entire intracellular domain (Bach *et al.*, 1997). Transcription of the human IFNgR1 genes gives rise to mRNA transcripts of 2.3 kb (Farrar and Schreiber, 1993). The receptor 1 chain polypeptide is synthesized in the endoplasmic reticulum (ER) and modified as it moves to the cell surface – the signal peptide is cleaved off, S-S bonds are formed, and N-linked carbohydrates are added (Hershey and Schreiber, 1989; Mao *et al.*, 1989).

The mature protein consists of 472 amino acids and has a predicted molecular mass of 52.5 kDa. It possesses a 223-amino acid intracellular domain, 21-amino acid transmembrane domain, and a 228-amino acid extracellular domain (Figure 2) that is organized into two fibronectin type III domains (Bazan, 1990). The extracellular domain contains 8 cysteine residues and five potential N-linked glycosylation sites. It was reported that disulfide bonds are

formed between residues Cys77-Cys85, Cys122-Cys167, Cys195-Cys200, and Cys214-Cys235, and are required for maximal activity (Stuber *et al.*, 1993). Based on experiments, all five potential glycosylation sites (Asn34, Asn79, Asn86, Asn179, and Asn240) appear to be occupied (Fischer *et al.*, 1990; Hershey and Schreiber, 1989; Mao *et al.*, 1989) and N-linked oligosaccharides contribute approximately 25 kDa to the apparent molecular mass of the fully mature protein. The size of fully mature IFNgR1 derived from different cell types ranges from 80 to 105 kDa depending on the extent of cell-specific glycosylation (Fischer *et al.*, 1990; Hershey and Schreiber, 1989; Mao *et al.*, 1989).

The intracellular domain is needed for signal transduction. Structure-function analyses performed on IFNgR1 revealed the presence of a functionally critical five amino acid region located at positions 457-461 near the C-terminus, containing the residues Tyr-Asp-Lys-Pro-His (YDKPH) (Farrar *et al.*, 1992). The tyrosine residue at position 457 was found to be a major substrate site for the activated JAKs (Greenlund *et al.*, 1994; Igarashi *et al.*, 1994). Mutational analysis of these five residues demonstrated that only Tyr457, Asp458, and His461 were functionally important (Greenlund *et al.*, 1995).

IFNgR1 is predominantly responsible for mediating high-affinity binding of IFNg with affinity of $K_d = 10^{-10}$ M with 2:1 stoichiometry (Marsters *et al.*, 1995) (Figure 2). It displays a strict species specificity in its ability to bind and respond to a ligand, i.e. the human IFNg receptor binds and responds only to human and not to murine IFNg, while the murine IFNg receptor binds and responds only to the murine ligand (reviewed in Farrar and Schreiber, 1993). The species-dependent binding mainly comes from the sequence differences of extracellular domains, not the intracellular domains as their functionally critical regions are preserved between mice and humans and thus no species-specificity is observed to contribute to signal transduction from these parts of receptor molecule (Axelrod *et al.*, 1994; Gibbs *et al.*, 1991).

Nearly all nucleated cells express IFNgR1 ubiquitously on their surface although at different level (250-25,000 sites/cell). Specifically, skin, nerve, and syncytial trophoblasts of the placenta express levels of IFNg receptor that are often 10-100 times higher than observed in spleen or on hematopoietic cells (Farrar and Schreiber, 1993).

2.2.2 Interferon gamma receptor 2

IFNgR2 (Uniprot P38484), also known as IFNg receptor β chain or Accessory Factor 1 (AF-1), belongs to the class 2 receptor family as well as IFNgR1. It is also a cell-surface glycoprotein and is encoded by a 33-kb gene (Rhee *et al.*, 1996) on chromosome 21 (Cook *et al.*, 1994; Soh *et al.*, 1994). The gene consists of 7 exons, the signal peptide being encoded by exons 1 and 2, the extracellular domain by exons 2, 3, 4, 5, and by part of exon 6. Exon 6 also encodes the whole transmembrane domain and part of the intracellular domain. Exon 7 encodes the remainder of the intracellular domain and contains the 3'-untranslated region (Rhee *et al.*, 1996).

The mature protein comprises of 310 amino acids and has a predicted molecular mass of 35 kDa. It consists of relatively short 69-amino acid intracellular domain, 21-amino acid transmembrane domain, and a 220-amino acid extracellular domain that is structured into two fibronectin type III domains. Extracellular domain contains 5 cysteine residues and 6 potential N-linked glycosylation sites (Asn56, Asn85, Asn110, Asn137, Asn219, and Asn231). Disulfide bonds were found to be between residues Cys86-Cys94 and Cys209-Cys234, while Cys174 remains uncoupled (unpublished data). IFNgR2 is heavily glycosylated and glycosylation contributes to the significant size heterogeneity seen in the mature protein, even when derived from the same cell type. The fully mature protein displays M_r values that range from 61 to 67 kDa (Bach *et al.*, 1995).

Cross-linking experiments with labeled human IFNg demonstrated that IFNgR2 associates with IFNg only when the IFNgR1 chain is present, indicating that IFNgR2 interacts with the IFNg/IFNgR1 complex primarily through the IFNgR1 chain, although it is likely that IFNgR2 also binds weakly to the ligand (Kotenko *et al.*, 1995; Pestka *et al.*, 1997). Thus, although IFNgR2 probably helps to stabilize the IFNg/IFNgR1 complex, its the main function is to promote signal transduction (see Chapter 2.2.3 below).

Expression patterns of the IFNgR2 gene generally follow those of the IFNgR1 gene, except in T lymphocytes, although the transcription may be tightly regulated (Ebensperger *et al.*, 1996). Th1 cells, which produce IFNg, down-regulate the expression of IFNgR2 and become IFNg-unresponsive. In contrast, Th2 cells, which do not produce IFNg, express IFNgR2 and remain IFNg-responsive. However, IFNgR2 down-regulation could also be induced in peripheral blood T cells upon exposure to IFNg (Bach *et al.*, 1995; Sakatsume and Finbloom, 1996). Interestingly, ligand-induced IFNgR2 down-regulation did not occur in certain

fibroblast cell lines. Thus, IFNg appears to regulate expression of IFNgR2 on certain cell types, which determines the ability of these cells to respond to subsequent exposure to IFNg (Bach *et al.*, 1995).

Table 1
Comparison of IFNgR1 and IFNgR2. Both receptors have different chromosome localization and their molecular size reflects their function. Extracellular domains consist of approximately the same amount of residues, because of the binding function of these domains. In contrast, the intracellular domain of IFNgR1 is almost three-times bigger than of IFNgR2, because it is associated with JAK1 kinase and includes a docking site for the STAT1 protein. Intracellular domain of IFNgR2 is smaller, as its main role is to bring the associated JAK2 protein in a close proximity of IFNgR1 and thus begin the signal transduction by phosphorylation. Expression of IFNgR1 on nearly all nucleated cells is constitutive, but IFNgR2 expression is highly regulated, therefore this receptor serves as the key molecule in IFNg signalization.

	IFNgR1 (or alpha)	**IFNgR2 (or beta)**
Chromosome localization	6	21
Extracellular domain	228 amino acids	220 amino acids
Intracellular domain	223 amino acids	69 amino acids
pI of ext. domain	4.84	6.18
Nr. of cysteines	8	5
Known structure	Yes (in complex with IFNg)	No
Role	Binding of IFNg; Signalization	Signalization
JAK associated	JAK1	JAK2
Expression on cells	Constitutive	Regulated

2.2.3 Signal transduction

IFNg primarily signals through the JAK/STAT pathway, which is used by over 50 cytokines, growth factors, and hormones to affect gene regulation (Subramaniam *et al.*, 2001). However, with the development of new techniques in recent years, which provided novel means to study the complexity of cell signaling, it has been shown that the classical model of JAK/STAT signaling was over-simplified, and that other ubiquitous pathways, including MAP kinase, PI3 kinase, CaM kinase II, and NFκB cooperate with or act in parallel to JAK/STAT signaling to regulate IFNg effects on the cell (Gough *et al.*, 2008; Liu *et al.*, 2008). There is a possibility that a certain level of signal specificity can be achieved through endocytosis and selective localization of the activated complexes within cellular membrane (Ahmed and Johnson, 2013; Blouin and Lamaze, 2013). It is now clear that our knowledge of IFNg trafficking and signaling is still incomplete. Many questions remain unanswered and more work is required for a complete understanding of the complex net of IFNg signaling pathways.

2.2.3.1 Classical model

According to the current model of IFNg signaling through JAK/STAT pathway (Figure 3), two IFNgR1 chains bind a dimeric IFNg molecule, forming thus the binary IFNg/IFNgR1 complex that is further connected with two IFNgR2 subunits. The IFNgR1 and IFNgR2 subunits were thought not to strongly associate with each other in the absence of ligand (Bach *et al.*, 1995; Gessani and Belardelli, 1998; Kaplan *et al.*, 1996; Marsters *et al.*, 1995; Sakatsume *et al.*, 1995), but newer techniques allowing the study of receptor chain interactions in intact cells have shown that the receptor complex is pre-assembled and their intracellular domains are in close proximity before ligand binding (Krause *et al.*, 2002).

Both IFNgR chains lack intrinsic kinase/phosphatase activity and so must associate with signaling machinery for signal transduction primarily through the JAK/STAT pathway. Binding motifs for the JAK1 and STAT1 proteins can be found within the IFNgR1 intracellular domain. The JAK1-binding motif LPKS is a membrane-proximal sequence located at IFNgR1 residues 283-286 (Farrar *et al.*, 1991; Greenlund *et al.*, 1994; Kaplan *et al.*, 1996) and STAT1-binding site YDKPH is positioned at residues 457-461 (Farrar *et al.*, 1992). This motif contains an essential Y457 phosphorylation site that is phosphorylated during signal transduction to allow STAT1 recruitment to the receptor (Cook *et al.*, 1992; Farrar *et al.*, 1992; Farrar *et al.*, 1991). Residues 458-DKPH-461 are responsible for the binding specificity of IFNgR1 and STAT1 (Cook *et al.*, 1992; Farrar *et al.*, 1992; Greenlund *et al.*, 1994).

The intracellular domain of IFNgR2 contains a noncontiguous binding motif consisting of two sites, 284-PPSIP-288 and 291-IEEYL-295, for association with JAK2 kinase (Bach *et al.*, 1996; Kotenko *et al.*, 1995). However, the IFNgR2 chain is not tyrosine phosphorylated during signal transduction (Kotenko *et al.*, 1995).

The inactive forms of the JAK1 and JAK2 kinases are constitutively associated with intracellular domain of IFNgR1 and IFNgR2, respectively (Bach *et al.*, 1997; Schroder *et al.*, 2004). After receptor complex assembly, JAK2 is activated by auto-transphosphorylation which leads to transactivation of JAK1 and phosphorylation of Y457 of IFNgR1. This residue is critical for forming a docking site for STAT1 that is further activated by phosphorylation, probably by JAK2 (Briscoe *et al.*, 1996). The four critical tyrosines (contained by JAK1, JAK2, IFNgR1, and STAT1) are phosphorylated within 1 minute of IFNg treatment (Greenlund *et al.*, 1994; Igarashi *et al.*, 1994).

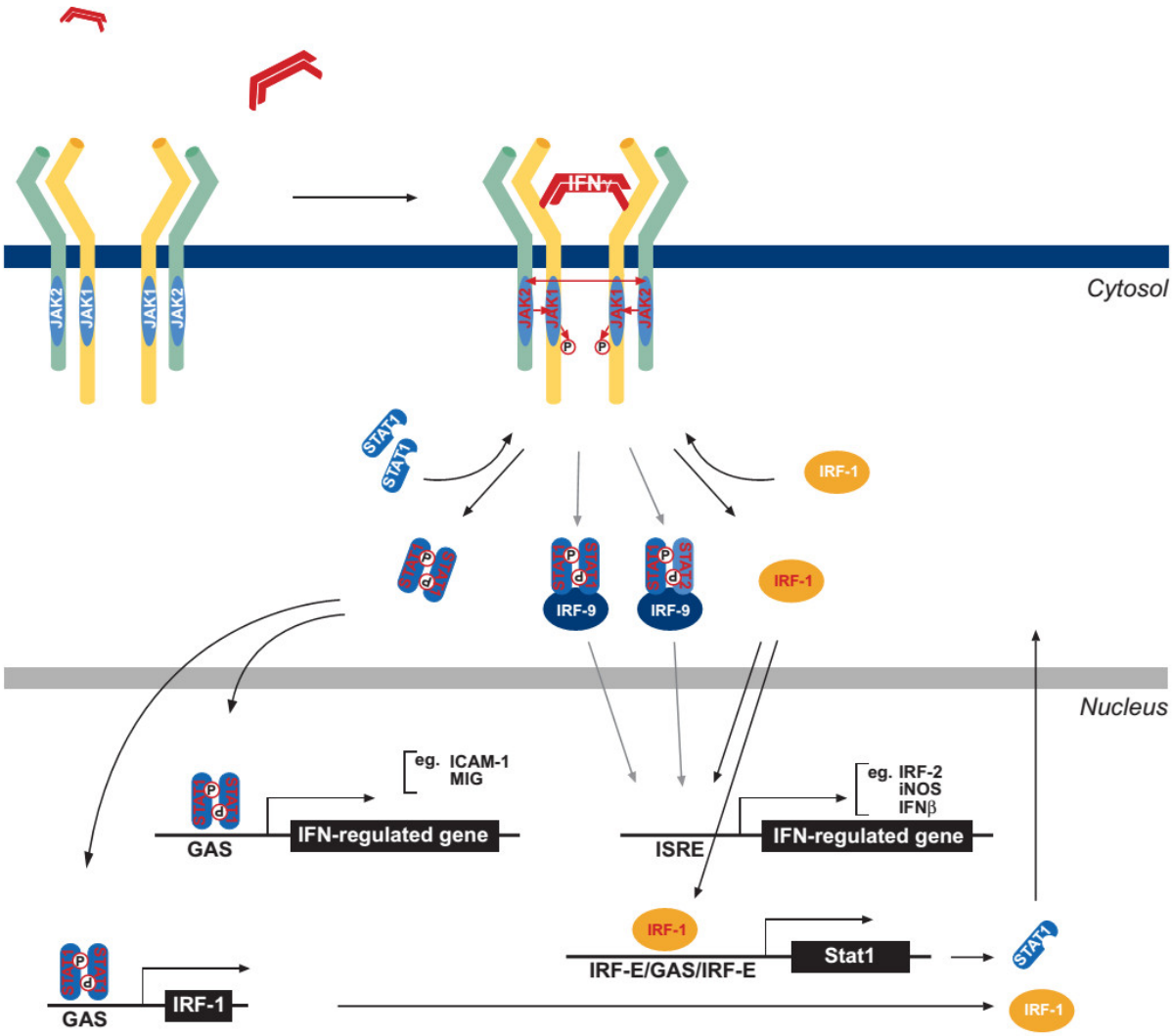

Figure 3
Classical model of IFNg signal transduction. Assembly of IFNg/IFNgR1/IFNgR2 ternary complex (IFNgR1, yellow; IFNgR2, green) on the cell surface brings in close proximity the JAK1 and JAK2 kinases which leads to the auto-transphosphorylation and activation of JAK2, which in turn transphosphorylate JAK1. The activated JAK1 further phosphorylates functionally critical tyrosine residue Y457 of each IFNgR1 chain to form two adjacent docking sites for the STAT1 protein. The receptor-recruited STAT1 is then phosphorylated inducing its homodimerization, dissociation from the receptor, and translocation into the cell nucleus. To a lesser extent, IFNg signaling also produces STAT1/STAT1/IRF-9 and STAT1/STAT2/IRF-9 complexes. Regardless of this, hundreds of IFNg-induced genes are transcribed. (Source: Schroder *et al.*, 2004).

Phosphorylation of STAT1 induces its homodimerization followed by dissociation from the receptor 1 (Greenlund *et al.*, 1995). STAT1 dimers are translocated into nucleus (Kotenko and Pestka, 2000), where they interact with specific DNA sequences called IFNg-activated sequences (GAS), located in the promoter regions of IFN-regulated genes (IRG) (also called

IFN-stimulated genes, ISGs), and in this way regulate their transcription (Aaronson and Horvath, 2002). Although the simplistic model involves only STAT1 homodimers alone, other active complexes such as STAT1 heterodimers (e.g., STAT1/STAT2) and heterotrimers (e.g., STAT1/STAT1/IRF-9 or STAT1/STAT2/IRF-9) form during signaling (Bluyssen *et al.*, 1996; Darnell *et al.*, 1994; Matsumoto *et al.*, 1999; Stark *et al.*, 1998). The first wave of IFNg-induced transcription occurs within 15-30 minutes of IFNg treatment (Kerr and Stark, 1991). Many of the induced genes are in fact transcription factors (for example, IRF-1) which are able to further drive regulation of the next wave of transcription (Paludan, 1998).

2.2.3.2 Non-canonical model

The non-canonical model of IFNg signaling proposed by Ahmed and Johnson (2013) (Figure 4) involves IFNg binding to IFNgR1 extracellular domain, followed by interaction with intracellular domain during endocytosis. The cytoplasmic binding increases the affinity of JAK2 for IFNgR1, which leads to autoactivation of the JAKs, phosphorylation of IFNgR1 cytoplasmic domain, and the binding and phosphorylation of STAT1 at IFNgR1. The complex of IFNgR1/STAT1/JAK1/JAK2 undergoes active nuclear transport where the classic polycationic nuclear localization sequence (NLS) of IFNg plays a key role for this transport to genes in the nucleus that are specifically activated by IFNg. Furthermore, the JAKs associated with the specific promoters were shown to be involved in epigenetic modifications (Ahmed and Johnson, 2013).

Other authors (Blouin and Lamaze, 2013), describe IFNg signaling pathways which include association of IFNg receptors with lipid microdomains at the plasma membrane and internalization of receptors through clathrin-coated pits (CCPs), or clustering of IFNg receptors with other proteins and triggering clathrin-independent endocytosis.

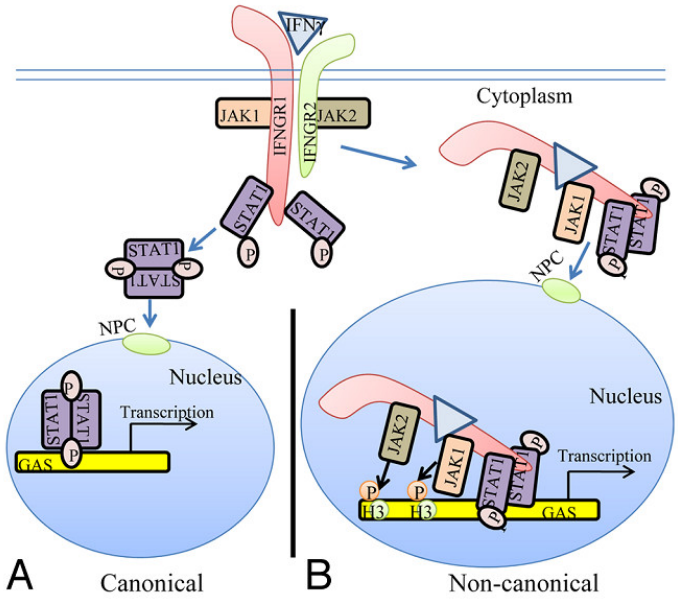

Figure 4
The classical and non-canonical IFNg signaling pathways. A) In the classical (canonical) model of IFNg signaling, assembly of ternary IFNg/IFNgR1/IFNgR2 complex causes cascades of phosphorylation events that result in dimerization of STAT1 protein and its translocation to the cell nucleus where the transcription of IFNg-induced genes is initiated. More details about the classical pathway is in the previous chapter. B) The non-canonical model of IFNg begins as classical pathway with IFNg binding to the receptor extracellular domain but then IFNg moves to the IFNgR1 intracellular domain in conjunction with endocytosis. In addition, JAK2 and STAT1 bind to the IFNgR1 and formed complex of IFNgR1/STAT1/JAK1/JAK2 undergoes active nuclear transport where regulates transcription of IFNg-induced genes. (Source: Ahmed and Johnson, 2013).

2.3 IFNg in diagnostics

Interferon gamma is the key molecule in the diagnostics of tuberculosis (TB), which, according to a World Health Organization (WHO), remains a major global health problem and one of the leading infectious causes of morbidity in the world (8 to 10 million cases per year). Besides, WHO reported that one third of the world's population is latently infected with *Mycobacterium tuberculosis* (MTB). It has been estimated that active disease will progress in 5% to 10% individuals with latent TB infection (LTBI) (Comstock *et al.*, 1974). In addition, immunosuppressed people have higher potential risk of developing active disease. Moreover, at least one third of HIV-infected persons worldwide are infected with MTB, and 8% to 10% of them develop clinical disease every year (data by WHO). Therefore, rapid diagnostic tests and effective treatment of LTBI are very important to reduce and control the TB burden (Comstock *et al.*, 1974; Hong *et al.*, 2012).

While it is relatively straightforward to diagnose active TB disease by the detection of *M. tuberculosis* in a clinical sample or by chest radiography, the diagnostic tools for the detection of LTBI are still limited, because both mentioned methods are either negative or normal in case of LTBI, and in addition latently infected persons don't show any symptoms (Pai *et al.*, 2014). Two mainly used methods for the identification of LTBI are the tuberculin skin test (TST) and IFNg release assays (IGRAs). Both methods depend on cell-mediated immunity and provide immunologic evidence of host sensitization to antigens of *M. tuberculosis*. Neither method can distinguish between LTBI and TB disease, and both methods display suboptimal performance in immunocompromised patients (Starke and Committee On Infectious Diseases, 2014).

Additional diagnostic markers are being investigated to enhance specificity and sensitivity of tuberculosis diagnostic tests as well as another diagnostic methods are being optimized to improve current detection of LTBI (Bibova *et al.*, 2012; Kim *et al.*, 2015; Ruhwald *et al.*, 2007; Yu *et al.*, 2012). For example, quantitative polymerase chain reaction (qPCR) was used to monitor mRNA levels in MTB antigen-activated peripheral blood mononuclear cells, and this method was claimed to enable distinguishing among healthy, LTBI, and active TB diseased individuals, respectively (Wu *et al.*, 2007). Another method could be the detection of markers on biosensors, which presents an attractive alternative to conventional techniques (Fan *et al.*, 2008).

The definitive diagnosis of LTBI is complicated and requires a case-by-case review. There is no current gold standard diagnostic measure (Pai *et al.*, 2006; Tsai *et al.*, 2013), which means that further studies, improvements of current tests, and development of new methods are highly required to reduce the number of latently infected people around the world.

2.3.1 Tuberculin skin test (TST)

The tuberculin skin test (TST) or Mantoux test has been the main standard for the diagnosis of LTBI so far (Pouchot *et al.*, 1997) and it has played an important role in the decline of TB disease. The TST is based on the detection of a cutaneous delayed-typed hypersensitivity response to purified protein derivative (PPD) that is a poorly defined mixture of more than two hundred *Mycobacterium tuberculosis* proteins, varying among batches and preparations. This is causing cross-reactivity with the bacille Calmette-Guérin (BCG) vaccination and many types

of environmental nontuberculous mycobacteria strains, resulting in false-positive results (Comstock *et al.*, 1974; Wang *et al.*, 2002). In addition, the TST is acknowledged to have poor sensitivity in individuals with compromised immune systems (e.g., patients with HIV infection, advanced TB, cancer, and children), resulting in false-negative results (Cobelens *et al.*, 2006). Another drawback is that the result depends on accurate intradermal injection and the the interpretation requires experienced medical personal. Additional difficulties come with improper handling of the PPD solution, which can cause false-negative results, and with the necessity of a return visit to read the results within 48 to 72 hours after injection. Despite all these limitations, the TST test is still the cheapest method for the detection of LTBI, and thus remains commonly used.

2.3.2 IFNg release assays (IGRAs)

Alternative immunodiagnostic method to the TST for the detection of LTBI is the IFNg release assays (IGRAs) (Lalvani *et al.*, 2001; Mandalakas *et al.*, 2008; Mori *et al.*, 2004; Richeldi, 2006). IGRAs are *ex vivo* blood tests that detect IFNg release from a patient's immune cells after stimulation by MTB-specific antigens, missing from all BCG strains (Mahairas *et al.*, 1996) and majority of environmental nontuberculous mycobacteria strains (except *M. Kansasi*, *M. szulgai*, *M. marinum*, *M. flavescens*, and *M. gastrii*) (Harboe *et al.*, 1996; Mahairas *et al.*, 1996; Shah *et al.*, 2012). Two commercial IGRAs kits are available: the QuantiFERON-TB Gold In-Tube Test (QFT) by Qiagen and the T-SPOT.*TB* assay (T-SPOT) by Oxford Immunotec. Both tests use Early Secreted Antigenic Target 6 (ESAT-6) protein and Culture Filter Protein 10 (CFP-10), in addition, the QFT uses a third antigen TB7.7. QFT is based on whole-blood ELISA, which measures the concentration of IFNg secretion, and T-SPOT is performed on peripheral blood mononuclear cells and is based on ELISpot, which directly counts the number of IFNg secreting T cells (Lalvani and Pareek, 2010).

Since there is no reference standard test for LTBI, it is hard to estimate the specificity and sensitivity of IGRAs. However, several studies have shown that the IGRAs have higher specificity than the TST and overall show great potential to reduce false-positive results, particularly among people who have received a BCG vaccine or have been exposed to nontuberculous mycobacteria strains (Lalvani, 2007; Lalvani and Millington, 2007; Lalvani and Millington, 2008a; Metcalfe *et al.*, 2011; Pai *et al.*, 2008; Sester *et al.*, 2011). The sensitivity of the IGRAs seems to be no better than that of TST and similar to TST, the IGRAs

have limited sensitivity in immunocompromised individuals and young children (Kim *et al.*, 2015; Starke and Committee On Infectious, 2014). Furthermore, IGRAs cannot differentiate between active pulmonary TB and LTBI (Mandalakas *et al.*, 2008). Further concerns have been raised about the reproducibility of the results (Gandra *et al.*, 2010; van Zyl-Smit *et al.*, 2009), since these can be affected by manufacturing issues, sample collection issues, such as inconsistencies in specimen collection, inadequate blood volume, delays in isolation and incubation of cells, and inadequate shaking (mixing) of the QFT collection tubes; laboratory issues caused by systematic or random error; and immunologic sources, including possible boosting of the response by a recently performed TST (van Zyl-Smit *et al.*, 2009).

In spite of these drawbacks, the IGRAs seem to be a better option than the TST, and the ongoing research lends hope that the next-generation assays are going to have higher sensitivity thanks to the incorporation of novel specific MTB-antigens (Dosanjh *et al.*, 2008; Harada *et al.*, 2008; Liu *et al.*, 2004) or the measurement of additional chemokines secreted by IFNg-activated macrophages (Lalvani and Millington, 2008b; Ruhwald *et al.*, 2008). The IGRAs have the advantages of requiring only a single health visit and having a more objective laboratory measurement. They are still more expensive than the TST, which makes them unusable in the developing countries on a regular basis.

2.3.3 New directions

Numerous cytokines and regulatory factors have been implicated in the pathogenesis and control of MTB infection (Azzurri *et al.*, 2005; Chegou *et al.*, 2009; Dlugovitzky *et al.*, 1999; Okamoto *et al.*, 2005; Pokkali *et al.*, 2008; Supriya *et al.*, 2008; Ulrichs *et al.*, 1998). There are several candidates, such as Interleukin-2, CXCL9, CXCL10 (also known as IFNg inducible protein 10, IP-10), CXCL11, and several others, tested in the context of tuberculosis diagnosis (Bibova *et al.*, 2012; Kim *et al.*, 2015; Ruhwald *et al.*, 2008). Real-time RT-PCR could be a good choice candidate for a potential diagnostic method, due to its ability to quantitate mRNA expression levels of selected targets after exposure of whole blood to TB antigens. Multiplex detection of mRNAs appears to be promising not only in its ability to detect TB exposure, but also to distinguish TB disease state (Bibova *et al.*, 2012; Kim *et al.*, 2015). However, further studies are needed to fully understand the strengths and limitations of this diagnostic approach.

Another new technique for TB diagnosis involves biosensors based on Surface Plasmon Resonance (SPR), which enable rapid, sensitive, and real-time analysis. SPR has been reported to be suitable for the detection of cytokines (Battaglia *et al.*, 2005; Chou *et al.*, 2010), including IFNg (Stigter *et al.*, 2005; Stybayeva *et al.*, 2010). Most frequently, antibodies are used as the biorecognition elements in biosensors, primarily due to their high specificity and wide availability. Neverthless, new alternative recognition molecules have emerged recently as the basis of novel assays (Van Dorst *et al.*, 2010). One of these alternative molecules are aptamers, single stranded DNA or RNA oligonucleotides with high affinity to a selected target (Sefah *et al.*, 2009), which are being used in a FRET-based assay for IFNg detection (Tuleuova *et al.*, 2010). Another molecules that could serve as biorecognition elements are protein scaffolds – small polypeptide molecules adapted to bind a variety of analytes using protein engineering methods (Gronwall and Stahl, 2009; Holliger and Hudson, 2005; Skerra, 2000). One of these scaffolds is the engineered albumin binding domain (ABD) of protein G from *Streptococcus* G148 selected by ribosome display to bind IFNg with high affinity (Ahmad *et al.*, 2012) and used in SPR-biosensor based assay for direct detection of IFNg (Šípová *et al.*, 2012).

2.4 High-affinity binders

Recognition between molecules is an important step in all processes of life. Biological function of many proteins is dependent on specific interactions with other biomolecules. High-affinity binders generated to specifically and with high affinity bind to other molecules have become an invaluable tool in molecular biology research and biotechnology (Gronwall and Stahl, 2009). They can be engaged in a wide range of *in vitro* and *in vivo* applications in clinical diagnostics, drug development, therapeutics, bioimaging, and bioseparations as well as in basic research (Arkin and Wells, 2004; Binz *et al.*, 2004; Chinai *et al.*, 2011; Jermutus *et al.*, 2001; Pommier and Marchand, 2012). High affinity and binding specificity are however not the only requirements. Depending on their final purpose they must possess various features such as specific kinetic properties, size, temperature and chemical stability, or compatibility with a number of detection methods.

Currently, antibodies are the most successful and widespread affinity proteins used in nearly all areas of life sciences for over three decades. Key to this success is their capability to be developed to virtually any given target with generally high affinity and specificity, and that the

technology is readily available. However, antibodies still have some limitations related to their molecular properties. The most used antibody type, the IgG molecule, is a large, bivalent, multidomain architecture with disulfide bonds and complex glycosylation pattern. This leads to an expensive manufacturing, batch to batch variations, and cross-reactivity with unrelated antigens (Lofblom *et al.*, 2010; Stumpp *et al.*, 2008).

To overcome some of the drawbacks of full-length antibodies, several smaller antibody derivatives (e.g. scFvs and Fab fragments) have been developed (He, 1997; Holliger and Hudson, 2005; Kanamori *et al.*, 2014) but they are still based on immunoglobulin scaffolds and, thus, some of the shortcomings of this class of protein will be difficult to correct. *In vitro* selection technologies, such as phage or ribosome display, have allowed the selection of specific high affinity binders without immunization. This has led to the development of non-immunoglobulin based scaffolds with attractive biophysical properties, such as small size, high stability and solubility. Examples (Figure 5) include DARPin (designed ankyrin repeat proteins), AdNectin, Affibody, Nanobody, Anticalin, Avimer, recombinant proteins and synthetic peptides, as well as aptamers (Ahmad *et al.*, 2012; Berezovski *et al.*, 2008; Binz *et al.*, 2004; Cooper and Waters, 2005; Holliger and Hudson, 2005; Lofblom *et al.*, 2011; Ng *et al.*, 2006; Nygren, 2008; Peczuh and Hamilton, 2000; Stumpp *et al.*, 2008).

There are two main complementary ways to engineer proteins with desired properties. One strategy is called “directed evolution” (Kuchner and Arnold, 1997; Stemmer, 1994) and the other one “rational design” (Chen, 1999; Chen *et al.*, 1996; Hurley *et al.*, 1996). Both approaches have their own pros and cons, as their basic ideas and methods are quite different.

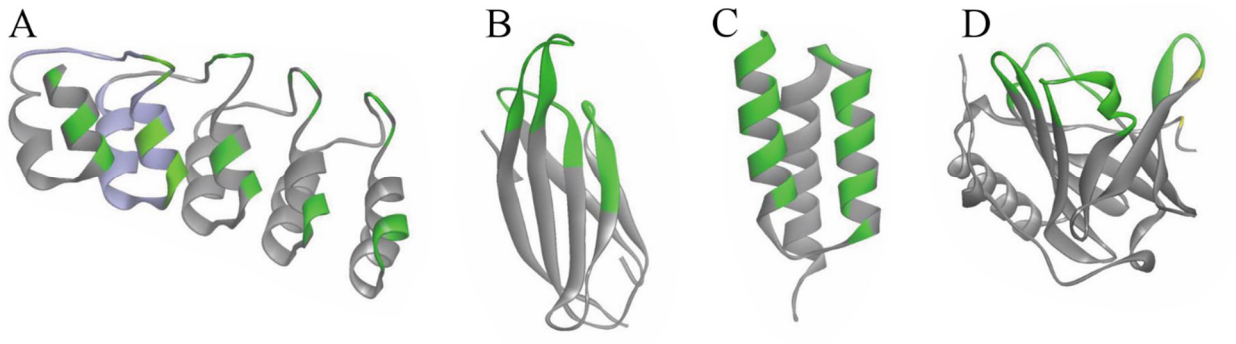

Figure 5
Examples of protein scaffolds. All scaffolds are crystal structures. Stretches of amino acids involved in binding are indicated in green. A) DARPin (PDB code: 4DX5); B) AdNectin (PDB code: 3QWQ); C) Affibody (PDB code: 1LP1); D) Anticalin (PDB code: 3BX7). (Source: Weidle *et al.*, 2013).

2.4.1 Directed evolution

Directed evolution is a protein engineering strategy that harnesses the power of natural selection to evolve proteins in the laboratory towards altered or non-natural properties. It employs a random process, in which protein variants are selected from a DNA library of mutagenized genes by high-throughput screening. The entry library can be created by several methods such as error-prone PCR, site-directed or saturation mutagenesis, gene shuffling, as well as *de novo* synthesis. Screening of the corresponding protein mutants can be accomplished by the so called "display" techniques, which include phage, bacterial, yeast, mRNA, ribosome display, and others (Gronwall and Stahl, 2009). All of these systems are based on a linkage between the genotype and phenotype of the selected proteins.

For example, in ribosome display (Figure 6) a non-covalent ternary complex is formed between the ribosome, mRNA (as it does not possess stop codon), and the encoded translated protein, and the complex is selected by binding to the target molecule. The complex is stabilized by magnesium ions and can be readily dissociated by the addition of EDTA (Hanes and Pluckthun, 1997). Another method called mRNA display is quite similar to ribosome display with the main modification that the mRNA and the protein are associated together via covalent bond using the antibiotics puromycin (Takahashi *et al.*, 2003). Other selection systems are based on similar principles with their own prerequisites (Gronwall and Stahl, 2009). Depending on the protein of interest and its desired properties, some molecular display methods can be more useful than others and it is not evident that one approach is advantageous over the others, since they all have their benefits and limitations.

One of the restrictions is the difficulty in creating the DNA library complex enough to cover all theoretically usable variants. Other problems come with the design of the high-throughput screening assay with the goal to pick up the anticipated protein variants from the large entry pool. In addition, realization of the whole procedures from the design of a library to getting the final product includes many steps, each prone to various faults, and the overall process is time- and money-consuming. Despite all these complications, directed evolution methods have been successfully applied throughout numerous studies (Ahmad *et al.*, 2012; Binz *et al.*, 2004; Chowdhury and Wu, 2005; Jermutus *et al.*, 2001; Kuchar *et al.*, 2014).

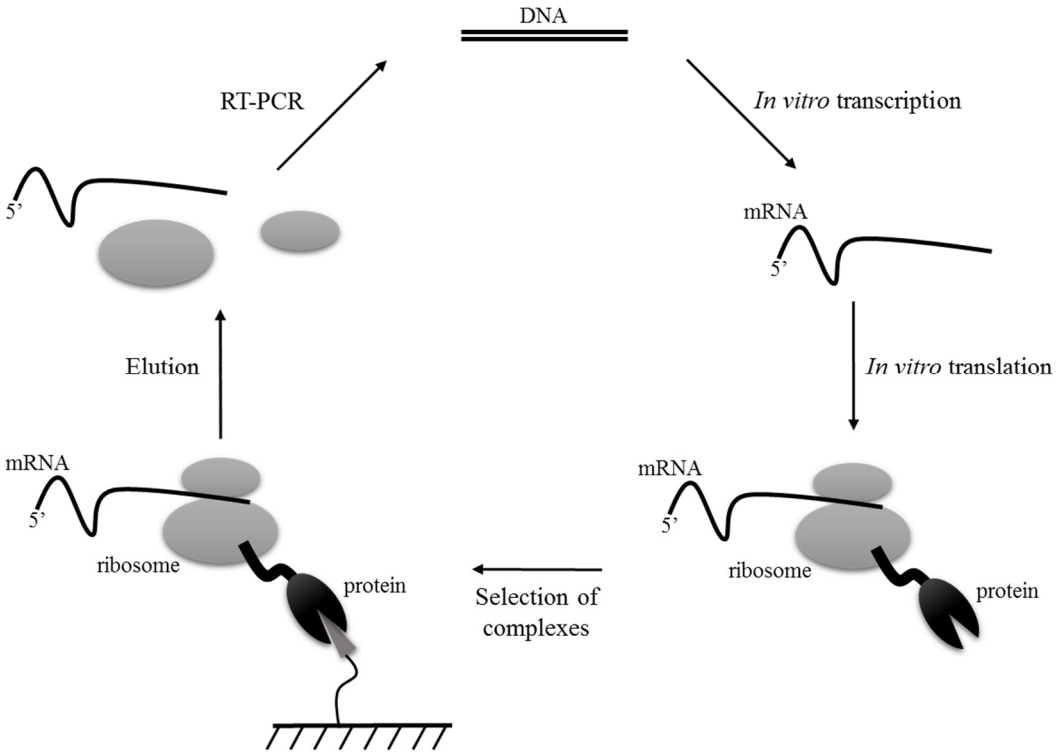

Figure 6
Schematic principle of ribosome display. A DNA library encoding protein variants lacking stop codon at the 3'-end is transcribed *in vitro*. The resultant mRNA is then purified and used for *in vitro* translation. The encoded protein is trapped within the mRNA-ribosome complex due to the absence of stop codon in the transcript. The mRNA-ribosome-protein complexes are used for affinity selection by an immobilized target or ligand molecule. Unbound complexes are washed away and bound complexes are eluted, followed by purification of mRNA that is reverse transcribed and PCR amplified. The PCR product can be used for next round of ribosome display.

2.4.2 Rational design

A group of computer-based techniques for the development of novel protein binders, sometimes called rational design, has recently emerged as a useful technique to study biomolecular recognition and to generate molecules for use in biotechnology, research, and biomedicine (Whitehead *et al.*, 2013). An important initial factor enabling structure-based rational design is availability of the structure of the wild type protein and a detailed knowledge about the relationships between sequence, structure, and function. However, an increasing number of the solved structures and enormous number of sequences deposited in public databases have facilitated progress in computational protein design. Also the effect of ever-increasing computer power is a significant factor helping to implement rational design.

Rational design can lead not only to optimizing the desired properties of proteins but it can also extend understanding of the fundamentals of protein binding or catalytic mechanisms of enzymes, thus increasing the success of future protein engineering efforts. The power of rational design has been demonstrated by number of studies, including the design of novel biocatalysts (Bolon and Mayo, 2001; Jiang *et al.*, 2008; Kaplan and DeGrado, 2004) and biosensors for non-natural molecules, redesign of proteins with greater binding specificity (Joachimiak *et al.*, 2006; Ogata *et al.*, 2003; Shifman *et al.*, 2006), design of proteins capable of binding non-biological cofactors (Cochran *et al.*, 2005), and redesign of proteins with improved binding affinity (Lazar *et al.*, 2006).

Structural analysis enabled better understanding of forces driving protein interactions, including van der Waals, electrostatic, hydrogen-bonding, and hydrophobic contacts. Computer modeling has been able to recapitulate some of these structural features to design novel protein-protein interactions (Huang *et al.*, 2007; Jha *et al.*, 2010; Karanicolas *et al.*, 2011) (Liu *et al.*, 2007). Using molecular modeling, it has been possible to predict how to modify proteins even if there are no structural data available and the structure of a homologous protein is used as a model (Kazlauskas, 2000). Despite all these successes, *de novo* design of protein binders is in its infancy (Whitehead *et al.*, 2013).

Rational design of interactions holds a great promise for extending our understanding of biomolecular recognition and ability to propose novel proteins with useful molecular functions (Fleishman and Baker, 2012). For the redesign of an improved protein-binding affinity, energy function accuracy is critical (Lippow and Tidor, 2007). A variety of strategies were developed for estimating protein energetics, ranging from methods based on the statistical analysis of known protein structures to more physically based methods. These are designated as Statistical (SEEF) and Physical (PEEF) Effective Energy Functions, respectively (Lazaridis and Karplus, 2000). A third class of methods, based mainly on empirical data derived from experimental work on proteins, called Empirical Effective Energy Functions (EEEF), are also widely used (Mendes *et al.*, 2002). One representative of the last group is FoldX force field (FOLDEF) that besides other things can evaluate the effect of mutations on the stability, folding, and dynamics of proteins or nucleic acids, and can calculate the free energy of macromolecules and complex formation (Schymkowitz *et al.*, 2005). Although the evaluation of protein-protein binding energy remains a challenging task, progress in computing performance and force-field parameterization are rapidly advancing our predictive capabilities (Barderas *et al.*, 2008; Park

and Jeon, 2011). In the upcoming years, the improvement in force-field development will improve both the accuracy and efficiency of computational design strategies (Wilson, 2015).

Computational protein design for a given function relies on optimizing a complex choreography of interactions with other molecules (Pantazes *et al.*, 2011). It was shown that certain critical residues make a major contribution to the binding free energy, therefore they are called "hot-spots" (Bogan and Thorn, 1998; Clackson and Wells, 1995; Cunningham and Wells, 1991; Keskin *et al.*, 2005). Hot-spots are found uniformly distributed across the interfaces and their direct periphery, and it is believed that these regions are most important in mediating protein-protein interactions (Keskin *et al.*, 2005; Sharabi *et al.*, 2009). Besides optimizing the hot-spot residues, alternative approach includes filling the cavities at the interaction interface, which can also lead to increase of affinity (Atwell *et al.*, 1997; Kawasaki *et al.*, 2010; Morellato-Castillo *et al.*, 2013).

In addition, recent studies indicate a role of conformational entropy in regulating binding affinity, providing a possible explanation for the effect of mutations remote from the interface (Tzeng and Kalodimos, 2012; Tzeng and Kalodimos, 2013). The non-negligible role of the non-interacting surface is supported by experimental mutagenesis studies that have revealed that both protein interior and the non-interacting surface do affect the free energy of binding (Kastritis and Bonvin, 2013; Kastritis *et al.*, 2011; Moal and Fernandez-Recio, 2012). Moreover, it has been shown that folding and thermal stability of a protein is influenced by interactions between its internal "core" residues (Černý *et al.*, 2015). Taken together, protein-protein affinity depends on the overall composition of the cognate molecules and could be altered by mutations not only on the interface, but also in cavities inside one of the interacting molecule.

3 Aims and objectives

The aims of this PhD thesis were to prepare the Interferon gamma receptor 1 variants with increased affinity to its ligand, IFNg, by combination of computational methods and experimental techniques, and to analyze the binding properties of the produced proteins with higher affinity.

Steps to achieve the aims:

A) Computer modeling to increase the IFNgR1 affinity to IFNg

This part included the analysis of the crystal structures of the IFNg/IFNgR1 complex, identification of cavities within the IFNgR1 molecule, *in silico* design of the interface and cavity variants, and determination of sequence conservancy of IFNgR1 residues. We worked towards developing a protocol that would enable to find mutations modulating the affinity between IFNgR1 and IFNg.

B) Experimental affirmation of the computer predictions

This part focused on the establishment and optimization of protocols for expression and purification of IFNg, IFNgR1 and its variants. We characterized the secondary structure and temperature stability of IFNgR1 variants and experimentally determined affinities of the designed IFNgR1 variants and analyzed the kinetics of binding to IFNg.

C) Comparison of predicted and measured affinities

This part comprised the analysis of internal dynamics of the IFNgR1 variants and we discussed computer-predicted and experimental affinities.

4 Materials

4.1 Chemicals

Acetic Acid; Lach-Ner, 10047-A99.
Acrylamide; Sigma-Aldrich, A8887.
Agarose; Sigma-Aldrich, A9539.
APS (Ammonium Persulfate); Sigma-Aldrich, 09913.
Beta-Mercaptoethanol; Sigma-Aldrich, M3148.
Bis-Acrylamide; Sigma-Aldrich, 146072.
Bromphenol Blue; Merck Millipore, 1.08122.
Coomassie Brilliant Blue G-250; Sigma-Aldrich, 27815.
Coomassie Brilliant Blue R-250; Sigma-Aldrich, 27816.
Cystamine; Sigma-Aldrich, C8707.
Cysteamine; Sigma-Aldrich, 30078.
dNTPs (Deoxynuleotide Mix); Sigma-Aldrich, D7295.
EDTA (Ethylenediaminetetraacetic Acid); Sigma-Aldrich, E5134.
Ethanol 96%; Lach-Ner, 20025-A96.
GelRed; Biotium, 41003.
GeneRuler DNA Ladder Mix, ready-to-use; Thermo Scientific, SM0333.
Glucose; Sigma-Aldrich, G7021.
Glycerol; Lach-Ner, 40058-AT0.
Glycine; Sigma-Aldrich, G8898.
HEPES; Sigma-Aldrich, H3375.
HyClone SFX-Insect Cell Culture Media; GE Healthcare, SH30278.
Hydrochloric Acid; Lach-Ner, 10033-A35.
Imidazole; Sigma-Aldrich, 56750.
IPTG; Enzo LifeSciences, ALX-582-001.
Kanamycin; Duchefa Biochemie, K0126.
KCl (Potassium Chloride); Lach-Ner, 30076-AP0.
KH_2PO_4 (Potassium Phosphate Monobasic); Sigma-Aldrich, P9791.
LB Agar; Sigma-Aldrich, L2897.
LB Medium; Sigma-Aldrich, L3022.
$MgSO_4.7H_2O$ (Magnesium Sulfate Heptahydrate); Merck Millipore, 1.05886.
$NaH_2PO_4.2H_2O$ (Sodium Phosphate Monobasic Dihydrate); Sigma-Aldrich, 71505.
$Na_2HPO_4.2H_2O$ (Sodium Phosphate Dibasic Dihydrate); Sigma-Aldrich, 71643.
NaCl (Sodium Chloride); Lach-Ner, 30093-AP0.
NDSB-201; Sigma-Aldrich, 82804.
$NiSO_4.6H_2O$ (Nickel(II) Sulfate Hexahydrate); Sigma-Aldrich, 227676.
PEG 8,000 (Polyethylene Glycol 8,000); Sigma-Aldrich, 81268.
Precision Plus Protein All Blue Prestained Standards; Bio-Rad, 161-0373.
SDS (Sodium Dodecyl Sulfate); Sigma-Aldrich, 75746.
SYPRO Orange dye; Sigma-Aldrich; S5692.
TEMED; Sigma-Aldrich, T7024.
Tris; Sigma-Aldrich, T6066.
Triton X-100; Sigma-Aldrich, T8787.
Tween20; Sigma-Aldrich, P9416.
Urea; Sigma-Aldrich, U5378.
Xylene Cyanol; Merck Millipore, 1.10590.

4.2 Equipment

ÄKTA Purifier 10; GE Healthcare.
Balance Pioneer PA2102C; OHAUS.
C1000 Touch Thermal Cycler; Bio-Rad.
Centrifuge Allegra X-22R with C0650 or C1015 rotors; Beckman Coulter.
Centrifuge Avanti J-30I with JA-10, JA-30.50Ti, JLA-9.1000, and JLA-16.250 rotors; Beckman Coulter.
Centrifuge Microfuge 18 with F241.5P rotor; Beckman Coulter.
Centrifuge Microfuge 22R with F241.5P rotor; Beckman Coulter.
CFX96 Touch Real-Time PCR Detection System, Bio-Rad.
Chirascan-plus CD Spectrophotometer; Applied Photophysics.
Finnpipette F2 Adjustable-Volume Pipettes; Thermo Scientific.
Gel Documentation System MF-ChemiBIS 3.2; DNR Bio-Imaging Systems.
HiLoad 16/600 Superdex 200 PG column; GE Healthcare.
Low-Profile 0.2 ml 8-Tube Strips without Caps; Bio-Rad.
Magnetic Stirrer RCT basic; IKA.
MaxQ 4000 Benchtop Orbital Shaker; Thermo Scientific.
MaxQ 5000 Floor-Model Shaker; Thermo Scientific.
Millex-GV Syringe Filter Unit (0.22 µm, PVDF membrane, 33 mm); Merck Millipore.
Mini Shaking Incubator NB-205; N-Biotek.
Mini-PROTEAN Tetra Cell SDS-PAGE Electrophoretic System; Bio-Rad.
Mini-Sub Cell GT Cell DNA Electrophoretic System; Bio-Rad.
Ni-NTA Agarose; Qiagen.
Optical Flat 8-Cap Strips; Bio-Rad.
Orion Star A211 pH Benchtop Meter; Thermo Scientific.
PowerPac Basic Power Supply for Electrophoretic Systems; Bio-Rad.
ProteOn HTG Sensor Chip; Bio-Rad.
ProteOn XPR36 Surface Plasmon Resonance (SPR) System; Bio-Rad.
SnakeSkin Dialysis Tubing (3.5K MWCO); Thermo Scientific.
SP Sepharose HP; GE Healthcare.
Spectrophotometer NanoDrop ND-1000; NanoDrop Technologies.
Spectrophotometer WPA Biowave II; Biochrom.
Superdex 200 10/300 GL column; GE Healthcare.
ThermoCell Mixing Block MB-102; Bioer Technology.
VivaSpin 2 Centrifugical Concentrators (10 kDa MWCO, Hydrosart Membrane); Sartorius.

4.3 Enzymes

T4 DNA Ligase; New England BioLabs, M0202.
Q5 High-Fidelity DNA Polymerase; New England BioLabs, M0491.
One*Taq* DNA Polymerase; New England BioLabs, M0480.
*Age*I Restriction Enzyme; New England BioLabs, R0552.
*Bgl*II Restriction Enzyme; New England BioLabs, R0144.
*Kpn*I Restriction Enzyme; New England BioLabs, R0142.
*Nco*I Restriction Enzyme; New England BioLabs, R0193.
*Nde*I Restriction Enzyme; New England BioLabs, R0111.
*Stu*I Restriction Enzyme; New England BioLabs, R0187.
*Xho*I Restriction Enzyme; New England BioLabs, R0146.

4.4 Solutions and buffers

30% Acrylamide Solution (29:1)
Acrylamide ..... 29% (w/v)
Bis-Acrylamide ..... 1% (w/v)

Agarose Gel Sample Buffer (6x concentrated)
Tris-HCl, pH 8.0 ..... 60 mM
Glycerol ..... 30% (v/v)
EDTA, pH 8.0 ..... 6 mM
Bromphenol Blue ..... 0.25% (w/v)
Xylene Cyanol ..... 0.25% (w/v)

Buffer A1, Buffer A2, Buffer A3, Buffer AW, Buffer A4; Macherey-Nagel
Limited information by supplier.

Buffer AE, Buffer NE; Macherey-Nagel
Tris-HCl, pH 8.5 ..... 5 mM

Buffer A
Tris-HCl, pH 8.0 ..... 50 mM

Buffer B (0.2 M Na-Phosphate buffer, pH 7.0)
$Na_2HPO_4.2H_2O$ ..... 0.54 g
$NaH_2PO_4.2H_2O$ ..... 0.30 g
Add distilled water to final volume 250 mL.

Buffer C
Tris-HCl, pH 8.0 ..... 50 mM
NaCl ..... 300 mM
Urea ..... 8 M

Buffer D
Tris-HCl, pH 8.0 ..... 50 mM
NaCl ..... 300 mM
Urea ..... 8 M
Imidazole, pH 8.0 ..... 250 mM

Buffer NTI, Buffer NT3; Macherey-Nagel
Limited information by supplier.

CutSmart Buffer (1x concentrated); New England Biolabs
Potassium Acetate ..... 50 mM
Tris-acetate ..... 20 mM
Magnesium Acetate ..... 10 mM
BSA ..... 100 µg/mL
pH 7.9 @ 25 °C

Medium A

Sterile LB medium supplemented with
$MgSO_4.7H_2O$.....10 mM
Glucose.....0.2% (w/v)

Medium B

Sterile LB medium supplemented with
Glycerol.....36% (w/v)
PEG 8,000 .....12% (w/v)
$MgSO_4.7H_2O$.....12 mM
Sterilized by filtration.

One*Taq* Standard Reaction Buffer (5x concentrated); New England Biolabs

Tris-HCl .....100 mM
NH_4Cl.....110 mM
KCl .....110 mM
$MgCl_2$ .....9 mM
IGEPAL CA-630..... 0.30%
Tween20..... 0.25%
pH 8.9 @ 25 °C

PBS Buffer

NaCl .....137 mM
KCl .....2.7 mM
$Na_2HPO_4.2H_2O$ .....10 mM
KH_2PO_4 .....2 mM
pH 7.4 @ 25 °C

PBST Buffer

NaCl .....137 mM
KCl .....2.7 mM
$Na_2HPO_4.2H_2O$ .....10 mM
KH_2PO_4 .....2 mM
Tween20..... 0.005% (v/v)
pH 7.4 @ 25 °C

Q5 Reaction Buffer (5x concentrated); New England Biolabs

Limited information by supplier except that contains 2 mM MgCl2 at final (1x) reaction concentrations.

QuikChange Reaction Buffer (10x concentrated); Agilent Technologies

Limited information by supplier.

Refolding Buffer

Tris-HCl, pH 8.0 .....100 mM
NaCl .....150 mM
EDTA, pH 8.0 .....2.5 mM
Cystamine.....0.5 mM
Cysteamine.....2.5 mM

SDS-PAGE gel (12.5%, 0.75 mm thick) – Separating

H_2O	0.98 mL
30% Acrylamide Solution	2.07 mL
1 M Tris-HCl, pH 8.8	1.87 mL
10% SDS (w/v)	50 µL
25% APS (w/v)	12.5 µL
TEMED	12.5 µL

SDS-PAGE gel (12.5%, 0.75 mm thick) – Stacking

H_2O	1.23 mL
30% Acrylamide Solution	0.27 mL
1 M Tris-HCl, pH 6.8	200 µL
10% SDS (w/v)	60 µL
25% APS (w/v)	20 µL
TEMED	5 µL

SDS-PAGE Running Buffer

Tris	25 mM
Glycine	192 mM
SDS	0.1% (w/v)

SDS-PAGE Sample Buffer (5x concentrated)

SDS	10% (w/v)
Glycerol	50% (v/v)
Tris-HCl, pH 6.8	0.3 M
Bromphenol Blue	0.05% (w/v)
Beta-Mercaptoethanol	25% (v/v)

SDS-PAGE Staining Solution

Coomassie Brilliant Blue G-250	100 mg/mL
Coomassie Brilliant Blue R-250	100 mg/mL
Acetic acid	0.003% (v/v)

T4 DNA Ligase Reaction Buffer (10x concentrated); New England Biolabs

Tris-HCl	500 mM
$MgCl_2$	100 mM
ATP	10 mM
DTT	100 mM
pH 7.5 @ 25 °C	

TAE Buffer (1x concentrated)

Tris	40 mM
Acetic acid	20 mM
EDTA, pH 8.0	1 mM

4.5 Synthetic oligonucleotides for mutagenesis

Variant	Oligonucleotides	Length
N65R	GTTTTTACCGTCGAAGTGAAACGTTATGGCGTGAAAAATAGCGA TCGCTATTTTTCACGCCATAACGTTTCACTTCGACGGTAAAAAC	44 bp
N70G	GAAAAACTATGGCGTGAAAGGCAGCGAATGGATCGATGCG CGCATCGATCCATTCGCTGCCTTTCACGCCATAGTTTTTC	40 bp
S95R	ATCATGTGGGCGACCCGCGTAACTCCCTGTGGGTT AACCCACAGGGAGTTACGCGGGTCGCCCACATGAT	35 bp
N96F	CATGTGGGCGACCCGAGTTTCTCCCTGTGGGTTCGTGTC GACACGAACCCACAGGGAGAAACTCGGGTCGCCCACATG	39 bp
N96W	GATCATGTGGGCGACCCGAGTTGGTCCCTGTGGGTTCGTGTCAA TTGACACGAACCCACAGGGACCAACTCGGGTCGCCCACATGATC	44 bp
K115Y	GAAAGAATCAGCGTATGCCTACTCGGAAGAATTCGCCGTG CACGGCGAATTCTTCCGAGTAGGCATACGCTGATTCTTTC	40 bp
T166M	ATGACCCGGAAACCATGTGTTACATTCGTG CACGAATGTAACACATGGTTTCCGGGTCAT	30 bp
T166Y	GTCGATTATGACCCGGAAACCTATTGTTACATTCGTGTTTATAACG CGTTATAAACACGAATGTAACAATAGGTTTCCGGGTCATAATCGAC	46 bp
H222R	TGAAGGCGTTCTGCGTGTCTGGGGTGTCA TGACACCCCAGACACGCAGAACGCCTTCA	29 bp
Y66L	CCGTCGAAGTGAAAAACCTGGGCGTGAAAAATAGCG CGCTATTTTTCACGCCCAGGTTTTTCACTTCGACGG	36 bp
S71E	GAAAAACTATGGCGTGAAAAATGAAGAATGGATCGATGCGTGCATC GATGCACGCATCGATCCATTCTTCATTTTTCACGCCATAGTTTTTC	46 bp
H222D	CTGAAGGCGTTCTGGATGTCTGGGGTGTC GACACCCCAGACATCCAGAACGCCTTCAG	29 bp
V35L	GTCCCGACCCCGACCAACTTGACGATTGAAAGTTACAAC GTTGTAACTTTCAATCGTCAAGTTGGTCGGGGTCGGGAC	39 bp
A114E	GAAAGAATCAGCGTATGAAAAATCGGAAGAATTCGCC GGCGAATTCTTCCGATTTTTCATACGCTGATTCTTTC	37 bp
D124N	CGCCGTGTGCCGTAATGGCAAAATCG CGATTTTGCCATTACGGCACACGGCG	26 bp
H222Y	CTGAAGGCGTTCTGTATGTCTGGGGTGTC GACACCCCAGACATACAGAACGCCTTCAG	29 bp

4.6 Plasmids

pET-22b(+); Novagen.
pET-26b(+); Novagen.
pET-28b(+); Novagen.
pMT/BiP/V5-His A; Invitrogen.
pPinkα-HC; Invitrogen.
Chaperone Plasmid Set; TaKaRa.

4.7 Cell strains and lines

Drosophila Schneider 2 (S2) Cells; Invitrogen.

Pichia pastoris cells included in PichiaPink Expression Strain Set; Invitrogen.

Escherichia coli XL1-Blue; Agilent Technologies. Genotype: *recA1 endA1 gyrA96 thi-1 hsdR17 supE44 relA1 lac* [F' *proAB lacI*^{q}*ZΔM15* Tn*10* (Tet^{r})].

Escherichia coli BL21(λDE3); Novagen. Genotype: F^{-} *ompT hsdS*$_{B}$(r_{B}^{-} m_{B}^{-}) *gal dcm* (DE3).

Escherichia coli SHuffle T7 Express; New England BioLabs. Genotype: *fhuA2 lacZ::T7 gene1* [lon] *ompT ahpC gal λatt::*pNEB3-r1-*cDsbC* (Spec^{R}, *lacI*^{q}) Δ*trxB sulA11 R(mcr-73::miniTn10--*Tet^{S})2 [dcm] *R(zgb-210::Tn10 --*Tet^{S}) *endA1* Δ*gor* Δ*(mcrC-mrr)114::IS10*.

Escherichia coli ArcticExpress (DE3); Agilent Technologies. Genotype: *E. coli* B F^{-} *ompT hsdS*(r_{B}^{-} m_{B}^{-}) *dcm*$^{+}$ Tet^{r} *gal* λ(DE3) *endA* Hte [*cpn10 cpn60* Gent^{r}].

4.8 Kits

NucleoSpin® Plasmid; Macherey-Nagel, 740588.
NucleoSpin® Gel and PCR clean-up; Macherey-Nagel, 740609.
QuikChange II Site-Directed Mutagenesis Kit; Agilent-Technologies, 200523.
Effectene Transfection Reagent; Qiagen, 301425.
iFOLD Protein Refolding System 1; Merck Millipore, 71552.
iFOLD Protein Refolding System 2; Merck Millipore, 71719.

4.9 Software

GROMACS; http://www.gromacs.org; (Van Der Spoel *et al.*, 2005).
OpenMM; https://simtk.org/home/openmm; (Eastman and Pande, 2010).
Zephyr; https://simtk.org/home/zephyr;(Friedrichs *et al.*, 2009).
CDNN software; Applied Photophysics.
FoldX; http://foldx.crg.es/; (Schymkowitz *et al.*, 2005).
Modeller suite of programs; http://salilab.org/modeller/; (Eswar *et al.*, 2003).
NEB temperature annealing calculator; http://tmcalculator.neb.com/.
PrimerX; http://www.bioinformatics.org/primerx/.
Program 3V; http://3vee.molmovdb.org;(Voss and Gerstein, 2010).
ProteOn Manager software (version 3.1.0.6); Bio-Rad.
ProtParam; http://web.expasy.org/protparam/.
Ugene; http://ugene.unipro.ru; (Okonechnikov *et al.*, 2012).
VMD program; http://www.ks.uiuc.edu/Research/vmd/; (Humphrey *et al.*, 1996).

5 Methods

5.1 Computational work

5.1.1 Modeling of missing residues

Modeller suite of programs (Eswar *et al.*, 2003) was used to model flexible residues missing ("not visible in the electron density") from the 1FG9 and 1FYH crystal structures. The loop and C-terminal residues were added. The missing residues were constructed employing the "`loopmodel`" routine and fast Molecular Dynamics (MD) refinement (by "`refine.fast`"). The lowest energy structure was chosen from ten models and used for the subsequent mutation analysis. All missing residues were outside the interface area.

5.1.2 Analysis of interfaces in crystal structures

The mutation analysis was based on analysis of the crystal structures of the complexes between the extracellular part of human Interferon gamma receptor 1 (IFNgR1) and human Interferon gamma (IFNg), of PDB code 1FG9 (Thiel *et al.*, 2000) and 1FYH (Randal and Kossiakoff, 2001) containing five crystallographically independent molecules of IFNgR1 in total; the asymmetric unit of 1FG9 contains three receptor molecules, but only two of them interact with IFNg; 1FYH has two receptor molecules interacting with IFNg. Therefore, there are four independent structures of the IFNg/IFNgR1 complex. Potential mutations were searched for in the IFNgR1 molecule, and the search was limited to its amino acid residues involved in direct interaction with IFNg. To make sure that all receptor residues potentially important for the interaction were included, we considered all residues within 6.0 Å from IFNg for mutation. A union of the four crystallographically unique interfaces consists of 40 receptor amino acid residues; they are depicted as wire models in Figure 7. The distances were calculated by the VMD program (Humphrey *et al.*, 1996).

5.1.3 FoldX calculations of ΔΔG values of interface variants

The variants potentially increasing the affinity of binding were selected by substituting each of the 40 residues of IFNgR1 forming the interface with IFNg by 20 (including self-mutations) standard amino acid residues and calculating the changes of the free energies, ΔΔG, caused by the mutations. Energies were calculated using locally installed binary of the program FoldX

(http://foldx.crg.es/) (Schymkowitz *et al.*, 2005) independently for each of the four crystallographic interfaces, two from crystal structure 1FG9 and two from 1FYH. Two sets of FoldX calculations were run: the first set of ΔΔG values estimated the influence of mutations on the stability of the whole IFNg/IFNgR1 complex, the second evaluated change of the interaction between the receptor molecule and the rest of the IFNg/IFNgR1 complex.

5.1.4 Identification of internal cavities and design of cavity variants

The program 3V (Voss and Gerstein, 2010) was used to identify internal cavities in all four available structures of IFNgR1 molecules in complex with IFNg. In total, 52 cavity-lining residues, which were identified as encapsulating the cavities in at least one of the four structures, were extracted using the VMD program (Humphrey *et al.*, 1996). Each of 52 amino acid residues identified as lining the internal receptor cavities was mutated in all four crystal IFNg/IFNgR1 complexes to 20 amino acid residues using the "`positionscan`" and "`analyzecomplex`" FoldX keywords. This represented 52 x 4 x 20 mutations (including self-mutations leading to ΔΔG = 0). Three types of changes of free energy (ΔΔG) were calculated using the program FoldX:

1) "ΔΔG of folding of IFNgR1 in complex" gauged the influence of mutations on the stability of the whole IFNg/IFNgR1 complex;

2) "ΔΔG of folding of free IFNgR1" estimated the effect of mutations on the stability of the isolated receptor;

3) "ΔΔG of binding" of complex between IFNgR1 and IFNg estimated the change of the interaction between the receptor molecule and the rest of the complex.

5.1.5 Molecular Dynamics (MD) of wild-type (WT) Complexes

MD simulations using the OpenMM (Eastman and Pande, 2010) Zephyr (Friedrichs *et al.*, 2009) implementation of GPU accelerated version of GROMACS (Van Der Spoel *et al.*, 2005) suite of programs were used to test the stability, dynamic properties, including analysis of values of root mean square fluctuations (RMSF) (Hess *et al.*, 2008), and interaction free energies (ΔG) of the IFNg/IFNgR1 complexes. The chains A, B, C, and D of the PDB structure

1FG9 and chains A, B, D, and E of the PDB structure 1FYH were used in the simulations. Missing residues were added using the Modeller suite of programs (Eswar *et al.*, 2003); the pdb2gmx program using parameters provided by the Zephyr program determined ionization state. All MD simulations were performed using the following setup. Implicit solvation (GBSA, $\varepsilon = 78.3$, with collision interval of 10.99 fs) was used in combination with parm96 force field (Kollman, 1996). The initial IFNg/IFNgR1 WT structure was optimized and the simulation was propagated at 300 K with time step of 2 fs. Snapshots of the geometry were saved every 10 ps throughout the simulation. RMSF of atoms in the analyzed proteins were calculated from the 100 ns trajectory to estimate flexibility of residues; they were calculated by "`g_rmsf`" program in 5 ns windows.

In order to test the stability of various structural predictions, we performed several MD simulations of the WT as well as mutated IFNg/IFNgR1 complexes. Three simulations of the WT complex consisted of a 100 ns MD run of the chains A, B, C, and D from 1FG9, which contain two interfaces, and two 20 ns runs for structure 1FYH, one for chains A, B and the other for chains D, E. These simulations demonstrated the stability of geometries of the crystal structures during the simulation. In the course of 100 ns 1FG9 simulation, instantaneous $\Delta\Delta G$ values of one IFNg/IFNgR1 interface switched to the value of the other interface and *vice versa*, suggesting sufficient sampling of the hypersurface of the free energy. For all the seventeen mutants, at least 10 ns MD simulations were run. They served as a reference for comparisons between calculated and measured affinities and to monitor the structural changes between the original crystal structures and the isolated solvated complexes.

To check the theoretical stability of the mutated receptor molecules, 20 ns MD simulations of their complexes with IFNg were performed; simulations were conducted according to the same protocol as for the WT complexes. The interaction ΔGs of the complexes were recalculated using FoldX on 1,000 snapshot structures from the converged second half of each MD simulation. The resulting values were used for comparison with the experimentally determined dissociation constants of the mutants.

5.1.6 Analysis of the sequence conservancy

The alignment was performed on 32 IFNg receptor sequences from 19 species: 12 sequences of primates (six human sequences, six from other primates), 15 sequences from other

mammals, three from birds, one amphibian, and one viral (the viral protein is not a cellular receptor but highly specific IFNg-binding protein). The list of their GenBank codes is below. The global sequence alignment was calculated using the KAlign (Lassmann *et al.*, 2009) algorithm as implemented in the program Ugene (http://ugene.unipro.ru/, Okonechnikov *et al.*, 2012); the resulting consensus sequence is shown in Figure 9.

1. gi|145975948 truncated interferon-gamma receptor 1 [Homo sapiens] human.
2. gi|4557880 interferon gamma receptor 1 precursor [Homo sapiens] human.
3. gi|189069218 unnamed protein product [Homo sapiens] human.
4. gi|62897165 interferon gamma receptor 1 variant [Homo sapiens] human.
5. gi|13562049 interferon-gamma receptor [Homo sapiens] human.
6. gi|632543 interferon-gamma receptor alpha chain [Homo sapiens] human.
7. gi|90083401 unnamed protein product [Macaca fascicularis] crab-eating macaque, species, primates.
8. gi|297291656 PREDICTED: interferon gamma receptor 1-like isoform 1 [Macacamulatta] crab-eating macaque, species, primates.
9. gi|297291658 PREDICTED: interferon gamma receptor 1-like isoform 2 [Macacamulatta] crab-eating macaque, species, primates.
10. gi|197100085 interferon gamma receptor 1 [Pongo abelii] Sumatran orangutan, species, primates.
11. gi|332213427 PREDICTED: interferon gamma receptor 1 isoform 1 [Nomascus leucogenys] Northern white-cheeked gibbon, species, primates.
12. gi|114609481 PREDICTED: interferon gamma receptor 1 isoform 5 [Pan troglodytes] chimpanzee, species, primates.
13. gi|296483981 interferon gamma receptor 1 [Bos taurus] cattle, species, even-toed ungulates.
14. gi|78050063 interferon gamma receptor 1 [Bos taurus] cattle, species, even-toed ungulates.
15. gi|45385782 interferon gamma receptor 1 [Bos taurus] cattle, species, even-toed ungulates.
16. gi|45385784 interferon gamma receptor 1 [Cervus elaphus] red deer, species, eventoed ungulates.
17. gi|295444941 interferon gamma receptor 1 [Sus scrofa] pig, species, even-toed ungulates.
18. gi|194216473 PREDICTED: similar to interferon gamma receptor 1 [Equus caballus] horse, species, odd-toed ungulates.
19. gi|74198189 unnamed protein product [Mus musculus] house mouse, species, rodents.
20. gi|6754306 interferon gamma receptor 1 precursor [Mus musculus] house mouse, species, rodents.
21. gi|309329 interferon-gamma receptor precursor [Mus musculus] house mouse, species, rodents.
22. gi|149039622 interferon gamma receptor 1 [Rattus norvegicus] Norway rat, species, rodents.
23. gi|38541396 Interferon gamma receptor 1 [Rattus norvegicus] Norway rat, species, rodents.
24. gi|16758624 interferon gamma receptor 1 [Rattus norvegicus] Norway rat, species, rodents.
25. gi|334324216 PREDICTED: interferon gamma receptor 1-like [Monodelphis domestica] gray short-tailed opossum, species, marsupials.
26. gi|57031680 PREDICTED: similar to Interferon-gamma receptor alpha chain precursor (IFN-gamma-R1) (CD119 antigen) (CDw119) [Canis familiaris] dog, subspecies, carnivores.
27. gi|281354680 hypothetical protein PANDA_003082 [Ailuropoda melanoleuca] giant panda, species, carnivores.
28. gi|224047948 PREDICTED: similar to interferon gamma receptor 1 [Taeniopygia guttata] zebra finch, species, birds.
29. gi|194332850 interferon gamma receptor 1 [Gallus gallus] chicken, species, birds.
30. gi|326915840 PREDICTED: interferon gamma receptor 1-like [Meleagris gallopavo] turkey, species, birds.
31. gi|118404146 interferon gamma receptor 1 [Xenopus (Silurana) tropicalis] western clawed frog, species, frogs & toads.
32. gi|211956284 soluble IFN-g receptor [Deerpox virus W-1170-84] Deerpox virus.

5.2 Experimental work

5.2.1 Preparation of plasmid DNA in small-scale (MiniPrep)

Minipreparations of plasmid DNA for routine work were obtained by using commercial kit called NucleoSpin Plasmid by company Macherey-Nagel. We followed the instructions provided by manufacturer. Briefly, the culture was inoculated with a single colony into 5 mL of LB medium containing appropriate antibiotic and was incubated at 37 °C with vigorous shaking over-night. Cells were harvested by centrifugation (8,000 g for 10 min at 4 °C) and supernatant was discarded. Pellet was resuspended in 250 μL of Buffer A1, transferred into 1.5 mL microcentrifuge tube, followed by addition of 250 μL of Buffer A2 and gentle mixing by inverting the tube 6-8 times. The mixture was incubated at room temperature (RT) for up to 5 min. Then 300 μL of Buffer A3 was added, mixed by inverting the tube, and centrifuged (8,000 g for 5 min at RT). Supernatant was placed onto the column and centrifuged (11,000 g for 1 min at RT). The column was washed by addition of 500 μL of Buffer AW and centrifugation (11,000 g for 1 min at RT). Second washing step included addition of 600 μL of Buffer A4 (supplemented with ethanol) and centrifugation (11,000 g for 1 min at RT). The column was dried by centrifugation (11,000 g for 2 min at RT). The DNA was eluted by addition of 50 μL of Buffer AE, incubation for 1 min at RT, and centrifugation (11,000 g for 1 min at RT). The final eluted DNA was stored at -20 °C.

5.2.2 Digestion of DNA with restriction enzymes

We used the restriction enzymes by New England BioLabs (NEB) company according to their recommendation. Typical reaction contained 0.2-1 μg of DNA, appropriate digestion buffer (CutSmart Buffer), 1 μL of restriction enzymes (5-10 units), and distilled water to final volume 50 μL. The mixture was incubated either 2-3 hours in case of PCR products or over-night in case of plasmid DNA. Digested DNA was recovered either directly from the mixture or from agarose gels.

5.2.3 Preparation of agarose gels

In our experiments we used home-made agarose gels to resolve DNAs. The agarose concentration differed from 0.6 % for larger fragments to 2.0 % for smaller fragments. Calculated amount of powdered agarose was added to a defined volume of TAE Buffer

(1x concentrated) and boiled in microwave until the agarose dissolved. The gel was casted after cooling the solution to 50 °C. Samples were mixed with Agarose Gel Sample Buffer (6x concentrated) supplemented with GelRed (60x concentrated) dye. Size marker used was the GeneRuler DNA Ladder Mix, ready-to-use. Electrophoresis was performed in TAE Buffer (1x concentrated) at 4 V/cm at room temperature. DNA was visualized on a gel documentation system.

5.2.4 Recovery of DNA fragments from agarose gels or reaction mixtures

Isolation of DNA from agarose gels or reaction mixtures was done by the commercial kit NucleoSpin Gel and PCR clean-up by company Macherey-Nagel. We followed the instructions provided by manufacturer. Briefly, DNA fragments from agarose gel were excised, transferred to fresh eppendorf tubes, dissolved in 200 µL of Buffer NTI for each 100 mg of gel, and incubated at 50 °C until the gel melted (5-10 min). For reaction mixtures (such as PCR), one volume of sample was mixed with two volumes of Buffer NTI. In both cases the resulting mixture was loaded on the column and centrifuged (11,000 g for 30 s at RT). Then the column was washed by addition of 700 µL Buffer NT3 and centrifuged (11,000 g for 30 s at RT). The washing step was repeated and then the column was dried by centrifugation (11,000 g for 1 min at RT). The DNA was eluted by addition of 30 µL of Buffer NE, incubation for 1 min at RT, and centrifugation (11,000 g for 1 min at RT). The final eluted DNA was stored at -20 °C.

5.2.5 Ligation of DNA fragments

All ligation reactions were set up with bacteriophage T4 DNA Ligase. For ligation of cohesive termini the plasmids and insert DNAs were digested with the appropriate restriction enzymes. The desired fragments were isolated from agarose gel and/or directly from reaction mixture. Ligation reaction were set up in a microcentrifuge tube as follows: 2 µL of T4 DNA Ligase Reaction Buffer (10x concentrated), 50 ng of Vector DNA, 3-fold molar excess of Insert DNA to Vector DNA, sterile water to 20 µL, and 0.5 µL of T4 DNA Ligase. Control reactions contained mixture with Vector DNA alone and with (to check background due to vector re-circularization) or without (to check background due to uncut vector) the T4 DNA Ligase. All ligation reactions were gently mixed by pipetting and incubated over-night at 16 °C or for

1 hour at room temperature. The 10 µL of ligation mixture were transformed into 50 µL of *E. coli* XL1-Blue competent cells.

5.2.6 Polymerase Chain Reaction (PCR) amplification

We used Q5 High-Fidelity DNA Polymerase for DNA amplification with low error rate according to manufacturer recommendations. PCR was usually performed in 50 µL reaction mixture (in 0.2 mL microcentrifuge thin-wall tube) containing 10 µL of Q5 Reaction Buffer (5x concentrated), 5 µL of 2 mM dNTPs (final concentration 200 µM), 2.5 µL of 10 µM Forward and Reverse primers (final concentration 0.5 µM), 1 µL of template DNA (amount <1,000 ng), 0.5 µL of Q5 High-Fidelity DNA Polymerase (final amount 1 U), and sterile water to 50 µL. Initiation of denaturation for 30 s at 98 °C was followed by 30-35 cycles of amplification consisting of denaturation step for 10 s at 98 °C, annealing step for 30 s at 50-72 °C (according to selected primers), and extension step for 20-30 s per kilobase pairs (kbp) at 72 °C. The last step was for 2 min at 72 °C and then reaction was cooled down to 4 °C. The annealing temperature of primers were determined by web-based NEB T_m Calculator.

5.2.7 Colony PCR

We used One*Taq* DNA Polymerase for Colony PCR that is a convenient high-throughput method for determining the presence or absence of insert DNA in plasmid constructs. PCR was usually performed in 15 µL reaction mixture (in 0.2 mL microcentrifuge thin-wall tube) containing 3 µL of One*Taq* Standard Reaction Buffer (5x concentrated), 1.5 µL of 2 mM dNTPs (final concentration 200 µM), 1.5 µL of 10 µM Forward and Reverse primers (final concentration 1 µM), 0.075 µL of One*Taq* DNA Polymerase (final amount 0.375 U), and sterile water to 15 µL. As a template DNA we picked up a single colony by a pipette tip and added directly to the PCR reaction. Initiation of denaturation for 3 min at 95 °C was followed by 30-35 cycles of amplification consisting of denaturation step for 10 s at 95 °C, annealing step for 30 s at 50-72 °C (according to selected primers), and extension step for 1 min per kilobase pairs (kbp) at 72 °C. The last step was for 10 min at 72 °C and then reaction was cooled down to 4 °C. The annealing temperatures of primers was determined by web-based NEB T_m Calculator.

5.2.8 Construction of plasmid DNA containing IFNgR1 or IFNg-SC gene

DNA sequence encoding open reading frame (ORF) covering the residues 18 to 245 (UniProt entry code P15260) of the extracellular domain of human IFNgR1 was codon-optimized to *E. coli*, synthetized, and cloned into general vector by GenScript. The ORF was then re-cloned in frame as an *Nco*I-*Xho*I fragment into pET-28b(+) vector (Novagen), resulting in the addition of N-terminal methionine (MEMGT) and C-terminal 6x His purification tag extension (SIKGLEHHHHHH).

DNA sequence encoding ORF of IFNg variant with sequence taken from previous report (Landar *et al.*, 2000) was codon-optimized to *E. coli*, synthetized, and cloned into general vector by GeneArt. The ORF was then re-cloned into pET-26b(+) vector (Novagen) as an *Nde*I-*Xho*I fragment containing C-terminal stop codon and in frame with N-terminal start codon not to add any peptide leader or tag.

The proper sequence of all constructs was verified by DNA sequencing that was performed in the Centre of DNA Sequencing (Institute of Microbiology CAS).

5.2.9 Site-directed mutagenesis

To prepare vectors carrying DNA sequence coding selected IFNgR1 variants with single-point amino acid mutations we used commercial QuikChange II Site-Directed Mutagenesis Kit by Agilent Technologies. We followed the instructions provided by manufacturer. Reaction was usually performed in 50 μL reaction mixture (in 0.2 mL microcentrifuge thin-wall tube) containing 5 μL of QuikChange Reaction Buffer (10x concentrated), 1 μL of dNTP mix, 1.5 μL of 10 μM Forward and Reverse primers (final concentration 0.3 μM), 2 μL of template DNA (MiniPrep), and sterile water to 50 μL. Then 1 μL of *PfuUltra* HF DNA Polymerase was added to the reaction mixture. Primers were designed by using web-based PrimerX program. As a template DNA served the vector carrying DNA sequence coding wild-type IFNgR1. Reaction was set up as follows: Initiation of denaturation for 30 s at 95 °C was followed by 18 cycles of amplification consisting of denaturation step for 30 s at 95 °C, annealing step for 60 s at 55 °C, and extension step for 1 min per kbp at 68 °C. The last step was cooling down to 37 °C. Then 1 μL of *Dpn*I restriction enzyme was added directly to the amplification reaction, gently mixed, and incubated at 37 °C for 1 hour to digest the parental (non-mutated) dsDNA. The 10 μL of reaction mixture were transformed into 100 μL of *E. coli* XL1-Blue competent cells.

The proper sequence of all constructs was verified by DNA sequencing that was performed in the Centre of DNA Sequencing (Institute of Microbiology CAS).

5.2.10 Preparation of *Escherichia coli* competent cells

Preparation of chemically highly competent *Escherichia coli* cells started with inoculation of 5 mL of LB medium (supplemented by appropriate antibiotics) by single colony and incubation over-night at 30 °C at 250 RPM. In the morning, 1 mL of over-night culture was transferred into 50 mL of Medium A (sterile LB medium supplemented with sterile 10 mM $MgSO_4.7H_2O$ and 0.2% Glucose) containing appropriate antibiotics. Culture was further incubated at 30 °C at 250 RPM until the Optical Density at 600 nm (OD_{600}) was around 0.4. Then the culture was cooled down on ice for 10 min and cells were harvested by centrifugation (8,000 g for 10 min at 4 °C). Medium was discarded and cells were resuspended in 0.5 mL of Medium A pre-cooled on ice followed by addition of 2.5 mL of Medium B (LB medium supplemented by 36% Glycerol (v/v), 12% PEG 8,000 (w/v), 12 mM $MgSO_4.7H_2O$, and sterilized by filtration) without any antibiotics also pre-cooled on ice. Treated cells were divided into aliquots and stored at -80 °C (quick freeze in liquid nitrogen was optional).

5.2.11 Transformation of competent cells

Competent cells (50 µL) stored at -80 °C were gently thawed on ice and 10 µL of ligation reaction or 1-2 µL of MiniPrep DNA were added. Suspension was incubated on ice for 30 min, then at 42 °C for 45 s and cooled on ice for 5 min. LB medium (950 µL) was added to transformed cells and incubation was performed at 37 °C for 1 hour without shaking to allow expression of the antibiotic resistance gene. Cell suspension were then centrifuged (13,000 g for 1 min at RT), 900 µL of supernatant were discarded, and cells were resuspended in the remaining medium (100 µL). The resulted cell suspension was platted on LB agar plates containing appropriate antibiotics for selection of bacterial cells containing recombinant vectors. Plates were incubated at 37 °C over-night.

5.2.12 SDS-PAGE analysis

Sodium Dodecyl Sulfate Poly-Acrylamide Gel Electrophoresis (SDS-PAGE) is the most widely used technique to separate and analyze proteins. Because the molecular size of IFNgR1 is 27 kDa and IFNg-SC is 32 kDa, the 12.5% gels (0.75 mm thick) were used with Precision Plus Protein All Blue Prestained Standards.

Protein samples (10-20 μL) were mixed with SDS-PAGE Sample Buffer (5x concentrated) and heated at 95 °C for 5 min. Samples were then loaded to SDS-PAGE gel consisting of lower Separating and upper Stacking gel, and run at 150 V in SDS-PAGE Running Buffer for 1 hour. Gels were further transferred into plastic box filled with distilled water, microwaved until just boiling, and shaken for 2 min at RT. Water was poured off, gel rinsed with new distilled water, SDS-PAGE Staining Solution added, microwaved again until just boiling, and shaken for 5 min at RT. Destaining procedure begins with pouring off the Staining Solution, gel rinsing with distilled water, addition of new distilled water with small amount of 96% Ethanol, soft microwaving (desired temperature is around 50 °C), and ends with shaking at RT. The destaining procedure may be repeated several times.

5.2.13 Cell cultivation

The *E. coli* strain BL21(λDE3) was used for protein expression. Small amount (5-50 mL) of LB medium supplemented with appropriate antibiotics was inoculated by several colonies of *E. coli* cells transformed by plasmid DNA and incubated over-night at 30 °C at 250 RPM. Next morning the culture was transferred into larger volume of fresh LB medium with antibiotics (dilution 1:100). In case of IFNgR1, cells were incubated at 37 °C shaking at 250 RPM until the Optical Density at 280 nm (OD_{600}) reached value 0.6, then IPTG to final concentration of 1 mM was added to induce protein expression that continued for 4 hours under same conditions (37 °C at 250 RPM). In the case of dimeric IFNg and IFNg-SC cells were incubated at 30 °C shaking at 250 RPM until the Optical Density at 280 nm (OD_{600}) reached value 0.4, then the temperature was decreased to 16 °C, and after another 30 min IPTG to final concentration of 1 mM was added to induce protein expression that continued for 20 hours under same conditions (16 °C at 250 RPM). In the end the cultivated cells were harvested by centrifugation (5,000 g for 15 min at 4 °C), washed by resuspending in smaller volume (10-20 mL) of PBS Buffer, and centrifuged again (8,000 g for 10 min at 4 °C). Supernatant was discarded and cells were stored at -20 °C.

5.2.14 Preparation of cytosolic and urea extract

Cells stored at -20 °C were thawed on ice and resuspended in 10 mL of buffer per 1 g of cells. Buffer A (50 mM Tris-HCl, pH 8.0) was used in case of IFNgR1 and Buffer B (20 mM Na-Phosphate buffer, pH 7.0) for IFNg-SC. Cells were further disrupted by ultrasound (pulse 20 s ON, 40 s OFF; total ON time 30 s per 1 mL of suspension) and centrifuged (40,000 g for 30 min at 4 °C) to get cytosolic extract. IFNg-SC was immediately purified from this cytosolic extract but because IFNgR1 is insoluble, its cytosolic extract was discarded and pellet containing inclusion bodies was dissolved in Buffer C (50 mM Tris-HCl, pH 8.0, 300 mM NaCl, 8 M Urea). Resulting suspension was incubated with shaking for 45-60 min at RT and then centrifuged again (40,000 g for 30 min at 4 °C) to get urea extract.

5.2.15 Purification on Ni-NTA agarose

Ni-NTA agarose was used for purification of IFNgR1 variants as they contain C-terminal 6x His Tag. All purification steps were performed as gravity flow at room temperature. The resin was equilibrated with Buffer C (50 mM Tris-HCl, pH 8.0, 300 mM NaCl, 8 M Urea), followed by urea extract application on the resin, and washing with Buffer C. The protein was eluted with Buffer D (50 mM Tris-HCl, pH 8.0, 300 mM NaCl, 8 M Urea, 250 mM Imidazole, pH 8.0) and EDTA to final concentration of 5 mM was added to the eluted fractions.

5.2.16 Purification on SP sepharose

SP Sepharose HP was used for purification of IFNg-SC as it has calculated pI around 8.99. All purification steps were performed on ÄKTA Purifier chromatography system at 4 °C. The resin was equilibrated with Buffer B (20 mM Na-Phosphate buffer, pH 7.0), followed by cytosolic extract application on the resin, and washing with Buffer B. The protein was eluted with linear gradient of NaCl up to 1 M in Buffer B.

5.2.17 Refolding

Since IFNgR1 variants formed inclusion bodies that were dissolved and purified in the presence of 8 M Urea, receptor had to be refolded. The eluted fractions from Ni-NTA agarose were dialyzed in SnakeSkin Dialysis Tubing (3.5K MWCO) against Refolding Buffer (100 mM

Tris-HCl, pH 8.0, 150 mM NaCl, 2.5 mM EDTA, pH 8.0, 0.5 mM Cystamine, 2.5 mM Cysteamine) in a ratio of at least 1:100 (protein to buffer volume).

5.2.18 Protein concentration measurement

Protein concentration was measured by Absorbance at 280 nm using NanoDrop ND-1000 instrument. The extinction coefficients were estimated from protein sequences using Expasy ProtParam tool.

5.2.19 Size exclusion chromatography

Final purification step for all proteins (IFNgR1 variants and IFNg-SC) included size exclusion chromatography on either Superdex 200 10/300 GL or HiLoad 16/600 Superdex 200 PG columns in PBS Buffer at flow rate 0.5 mL/min or 0.8 mL/min, respectively. Purification was performed on ÄKTA Purifier chromatography system at 4 °C. Samples were concentrated using VivaSpin Centrifugical Concentrators when necessary and filtrated through 0.22 μm Millex-GV Syringe Filter Unit (PVDF membrane).

5.2.20 Circular dichroism (CD) spectrometry

CD spectra were recorded using "Chirascan-plus" (Applied Photophysics) spectrometer in steps of 1 nm over the wavelength range of 190-260 nm. Samples at a concentration of 0.2 mg/mL were placed into quartz cell to the thermostated holder and individual spectra were recorded at the temperature of 25 °C. The CD signal was expressed as the difference between the molar absorption of the right- and left-handed circularly polarized light and the resulting spectra were buffer-subtracted. To analyze the ratio of the secondary structures we used the CDNN program provided with Chirascan CD spectrometer (Bohm *et al.*, 1992).

5.2.21 Melting temperature by CD spectrometry

For CD melting measurements, samples at a concentration of 1.5 mg/mL were placed into 10 mm path-length quartz cell to the thermostated holder and CD signal at 280 nm was recorded at 1 °C increment at rate of 1.0 °C/min over the temperature range of 25 to 65 °C with

an averaging time of 10 s. CD melting curves were normalized to relative values between 1.0 and 0.0.

5.2.22 Melting temperature by Thermal Shift Assay (TSA)

Melting temperature (T_m) curves of the WT and selected variants were obtained from fluorescence-based thermal shift assay (TSA) using fluoroprobe. Experiment was performed in "CFX96 Touch Real-Time PCR Detection System" (Bio-Rad) using FRET Scan Mode. The concentration of fluorescent SYPRO Orange dye (Sigma Aldrich) was 8-fold dilution from 5,000-fold stock and protein concentration was 2 µL in final volume of 25 µL. As a reference we used only buffer (PBS Buffer) without protein. Thermal denaturation of proteins was performed in capped "Low Tube Strips, CLR" (Bio-Rad) and possible air bubbles in samples were removed by centrifugation immediately before the assay. The samples were heated from 20 to 75 °C with stepwise increment of 0.5 °C/min and a 30 s hold step for every point, followed by the fluorescence reading. Data (after subtraction of reference sample) were normalized and used for first derivative calculation to estimate the melting temperature.

5.2.23 SPR

His-tagged receptor molecules were diluted to concentration of 10 µg/mL in PBST running buffer (PBS Buffer, 0.005% Tween20) and immobilized on a HTG sensor chip activated with Ni^{2+} cations at a flow rate 30 µL/min for 60 s to gain similar surface protein density. Purified IFNg-SC was diluted in running buffer to concentrations ranging from 0.1 to 9 nM and passed over the sensor chip for 90 s at a flow rate 100 µL/min (association phase). Dissociation was measured in the running buffer for 10 min at the same flow rate. Correction for nonspecific binding of IFNg-SC to the chip surface was done by subtraction of the response measured on uncoated interspots and reference channel coated with His-tagged Fe-regulated protein D (FrpD) from Neisseria meningitides (Sviridova *et al.*, 2010). Data were processed in the ProteOn Manager software (version 3.1.0.6) and the doubly referenced data were fitted to the 1:1 "Langmuir with drift" binding model.

6 Results

We applied two strategies to increase the affinity of extracellular part of human Interferon gamma receptor 1 (IFNgR1) to its ligand Interferon gamma (IFNg). The first set of mutations was aimed at changing residues on the interface between IFNg and its receptor, in this approach, the mutated residues on receptor molecule were in direct contact with IFNg amino acids. The second way to influence the affinity was innovative, as we targeted the residues within the "cavities" of the receptor molecule, in this approach, the mutated residues were not in direct contact with IFNg. All selected variants were expressed in *E. coli*, purified, and affinities were measured by the Surface Plasmon Resonance (SPR) method.

6.1 Analysis of interfaces in the IFNg/IFNgR1 crystal structures

Our analysis included two crystal structures of IFNg/IFNgR1 complex with PDB codes 1FG9 (Thiel *et al.*, 2000) and 1FYH (Randal and Kossiakoff, 2001), and we identified 40 amino acids in the receptor molecule that were within the range of 6.0 Å from IFNg in the crystal structures to mutate. We selected receptor chain D of 1FG9 as a reference chain for comparison of root mean square deviations (rmsd) between the main chain atoms of these 40 residues at the interface and 40 randomly chosen residues outside the interface. Table 3 shows that all four IFNgR1 molecules are quite similar, as the amino acids interacting directly with IFNg differ from the reference chain D of 1FG9 by less than 0.5 Å and residues outside the interface less than 2.0 Å. The receptor chain E of 1FG9 is not in direct contact with IFNg and varies from the other receptor molecules by more than 4.0 Å, so we did not include this chain in further calculations.

6.2 *In silico* design of interface variants

We replaced the selected 40 receptor interface residues by the 20 (including self-mutations) amino acids *in silico* and calculated two types of changes of free energy (ΔΔG) using the program FoldX (Schymkowitz *et al.*, 2005) to identify mutations increasing the affinity of IFNgR1 to IFNg. First, we predicted the stability of the mutated receptor in the complex by calculating ΔΔG (stability). Second, we tested the change of affinity of receptor to IFNg by calculating ΔΔG (affinity). Two sample matrices of ΔΔG values are shown in Table 2.

Table 2

Color-coded values of ΔΔG calculated using FoldX for chains C/ABD of the PDB structure 1FG9. Red indicates stabilization, blue destabilization. A) The first set of ΔΔG values estimates the influence of mutations on stability of the whole IFNg/IFNgR1 complex; B) the second set of ΔΔG values estimates (de)stabilization of the interaction between the receptor molecule and the rest of the IFNg/IFNgR1 complex.

A)

res	G	A	V	L	I	S	T	C	M	N	Q	K	R	H	P	D	E	F	Y	W
K_64	3.33	1.7	0.32	-	0.2	2.85	2.47	1.2	0.6	2.12	0.59	0.0	-	24.2	8.1	4.91	5.72	9.7	14.4	9.97
N_65	0.38	-	-	-	-	-	-	-	-	0.0	-	-	-	-0.44	-	0.76	0.84	-	-1.57	-
Y_66	2.90	1.6	1.77	1.12	1.6	2.41	3.13	1.5	-	1.83	2.54	0.22	0.24	1.37	3.4	3.41	4.56	-	0.00	-
G_67	0.0	3.0	4.22	1.51	3.0	4.25	5.46	3.4	3.2	3.32	2.66	2.65	5.04	3.61	9.5	2.46	3.74	2.7	3.10	4.23
V_68	2.22	0.6	0.0	-	-	1.66	1.31	0.8	1.0	0.38	1.15	1.59	1.20	3.73	6.0	2.54	1.14	4.1	5.38	5.19
K_69	0.08	-	0.17	0.02	0.1	-	-	0.0	0.3	0.36	0.15	0.0	-	0.35	-	-	0.05	0.0	0.05	0.13
N_70	-	-	0.19	-	-	-	0.29	-	-	0.0	-	-	-	-0.64	-	-	-	-	-0.62	-
S_71	0.47	1.1	1.51	0.54	1.8	0.0	0.98	0.5	0.9	0.07	0.61	0.38	0.73	1.07	0.8	0.98	0.94	0.2	0.32	0.21
E_72	-	-	0.31	0.24	0.1	-	-	0.0	0.6	0.40	0.19	0.05	0.26	0.32	-	0.25	0.0	-	-0.77	0.26
W_73	2.37	2.3	1.99	1.36	1.9	3.06	2.73	2.3	0.9	3.14	3.31	3.58	4.01	2.83	1.1	2.76	2.87	1.8	1.29	0.0
D_93	0.53	-	2.66	-	-	0.39	-	-	-	1.00	-	-	0.15	0.61	-	0.0	-	-	0.10	-
S_95	1.32	0.7	-	-	-	0.0	-	0.3	0.2	0.84	-	0.05	-	4.37	1.0	1.82	2.57	2.3	2.53	4.05
N_96	0.89	0.4	0.34	-	-	0.96	0.41	0.5	-	0.0	0.42	0.47	-	0.18	3.8	0.35	1.61	-	-0.21	-
S_97	-	-	-	-	-	0.0	-	-	-	-	-	-	1.68	-1.42	-	-	-	-	-2.84	-
W_99	2.90	1.7	0.00	0.63	-	2.15	1.07	1.4	0.5	2.54	1.52	2.06	3.52	2.24	3.0	3.35	3.24	0.3	1.21	0.0
K_115	0.94	0.6	0.15	-	-	0.65	0.35	0.3	-	0.73	0.23	0.0	1.05	0.86	0.3	0.83	0.39	-	-1.50	0.43
S_116	0.18	-	2.04	-	0.1	0.0	0.42	0.5	-	-	1.89	1.92	2.26	7.47	3.2	2.27	2.01	7.8	10.3	7.19
E_118	-	-	0.35	-	1.0	-	0.22	-	-	-	-	-	-	0.12	-	0.03	0.0	-	-0.90	-
R_123	2.44	1.3	2.30	0.92	2.5	2.39	2.46	1.6	1.6	1.62	2.27	1.11	0.0	2.01	0.7	4.48	4.24	1.2	0.97	2.46
E_164	-	0.2	2.00	0.26	2.1	0.38	1.42	0.0	0.2	-	-	-	0.12	-0.17	2.6	0.09	0.0	-	-0.11	0.08
T_165	0.85	0.1	0.35	-	-	0.00	0.0	0.3	-	1.22	0.56	-	-	1.00	2.5	3.63	2.40	2.2	1.71	6.09
T_166	-	-	-	-	-	-	0.0	-	-	-	-	-	0.26	0.17	-	0.88	1.15	-	-0.94	-
Y_168	-	-	-	0.34	0.2	-	-	-	0.4	-	0.71	-	0.29	0.11	2.0	2.67	2.49	-	0.00	0.17
R/F_17	-	-	-	-	-	0.29	-	-	-	0.45	-	-	0.0	-1.28	2.0	-	-	-	-2.47	-
V_171	2.42	1.1	0.0	0.69	0.0	1.76	1.33	0.8	1.2	1.18	0.57	0.71	1.17	1.67	0.8	1.65	1.13	0.7	1.89	1.20
K_186	0.29	0.3	0.64	-	0.3	0.04	0.58	-	-	0.02	0.20	0.0	0.45	0.64	-	-	-	-	0.21	0.07
T_189	0.92	-	-	-	0.4	0.33	0.0	0.6	-	0.84	0.00	0.47	0.44	1.78	1.7	2.07	1.51	0.4	0.71	0.90
Q_190	-	-	-	-	-	-	-	-	-	-	0.0	0.40	0.92	0.23	0.3	-	0.49	-	-0.60	-
K_191	0.60	0.0	0.73	-	0.3	0.49	0.73	0.6	-	0.00	-	0.0	0.33	0.52	-	0.00	-	0.5	0.39	0.02
E_192	-	-	0.02	-	0.6	-	-	-	0.6	-	0.35	0.76	1.41	0.56	5.8	-	0.0	0.2	2.37	2.60
D_193	-	-	0.28	-	0.2	-	0.09	-	0.0	-	-	-	-	-0.39	-	0.0	-	-	-0.45	-
E_197	-	-	0.02	-	-	-	0.17	0.1	-	0.12	-	-	-	0.40	-	0.33	0.0	-	-0.45	0.12
V_220	2.56	1.4	0.0	0.10	-	2.26	1.61	1.4	1.0	2.49	1.66	1.86	2.10	1.92	4.0	2.22	1.11	0.5	0.94	1.09
L_221	3.13	2.6	2.70	0.0	2.6	2.13	2.02	2.2	1.7	3.20	3.15	2.47	2.90	1.68	3.5	4.78	4.11	2.2	8.35	3.80
H_222	-	-	0.22	-	0.1	-	0.13	-	-	-	-	-	-	0.00	-	-	-	-	-1.69	-
V_223	1.29	2.0	0.0	-	-	2.42	1.21	0.8	-	1.55	0.83	0.14	2.10	34.5	3.4	2.30	2.27	3.8	5.30	5.32
W_224	3.33	3.0	2.90	1.91	2.9	3.81	4.23	3.0	2.2	4.20	3.54	2.82	3.10	2.42	2.2	4.52	4.45	1.0	1.53	0.0
G_225	0.0	1.8	6.50	4.89	8.0	2.78	5.98	3.0	4.1	2.94	5.28	3.55	4.48	5.09	7.4	4.21	5.79	4.4	5.26	5.03
V_226	1.26	0.4	0.0	-	-	0.65	0.98	0.3	0.0	0.79	0.80	0.42	0.49	1.94	-	1.48	0.94	0.0	0.41	1.34
T_227	0.13	-	-	-	-	-	0.0	-	-	-	-	-	-	-0.12	-	0.70	-	-	-0.94	-

B)

res	G	A	V	L	I	S	T	C	M	N	Q	K	R	H	P	D	E	F	Y	W
K_64	1.68	1.7	1.22	1.15	1.3	1.66	1.93	1.2	1.2	1.76	0.53	0.0	-	0.96	1.6	3.31	3.75	3.0	3.80	2.79
N_65	0.29	0.2	-	-	-	0.20	-	0.0	-	0.0	-	-	-	0.00	0.1	0.11	0.09	0.0	0.01	0.03
Y_66	4.20	3.5	2.86	2.85	4.1	4.30	4.20	3.5	1.1	4.46	3.61	1.83	1.16	2.52	3.5	4.73	4.24	-	0.0	1.16
G_67	0.0	0.9	0.14	-	-	1.24	1.22	0.7	-	0.96	-	0.31	1.20	0.74	2.0	-	0.41	0.1	0.23	0.90
V_68	1.92	0.7	0.0	1.97	0.5	0.91	1.68	0.3	2.0	-	-	1.11	0.97	1.86	5.2	0.50	0.04	0.3	2.04	2.18
K_69	1.40	1.4	1.45	1.39	1.4	1.42	1.44	1.4	1.4	1.45	1.41	0.0	1.46	1.43	1.1	1.19	1.44	1.3	1.37	1.37
N_70	0.02	-	0.21	0.18	0.2	-	0.15	0.0	0.1	0.0	0.11	0.08	0.03	0.04	-	0.29	0.17	0.0	0.07	0.14
S_71	2.21	2.2	1.96	1.49	1.5	0.0	0.18	1.8	1.5	1.62	1.70	1.30	1.17	1.99	1.8	2.19	2.09	1.4	1.69	1.52
E_72	-	-	-	-	-	-	-	-	-	-	-	-	-	-	-	-	0.0	-	-	-
W_73	0.25	0.1	-	0.18	0.0	0.10	-	0.1	0.1	-	0.29	-	0.01	-	-	0.08	0.07	-	0.40	0.0
D_93	0.05	-	-	-	-	0.09	0.07	-	-	0.10	0.06	0.07	0.27	0.35	-	0.0	-	0.2	0.29	0.19
S_95	0.51	0.2	0.10	-	-	0.0	0.22	0.2	-	0.19	0.12	-	-	0.33	0.4	0.39	0.98	0.1	0.29	-
N_96	-	-	-	-	-	-	-	-	-	0.0	-	-	-	-	-	0.04	0.22	-	-	-
S_97	-	0.2	-	0.04	-	0.00	0.32	-	-	-	0.20	-	0.0	-	-	-	-	-	-	-
W_99	0.63	0.4	0.29	0.24	-	0.62	0.50	0.2	-	0.74	1.09	-	1.89	0.72	0.3	-	0.97	0.6	-	0.0
K_115	0.04	0.1	0.17	0.21	0.1	0.23	0.10	0.2	0.2	0.48	0.01	0.0	-	0.15	0.0	0.18	0.40	0.2	0.22	0.23
S_116	-	-	-	-	0.0	0.0	-	-	-	-	-	-	-	-	-	-	-	-	-	-
E_118	-	-	-	-	-	-	-	-	-	-	-	-	-	-	-	-	0.0	-	-	-
R_123	1.40	1.1	1.32	1.60	1.5	1.26	1.27	1.2	1.9	1.58	2.20	0.94	0.0	1.29	0.9	2.20	2.47	1.1	0.93	1.41
E_164	0.30	0.3	0.62	0.47	0.4	0.35	0.39	0.3	0.2	0.26	0.26	0.29	0.34	0.33	0.3	0.16	0.0	0.4	0.45	0.46
T_165	0.03	0.0	0.15	0.07	0.1	0.02	0.0	0.0	0.0	0.11	0.06	0.05	0.13	0.19	0.0	0.29	0.10	0.3	0.28	0.02
T_166	0.43	0.5	-	-	-	0.01	0.0	-	-	-	-	0.22	0.09	0.67	0.1	1.98	1.43	0.1	-	-
Y_168	0.14	0.0	-	-	-	0.09	-	0.0	-	0.12	-	-	-	-	-	0.07	-	0.1	0.0	-
R/F_17	0.30	0.2	0.30	0.29	0.3	0.29	0.30	0.3	0.2	-	0.56	0.13	0.0	0.29	0.3	0.41	0.50	0.2	0.27	0.27
V_171	-	-	0.0	0.00	0.0	-	-	-	-	-	0.31	-	-	-	-	-	-	-	-	0.08
K_186	-	-	-	-	-	-	-	-	-	-	-	0.0	0.04	-	-	-	-	0.0	0.04	0.10
T_189	0.00	-	0.00	0.00	0.0	0.00	0.0	0.0	0.0	0.00	0.00	0.02	0.08	0.01	0.0	-	-	0.0	0.10	-
Q_190	-	-	-	-	-	-	-	-	-	-	0.0	-	-	-	-	-	-	0.1	0.09	0.45
K_191	-	-	0.11	0.17	0.0	-	0.13	-	-	-	0.06	0.0	0.01	-	0.0	-	0.05	0.1	-	0.46
E_192	0.04	0.0	0.04	0.04	0.0	0.04	0.04	0.0	0.0	0.04	0.04	0.04	0.04	0.04	0.1	-	0.0	0.0	0.07	0.03
D_193	0.06	0.0	0.06	0.06	0.0	0.06	0.06	0.0	0.0	0.06	0.06	0.08	0.12	0.10	0.0	0.0	0.01	0.0	0.06	0.06
E_197	0.10	0.0	0.10	0.10	0.1	0.10	0.13	0.1	0.1	0.09	0.10	0.11	0.14	0.09	0.1	-	0.0	0.0	0.09	0.09
V_220	-	-	0.0	0.01	0.0	-	0.03	-	0.1	0.39	0.12	0.46	0.76	0.19	-	-	-	0.3	0.37	-
L_221	-	0.0	0.12	0.0	0.0	0.05	0.04	-	-	-	-	-	-	-	0.3	-	-	-	-	-
H_222	-	0.0	-	-	-	0.00	-	-	-	-	-	-	-	0.0	-	0.04	-	-	-	-
V_223	1.62	1.2	0.0	0.49	0.0	0.76	1.05	0.3	-	1.58	1.03	0.42	0.58	2.89	1.7	2.88	2.34	4.6	6.32	5.13
W_224	1.61	1.8	1.82	1.15	1.5	1.99	1.86	1.8	0.7	2.53	2.04	1.66	1.60	1.11	1.7	2.02	2.84	1.0	1.27	0.0
G_225	0.0	0.1	2.31	2.00	4.7	0.58	2.48	1.3	1.5	0.94	2.42	1.10	0.35	2.60	1.3	1.54	2.60	2.2	2.45	2.21
V_226	0.00	0.0	0.0	-	-	0.00	0.00	0.0	0.0	-	-	-	-	0.00	0.1	0.02	-	-	-	-
T_227	0.00	0.0	0.01	0.12	0.0	0.00	0.0	0.0	0.1	0.01	-	0.04	0.06	0.10	0.0	-	-	0.2	0.42	0.17

Because we use four crystallographic interfaces for analysis and the calculated ΔΔG values may differ between them, we calculated both types of the ΔΔG matrices independently for all four interfaces. Because the four receptor molecules interacting with IFNg are structurally similar (Table 3), the differences between corresponding ΔΔG values in "stability" and "affinity" matrices are usually quite small.

Table 3
Structural similarity of the IFNgR1 molecules at and outside the interface with IFNg. Four receptor chains from crystal structures 1FG9 (Thiel *et al.*, 2000) and 1FYH (Randal and Kossiakoff, 2001) are compared to receptor chain D of 1FG9. Almost all chains are pretty similar to each other except the 1FG9:E chain that differs from the others by more than 4.0 Å.

PDB Code:chain	**rmsd (Å)[1] Interface**	**rmsd (Å)[2] Outside**
1FG9:C	0.60	1.66
1FG9:E	4.16	4.32
1FYH:B	0.58	1.42
1FYH:E	0.59	1.06

[1] Root mean square deviations (rmsd) between the four IFNgR1 molecules and the chain D of 1FG9. Deviations are calculated between the positions of the main chain atoms of the 40 residues forming the interface with IFNg.
[2] Root mean square deviations (rmsd) between the four IFNgR1 molecules and the chain D of 1FG9. Deviations are calculated between the positions of the main chain atoms randomly selected outside the 40 residues forming the interface with IFNg.

We further supported the selection of mutable residues by sequence analysis of conserved amino acids (see below Chapter 6.5), as the residues conserved in more than 65 % of 32 IFNg receptor sequences from 19 species were considered for mutation. By combining energy-based criteria and sequence variability, we choose nine most promising variants (Table 4).

Moreover, we designed combinations of these nine single amino acids variants to evaluate their possible cooperative effects. To this end, we combined three mutations, N70G, S95R, and H222R, which are distant from each other, into one triple and three double variants to cover all seven possible mutual combinations. Selected variants are illustrated in Figure 7 and listed in Table 4 under numbers 1-13.

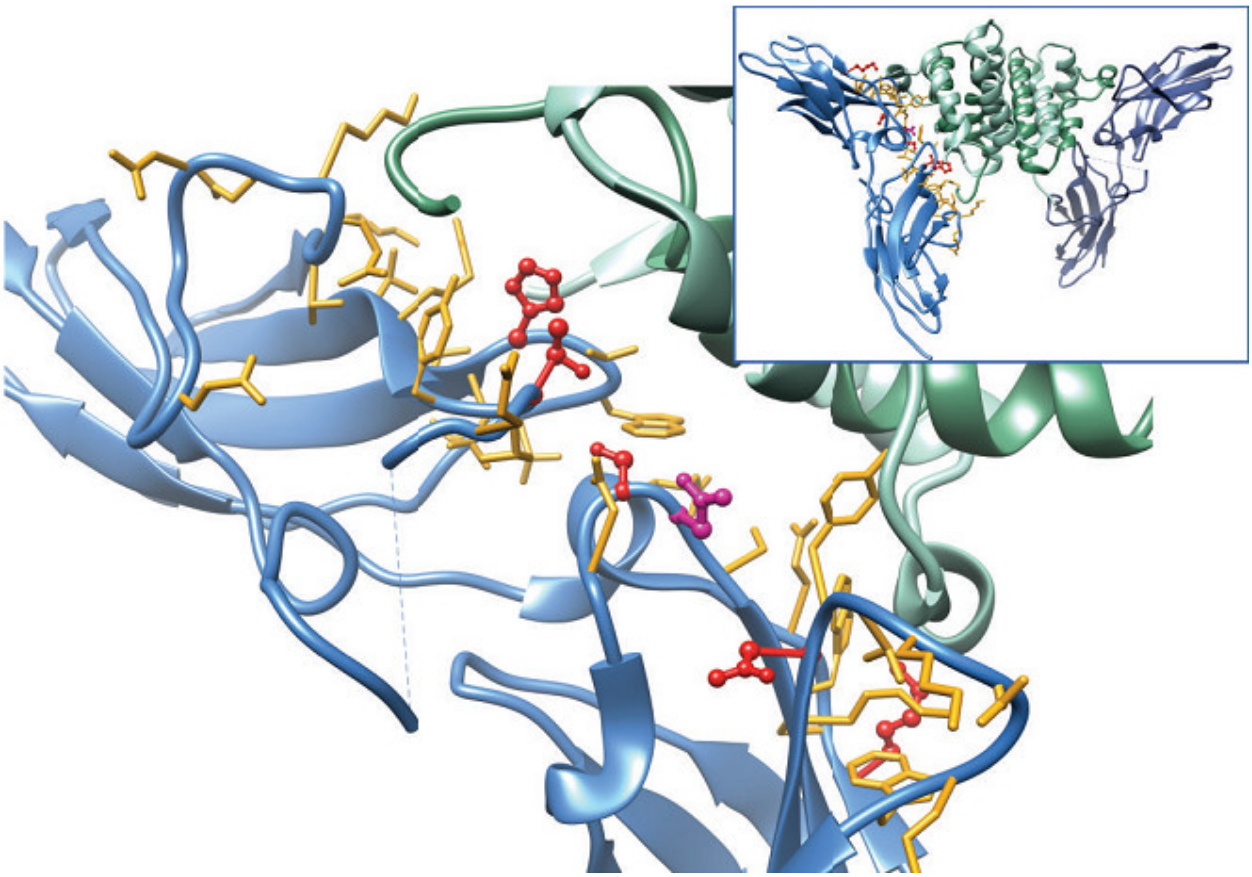

Figure 7
The interface between IFNg and the extracellular part of its receptor 1 (IFNgR1) from crystal structure 1FG9 (Thiel *et al.*, 2000). Two IFNgR1 molecules are drawn as blue cartoon and IFNg homodimer as green cartoon. The receptor residues forming the interface with IFNg are drawn as yellow sticks, the residues selected for mutations are highlighted in red, and the residue N96 in magenta. All the selected mutations are listed in Table 4.

6.3 Internal cavities identified in IFNgR1

Our analysis of internal cavities included four IFNgR1 molecules from crystal structures with PDB entries 1FYH and 1FG9, used previously for searching of interface variants (see Chapter 6.1). We did not include chain E from crystal structure 1FG9 because of no direct contact with IFNg. Generally number and size of cavities differed for each IFNgR1 molecule and their characteristics are listed in Table 5. Figure 8 highlights their location within the representative receptor molecule (PDB entry 1FG9, chain C). We combined all amino acids lining cavities in all four IFNgR1 proteins complexed with IFNg, resulting in a total of 52 residues used in subsequent *in silico* analysis.

Table 4
Calculated and experimental values of the changes of free energy (ΔΔG) of the interaction between IFNgR1 variants and IFNg-SC relative to the wild-type receptor.

ID[1]	Variant[2]	The best ΔΔG[3] (kJ/mol)	ΔΔG from MD[4] (kJ/mol)	Experimental ΔΔG[5] (kJ/mol)	Esd[6] (kJ/mol)
1	N65R	-5.4	17.3	2.1	-
2	N70G	-5.4	0.3	-0.6	-
3	S95R	-8.3	11.8	2.1	-
4	N96F	-13.0	-0.6	-0.2	-
5	N96W	-9.9	-6.1	-3.9	0.2
6	K115Y	-0.3	-9.6	0.7	-
7	T166M	-5.8	-5.4	2.0	-
8	T166Y	-9.8	0.9	2.5	-
9	H222R	-6.9	-15.8	-0.1	0.2
10	N70G + S95R	-7.3	2.7	1.5	-
11	N70G + H222R	-4.6	-7.3	-0.3	-
12	S95R + H222R	-11.4	-10.8	1.5	-
13	N70G + S95R + H222R	-15.8	-5.6	0.5	0.1
14	Y66L	2.1	11.8	0.0	-
15	S71E	9.6	19.6	1.6	-
16	H222D	6.7	5.8	2.0	-

[1] Variants 1-13 are single, double, and triple mutants designed to increase affinity to IFNg compared to WT. Variants 14-16 were designed to lower the affinity between IFNg and IFNgR1 but not to destabilize the unbound IFNgR1.
[2] Residues are numbered as in the UniProt entry code P15260.
[3] For variants 1-13, the most negative (most stabilizing) values obtained at the four crystal interfaces by FoldX (Schymkowitz *et al.*, 2005). For variants 14-16, the listed ΔΔG are for the least positive (least destabilizing) interface.
[4] Averaged ΔΔG values calculated by FoldX on structures taken from snapshots of 10 to 20 ns MD runs by GROMACS (Van Der Spoel *et al.*, 2005).
[5] ΔΔG values determined from experimental SPR values of dissociation equilibrium constants K_d as $\Delta\Delta G = -RT\ln\{(K_d)_{WT}/(K_d)_{mut}\}$.
[6] Estimated standard deviations (Esd) for the experimental values of ΔΔG with the number of independent SPR measurements $N > 2$.

Table 5
Cavities in the four molecules of the IFNgR1 receptor in crystal structures 1FG9 (Thiel *et al.*, 2000) and 1FYH (Randal and Kossiakoff, 2001). The receptor molecules are labeled by chain ID (chains C and D from 1FG9, chains B and E from 1FYH).
Figure 8 shows cavities 1-8 as they project into the chain C of 1FG9.

	Surface (Å²)[1]	**Number of residues lining the cavity[2]**	**Residues selected for mutation**	**Cavity observed in IFNgR1 chain**	
				1FG9	1FYH
1	134	7	V35, A114	C D	-
2	133	5	-	-	B E
3	470	14	D124	C D	-
4	262	9	H222	C D	B E
5	120	6	-	C D	E
6	165	7	-	C D	E
7	177	7	-	D	B E
8	138	5	-	C	B

[1] Surface calculated with a probe radius of 0.25 Å for cavities combined from all relevant receptor chains.
[2] Some residues are shared among neighboring cavities.

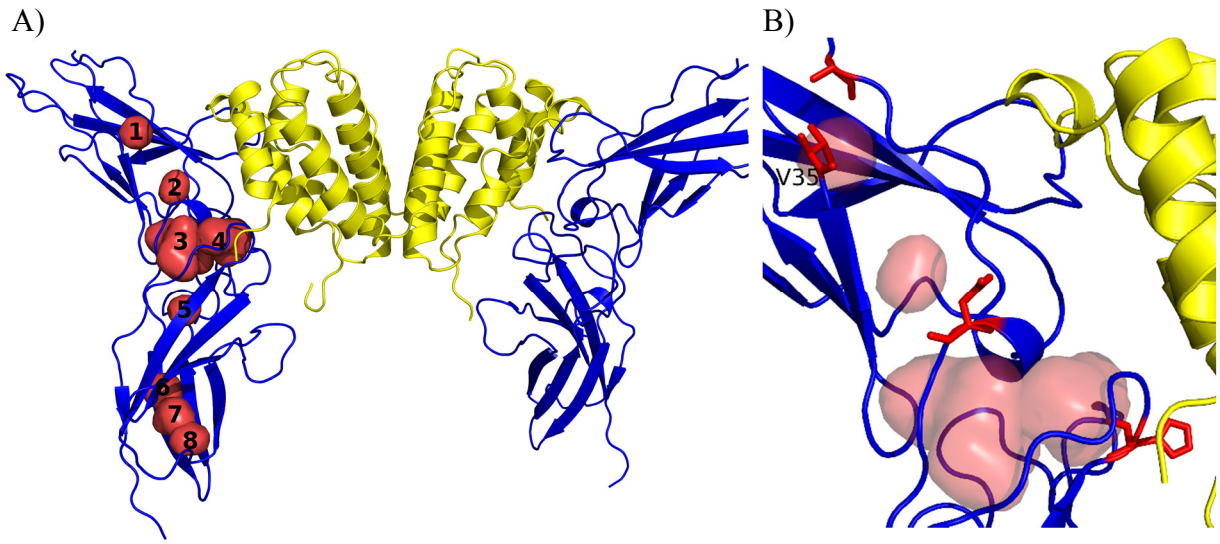

Figure 8
A) The complex between IFNg and the extracellular part of its receptor 1 (IFNgR1) from crystal structure of PDB code 1FG9 (Thiel *et al.*, 2000). The two IFNgR1 molecules are drawn as blue cartoon and IFNg homodimer as yellow cartoon. The eight identified cavities in the receptor molecule are shown as numbered red surfaces.
B) A close-up of the mutated cavities. The receptor cavities are drawn as red surface and residues selected for mutations as red sticks, valine 35 is labeled.

6.4 *In silico* design of cavity variants

We included all 52 amino acids forming the cavities of the receptor molecules from crystal structures in mutation analysis by FoldX. We calculated "binding" ΔΔG values and ordered them by their potential to increase the affinity. We narrowed the selection to first 50 best mutations from each receptor chain (200 mutations in total) and then we suggested 12 promising positions that were predicted in all four or at least three crystal structures. These 12 residues are listed in Table 7 with ΔΔG values calculated for one crystal structure.

We observed significant differences between ΔΔG predicted directly from the crystal structures and from structures after molecular dynamics (MD) relaxation in analysis of interface variants, therefore we performed short (10 ns) MD simulations of the four crystal structures of wild-type IFNgR1/IFNg complexes. Subsequently, from these MD trajectories we extracted 500 snapshots that were the basis for FoldX analysis to get ΔΔG values of the predicted 12 positions nominated for mutations. Last steps were averaging of ΔΔG values and final selection of the four candidate variants that are listed in Table 6 together with the changes of their binding free energies averaged over the 500 MD snapshots.

Table 6
Predicted changes of free energy changes (ΔΔG) of the four selected IFNgR1 variants with cavity-lining mutations relative to the wild-type receptor. All energy values are in kcal/mol.

Variant	ΔΔG of folding of IFNgR1 in complex [1]	ΔΔG of folding of free IFNgR1 [2]	ΔΔG of binding of IFNgR1/IFNg complex [3]	Sequence conservation [4]
V35L	-0.88	-0.85	-0.02	80 %
A114E	0.28	0.46	-0.20	60 %
D124N	0.65	0.88	-0.21	40 %
H222Y	-0.72	-0.69	0.15	40 %

[1] "ΔΔG of folding of IFNgR1 in complex" measures the influence of mutations on the stability of the whole complex.
[2] "ΔΔG of folding of free IFNgR1" represents changes of the stability of the isolated receptor.
[3] "ΔΔG of binding" of the whole complex between IFNgR1 and IFNg estimates the change of the affinity between the receptor molecule and the rest of the complex.
[4] Sequence conservation of amino acid residues at position 35, 114, 124, and 222. It was based on the global alignment of 32 sequences of the extracellular part of IFNgR1 (Figure 9).

Table 7
Color-coded values of ΔΔG calculated using the program FoldX – red colored matrix fields indicate stabilization, blue ones destabilization. Shown are only values of ΔΔG calculated using PDB 1FG9 (Thiel *et al.*, 2000), receptor chain C. Analogical matrices are calculated for 1FG9 receptor chain D, and for receptor chains B and E from the structure 1FYH (Randal and Kossiakoff, 2001) but data are not shown here.
[1] "ΔΔG of folding of IFNgR1 in complex" gauged the influence of mutations on the stability of the whole IFNg/IFNgR1 complex.
[2] "ΔΔG of folding of free IFNgR1" estimated the effect of mutations on the stability of the isolated receptor.
[3] "ΔΔG of binding" of complex between IFNgR1 and IFNg made an estimate of change of the interaction between the receptor molecule and the rest of the complex.

(1)		GLY	ALA	VAL	LEU	ILE	SER	THR	CYS	MET	ASN	GLN	LYS	ARG	HIS	PRO	ASP	GLU	PHE	TYR	TRP
VAL	35	2.8	2.0	0.0	-0.9	-0.4	2.9	1.6	1.3	0.1	2.0	2.5	3.5	5.1	4.7	1.2	3.4	3.5	4.3	7.3	10.6
VAL	46	3.8	2.2	0.0	-0.1	-0.3	3.1	1.8	1.8	0.6	2.4	3.0	4.1	6.4	6.4	2.0	3.6	3.7	4.0	6.6	9.1
VAL	100	5.6	3.7	0.0	0.3	-0.3	4.2	2.4	2.7	0.8	3.6	3.9	5.4	7.6	6.2	5.0	5.5	5.1	4.0	6.8	9.8
VAL	102	5.2	3.3	0.0	1.2	-0.4	4.0	2.2	2.5	1.8	3.6	4.1	7.1	11.9	9.4	4.8	4.9	4.9	7.5	11.2	15.6
ALA	114	1.0	0.0	-0.2	0.1	0.1	0.3	0.2	0.1	0.3	0.6	0.2	0.2	0.7	3.3	2.3	1.1	0.3	0.7	1.0	1.9
ASP	124	3.0	2.2	2.5	1.4	2.5	2.3	2.7	2.0	1.7	0.7	1.4	1.8	2.1	2.3	5.7	0.0	1.5	1.4	1.6	2.5
GLY	125	0.0	2.0	6.0	6.4	7.7	2.9	5.6	3.0	4.7	5.7	6.8	8.1	10.1	31.3	6.2	7.1	7.1	12.0	14.1	21.8
ILE	169	5.1	3.7	1.1	0.1	0.0	4.7	3.2	2.9	0.3	3.0	3.2	4.1	5.5	3.9	1.8	4.2	3.6	1.9	4.7	7.0
HIS	222	0.7	0.1	0.8	-0.3	1.1	-0.3	0.6	0.4	-0.3	-0.6	0.5	-0.1	0.3	0.0	2.9	-0.1	0.5	-1.1	-0.7	1.1
VAL	223	2.5	2.0	0.0	0.7	0.3	3.7	1.4	2.3	0.9	3.0	3.2	3.8	6.3	14.2	7.3	4.6	4.9	7.6	11.5	15.6
TRP	224	5.5	4.7	3.5	2.8	3.1	5.5	4.9	4.5	2.4	4.8	4.2	4.2	4.0	3.3	4.6	5.9	5.2	1.1	1.5	0.0
GLY	225	0.0	1.5	3.3	2.0	3.4	2.0	3.3	1.8	1.6	2.1	2.5	2.6	2.9	4.7	4.3	2.9	3.0	2.4	2.6	2.9

(2)		GLY	ALA	VAL	LEU	ILE	SER	THR	CYS	MET	ASN	GLN	LYS	ARG	HIS	PRO	ASP	GLU	PHE	TYR	TRP
VAL	35	2.8	2.0	0.0	-0.9	-0.4	2.9	1.6	1.3	0.1	2.0	2.5	3.6	5.3	4.5	1.2	3.4	3.5	4.3	7.3	10.7
VAL	46	5.0	3.0	0.0	-0.2	-0.5	4.1	2.4	2.4	0.5	3.2	3.8	5.1	8.1	7.6	2.9	4.8	4.8	4.4	7.9	11.5
VAL	100	5.7	3.8	0.0	0.3	-0.3	4.2	2.4	2.7	0.8	3.7	4.0	5.5	7.7	5.9	5.0	5.5	5.1	4.1	6.8	9.7
VAL	102	5.2	3.3	0.0	1.2	-0.4	4.0	2.2	2.5	1.8	3.6	4.1	7.1	11.9	9.5	4.8	4.9	4.9	7.5	11.2	15.7
ALA	114	1.0	0.0	-0.2	0.2	0.2	0.3	0.2	0.1	0.4	0.7	0.3	0.3	0.7	3.4	2.3	1.2	0.5	0.8	1.1	2.0
ASP	124	2.4	1.6	2.0	0.7	1.7	1.8	2.1	1.6	0.9	0.9	1.3	1.0	1.4	1.5	4.8	0.0	1.4	1.0	1.2	1.8
GLY	125	0.0	2.0	6.0	6.4	7.8	2.9	5.6	3.0	4.8	5.8	6.8	8.2	10.2	32.2	6.2	7.1	7.2	12.1	14.2	21.9
ILE	169	5.1	3.7	1.1	0.1	0.0	4.7	3.2	2.9	0.3	3.0	3.2	4.2	5.6	3.8	1.8	4.2	3.7	1.9	4.7	7.0
HIS	222	-0.1	-0.6	0.5	-0.4	0.6	-1.0	0.2	-0.1	-0.4	-0.7	0.2	-0.5	0.0	0.0	2.3	-0.3	-0.2	-0.9	-0.7	0.6
VAL	223	0.9	0.6	0.0	0.2	-0.2	1.7	0.4	1.2	0.1	1.2	1.1	0.5	0.9	1.0	5.6	1.6	1.2	0.1	0.3	0.6
TRP	224	2.7	2.1	1.3	1.2	1.1	2.5	2.1	1.9	0.9	2.2	1.9	1.6	2.0	2.0	2.2	2.4	2.0	0.3	0.6	0.0
GLY	225	0.0	1.2	1.9	0.8	1.7	1.2	1.7	1.1	0.6	0.9	0.9	0.8	1.0	1.0	2.8	1.0	1.0	0.4	0.5	0.3

(3)		GLY	ALA	VAL	LEU	ILE	SER	THR	CYS	MET	ASN	GLN	LYS	ARG	HIS	PRO	ASP	GLU	PHE	TYR	TRP
VAL	35	0.0	0.0	0.0	0.0	0.0	0.0	0.0	0.0	0.0	0.0	0.0	-0.1	-0.2	0.0	0.0	0.0	0.0	0.0	0.0	-0.1
VAL	46	0.0	0.0	0.0	0.0	0.0	0.0	0.0	0.0	0.0	0.0	0.0	0.0	0.0	0.0	0.0	0.0	0.0	0.0	0.0	0.0
VAL	100	0.0	0.0	0.0	0.0	0.0	0.0	0.0	0.0	0.0	0.0	0.0	0.0	0.0	0.0	0.0	0.0	0.0	0.0	0.0	0.0
VAL	102	0.0	0.0	0.0	0.0	0.0	0.0	0.0	0.0	0.0	0.0	0.0	0.0	0.0	0.0	0.0	0.0	0.0	0.0	0.0	0.0
ALA	114	0.0	0.0	0.0	-0.1	-0.1	0.0	0.0	0.0	-0.1	-0.1	-0.1	-0.1	0.0	-0.1	0.0	-0.1	-0.2	-0.1	-0.1	-0.1
ASP	124	0.2	0.1	0.0	-0.1	0.1	0.1	0.0	-0.1	-0.1	-0.2	-0.2	-0.1	-0.1	0.1	0.2	0.0	-0.1	-0.1	-0.1	0.1
GLY	125	0.0	0.0	0.0	0.0	-0.1	0.0	0.0	0.0	0.0	0.0	0.0	-0.1	-0.1	-0.1	-0.1	0.0	0.0	-0.1	-0.1	-0.1
ILE	169	0.0	0.0	0.0	0.0	0.0	0.0	0.0	0.0	0.0	0.0	0.0	0.0	0.0	0.0	0.0	0.0	0.0	0.0	0.0	0.0
HIS	222	1.3	1.2	0.9	0.7	0.8	1.1	0.9	0.7	0.4	0.3	0.5	0.4	0.2	0.0	1.2	0.5	0.6	0.1	0.2	0.8
VAL	223	1.7	1.4	0.0	0.1	0.4	2.0	0.8	1.2	0.3	1.5	1.6	2.0	3.2	6.1	2.2	2.7	2.9	5.7	8.2	10.4
TRP	224	3.3	3.1	2.6	1.8	2.2	3.3	3.0	3.0	1.4	2.9	2.3	2.4	2.0	1.3	2.8	3.6	3.1	0.9	0.8	0.0
GLY	225	0.0	0.3	1.1	0.6	1.2	0.6	1.2	0.4	0.3	0.8	0.9	0.9	0.9	2.9	1.3	1.4	1.3	1.1	1.1	1.4

6.5 Sequence conservation of IFNgR1 residues

We supplemented the energy-based selection of variants by considering the residue conservation. 32 receptor sequences from 19 organisms were used in a global alignment (Figure 9) of the extracellular part of IFNgR1 by Kalign algorithm implemented in program Ugene (Okonechnikov *et al.*, 2012). In the case of interface variants, we wanted to avoid mutating highly conserved residues that can play structural or functional role (Ma *et al.*, 2003; Valdar and Thornton, 2001). We checked this feature by mutational analysis of residues which are conserved at the 90 % level, namely S97X (X = L, N, W) and E118X (X = M, F, Y, W). An SPR experiment showed that none of the mentioned variants bind IFNg-SC, although they were predicted to have higher affinity than WT. Based on this observation, we excluded mutations of interface amino acids conserved by more than 65 % from further analysis. In contrast, such a close correlation between sequence conservation and mutability is less obvious in the case of cavity variants. Global alignment showed conservation between 40 to 98 % for cavity-lining positions, for example residue V35 is well conserved at 80% level, however, its mutation (V35L) still increases the affinity.

6.6 Production and purification of IFNg and its variant IFNg-SC

We have developed a new protocol for production and purification of dimeric IFNg and its "single-chain" variant called hereafter IFNg-SC. IFNg-SC has the two peptide chains of the IFNg dimer linked together by a seven-residue linker and His111 changed to an aspartic acid residue in the first chain (Landar *et al.*, 2000); cloning into the expression vector is described in more detail in Methods (Chapter 5.2.8). Although wild-type IFNg as well as IFNg-SC are expressed in insoluble form in *E. coli* according to the literature (Haelewyn and De Ley, 1995; Landar *et al.*, 2000; Mohammadian-Mosaabadi *et al.*, 2007; Petrov *et al.*, 2014), we produced IFNg-SC in *E. coli* BL21(λDE3) as a soluble protein by lowering the temperature of expression to 16 °C. We did not include any purification tag or extra amino acids to IFNg to get a higher yield of the native protein for further biophysical measurements. IFNg has a high isoelectric point (pI) of about 8.99, so that we could use cation exchange chromatography (SP Sepharose) as the first purification step and size exclusion chromatography (Superdex column) as the second final step. The details of purification, SDS-PAGE gels and chromatograms, are depicted in Figure 10.

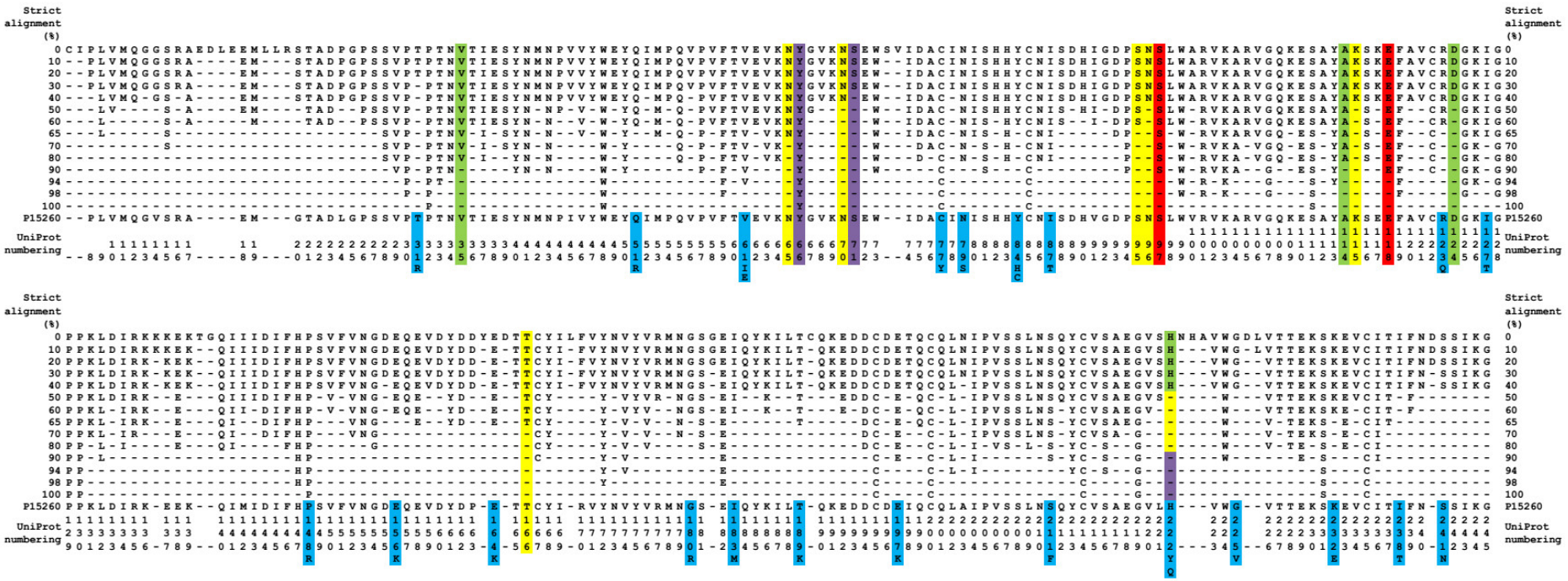

Figure 9

Conserved residues of the extracellular part of IFNg receptor 1 and their mutability. The conservancy of residues was determined by strict alignment of 32 sequences from 19 species. Percentages of the conservation are shown on the left and right sides, sequence and numbering of UniProt entry code P15260 on the bottom. Sequences used for the alignment are listed in Chapter 5.1.6. The numbering of the PDB entry 1FG9 can be derived from the UniProt one by subtracting 17. The alignment was computed by KAlign (Lassmann *et al.*, 2009) as implemented in program Ugene (Okonechnikov *et al.*, 2012).

Yellow – The receptor residues forming the interface with IFNg (i.e., residues no further than 6 Å from an IFNg atom) and selected for mutations.

Green – The residues lining the cavities and selected for mutations after MD simulations.

Purple – The residues predicted to lower the receptor affinity but still increase the stability of receptor molecule itself.

Red – The highly conserved residues; their mutation abolished binding of IFNgR1 to IFNg.

Blue – IFNgR1 variants occurring naturally in humans.

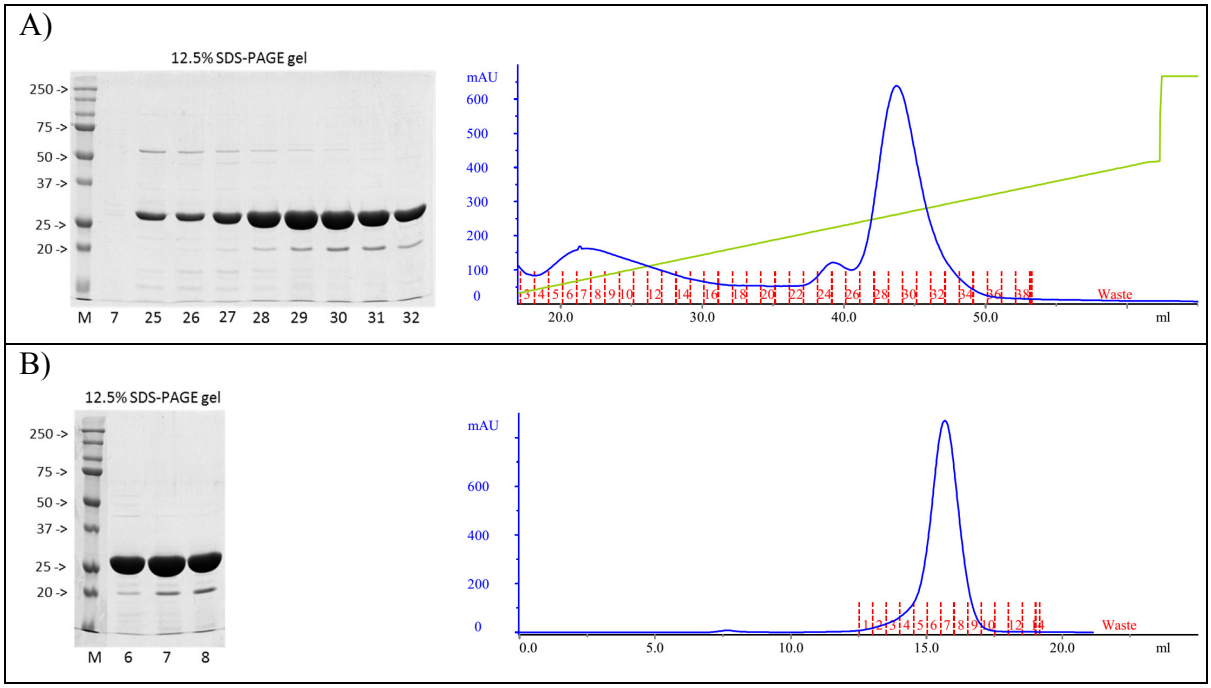

Figure 10
Purification of IFNg Single Chain (IFNg-SC) variant (31 kDa). A) Purification on SP Sepharose HP. B) Purification on Size exclusion chromatography (Superdex 200 10/300 GL). Left – 12.5% SDS-PAGE gel under reducing conditions showing molecular size marker (M) in kDa and fractions from chromatogram (Numbers); Right – Chromatogram from purification on ÄKTA Purifier (Blue – Absorbance at 280 nm; Green – Concentration of NaCl; Red – Fractions).

Stability of all tested IFNg constructs was low. It is most probably caused by low integrity of the IFNg C-terminal tail and its sensitivity to proteolysis (Landar *et al.*, 2000; Lundell *et al.*, 1991). Each affinity measurement was therefore performed by using a new batch of IFNg protein. Interpretation of the SPR experiments was to a certain degree complicated by the fact that different batches of IFNg-SC showed different affinity values to IFNgR1 variants.

The IFNg-SC construct described above is more appropriate for SPR measurements than the native IFNg homodimer. Use of the IFNg-SC variant has three main advantages. Firstly, it significantly simplifies interpretation of the SPR kinetic data because it binds only one IFNgR1 molecule (Landar *et al.*, 2000) and we could use 1:1 kinetic model for data fitting. Secondly, it is more stable than the native IFNg dimer. Thirdly, the native IFNg dimer exhibited high non-specific binding to the SPR chip surface so that its use for SPR measurements was highly problematic and we did not observe such an extensive non-specific binding with IFNg-SC.

6.7 Production and purification of IFNgR1 and its variants

We tested three different expression systems for production of extracellular part of IFNgR1 – insect Schneider 2 cells (S2 cells), yeast *Pichia pastoris*, and bacteria *Escherichia coli*. We were able to produce the wild-type receptor in all three organisms but we put most of our effort to the bacterial system for its relatively fast and cheap production.

6.7.1 Schneider S2 cells

We cloned DNA sequence (with native human codons) encoding extracellular domain of IFNgR1 into the pMT/BiP/V5-His A vector digested by *Bgl*II and *Age*I restriction enzymes to create a construct with N-terminal insect BiP signal peptide and C-terminal 6x His purification tag extension. We transfected the S2 cells using Effectene Tranfection Reagent according to manufacturer recommendations and used HyClone SFX-Insect medium for cell culturing and expression. The IFNgR1 protein was successfully secreted into culture medium but the final yield of purified protein was not much higher than from bacterial production.

6.7.2 *Pichia pastoris* cells

We cloned DNA sequence (with codons optimized for expression in *P. pastoris*) cells encoding extracellular domain of IFNgR1 with C-terminal 6x His purification tag extension into the pPINKα-HC vector digested by *Stu*I and *Kpn*I restriction enzymes to create a construct with N-terminal yeast α-mating factor signal peptide. We transformed four different Pichia PINK cells by electroporation and worked with cells according to manufacturer recommendations. The IFNgR1 protein was successfully secreted into culture medium but the final yield of purified protein was low compared to production from bacteria or insect cells.

6.7.3 *Escherichia coli* cells

Bacterial production is still the cheapest and fastest expression system available, so we put effort into expressing our IFNgR1 variants in *E. coli*, despite the fact that it is a human glycosylated protein with 8 cysteines. Previous studies showed that glycosylation is not necessary for interaction between IFNgR1 and IFNg (Fountoulakis and Gentz, 1992; Gentz *et al.*, 1992) and IFNgR1 can be purified from *E. coli* (Fountoulakis *et al.*, 1990). We followed

the protocol of Fountoulakis *et al.* (1990) but the yield of monomeric receptor was very low and we needed to optimize the production and purification protocols.

We searched for the best combination of constructs among *E. coli* strains BL21(λDE3), SHuffle T7 Express, ArcticExpress (DE3), and others, culture conditions (medium, temperature, IPTG concentration, times, *etc.*), co-expression with chaperones, and purification protocols to get stable monomeric wild-type IFNgR1. Early on, we found out that there was a problem with expression with the native codon sequence so we optimized DNA sequence with codons for *E. coli* expression system, and this DNA was used for further work. We prepared several different constructs in the pET vectors (with T7 promotor) including N- and C-terminal purification tags (6x His Tag, Strep Tag, and AviTag), N-terminal solubility tags (MBP – Maltose Binding Protein, GST – Glutathione S-Tranferase, and TRX – Thioredoxin), and their combinations and used them with various success, getting insoluble or oligomeric products in most cases. Some of these constructs are discussed in the following text.

Because of cysteine residues in the receptor molecule we started expression in SHuffle T7 Express cells that can form disulfide bonds in the cytoplasm. The best conditions were cultivation in LB medium, induction by 0.4 mM IPTG, expression at 16 °C for 20 hours. Protein is partially soluble but we observed that protein is not monomeric after purification on size exclusion chromatography.

We also tested the expression into the periplasm of *E. coli* where the disulfide bonds can be formed. We cloned receptor into vectors bearing signal peptide pelB (pET-22b(+) and pET-26b(+) vectors) and cultivated cells under various conditions. We were able to obtain purified monomeric receptor, but the overall yield was very low. Most of the protein remains insoluble inside the cytoplasm of the cells.

We tried to get soluble IFNgR1 receptor by fusing it with solubility tags such as MBP, GST, or TRX. We were able to get soluble protein in large quantities, but unfortunately protein was oligomeric again and removal of tags led to its precipitation.

Another strategy to produce soluble receptor was its co-expression with chaperones included in the Chaperone Plasmid Set by TaKaRa. Some of the chaperones helped to solubilize the receptor but in this case chaperones were co-purified with the receptor and formed further unspecified higher oligomeric forms.

Because we were not able to get soluble monomeric receptor by any of the above mentioned protocols, we decided to refold the protein from inclusion bodies. We attempted to determine the optimal refolding conditions by "iFOLD Protein Refolding System 1 and 2" in 96-well plates. We got a few promising hits but after closer examination we observed that percentage of monomeric receptor was quite low. Therefore, we performed a series of refolding trials with different buffers (Tris-HCl, Phosphate buffer, HEPES, *etc*), pH's, additives (Glycerol, L-Arginine, NDSB-201, Tween20, Triton X-100, *etc*), and several others. We also tried different ways of refolding such as dilution, dialysis, on-column refolding, or refolding on size exclusion chromatography column. After scanning of hundreds of various protocols we decided for the one with acceptable yields and used it for preparation of IFNgR1 variants. Final protocols are described in Methods (Chapter 5.2), the results from of purification, SDS-PAGE gels and chromatograms, are depicted in Figure 11.

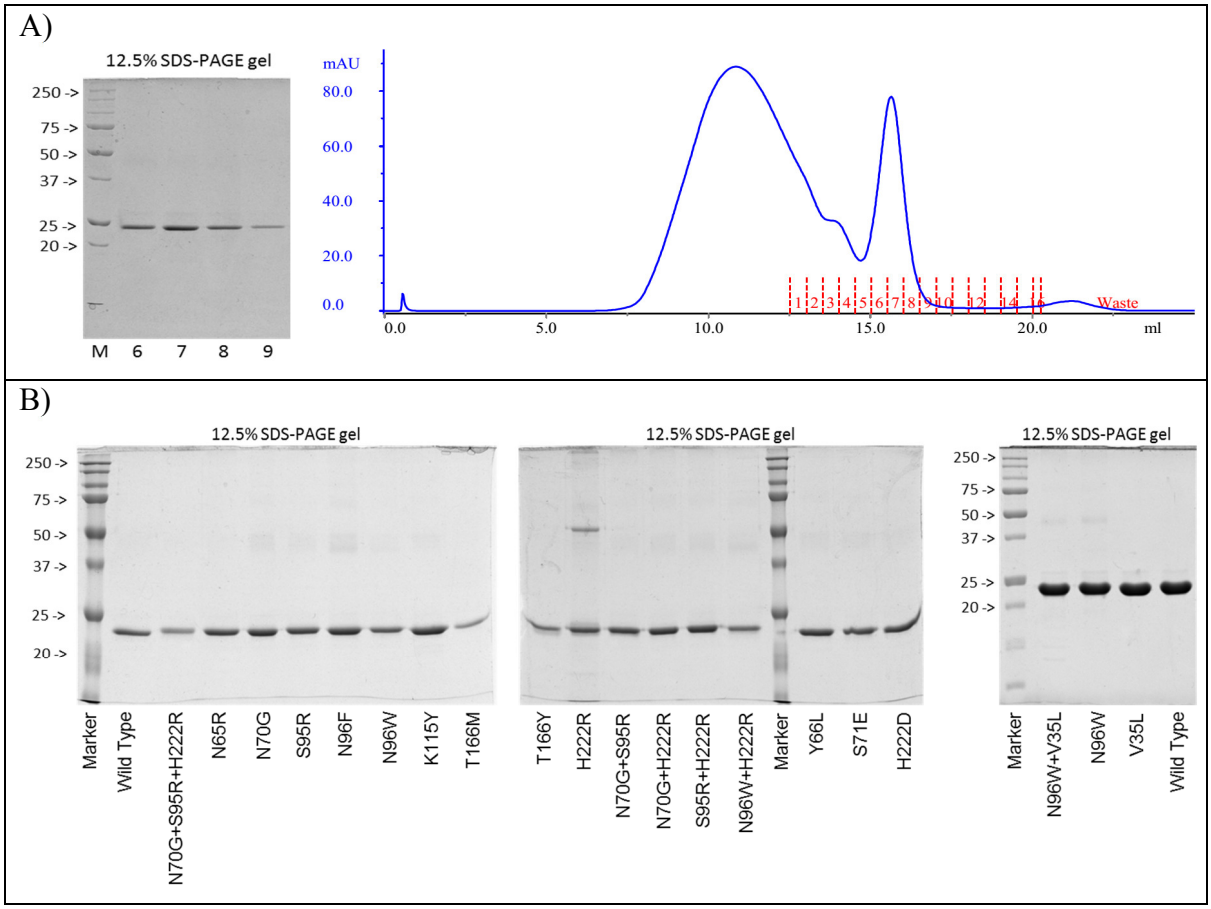

Figure 11
A) Purification of wild-type IFNgR1, final purification step on Size exclusion chromatography (Superdex 200 10/300 GL). Left – 12.5% SDS-PAGE gel under non-reducing conditions showing molecular size marker (M) in kDa and fractions from chromatogram (Numbers); Right – Chromatogram from purification on ÄKTA Purifier (Blue – Absorbance at 280 nm; Red – Fractions). B) 12.5% SDS-PAGE gel under non-reducing conditions showing IFNgR1 variant purified same way as wild-type receptor.

6.8 Experimental determination of affinities of the IFNgR1 variants

We measured affinities of WT and all variants to IFNg-SC by method called Surface Plasmon Resonance (SPR). Data are summarized in Table 4 and Figure 12, and SPR sensorgrams for a few selected variants are depicted in Figure 13.

We could qualitatively sort the variants into three groups in comparison to WT receptor. The first group included variants with lower affinity (higher K_d values) such as interface variants N65R, S95R, or T166Y, which have their affinities about two to three times lower than WT. The second group comprises a large collection of variants with similar affinity as WT, for example interface variants N70G and N96F, or all four selected cavity single amino acid mutation variants (although a modest increase was observed for the V35L variant). The third group included variants with affinity higher than WT (lower K_d values). A significant, about five-fold, increase of affinity compared to WT was observed for interface N96W variant.

In addition to the search for mutations increasing the affinity, we decided to select a smaller set of variants to test the non-randomness of predictions to increase the receptor affinity to IFNg. We selected three variants (listed in Table 4 under numbers 15-16) that were predicted to lower the receptor affinity but still increase the stability of receptor molecule itself. The dissociation constants of mutants H222D and S71E are about two times lower than K_d of WT (2.2 and 2.0 times, resp.); the third variant, Y66L, has about the same affinity as WT. Based on these experimental data, we suggest that we can apply our computer prediction and modeling protocol to design mutations leading to desired effects that would be affinity increase or decrease.

We verified the cooperativity of sequentially and spatially distant mutations on the binding to IFNg-SC by combining three interface single mutations to produce three double and one triple variants (listed in Table 4 under numbers 10-13). The selected mutations, N70G, S95R, and H222R, were about 25 amino acids apart in sequence and more than 20 Å apart in 3D space. We checked the cooperativity by comparing the changes of experimental binding affinities ($\Delta\Delta G$) for the seven variants in series and discovered that experimental values (Table 4) of $\Delta\Delta G$ of the double variants are approximately the sum of contributions from the single ones and $\Delta\Delta G$ of the triple variant is the sum of the values for the three single variants.

Despite that there was no cooperativity between interface mutations we decided to test if the cavity and interface are independent. We combined the four cavity variants with the interface

mutant with the highest affinity to IFNg, N96W. The results were quite inspiring. Although affinity of one double variant (N96W+H222Y) is neutral and one (N96W+D124N) had affinity slightly decreased compared to N96W variant, two double variants (N96W+A114E and N96W+V35L) showed an affinity increase. In case of N96W+V35L variant the increment is significant, the affinity being seven times higher than the affinity of WT.

6.9 Kinetics and equilibrium of binding

The ability of Surface Plasmon Resonance (SPR) technique to measure kinetics of binding in real time was important in our study. We found out that IFNg receptor 1 variants associate with IFNg-SC with similar kinetics (association rate constant, k_a) and in most cases fast association is followed by fast dissociation (dissociation rate constant, k_d). However, the two variants with significantly increased affinity to IFNg-SC, namely N96W and N96W+V35L, exhibit different kinetic behavior. It is illustrated in Figure 13, which represents SPR interaction sensograms of WT and V35L receptor variants with fast ligand release and a much slower release of high-affinity N96W and N96W+V35L variants. Their noticeably slower dissociations are mainly responsible for their higher affinity to IFNg-SC: $K_d = k_d/k_a$; where K_d is the equilibrium dissociation constant, and k_d and k_a are kinetic constants of dissociation and association, respectively. Thus, these two variants are interesting not only for their thermodynamic properties, i.e. their affinity or equilibrium dissociation constant, but also for the different kinetic characteristics of the interaction.

A)

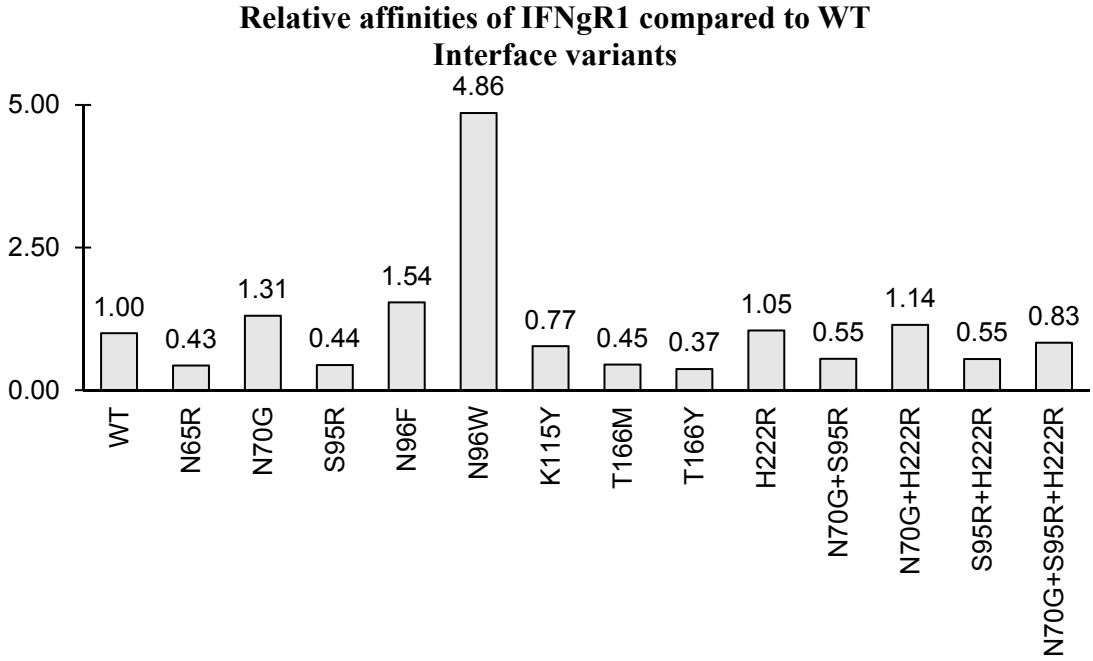

B)

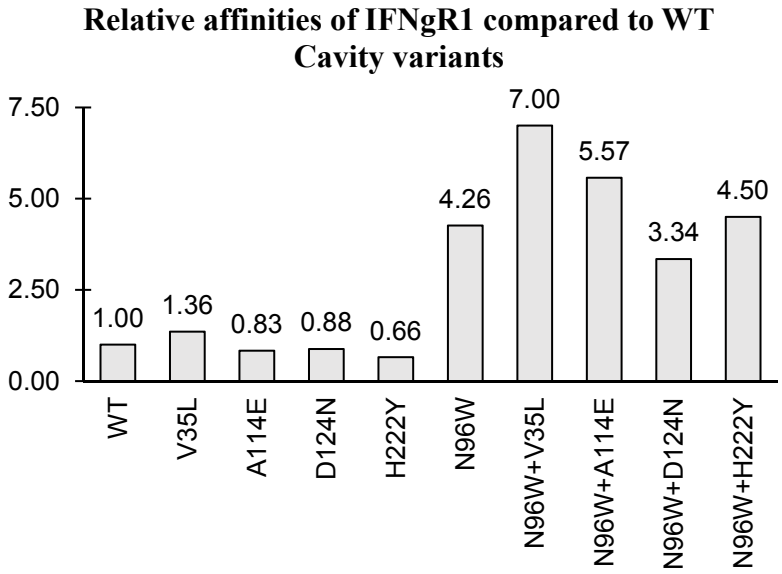

Figure 12
Affinities of the wild-type IFNgR1 (WT) and variants to IFNg-SC obtained from SPR measurements. Graphs represents relative affinities of IFNgR1 variants compared to WT.
A) Interface variants. They could be divided into three groups – lower, similar, and higher affinity compared to WT. Variant N96W has significantly, about five fold, increase of affinity than WT.
B) Cavity variants. All selected cavity single amino acid mutation variants bind to the IFNg-SC with similar affinity as WT, but the V35L variant has slightly higher affinity itself and further increases the affinity of interface variant N96W if combined together.

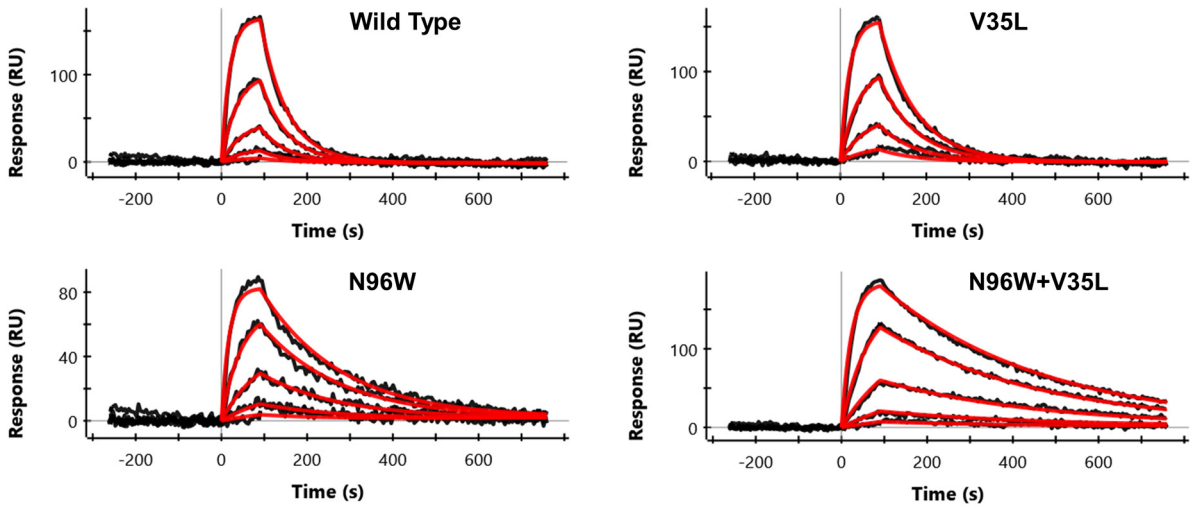

Figure 13
SPR sensorgrams showing the interaction between IFNg-SC and selected IFNgR1 variants. V35L variant behaves similarly as WT displaying fast association and dissociation phases. Two variants (N96W and N96W+V35L) with higher affinities compared to WT bind IFNg-SC with slower dissociation phase, thus increasing the affinity. Measured SPR signal is in black and calculated fitted curves are in red; concentrations of IFNg-SC used for SPR measurements were as follows: 0.1, 0.3, 1.0, 3.0, and 9.0 nM.

6.10 Secondary structure of IFNgR1 variants

We measured the secondary structure of WT receptor and three variants (V35L, N96W, and N96W+V35L) by circular dichroism (CD). The results showed that CD spectra (Figure 14) of all four proteins are highly similar, indicating that the mutations did not cause any major global structural rearrangements. Additionally, the spectra are in agreement with the spectrum published previously for WT of IFNgR1 (Fountoulakis and Gentz, 1992).

IFNgR1 molecule contains 8 cysteines that should form disulfide bonds. We checked their formation in the refolded proteins by mass spectroscopy (done by Zdeněk Kukačka from Laboratory of Molecular Structure Characterization, Institute of Microbiology CAS). We found out that our proteins comprise same disulfide bonds as already published (Stuber *et al.*, 1993): Cys77-Cys85, Cys122-Cys167, Cys195-Cys200, and Cys214-Cys235. Similarly to other groups (Fountoulakis *et al.*, 1990; Gentz *et al.*, 1992), we saw faster protein mobility (showing smaller size) under non-reducing conditions compared to reducing during SDS-PAGE analysis. This effect implied that disulfide bonds were formed and that their presence under non-reducing conditions led to a more compact protein structure.

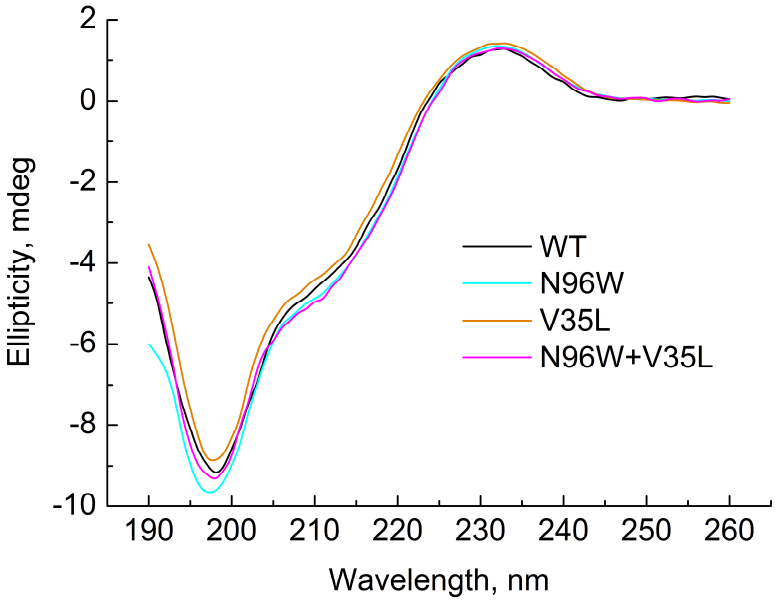

Figure 14
Circular dichroism (CD) spectra of IFNgR1 variants (WT, N96W, V35L, and N96W+V35L) measured in water at 25 ºC. The shape of CD curves is comparable suggesting that mutations don't change the secondary structure of IFNgR1.

6.11 Thermal stability

We used circular dichroism (CD) instrument to study the thermal stability of WT receptor and three variants, V35L, N96W, and N96W+V35L, depicted on Figure 15. The CD-measured melting temperatures of V35L, N96W, N96W+V35L, and of WT are 53, 48, 50, and 54 °C, respectively. Their melting temperatures were independently confirmed by Thermal Shift Assay (TSA) with similar result (Figure 16). Both variants with the highest affinity, N96W and N96W+V35L, have melting temperatures slightly lower than WT, so that mutation from asparagine to tryptophan at the position 96 apparently causes a decrease of IFNgR1 thermal stability. However, according to the CD spectra (Figure 14) there is no change in secondary structure caused by mutations.

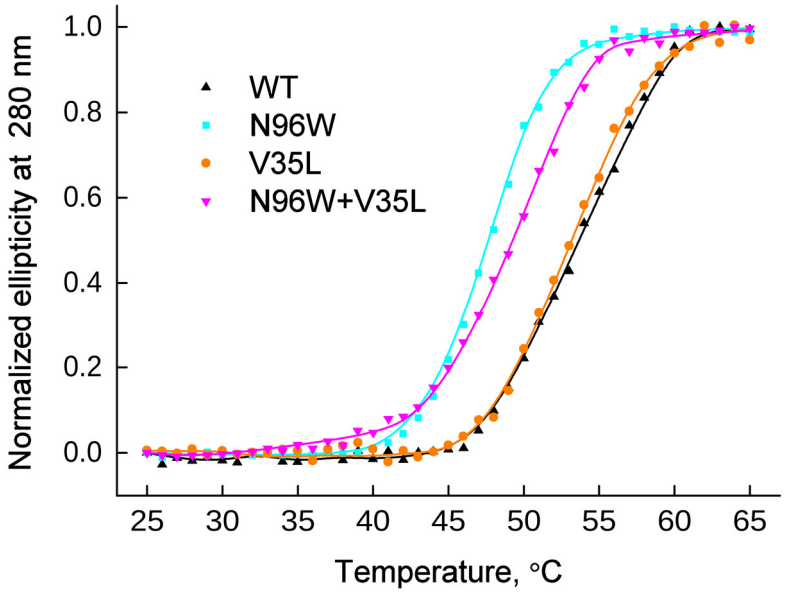

Figure 15
Normalized melting curves of IFNgR1 variants measured by temperature-dependent near ultraviolet circular dichroism (CD) spectra. Each data point is from the intensity measured at 280 nm. IFNgR1 WT, V35L, N96W, and N96W+V35L variants were measured in PBS buffer between 25 and 65 °C at steps 1 ºC/minute. The melting temperature (T_m) of IFNgR1 variants was determined as 54 °C for WT, 53 °C for V35L, 50 °C for N96W+V35L, and 48 °C for N96W, respectively.

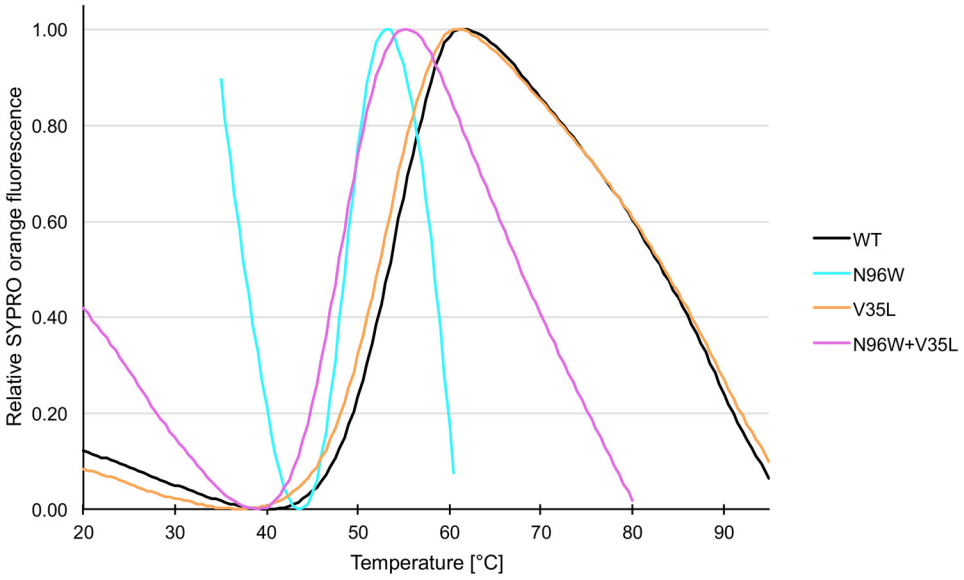

Figure 16
Melting temperatures of selected IFNgR1 variants determined by Thermal Shift Assay. Plotted are normalized data of reference-subtracted fluorescence intensities of IFNgR1 WT, V35L, N96W, and N96W+V35L. The melting temperatures (T_m) of IFNgR1 variants were determined from the first derivatives of the curves plotted in figure: 55 °C for WT, 53 °C for V35L, 49 °C for N96W, and 48 °C for N96W+V35L. The T_m values determined by temperature-dependent CD spectra and Thermal Shift Assay are within 1 °C the same.

6.12 Computer analysis of the internal dynamics of the IFNgR1 variants

Using the tools of molecular modeling, we analyzed the root-mean square fluctuations (RMSF) of the selected IFNgR1 variants (WT, N96W, and N96W+V35L) to examine the effect of a mutation on the flexibility of the receptor molecule in unbound and bound states. Figure 17 and Figure 18 show comparison of RMSF sorted by their values, "ranked RMSF", and these plots revealed significant differences between dynamics of the selected variants.

In case of N96W+V35L variant, the flexibility of its amino acids located within interface region is similar for both unbound and bound state. On the other hand, interface residues of N96W and WT are more flexible in the free receptor rather than in the complex (Figure 17a, c). This indicates that binding of the N96W+V35L variant to IFNg is more entropically driven compared to the other two IFNgR1 molecules.

However, the source of this behavior differs in the N- and C-terminal domains of the IFNgR1 molecule. In the N-terminal domain (Figure 17c), the flexibility of the interface residues of all tested receptor variants is similar in the bound state, while being different in unbound state – they are most flexible in N96W, the least in N96W+V35L. On the other hand, in the C-terminal domain (Figure 17d), the flexibility of the three receptor variants is similar in their unbound states, but it varies in the bound state between N96W, which has the lowest flexibility, and WT with the highest flexibility.

Furthermore, the V35L mutation causes non-local stiffening of the receptor molecule and makes especially the C-terminal interface amino acids more flexible in the bound state compared to the N96W mutant (Figure 17d).

To sum up, the V35L mutation decreases the difference in flexibility between unbound and bound states, indicating reduced entropy penalty of binding and resulting in the higher affinity of the N96W+V35L double mutant compared to N96W mutant.

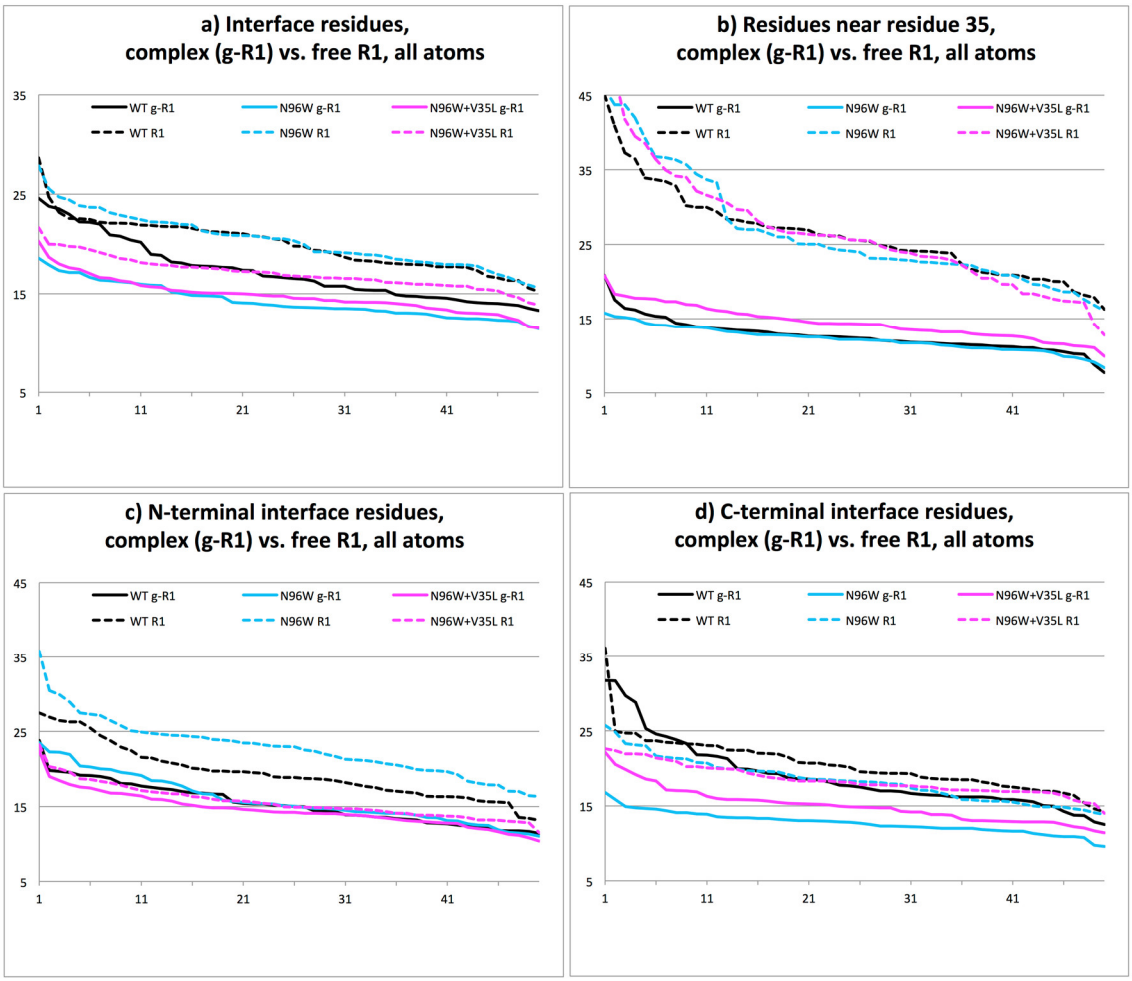

Figure 17
Ranked RMSF values collected from the last 50 ns of the 100 ns MD simulations of WT, N96W, and N96W+V35L variants of IFNgR1. Solid lines labeled g-R1 are for the IFNg/IFNgR1 complex, dashed lines labeled R1 for IFNgR1 alone. Shown are a) RMSF values of all interface residues; b) residues near positions 35; c), d) the interface residues from the N-terminal and C-terminal domains, respectively. The RMSF values are on the y-axis, the rank of the values (1-50) on the x-axis. List of residues in each group is in Figure 18, which also shows RMSF values separately for the main and side chain atoms.

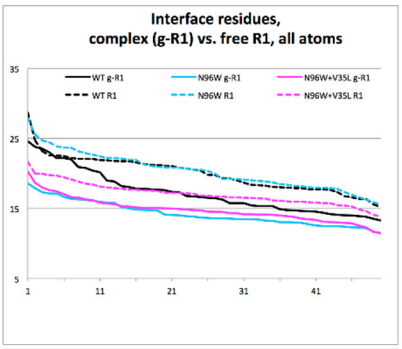
Interface residues,
complex (g-R1) vs. free R1, all atoms
WT g-R1
N96W g-R1
N96W+V35L g-R1
WT R1
N96W R1
N96W+V35L R1

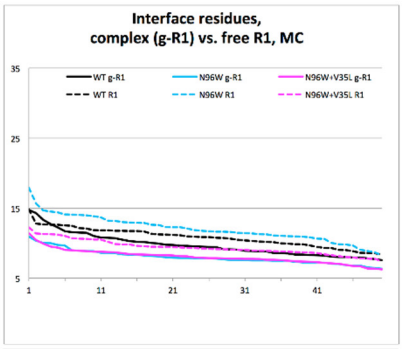
Interface residues,
complex (g-R1) vs. free R1, MC
WT g-R1
N96W g-R1
N96W+V35L g-R1
WT R1
N96W R1
N96W+V35L R1

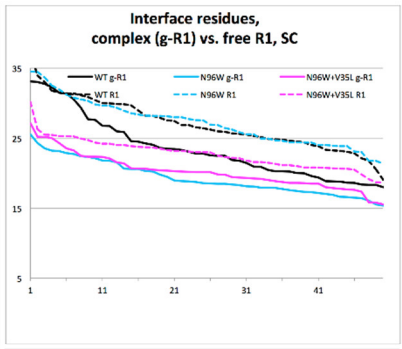
Interface residues,
complex (g-R1) vs. free R1, SC
WT g-R1
N96W g-R1
N96W+V35L g-R1
WT R1
N96W R1
N96W+V35L R1

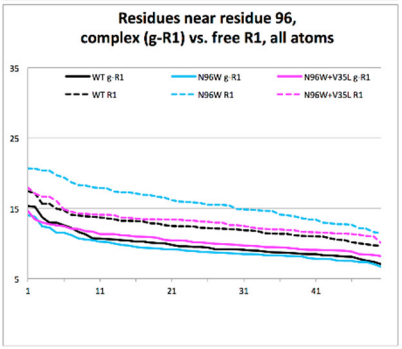
Residues near residue 96,
complex (g-R1) vs. free R1, all atoms
WT g-R1
N96W g-R1
N96W+V35L g-R1
WT R1
N96W R1
N96W+V35L R1

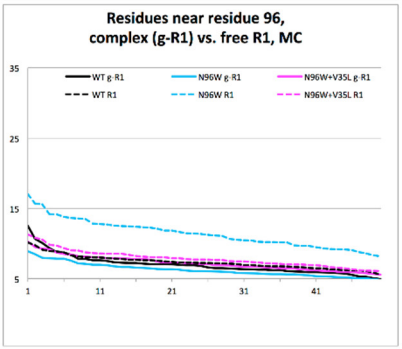
Residues near residue 96,
complex (g-R1) vs. free R1, MC
WT g-R1
N96W g-R1
N96W+V35L g-R1
WT R1
N96W R1
N96W+V35L R1

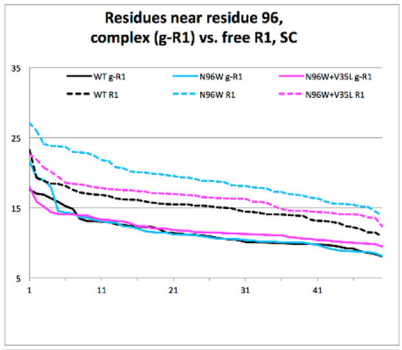
Residues near residue 96,
complex (g-R1) vs. free R1, SC
WT g-R1
N96W g-R1
N96W+V35L g-R1
WT R1
N96W R1
N96W+V35L R1

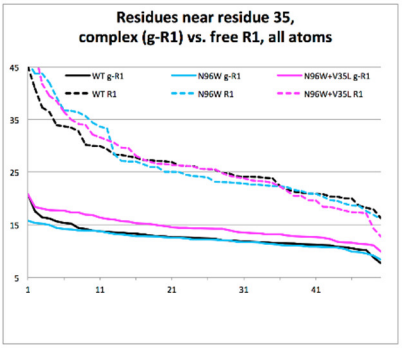
Residues near residue 35,
complex (g-R1) vs. free R1, all atoms
WT g-R1
N96W g-R1
N96W+V35L g-R1
WT R1
N96W R1
N96W+V35L R1

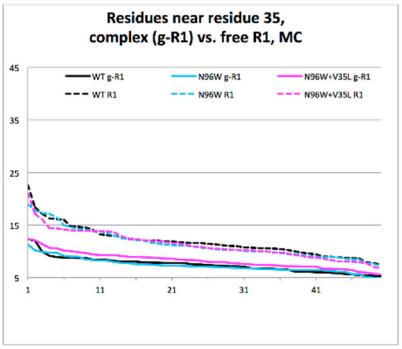
Residues near residue 35,
complex (g-R1) vs. free R1, MC
WT g-R1
N96W g-R1
N96W+V35L g-R1
WT R1
N96W R1
N96W+V35L R1

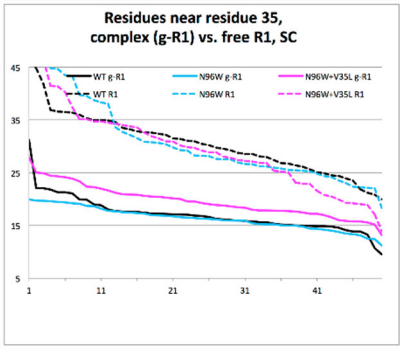
Residues near residue 35,
complex (g-R1) vs. free R1, SC
WT g-R1
N96W g-R1
N96W+V35L g-R1
WT R1
N96W R1
N96W+V35L R1

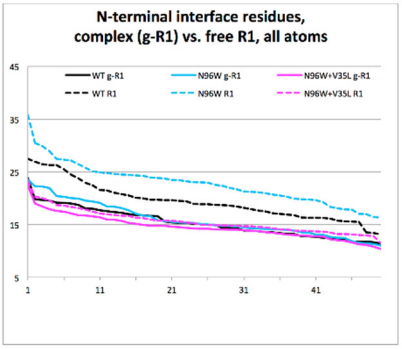
N-terminal interface residues,
complex (g-R1) vs. free R1, all atoms
WT g-R1
N96W g-R1
N96W+V35L g-R1
WT R1
N96W R1
N96W+V35L R1

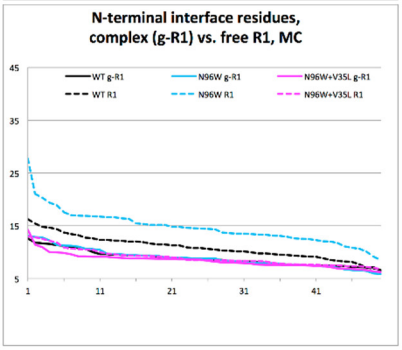
N-terminal interface residues,
complex (g-R1) vs. free R1, MC
WT g-R1
N96W g-R1
N96W+V35L g-R1
WT R1
N96W R1
N96W+V35L R1

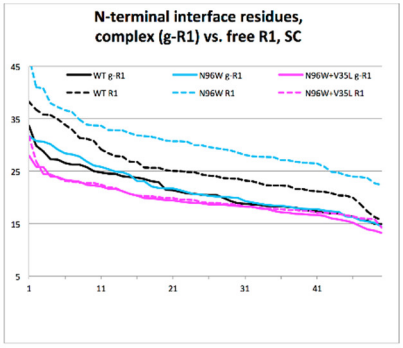
N-terminal interface residues,
complex (g-R1) vs. free R1, SC
WT g-R1
N96W g-R1
N96W+V35L g-R1
WT R1
N96W R1
N96W+V35L R1

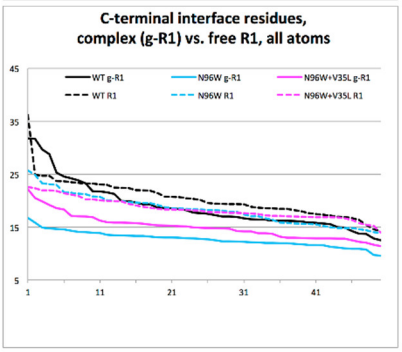
C-terminal interface residues,
complex (g-R1) vs. free R1, all atoms
WT g-R1
N96W g-R1
N96W+V35L g-R1
WT R1
N96W R1
N96W+V35L R1

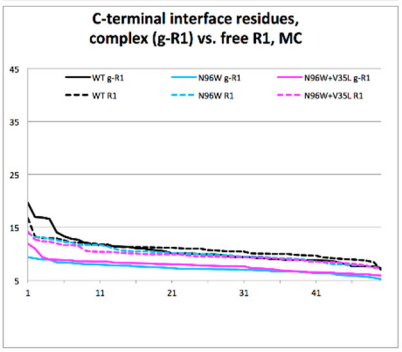
C-terminal interface residues,
complex (g-R1) vs. free R1, MC
WT g-R1
N96W g-R1
N96W+V35L g-R1
WT R1
N96W R1
N96W+V35L R1

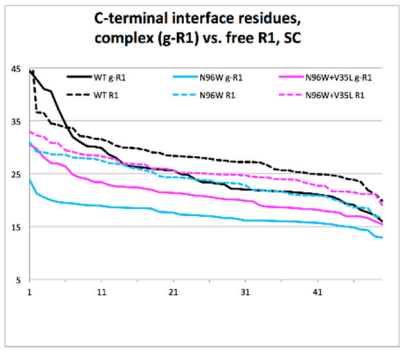
C-terminal interface residues,
complex (g-R1) vs. free R1, SC
WT g-R1
N96W g-R1
N96W+V35L g-R1
WT R1
N96W R1
N96W+V35L R1

Figure 18
Ranked RMSF values collected at the last 50 ns of the 100 ns MD simulations of WT, N96W, and N96W+V35L variants of IFNgR1. Solid lines labeled g-R1 denote RMSF values of the IFNg/IFNgR1 complex, dashed lines labeled R1 denote values of IFNgR1 alone. Shown are RMSF values of all atoms, main chain atoms (MC), and side chain atoms (SC) for the following residues:
All 40 interface residues (i. e. residue numbers 64, 65, 66, 67, 68, 69, 70, 71, 72, 73, 93, 95, 96, 97, 99, 115, 116, 118, 123, 164, 165, 166, 168, 170, 171, 186, 189, 190, 191, 192, 193, 197, 220, 221, 222, 223, 224, 225, 226, 227);
residues within 6 Å of residue 96 (i. e. residue numbers 65, 66, 67, 91, 92, 93, 94, 95, 96, 97, 98, 119, 120, 121, 224);
residues within 6 Å of residue and 35 (i. e. residue numbers 32, 33, 34, 35, 36, 37, 46, 47, 48, 49, 100, 101, 102, 114, 115, 116, 117);
the interface residues from the N-terminal domain (i. e. residues 64 to 123);
the interface residues from the C-terminal domain (i. e. residues 164 to 227).
The RMSF values are on the y-axis, the rank of the values on the x-axis.

7 Discussion

Two main complementary approaches are broadly used to modify proteins so that they acquire or enhance desired properties. First strategy is called "directed evolution" and depends on high-throughput screening of protein variants from a DNA library of mutagenized genes.

However, we concentrated on the use of the other strategy to create proteins with higher affinities, namely application of computational methods to predict the mutations that would influence affinity of proteins in the preferred way. Applicability of this computer-aided approach, sometimes called rational design, relies on availability of experimentally determined structures of the studied proteins that provides better knowledge about the relationship between sequence, structure, and function. As these initial structural models for search of energetically favorable replacements of amino acid residues can be used crystal structures even at a relatively low crystallographic resolution around 3 Å.

The application of computational methods for the evaluating of the effect of mutation on protein-protein interactions is an attractive strategy, because the predictions are relatively fast and cost-effective. Here, we developed a new computational strategy to find mutations within the extracellular part of Interferon gamma receptor 1 (IFNgR1) leading to increase of affinity to its native ligand Interferon gamma (IFNg). We measured affinities of selected IFNgR1 variants by Surface Plasmon Resonance (SPR) and analyzed their kinetic properties.

We started with optimizing residues on the interface between the protein components of the IFNg/IFNgR1 complex. The affinity of interaction can be strongly influenced by a few residues at the interface or its direct periphery, so called "hot-spots" (Keskin *et al.*, 2005; Sharabi *et al.*, 2009). Our initial analysis was based on two crystal structures of IFNg/IFNgR1 complex with PDB codes 1FG9 (Thiel *et al.*, 2000) and 1FYH (Randal and Kossiakoff, 2001). We decided to identify amino acids on IFNgR1 molecule that are closer to the IFNg than 6.0 Å, not to miss any possible contact between these two proteins. We got a set of 40 residues that seemed to be suitable for mutation.

In search for mutations increasing the affinity of IFNgR1 to IFNg, we replaced each of the 40 selected receptor residues by the 20 (including self-mutations) amino acids and calculated change of free energy ($\Delta\Delta G$). Protein energetics and energy function accuracy is important for design of altered protein binding affinity (Lippow and Tidor, 2007). There is plenty of

approaches for energy calculations based on statistical analysis or physically based methods (Lazaridis and Karplus, 2000); based on previous experience of the members of the laboratory, we decided to apply empirical energy function coming from experimental work on proteins and used the program FoldX for energy calculations (Schymkowitz *et al.*, 2005). Specifically we calculated two types of free energy changes (ΔΔG) to predict (a) the stability of the mutated receptor in the complex and (b) change of receptor affinity to IFNg. The calculated energy changes (ΔΔG) were relatively small, meaning that the predicted single point mutation may not cause dramatic affinity increase in real samples. This result can be explained by the fact that the affinity of the soluble receptor to the IFNg is already in nanomolar range (Landar *et al.*, 2000; Marsters *et al.*, 1995; Walter *et al.*, 1995) and further improvement is apparently a challenging task.

In addition to the energy-based criteria for the selection of mutations, we performed global sequence alignment to find conserved amino acids within the extracellular part of IFNgR1. Highly conserved residues are usually suspected of playing structural or functional role in protein binding (Ma *et al.*, 2003; Valdar and Thornton, 2001). We tested some of the receptor residues conserved at the 90 % or higher level (S97 and E118). In spite of the fact that some of the mutations of these residues were predicted to increase the affinity, the experimental determination showed its complete loss. Therefore, the final selection criteria comprised of (a) calculated stability of mutated receptor molecule in the complex with IFNg, (b) predicted affinity increase, and (c) conservancy ≤ 60 %. We selected nine most promising variants on the interface region of the IFNgR1 for experimental work.

We tested several expression systems to produce extracellular part of IFNgR1 receptor. We successfully expressed protein in insects Schneider S2 cells but we decided not to use it routinely for production of several new mutants because tissue culturing was rather expensive, long compared to other tested expression systems, and the overall yield of purified protein was not higher than in *Escherichia coli*. Another used expression system was yeast *Pichia pastoris*, but the production of IFNgR1 was not sufficient for further work. Finally, we expressed extracellular part of IFNgR1 in *E. coli* for its speed and cheap production, even though it is a human glycosylated protein. Previous studies showed that IFNgR1 can be purified from *E. coli* (Fountoulakis *et al.*, 1990) and glycosylation does not affect its capacity to bind IFNg (Fountoulakis and Gentz, 1992; Gentz *et al.*, 1992). However, the expression in *E. coli* was not straightforward from the beginning. Our intended IFNgR1 construct should contain C-terminal

6x His Tag because we planned to measure the kinetics of binding by SPR technique where one binding partner (analyte – IFNg-SC) freely flows over the other binding partner (ligand – IFNgR1) anchored to the chip surface. The defined attachment of IFNgR1 to the chip by the 6x His Tag thus served not only for purification but also to simulate situation analogous to its binding to the cell surface.

There was a problem with expression of IFNgR1 with C-terminal His Tag using the native human codon sequence in *E. coli* that was solved by codon optimization. Another challenge was to optimize the combination of production and purification strategies including various *E. coli* strains, culture conditions, even co-expression with chaperones, or hundreds of refolding protocols. Because of 8 cysteines within the receptor molecule we tried to express the receptor to periplasmic space of *E. coli* where disulfide bridges could be formed. Unfortunately, majority of the protein remains insoluble in the cytoplasm. Among others things, we found conditions to express the receptor soluble within the cytoplasm of *E. coli* but the receptor was not monomeric. Therefore we focused on refolding of IFNgR1 from inclusion bodies and applied many refolding approaches, more systematic such as iFOLD Protein Refolding System 1 and 2, or *ad hoc* in different buffers, pH, and using various additives. Our refolding procedures included various types of dilution, dialysis, on-column refolding, or refolding on size exclusion chromatography column. Every time we faced the very same problem – oligomerization of a yet soluble receptor. After scanning of a large number of different strategies we decided to use one protocol that was relatively easy and produced sufficient amount of monomeric receptor for protein characterization and SPR measurement.

There is always a possibility that refolded protein will be non-active or have a wrong fold. We therefore tested various properties of receptor prepared by our protocol. We checked the secondary structure by circular dichroism (CD) measurement and the CD spectra of IFNgR1 variants were virtually identical to already published one of WT (Fountoulakis and Gentz, 1992). Moreover, we performed mass spectroscopy analysis that verified formation of the correct S-S bridges between the eight cysteine residues (Stuber *et al.*, 1993). Another indication of created disulfide bonds in the case of IFNgR1 is different protein mobility under non-reducing and reducing electrophoretic conditions (Fountoulakis *et al.*, 1990; Gentz *et al.*, 1992), and we saw similar behavior of our refolded protein on SDS-PAGE, protein displayed smaller molecular mass under non-reducing conditions.

The crucial experiment was the measurement of affinities between IFNgR1 variants and IFNg-SC by Surface Plasmon Resonance technique. The advantages of these methods are measurement of binding kinetics in real-time, relatively straightforward set up, and reasonably small protein consumption compared to other techniques such as isothermal titration calorimetry (ITC). We successfully utilized C-terminal 6x His Tag of IFNgR1 for its orientated attachment to the surface of HTG ("Ni-NTA") chip as described above. As an analyte (freely flowing protein) we applied recombinant IFNg Single Chain (IFNg-SC) variant that was derived by linking the two peptide chains of the IFNg dimer by a seven-residue linker and changing His111 in the first chain to an aspartic acid residue (Landar *et al.*, 2000). There were two main benefits in using this protein construct – (a) it supposedly binds only one IFNgR1 (Landar *et al.*, 2000) so we could use 1:1 kinetic model for data fitting, (b) it was more stable than native IFNg, primarily in the SPR instrument itself. Although the stability of IFNg-SC was higher than that of the wild type homodimer, it was still limited and we also saw variability of affinities with different batches of IFNg-SC. Similar effect was observed by others, and it is probably caused by low integrity of C-terminal tail and its sensitivity to proteolysis (Landar *et al.*, 2000; Lundell *et al.*, 1991). Therefore, the individual values of K_d from measurements using different batches of IFNg-SC cannot be directly compared. To allow comparison of different measurements, we used wild-type (WT) receptor as an internal control in all SPR measurements.

A significant success of our computer predictions was that all selected IFNgR1 variants could bind IFNg-SC in nanomolar range. This was case for all mutations except those of highly conserved interface residues, which eliminated the binding completely. When we compared the measured affinity values of IFNgR1 variants to WT receptor, we classified variants into three groups. First category comprised variants with affinity about two or three times lower than WT, such as N65R, S95R, or T166Y variants. The majority of variants fell into a second group of mutations causing almost no change in affinity, for example variants N70G or N96F. Third class included variants with affinity higher than WT. A significant, about five-fold, increase of affinity compared to WT was observed for the N96W interface variant.

Small calculated energy changes ($\Delta\Delta G$) suggested that single point mutations would not have high impact on affinity change. This result is not completely surprising because the affinity of IFNgR1 to IFNg is already in nanomolar range (Landar *et al.*, 2000; Marsters *et al.*, 1995; Walter *et al.*, 1995). From this point of view, the achieved five-fold increase by single point

mutation is promising result and is fully comparable to other published studies. In the case of computer modeling of interaction between acetylcholinesterase and snake toxin fasciculin, one mutation within acetylcholinesterase enhanced the affinity about seven-fold (Sharabi *et al.*, 2009). Another study regarding single amino acid substitutions in Toll-like Receptor 4 (TLR4) Decoy Receptor showed three variants with a binding affinities about ten-fold higher than wild-type decoy receptor (Han *et al.*, 2012). Furthermore, study about the rational design of intercellular adhesion molecule-1 (ICAM-1) variants showed about twenty-fold increase of affinity by five amino acid substitutions (Song *et al.*, 2006).

In addition to the single point mutations, we tested their possible cooperative effects on the binding to IFNg-SC by combining three interface mutations (N70G, S95R, and H222R). We produced all possible combinations (one triple and three double variants) using the interface residues that were distant sequentially and spatially from each other. We observed that experimental affinity values of the double variants are actually approximately the sum of contributions from the single mutations and $\Delta\Delta G$ of the triple variant is the sum of the values for the three mutations. This means that the effect of the relatively isolated mutations is additive and does not show any cooperative effect. However, our observation of the additive effects of the mutated residues should not be considered as general rule, as non-additive energetic effects have been observed in different systems (Pierce *et al.*, 2010).

We tested whether a relative success of the computer predictions of higher receptor affinity to IFNg was random or reflected correct computational description of complex molecular systems. To this end, we selected a smaller set of variants that were predicted to decrease the affinity but at the same time not the receptor molecule stability. Perhaps surprisingly, there were not many variants fulfilling both these conditions and those that did destabilize the interaction by a fairly small margin. The dissociation constant of one such variant (Y66L) was similar to WT and two variants (H222D and S71E) had affinity about two times lower compared to WT. Thus our results indicate general applicability of the computer predictions and the ability of our computer modeling protocol to suggest mutations that lead to the desired effects, be it affinity increase or decrease.

Mutating the interface residues directly interacting with ligand is intuitively obvious strategy but we decided to test also an alternative approach. It attempts to increase affinity by filling cavities of one of the interacting partners. Some such attempts mutated residues in cavities near the interacting interface (Atwell *et al.*, 1997; Kawasaki *et al.*, 2010; Morellato-Castillo *et al.*,

2013) but we searched for cavities within the whole extracellular part of IFNgR1. Recent studies support this idea as they suggest that mutations distant from the interface can influence the binding affinity (Tzeng and Kalodimos, 2012; Tzeng and Kalodimos, 2013). Moreover, experimental mutagenesis studies showed that both protein interior and the non-interacting surface can have impact on the free energy of binding (Kastritis and Bonvin, 2013; Kastritis *et al.*, 2011; Moal and Fernandez-Recio, 2012).

In search for internal cavities within the IFNgR1 molecule, we used same four chains from crystal structures of PDB entries 1FYH and 1FG9, as before for identification of interface variants. We listed all residues forming cavities in all four IFNgR1 chains to get 52 amino acids for *in silico* analysis by FoldX. We calculated the changes of free energy (ΔΔG) of binding in a similar way to the case of interface variants by replacing the selected receptor residues by side chains of the remaining 19 natural amino acids. Because cavities differed in each receptor chain, we organized the predicted variants by their ΔΔG values and the first 50 best mutations from each chain were included in a more detailed analysis. From a total of 200 variants we looked for those that occurred in all four or at least three receptor chains. This procedure led to twelve promising residues that were subjected to molecular dynamics relaxation analysis to suggest four variants for experimental work.

The calculations of ΔΔG (listed in Table 6 and Table 7) show only modest potential gains in interaction affinity, perhaps due to small cavity volumes and also due to the fact that they are often lined by highly conserved residues. In the case of interface variants, the predicted ΔΔGs of IFNgR1 binding to IFNg (combined with no decrease of ΔΔG of the IFNgR1 stability) could be used for selection of interface mutations increasing affinity, but there was no clear criterion for the selection of internal cavity mutations that would improve interaction energy. We could divide the selected mutations listed in Table 6 into two groups. First one included variants V35L and H222Y that were predicted to increase both ΔΔG of folding of IFNgR1 in complex (type ^{1}) and free IFNgR1 (type ^{2}) to a similar extent, while calculated values of their ΔΔG of binding (type ^{3}) was almost zero. The second group comprised variants A114E and D124N that were predicted to slightly improve ΔΔG of binding (type ^{3}) while both types of their ΔΔG (type ^{1} and ^{2}) of folding were destabilizing. The experimental affinities measured by SPR showed that all four designated variants had affinity comparable to the wild-type receptor, only the V35L variant had a slightly higher affinity.

In analogy with the interface IFNgR1 variants, we decided to combine the best interface variant, N96W, with each of the four selected cavity mutants in order to test the additive effect on the overall affinity of these distant mutations. The results were quite encouraging. Despite the fact that one double variant (N96W+H222Y) had affinity similar to WT receptor and one (N96W+D124N) even a little bit decreased, two double variants (N96W+A114E and N96W+V35L) displayed increased affinity to IFNg-SC. Actually, the combination of interface N96W mutation with cavity V35L mutation led to a significant seven-fold increase of affinity compared to WT receptor. Altogether, we suggest that mutations of cavity amino acids with no direct contact with the ligand can contribute to the overall increase of affinity in combination with interface mutations.

We made use of the Surface Plasmon Resonance method and its unique feature to measure the kinetics of binding in real time. This technique was already used to measure the influence of 14 mutations and 5 environmental variables (buffer perturbation) on the association (k_a) and dissociation (k_d) rate of an antibody interacting with lysozyme (De Genst *et al.*, 2002). We discovered that most of the IFNgR1 variants exhibited quite similar fast association to IFNg-SC followed also by fast dissociation. However, we observed slower release of IFNg-SC from N96W and N96W+V35L variants which evinced significantly higher affinity, and their altered kinetic behavior distinguishes them from the other variants. Actually, this slower dissociation is the reason for their higher affinity, according to the dissociation equilibrium constant equation, $K_d = k_d/k_a$.

In contrast to our results, other studies (Lengyel *et al.*, 2007; Marvin and Lowman, 2003; Schreiber *et al.*, 2006; Selzer *et al.*, 2000) showed that faster binding rather than slower release is the reason for affinity increase of their mutants. For example, the rate of association and the affinity between TEM1 beta-lactamase and its protein inhibitor BLIP was enhanced by increasing the electrostatic attraction by incorporating charged residues in the vicinity of the binding interface (Selzer *et al.*, 2000). The importance of such electrostatic interactions for the association of two proteins was experimentally verified by Schreiber and Fersht (Schreiber and Fersht, 1996), working with mutants of proteins barnase and barstar. This strategy, optimization of electrostatic contributions for protein-protein interactions, has been recently reviewed (Gorham *et al.*, 2011). In practice, the association rate constant (k_a) is limited by diffusion and rotational alignment of the binding sites, including the desolvation of the binding interface (Janin, 1997; Northrup and Erickson, 1992), and falls in a remarkably small window,

typically between 1 x 10^5 and 1 x 10^6 $M^{-1}s^{-1}$ (Northrup and Erickson, 1992). Thus affinity improvements usually are caused by slower dissociation rates (Luginbuhl *et al.*, 2006) and this is also the case of our two best IFNgR1 variants, N96W and N96W+V35L.

Additionally, we indirectly validated the FoldX predictions by retrospective analysis of ΔΔGs of naturally occurring IFNgR1 single-point mutations collected in the database of single nucleotide polymorphism (dbSNP) (Sherry *et al.*, 2001). In this database we found 25 nucleotide mutations at 22 unique positions (Figure 9) within the extracellular part of the IFNgR1 molecule (exons only). Most of the ΔΔG predictions for these natural mutants showed neutral effect on the stability of free IFNgR1 and on its complex with IFNg. This correlates with the fact that only two of the natural variants exhibit harmful or pathological phenotype.

We investigated the secondary structure of WT receptor and its three designed variants, namely V35L, N96W, and N96W+V35L, by circular dichroism (CD) to confirm their structural integrity upon mutation. The measured CD spectra showed high similarity of all four proteins, therefore we could conclude that mutations did not cause any major global structural reorganization. In addition, we measured melting temperatures (T_m) of these for proteins using CD instrument and we independently confirmed the values by Thermal Shift Assay (TSA). The WT receptor and V35L variant had similar values of T_m, 54 °C and 53 °C, respectively. In contrast, variants with the highest affinities, specifically N96W and N96W+V35L, demonstrated slightly lower melting temperatures, 48 °C and 50 °C, respectively. Although the secondary structures of IFNgR1 proteins clearly remained the same according to the measured CD spectra, N96W mutation led to a decrease of IFNgR1 thermal stability. We suggest a possible explanation of this observation in the next paragraph.

In order to elucidate the increase of affinity on structural level, we looked at the snapshots from molecular dynamics (MD) simulations but unfortunately the results were not entirely clear. The mutation of asparagine to tryptophan (N96W) did not create any easily identifiable interactions such as hydrogen bonds or stacking between the tryptophan aromatic ring and the rest of the receptor molecule or nearby atoms of IFNg-SC. On the contrary, one H-bond present in the WT complex is actually weakened. In addition, the tryptophan increased the mobility of several receptor residues, for example N65 and Y66, instead of the expected stiffening of the nearby groups. On the other hand, the replacement of a smaller asparagine by a large tryptophan resulted in large number of stabilizing van der Waals contacts. We suggest that slower dissociation (in other words, higher stability of the complex) was driven by the entropic

stabilization of a tryptophan amino acid when it was in contact with IFNg-SC. The MD simulations for N96W variants indicated the hydrophobic destabilization at the position 96 and the related higher flexibility of the receptor molecule, and these effects could explain the measured lower melting temperatures compared to WT. However, better understanding of the stabilization effect of the large tryptophan at the position 96 of the IFNgR1 clearly requires further study including full thermodynamic description of the IFNg-SC/IFNgR1 complex.

We also analyzed the internal dynamics of the IFNgR1 variants, especially the impact of a cavity-filling mutation on the flexibility of receptor molecule in unbound and bound states. We found out that interface residues of the N96W and WT variants showed higher flexibility in the unbound state rather than in the complex with IFNg, while the interface residues of N96W+V35L variant displayed similar flexibility in both unbound and bound states. Thus we propose that binding of the N96W+V35L variant to IFNg is entropically more favorable compared to the other two IFNgR1 receptors. But the origin of this effect is different in the N- and C-terminal domains of the IFNgR1 molecule. In case of the N-terminal part, the interface residues of all variants showed comparable flexibility in the bound, but varied in unbound state. In the C-terminal domain the behavior was more complicated, the flexibility in the unbound state was similar for all variants, while the flexibility in bound state differed between variants, specifically the N96W variant had the lowest flexibility and WT the highest.

We further found out that the action of V35L mutation to stiffen the receptor molecule is mainly non-local as the V35L mutation actually caused *higher* flexibility especially of the C-terminal interface residues in the bound state compared to the N96W variant. The main beneficial effect of the cavity V35L mutation originated from decreasing the difference between flexibility of the bound and unbound states of IFNgR1. We suggest that the resulting reduced entropy penalty of binding led to higher affinity of N96W+V35L variant compared to N96W mutant. There could also be several other mechanisms how the cavity-filling mutations may stabilize the interaction. For example, mutation can stiffen the interacting proteins in their unbound state resulting in reduced entropic penalty of complexation, or indirectly destabilize the intermediate molten globule state rather than stabilize the folded protein (Sengupta *et al.*, 2009). These compensatory effects demonstrate complexity of protein-protein interactions (and/or folding) and the known limits of computational methods to design increased affinity between proteins (Chen and Keating, 2012).

When we compared the computer-predicted and experimental affinities as the changes of binding free energies (ΔΔG), we noticed that the main difference appeared to be the scale. The computer calculations evidently overestimated the magnitude of ΔΔGs. The comparison of FoldX-calculated values of ΔΔG at the four used crystallographic interfaces showed large variations in some components of the FoldX force field, particularly in the solvation and electrostatic contributions, despite their structural similarity. We therefore suggest that limiting factors of the prediction accuracy are the energy terms describing solvation effects, the equilibrium between charged and uncharged states, and also the contribution of polarizability of large ionized particles including amino acid residues. It seems that the computational methods are probably underestimating (or even ignoring) a possible mutation-induced movements of the backbone. In addition, FoldX program likely overestimated the interaction energy of charged arginine, at least in our case. It repeatedly recommended to mutate various residues to arginine (namely mutations N65R, S95R, and H222R were predicted to be highly complex stabilizing) but experimental data did not confirm their calculated potential. However, the overall performance of the FoldX force field was acceptable, especially in the light of a recent report showing that no empirical potential predicts correctly all types of interaction (Sharabi *et al.*, 2011).

Current predominant opinion is that long MD simulations are crucial for reliable description of molecular systems and prediction of affinity modulation (Bradshaw *et al.*, 2012). Our experimental data do not support this view, as our 10-20 ns MD simulations did not show clear systematic similarity with the experimental ΔΔGs. These values were shifted in both directions, to be more comparable with experimental values in case of N65R, S95R, and N96F, or on contrary to be more different in case of K115Y and H222R. Therefore, we suggest that predicted interface mutations based on simply relaxed crystal structure could be as beneficial as predictions based on much more computationally demanding and expensive MD simulations. Also other authors (Bradshaw *et al.*, 2011) have observed that full MD simulation is not more successful in prediction of mutants than simpler approaches, and that the inclusion of non-local flexibility of the to-be mutated protein structure led to a higher number of false positive predictions (Clark *et al.*, 2006).

Protein-protein interactions are a complex phenomenon, while computational methods operate with simplified models of reality and face many obstacles coming out from insufficient understanding of complex protein-protein interactions. In the light of these facts, it is not

surprising that our protocol based on a straightforward geometric analysis of the crystal interface and the changes of the interaction free energy led to a decrease of affinity in about a half of the variants designed to actually increase the affinity. We assume that a disadvantage of computational design based on energy calculations includes misinterpretation of the ratio between true and false positives. Because many predicted mutations calculated to be stabilizing are in fact destabilizing, we should expect not only false positive but also false negative error (type II error). As the false negative predictions are never tested, some mutations can be omitted from the final selection although they would stabilize the complex more than any of the actually tested variants. In contrast, experimental methods, such as ribosome display, are based on random mutations and are capable of scanning much larger portion of overall sequence space without any prejudice.

Binding of IFNg to its Receptor 1 on the cell surface is just the first step of the interferon gamma signaling cascade leading to the regulation of hundreds of genes. New knowledge about this initial event of this signaling pathway, which is one the most critical in responding against pathogens and tumors, could help better understanding of the following step, formation of the ternary complex between IFNg, IFNgR1, and IFNgR2. We still miss information about the structural and biophysical features of IFNgR2 itself and especially the ternary complex, research in this direction is highly timely.

Our results demonstrated that computer-aided design of mutations within the receptor molecule, on the interface, in cavities or their combination, is a useful approach to increase the binding between two proteins with already evolutionary highly optimized interface and the affinity in the nanomolar range.

8 Conclusions

In this thesis, we combine the computational methods with experimental techniques to identify amino acids within extracellular domain of Interferon gamma receptor 1 (IFNgR1) suitable for modulation of affinity to its natural ligand Interferon gamma (IFNg).

A) Computer modeling to increase the IFNgR1 affinity to IFNg

In search for mutations modulating the affinity between our model proteins IFNgR1 and IFNg we developed a new protocol that is based on *in silico* analysis of crystal structures 1FG9 (Thiel *et al.*, 2000) and 1FYH (Randal and Kossiakoff, 2001), sequence conservancy, and free energy calculations by a FoldX empirical force field (Schymkowitz *et al.*, 2005). We applied our protocol to design several single-point IFNgR1 variants, together with multiple-site variants comprising also combination of interface mutations with cavity filling mutations.

B) Experimental affirmation of the computer predictions

We developed new protocols for the production and purification of Interferon gamma as well as wild-type Interferon gamma receptor 1 and its variants. We tested a large number of protocols to produce IFNgR1 in different expression systems such as insect S2 cells, yeast *Pichia pastoris* cells, and bacteria *Escherichia coli*. All selected IFNgR1 variants were successfully expressed in *E. coli*, refolded, purified to homogeneity, and their affinities to IFNg were measured by Surface Plasmon Resonance (SPR). The best interface variant N96W has affinity five-fold higher than wild-type (WT) receptor and this affinity is enhanced to seven-fold by the addition of a cavity mutation V35L, although the V35L variant itself has similar affinity to WT.

We measured the thermal stabilities of the best IFNg binders and confirmed by CD spectra that their affinity increases were not accompanied by major global structural rearrangements. It became apparent from the SPR results that the affinity increase was mainly caused by dissociation slowdown of free IFNg from IFNgR1 variants coated on the surface of the chip.

C) Comparison of the predicted and measured affinities

We compared computer predictions with the experimental results in an attempt to identify the structural source of the affinity increase. Interpretation of molecular dynamics (MD) simulations indicated that slower dissociation rate of the N96W interface variant and therefore its higher affinity is caused by an entropic stabilization of the introduced tryptophan residue in the complex with IFNg relative to the free state. There are also signs of hydrophobic destabilization of the free receptor at position 96. Although the cavity IFNgR1 variants have similar affinities to the WT receptor, they can enhance the binding of the interface variants by restricting molecular fluctuations, which can be related to reduced entropy penalty upon binding (Marlow *et al.*, 2010; Wand, 2013). However, we still need a more complete thermodynamic characterization of the IFNgR1 variants and their complexes to better comprehend the impact of mutations on the affinity between IFNgR1 and IFNg.

Summary

In this study, we faced the challenging task of increasing the binding between two proteins with already high affinity in a nanomolar range by employing computational methods. Our results demonstrate that computational design of protein variants supported by their experimental measurements can be an applicable approach for affinity modulation and can help in further understanding of the forces governing the protein-protein interactions.

9 Abbreviations

Å	Angstrom
aa	Amino Acids
ABD	Albumin Binding Domain
AF-1	Accessory Factor 1
Asn	Asparagine
Asp	Aspartic acid
BCG	Bacille Calmette-Guérin
CaM kinase	Calcium/Calmodulin-dependent Protein Kinase
CCPs	Clathrin-Coated Pits
CD	Circular Dichroism
cDNA	Complementary DNA
CFP-10	Culture Filter Protein 10
Cys	Cysteine
DC cells	Dendritic cells
DNA	Deoxyribonucleic Acid
EEEF	Empirical Effective Energy Functions
ER	Endoplasmic reticulum
ESAT-6	Early Secreted Antigenic Target 6
Esd	Estimated Standard Deviations
FRET	Förster Resonance Energy Transfer (Fluorescence Resonance Energy Transfer)
FrpD	Fe-regulated protein D
GAS	Interferon gamma Activated Sequences
Gly	Glycine
GST	Glutathione S-Transferase
His	Histidine
ICAM-1	Intercellular Adhesion Molecule 1
IFN	Interferon
IFNAR1	IFNα Receptor 1
IFNAR2	IFNα Receptor 2
IFNg	Interferon gamma
IFNgR1	Interferon gamma receptor 1
IFNgR2	Interferon gamma receptor 2
IFNg-SC	Interferon gamma Single Chain
IFNLR1	Interferon lambda receptor 1
IGRAs	Interferon gamma Release Assays
IL	Interleukin
IRF9	Interferon Regulatory Factor 9
IRGs	Interferon Regulated Genes
ISGs	Interferon Stimulated Genes
ITC	Isothermal Titration Calorimetry
JAK	Janus Kinase
k_a	Association Rate Constant
kb	Kilobase
kbp	Kilobase Pairs
K_d	Dissociation Constant
k_d	Dissociation Rate Constant
kDa	Kilodalton

LTBI	Latent Tuberculosis Infection
Lys	Lysine
M	Molar (as unit) or Marker (on SDS-PAGE gels)
MAP kinase	Mitogen-Activated Protein Kinase
MBP	Maltose Binding Protein
MD	Molecular Dynamics
M_r	Molecular Weight
mRNA	Messenger RNA
MS	Multiple Sclerosis
MTB	*Mycobacterium tuberculosis*
mut	Mutant
NFκB	Nuclear Factor κB
NK cells	Natural Killer cells
NKT cells	Natural Killer T cells
NLS	Nuclear Localization Sequence
nm	Nanometer
nM	Nanomolar
ORF	Open Reading Frame
PCR	Polymerase Chain Reaction
PDB	Protein Database
PEEF	Physical Effective Energy Functions
pI	Isoelectric point
PI3 kinase	Phosphoinositide 3-kinase
PPD	Purified Protein Derivative
Pro	Proline
QFT	QuantiFERON-TB
qPCR	Quantitative Polymerase Chain Reaction
RA	Rheumatoid Arthritis
rmsd	Root Mean Square Deviations
RMSF	Root Mean Square Fluctuations
RNA	Ribonucleic Acid
RPM	Revolutions Per Minute
RT	Room Temperature
RT-PCR	Real-Time Polymerase Chain Reaction
RU	Response Unit
S2 cells	Schneider 2 cells
SDS-PAGE	Sodium Dodecyl Sulfate Poly-Acrylamide Gel Electrophoresis
SEEF	Statistical Effective Energy Functions
SLE	Systemic Lupus Erythematous
SPR	Surface Plasmon Resonance
STAT	Signal Transducer and Activator of Transcription
TB	Tuberculosis
Th1 cells	T helper 1 cells
Th17 cells	T helper 17 cells
Th2 cells	T helper 2 cells
TLR4	Toll-like Receptor 4
T_m	Melting temperature
TRX	Thioredoxin
TSA	Thermal Shift Assay
T-SPOT	T-SPOT.*TB*

TST	Tuberculin Skin Test
TYK	Tyrosine Kinase
Tyr	Tyrosine
WHO	World Health Organization
WT	Wild-Type
ΔΔG	Change of free energy

10 References

Aaronson, D.S., and Horvath, C.M. (2002). "A road map for those who don't know JAK-STAT." Science **296**(5573): 1653-1655.

Aguet, M., Dembic, Z., and Merlin, G. (1988). "Molecular cloning and expression of the human interferon-gamma receptor." Cell **55**(2): 273-280.

Ahmad, J.N., Li, J., Biedermannova, L., Kuchar, M., Sipova, H., Semeradtova, A., Cerny, J., Petrokova, H., Mikulecky, P., Polinek, J., Stanek, O., Vondrasek, J., Homola, J., Maly, J., Osicka, R., Sebo, P., and Maly, P. (2012). "Novel high-affinity binders of human interferon gamma derived from albumin-binding domain of protein G." Proteins **80**(3): 774-789.

Ahmed, C.M., and Johnson, H.M. (2013). "The role of a non-canonical JAK-STAT pathway in IFN therapy of poxvirus infection and multiple sclerosis: An example of Occam's Broom?" JAKSTAT **2**(4): e26227.

Arkin, M.R., and Wells, J.A. (2004). "Small-molecule inhibitors of protein-protein interactions: progressing towards the dream." Nat Rev Drug Discov **3**(4): 301-317.

Atwell, S., Ultsch, M., De Vos, A.M., and Wells, J.A. (1997). "Structural plasticity in a remodeled protein-protein interface." Science **278**(5340): 1125-1128.

Axelrod, A., Gibbs, V.C., and Goeddel, D.V. (1994). "The interferon-gamma receptor extracellular domain. Non-identical requirements for ligand binding and signaling." J Biol Chem **269**(22): 15533-15539.

Azzurri, A., Sow, O.Y., Amedei, A., Bah, B., Diallo, S., Peri, G., Benagiano, M., D'Elios, M.M., Mantovani, A., and Del Prete, G. (2005). "IFN-gamma-inducible protein 10 and pentraxin 3 plasma levels are tools for monitoring inflammation and disease activity in Mycobacterium tuberculosis infection." Microbes Infect **7**(1): 1-8.

Bach, E.A., Aguet, M., and Schreiber, R.D. (1997). "The IFN gamma receptor: a paradigm for cytokine receptor signaling." Annu Rev Immunol **15**: 563-591.

Bach, E.A., Szabo, S.J., Dighe, A.S., Ashkenazi, A., Aguet, M., Murphy, K.M., and Schreiber, R.D. (1995). "Ligand-induced autoregulation of IFN-gamma receptor beta chain expression in T helper cell subsets." Science **270**(5239): 1215-1218.

Bach, E.A., Tanner, J.W., Marsters, S., Ashkenazi, A., Aguet, M., Shaw, A.S., and Schreiber, R.D. (1996). "Ligand-induced assembly and activation of the gamma interferon receptor in intact cells." Mol Cell Biol **16**(6): 3214-3221.

Barderas, R., Desmet, J., Timmerman, P., Meloen, R., and Casal, J.I. (2008). "Affinity maturation of antibodies assisted by in silico modeling." Proc Natl Acad Sci U S A **105**(26): 9029-9034.

Battaglia, T.M., Masson, J.F., Sierks, M.R., Beaudoin, S.P., Rogers, J., Foster, K.N., Holloway, G.A., and Booksh, K.S. (2005). "Quantification of cytokines involved in wound healing using surface plasmon resonance." Anal Chem **77**(21): 7016-7023.

Bazan, J.F. (1990). "Structural design and molecular evolution of a cytokine receptor superfamily." Proc Natl Acad Sci U S A **87**(18): 6934-6938.

Berezovski, M.V., Lechmann, M., Musheev, M.U., Mak, T.W., and Krylov, S.N. (2008). "Aptamer-facilitated biomarker discovery (AptaBiD)." J Am Chem Soc **130**(28): 9137-9143.

Bibova, I., Linhartova, I., Stanek, O., Rusnakova, V., Kubista, M., Suchanek, M., Vasakova, M., and Sebo, P. (2012). "Detection of immune cell response to M. tuberculosis-specific antigens by quantitative polymerase chain reaction." Diagn Microbiol Infect Dis **72**(1): 68-78.

Binz, H.K., Amstutz, P., Kohl, A., Stumpp, M.T., Briand, C., Forrer, P., Grutter, M.G., and Pluckthun, A. (2004). "High-affinity binders selected from designed ankyrin repeat protein libraries." Nat Biotechnol **22**(5): 575-582.

Blatt, L.M., Davis, J.M., Klein, S.B., and Taylor, M.W. (1996). "The biologic activity and molecular characterization of a novel synthetic interferon-alpha species, consensus interferon." J Interferon Cytokine Res **16**(7): 489-499.

Blouin, C.M., and Lamaze, C. (2013). "Interferon gamma receptor: the beginning of the journey." Front Immunol **4**: 267.

Bluyssen, A.R., Durbin, J.E., and Levy, D.E. (1996). "ISGF3 gamma p48, a specificity switch for interferon activated transcription factors." Cytokine Growth Factor Rev **7**(1): 11-17.

Boehm, U., Klamp, T., Groot, M., and Howard, J.C. (1997). "Cellular responses to interferon-gamma." Annu Rev Immunol **15**: 749-795.

Bogan, A.A., and Thorn, K.S. (1998). "Anatomy of hot spots in protein interfaces." J Mol Biol **280**(1): 1-9.

Bohm, G., Muhr, R., and Jaenicke, R. (1992). "Quantitative analysis of protein far UV circular dichroism spectra by neural networks." Protein Eng **5**(3): 191-195.

Bolen, C.R., Ding, S., Robek, M.D., and Kleinstein, S.H. (2014). "Dynamic expression profiling of type I and type III interferon-stimulated hepatocytes reveals a stable hierarchy of gene expression." Hepatology **59**(4): 1262-1272.

Bolon, D.N., and Mayo, S.L. (2001). "Enzyme-like proteins by computational design." Proc Natl Acad Sci U S A **98**(25): 14274-14279.

Bradshaw, R.T., Aronica, P.G.A., Tate, E.W., Leatherbarrow, R.J., and Gould, I.R. (2012). "Mutational Locally Enhanced Sampling (MULES) for quantitative prediction of the effects of mutations at protein–protein interfaces." Chemical Science **3**(5): 1503.

Bradshaw, R.T., Patel, B.H., Tate, E.W., Leatherbarrow, R.J., and Gould, I.R. (2011). "Comparing experimental and computational alanine scanning techniques for probing a prototypical protein-protein interaction." Protein Eng Des Sel **24**(1-2): 197-207.

Briscoe, J., Rogers, N.C., Witthuhn, B.A., Watling, D., Harpur, A.G., Wilks, A.F., Stark, G.R., Ihle, J.N., and Kerr, I.M. (1996). "Kinase-negative mutants of JAK1 can sustain interferon-gamma-inducible gene expression but not an antiviral state." EMBO J **15**(4): 799-809.

Černý, J., Biedermannová, L., Mikulecký, P., Zahradník, J., Charnavets, T., Šebo, P., and Schneider, B. (2015). "Redesigning Protein Cavities as a Strategy for Increasing Affinity in Protein-Protein Interaction: Interferon-γReceptor 1 as a Model." Biomed Res Int **2015**: 1-12.

Chegou, N.N., Black, G.F., Kidd, M., van Helden, P.D., and Walzl, G. (2009). "Host markers in QuantiFERON supernatants differentiate active TB from latent TB infection: preliminary report." BMC Pulm Med **9**: 21.

Chen, R. (1999). "A general strategy for enzyme engineering." Trends Biotechnol **17**(9): 344-345.

Chen, R., Greer, A., and Dean, A.M. (1996). "Redesigning secondary structure to invert coenzyme specificity in isopropylmalate dehydrogenase." Proc Natl Acad Sci U S A **93**(22): 12171-12176.

Chen, T.S., and Keating, A.E. (2012). "Designing specific protein-protein interactions using computation, experimental library screening, or integrated methods." Protein Sci **21**(7): 949-963.

Chinai, J.M., Taylor, A.B., Ryno, L.M., Hargreaves, N.D., Morris, C.A., Hart, P.J., and Urbach, A.R. (2011). "Molecular recognition of insulin by a synthetic receptor." J Am Chem Soc **133**(23): 8810-8813.

Chou, T.H., Chuang, C.Y., and Wu, C.M. (2010). "Quantification of Interleukin-6 in cell culture medium using surface plasmon resonance biosensors." Cytokine **51**(1): 107-111.

Chowdhury, P.S., and Wu, H. (2005). "Tailor-made antibody therapeutics." Methods **36**(1): 11-24.

Clackson, T., and Wells, J.A. (1995). "A hot spot of binding energy in a hormone-receptor interface." Science **267**(5196): 383-386.

Clark, L.A., Boriack-Sjodin, P.A., Eldredge, J., Fitch, C., Friedman, B., Hanf, K.J., Jarpe, M., Liparoto, S.F., Li, Y., Lugovskoy, A., Miller, S., Rushe, M., Sherman, W., Simon, K., and Van Vlijmen, H. (2006). "Affinity enhancement of an in vivo matured therapeutic antibody using structure-based computational design." Protein Sci **15**(5): 949-960.

Cobelens, F.G., Egwaga, S.M., van Ginkel, T., Muwinge, H., Matee, M.I., and Borgdorff, M.W. (2006). "Tuberculin skin testing in patients with HIV infection: limited benefit of reduced cutoff values." Clin Infect Dis **43**(5): 634-639.

Cochran, F.V., Wu, S.P., Wang, W., Nanda, V., Saven, J.G., Therien, M.J., and DeGrado, W.F. (2005). "Computational de novo design and characterization of a four-helix bundle protein that selectively binds a nonbiological cofactor." J Am Chem Soc **127**(5): 1346-1347.

Comstock, G.W., Livesay, V.T., and Woolpert, S.F. (1974). "The prognosis of a positive tuberculin reaction in childhood and adolescence." Am J Epidemiol **99**(2): 131-138.

Cook, J.R., Emanuel, S.L., Donnelly, R.J., Soh, J., Mariano, T.M., Schwartz, B., Rhee, S., and Pestka, S. (1994). "Sublocalization of the human interferon-gamma receptor accessory factor gene and characterization of accessory factor activity by yeast artificial chromosomal fragmentation." J Biol Chem **269**(9): 7013-7018.

Cook, J.R., Jung, V., Schwartz, B., Wang, P., and Pestka, S. (1992). "Structural analysis of the human interferon gamma receptor: a small segment of the intracellular domain is specifically required for class I major histocompatibility complex antigen induction and antiviral activity." Proc Natl Acad Sci U S A **89**(23): 11317-11321.

Cooper, W.J., and Waters, M.L. (2005). "Molecular recognition with designed peptides and proteins." Curr Opin Chem Biol **9**(6): 627-631.

Cunningham, B.C., and Wells, J.A. (1991). "Rational design of receptor-specific variants of human growth hormone." Proc Natl Acad Sci U S A **88**(8): 3407-3411.

Dalton, D.K., Pitts-Meek, S., Keshav, S., Figari, I.S., Bradley, A., and Stewart, T.A. (1993). "Multiple defects of immune cell function in mice with disrupted interferon-gamma genes." Science **259**(5102): 1739-1742.

Darnell, J.E., Jr., Kerr, I.M., and Stark, G.R. (1994). "Jak-STAT pathways and transcriptional activation in response to IFNs and other extracellular signaling proteins." Science **264**(5164): 1415-1421.

De Genst, E., Areskoug, D., Decanniere, K., Muyldermans, S., and Andersson, K. (2002). "Kinetic and affinity predictions of a protein-protein interaction using multivariate experimental design." J Biol Chem **277**(33): 29897-29907.

de Veer, M.J., Holko, M., Frevel, M., Walker, E., Der, S., Paranjape, J.M., Silverman, R.H., and Williams, B.R. (2001). "Functional classification of interferon-stimulated genes identified using microarrays." J Leukoc Biol **69**(6): 912-920.

Diaz, M.O., Bohlander, S., and Allen, G. (1996). "Nomenclature of the human interferon genes." J Interferon Cytokine Res **16**(2): 179-180.

Dlugovitzky, D., Bay, M.L., Rateni, L., Urizar, L., Rondelli, C.F., Largacha, C., Farroni, M.A., Molteni, O., and Bottasso, O.A. (1999). "In vitro synthesis of interferon-gamma, interleukin-4, transforming growth factor-beta and interleukin-1 beta by peripheral blood mononuclear cells from tuberculosis patients: relationship with the severity of pulmonary involvement." Scand J Immunol **49**(2): 210-217.

Dosanjh, D.P., Hinks, T.S., Innes, J.A., Deeks, J.J., Pasvol, G., Hackforth, S., Varia, H., Millington, K.A., Gunatheesan, R., Guyot-Revol, V., and Lalvani, A. (2008). "Improved diagnostic evaluation of suspected tuberculosis." Ann Intern Med **148**(5): 325-336.

Ealick, S.E., Cook, W.J., Vijay-Kumar, S., Carson, M., Nagabhushan, T.L., Trotta, P.P., and Bugg, C.E. (1991). "Three-dimensional structure of recombinant human interferon-gamma." Science **252**(5006): 698-702.

Eastman, P., and Pande, V. (2010). "OpenMM: A Hardware-Independent Framework for Molecular Simulations." Computing in Science & Engineering **12**(4): 34-39.

Ebensperger, C., Rhee, S., Muthukumaran, G., Lembo, D., Donnelly, R., Pestka, S., and Dembic, Z. (1996). "Genomic organization and promoter analysis of the gene ifngr2 encoding the second chain of the mouse interferon-gamma receptor." Scand J Immunol **44**(6): 599-606.

Eswar, N., John, B., Mirkovic, N., Fiser, A., Ilyin, V.A., Pieper, U., Stuart, A.C., Marti-Renom, M.A., Madhusudhan, M.S., Yerkovich, B., and Sali, A. (2003). "Tools for comparative protein structure modeling and analysis." Nucleic Acids Res **31**(13): 3375-3380.

Fan, X., White, I.M., Shopova, S.I., Zhu, H., Suter, J.D., and Sun, Y. (2008). "Sensitive optical biosensors for unlabeled targets: a review." Anal Chim Acta **620**(1-2): 8-26.

Farrar, M.A., Campbell, J.D., and Schreiber, R.D. (1992). "Identification of a functionally important sequence in the C terminus of the interferon-gamma receptor." Proc Natl Acad Sci U S A **89**(24): 11706-11710.

Farrar, M.A., Fernandez-Luna, J., and Schreiber, R.D. (1991). "Identification of two regions within the cytoplasmic domain of the human interferon-gamma receptor required for function." J Biol Chem **266**(29): 19626-19635.

Farrar, M.A., and Schreiber, R.D. (1993). "The molecular cell biology of interferon-gamma and its receptor." Annu Rev Immunol **11**: 571-611.

Fasler-Kan, E., Pansky, A., Wiederkehr, M., Battegay, M., and Heim, M.H. (1998). "Interferon-alpha activates signal transducers and activators of transcription 5 and 6 in Daudi cells." Eur J Biochem **254**(3): 514-519.

Filipe-Santos, O., Bustamante, J., Chapgier, A., Vogt, G., de Beaucoudrey, L., Feinberg, J., Jouanguy, E., Boisson-Dupuis, S., Fieschi, C., Picard, C., and Casanova, J.L. (2006). "Inborn errors of IL-12/23- and IFN-gamma-mediated immunity: molecular, cellular, and clinical features." Semin Immunol **18**(6): 347-361.

Fischer, T., Thoma, B., Scheurich, P., and Pfizenmaier, K. (1990). "Glycosylation of the human interferon-gamma receptor. N-linked carbohydrates contribute to structural heterogeneity and are required for ligand binding." J Biol Chem **265**(3): 1710-1717.

Fleishman, S.J., and Baker, D. (2012). "Role of the biomolecular energy gap in protein design, structure, and evolution." Cell **149**(2): 262-273.

Fountoulakis, M., and Gentz, R. (1992). "Effect of glycosylation on properties of soluble interferon gamma receptors produced in prokaryotic and eukaryotic expression systems." Biotechnology (N Y) **10**(10): 1143-1147.

Fountoulakis, M., Juranville, J.F., Stuber, D., Weibel, E.K., and Garotta, G. (1990). "Purification and biochemical characterization of a soluble human interferon gamma receptor expressed in Escherichia coli." J Biol Chem **265**(22): 13268-13275.

Friedrichs, M.S., Eastman, P., Vaidyanathan, V., Houston, M., Legrand, S., Beberg, A.L., Ensign, D.L., Bruns, C.M., and Pande, V.S. (2009). "Accelerating molecular dynamic simulation on graphics processing units." J Comput Chem **30**(6): 864-872.

Gandra, S., Scott, W.S., Somaraju, V., Wang, H., Wilton, S., and Feigenbaum, M. (2010). "Questionable effectiveness of the QuantiFERON-TB Gold Test (Cellestis) as a screening tool in healthcare workers." Infect Control Hosp Epidemiol **31**(12): 1279-1285.

Gentz, R., Hayes, A., Grau, N., Fountoulakis, M., Lahm, H.W., Ozmen, L., and Garotta, G. (1992). "Analysis of soluble human and mouse interferon-gamma receptors expressed in eukaryotic cells." Eur J Biochem **210**(2): 545-554.

Gessani, S., and Belardelli, F. (1998). "IFN-gamma expression in macrophages and its possible biological significance." Cytokine Growth Factor Rev **9**(2): 117-123.

Gibbs, V.C., Williams, S.R., Gray, P.W., Schreiber, R.D., Pennica, D., Rice, G., and Goeddel, D.V. (1991). "The extracellular domain of the human interferon gamma receptor interacts with a species-specific signal transducer." Mol Cell Biol **11**(12): 5860-5866.

Gorham, R.D., Jr., Kieslich, C.A., and Morikis, D. (2011). "Electrostatic clustering and free energy calculations provide a foundation for protein design and optimization." Ann Biomed Eng **39**(4): 1252-1263.

Gough, D.J., Levy, D.E., Johnstone, R.W., and Clarke, C.J. (2008). "IFNgamma signaling-does it mean JAK-STAT?" Cytokine Growth Factor Rev **19**(5-6): 383-394.

Gray, P.W., and Goeddel, D.V. (1982). "Structure of the human immune interferon gene." Nature **298**(5877): 859-863.

Gray, P.W., and Goeddel, D.V. (1983). "Cloning and expression of murine immune interferon cDNA." Proc Natl Acad Sci U S A **80**(19): 5842-5846.

Gray, P.W., Leung, D.W., Pennica, D., Yelverton, E., Najarian, R., Simonsen, C.C., Derynck, R., Sherwood, P.J., Wallace, D.M., Berger, S.L., Levinson, A.D., and Goeddel, D.V. (1982). "Expression of human immune interferon cDNA in E. coli and monkey cells." Nature **295**(5849): 503-508.

Greenlund, A.C., Farrar, M.A., Viviano, B.L., and Schreiber, R.D. (1994). "Ligand-induced IFN gamma receptor tyrosine phosphorylation couples the receptor to its signal transduction system (p91)." EMBO J **13**(7): 1591-1600.

Greenlund, A.C., Morales, M.O., Viviano, B.L., Yan, H., Krolewski, J., and Schreiber, R.D. (1995). "Stat recruitment by tyrosine-phosphorylated cytokine receptors: an ordered reversible affinity-driven process." Immunity **2**(6): 677-687.

Gronwall, C., and Stahl, S. (2009). "Engineered affinity proteins--generation and applications." J Biotechnol **140**(3-4): 254-269.

Haelewyn, J., and De Ley, M. (1995). "A rapid single-step purification method for human interferon-gamma from isolated Escherichia coli inclusion bodies." Biochem Mol Biol Int **37**(6): 1163-1171.

Hamming, O.J., Terczynska-Dyla, E., Vieyres, G., Dijkman, R., Jorgensen, S.E., Akhtar, H., Siupka, P., Pietschmann, T., Thiel, V., and Hartmann, R. (2013). "Interferon lambda 4 signals via the IFNlambda receptor to regulate antiviral activity against HCV and coronaviruses." EMBO J **32**(23): 3055-3065.

Han, J., Kim, H.J., Lee, S.C., Hong, S., Park, K., Jeon, Y.H., Kim, D., Cheong, H.K., and Kim, H.S. (2012). "Structure-based rational design of a Toll-like receptor 4 (TLR4) decoy receptor with high binding affinity for a target protein." PLoS One **7**(2): e30929.

Hanes, J., and Pluckthun, A. (1997). "In vitro selection and evolution of functional proteins by using ribosome display." Proc Natl Acad Sci U S A **94**(10): 4937-4942.

Harada, N., Higuchi, K., Yoshiyama, T., Kawabe, Y., Fujita, A., Sasaki, Y., Horiba, M., Mitarai, S., Yonemaru, M., Ogata, H., Ariga, H., Kurashima, A., Wada, A., Takamori, M., Yamagishi, F., Suzuki, K., Mori, T., and Ishikawa, N. (2008). "Comparison of the sensitivity and specificity of two whole blood interferon-gamma assays for M. tuberculosis infection." J Infect **56**(5): 348-353.

Harboe, M., Oettinger, T., Wiker, H.G., Rosenkrands, I., and Andersen, P. (1996). "Evidence for occurrence of the ESAT-6 protein in Mycobacterium tuberculosis and virulent Mycobacterium bovis and for its absence in Mycobacterium bovis BCG." Infect Immun **64**(1): 16-22.

Harty, J.T., and Bevan, M.J. (1995). "Specific immunity to Listeria monocytogenes in the absence of IFN gamma." Immunity **3**(1): 109-117.

He, M. (1997). "Antibody-ribosome-mRNA (ARM) complexes as efficient selection particles for in vitro display and evolution of antibody combining sites." Nucleic Acids Res **25**(24): 5132-5134.

Hershey, G.K., and Schreiber, R.D. (1989). "Biosynthetic analysis of the human interferon-gamma receptor. Identification of N-linked glycosylation intermediates." J Biol Chem **264**(20): 11981-11988.

Hertzog, P., Forster, S., and Samarajiwa, S. (2011). "Systems biology of interferon responses." J Interferon Cytokine Res **31**(1): 5-11.

Hess, B., Kutzner, C., van der Spoel, D., and Lindahl, E. (2008). "GROMACS 4: Algorithms for Highly Efficient, Load-Balanced, and Scalable Molecular Simulation." Journal of Chemical Theory and Computation **4**(3): 435-447.

Hoffmann, H.H., Schneider, W.M., and Rice, C.M. (2015). "Interferons and viruses: an evolutionary arms race of molecular interactions." Trends Immunol **36**(3): 124-138.

Holliger, P., and Hudson, P.J. (2005). "Engineered antibody fragments and the rise of single domains." Nat Biotechnol **23**(9): 1126-1136.

Hong, J.Y., Jung, G.S., Kim, H., Kim, Y.M., Lee, H.J., Cho, S.N., Kim, S.K., Chang, J., and Kang, Y.A. (2012). "Efficacy of inducible protein 10 as a biomarker for the diagnosis of tuberculosis." Int J Infect Dis **16**(12): e855-859.

Hu, X., and Ivashkiv, L.B. (2009). "Cross-regulation of signaling pathways by interferon-gamma: implications for immune responses and autoimmune diseases." Immunity **31**(4): 539-550.

Huang, P.S., Love, J.J., and Mayo, S.L. (2007). "A de novo designed protein protein interface." Protein Sci **16**(12): 2770-2774.

Huang, S., Hendriks, W., Althage, A., Hemmi, S., Bluethmann, H., Kamijo, R., Vilcek, J., Zinkernagel, R.M., and Aguet, M. (1993). "Immune response in mice that lack the interferon-gamma receptor." Science **259**(5102): 1742-1745.

Humphrey, W., Dalke, A., and Schulten, K. (1996). "VMD: visual molecular dynamics." J Mol Graph **14**(1): 33-38, 27-38.

Hurley, J.H., Chen, R., and Dean, A.M. (1996). "Determinants of cofactor specificity in isocitrate dehydrogenase: structure of an engineered NADP+ --> NAD+ specificity-reversal mutant." Biochemistry **35**(18): 5670-5678.

Igarashi, K., Garotta, G., Ozmen, L., Ziemiecki, A., Wilks, A.F., Harpur, A.G., Larner, A.C., and Finbloom, D.S. (1994). "Interferon-gamma induces tyrosine phosphorylation of interferon-gamma receptor and regulated association of protein tyrosine kinases, Jak1 and Jak2, with its receptor." J Biol Chem **269**(20): 14333-14336.

Ikeda, H., Old, L.J., and Schreiber, R.D. (2002). "The roles of IFN gamma in protection against tumor development and cancer immunoediting." Cytokine Growth Factor Rev **13**(2): 95-109.

Jaitin, D.A., Roisman, L.C., Jaks, E., Gavutis, M., Piehler, J., Van der Heyden, J., Uze, G., and Schreiber, G. (2006). "Inquiring into the differential action of interferons (IFNs): an IFN-alpha2 mutant with enhanced affinity to IFNAR1 is functionally similar to IFN-beta." Mol Cell Biol **26**(5): 1888-1897.

Janin, J. (1997). "The kinetics of protein-protein recognition." Proteins **28**(2): 153-161.

Jermutus, L., Honegger, A., Schwesinger, F., Hanes, J., and Pluckthun, A. (2001). "Tailoring in vitro evolution for protein affinity or stability." Proc Natl Acad Sci U S A **98**(1): 75-80.

Jha, R.K., Leaver-Fay, A., Yin, S., Wu, Y., Butterfoss, G.L., Szyperski, T., Dokholyan, N.V., and Kuhlman, B. (2010). "Computational design of a PAK1 binding protein." J Mol Biol **400**(2): 257-270.

Jiang, L., Althoff, E.A., Clemente, F.R., Doyle, L., Rothlisberger, D., Zanghellini, A., Gallaher, J.L., Betker, J.L., Tanaka, F., Barbas, C.F., 3rd, Hilvert, D., Houk, K.N., Stoddard, B.L., and Baker, D. (2008). "De novo computational design of retro-aldol enzymes." Science **319**(5868): 1387-1391.

Joachimiak, L.A., Kortemme, T., Stoddard, B.L., and Baker, D. (2006). "Computational design of a new hydrogen bond network and at least a 300-fold specificity switch at a protein-protein interface." J Mol Biol **361**(1): 195-208.

John, B., Rajagopal, D., Pashine, A., Rath, S., George, A., and Bal, V. (2002). "Role of IL-12-independent and IL-12-dependent pathways in regulating generation of the IFN-gamma component of T cell responses to Salmonella typhimurium." J Immunol **169**(5): 2545-2552.

Jouanguy, E., Doffinger, R., Dupuis, S., Pallier, A., Altare, F., and Casanova, J.L. (1999). "IL-12 and IFN-gamma in host defense against mycobacteria and salmonella in mice and men." Curr Opin Immunol **11**(3): 346-351.

Kalie, E., Jaitin, D.A., Podoplelova, Y., Piehler, J., and Schreiber, G. (2008). "The stability of the ternary interferon-receptor complex rather than the affinity to the individual subunits dictates differential biological activities." J Biol Chem **283**(47): 32925-32936.

Kanamori, T., Fujino, Y., and Ueda, T. (2014). "PURE ribosome display and its application in antibody technology." Biochimica et Biophysica Acta (BBA) - Proteins and Proteomics **1844**(11): 1925-1932.

Kaplan, D.H., Greenlund, A.C., Tanner, J.W., Shaw, A.S., and Schreiber, R.D. (1996). "Identification of an interferon-gamma receptor alpha chain sequence required for JAK-1 binding." J Biol Chem **271**(1): 9-12.

Kaplan, D.H., Shankaran, V., Dighe, A.S., Stockert, E., Aguet, M., Old, L.J., and Schreiber, R.D. (1998). "Demonstration of an interferon gamma-dependent tumor surveillance system in immunocompetent mice." Proc Natl Acad Sci U S A **95**(13): 7556-7561.

Kaplan, J., and DeGrado, W.F. (2004). "De novo design of catalytic proteins." Proc Natl Acad Sci U S A **101**(32): 11566-11570.

Karanicolas, J., Corn, J.E., Chen, I., Joachimiak, L.A., Dym, O., Peck, S.H., Albeck, S., Unger, T., Hu, W., Liu, G., Delbecq, S., Montelione, G.T., Spiegel, C.P., Liu, D.R., and Baker, D. (2011). "A de novo protein binding pair by computational design and directed evolution." Mol Cell **42**(2): 250-260.

Karanicolas, J., and Kuhlman, B. (2009). "Computational design of affinity and specificity at protein-protein interfaces." Curr Opin Struct Biol **19**(4): 458-463.

Kastritis, P.L., and Bonvin, A.M. (2013). "Molecular origins of binding affinity: seeking the Archimedean point." Curr Opin Struct Biol **23**(6): 868-877.

Kastritis, P.L., Moal, I.H., Hwang, H., Weng, Z., Bates, P.A., Bonvin, A.M., and Janin, J. (2011). "A structure-based benchmark for protein-protein binding affinity." Protein Sci **20**(3): 482-491.

Kawasaki, Y., Chufan, E.E., Lafont, V., Hidaka, K., Kiso, Y., Mario Amzel, L., and Freire, E. (2010). "How much binding affinity can be gained by filling a cavity?" Chem Biol Drug Des **75**(2): 143-151.

Kazlauskas, R.J. (2000). "Molecular modeling and biocatalysis: explanations, predictions, limitations, and opportunities." Curr Opin Chem Biol **4**(1): 81-88.

Kelker, H.C., Le, J., Rubin, B.Y., Yip, Y.K., Nagler, C., and Vilcek, J. (1984). "Three molecular weight forms of natural human interferon-gamma revealed by immunoprecipitation with monoclonal antibody." J Biol Chem **259**(7): 4301-4304.

Kerr, I.M., and Stark, G.R. (1991). "The control of interferon-inducible gene expression." FEBS Lett **285**(2): 194-198.

Keskin, O., Ma, B., and Nussinov, R. (2005). "Hot regions in protein--protein interactions: the organization and contribution of structurally conserved hot spot residues." J Mol Biol **345**(5): 1281-1294.

Kim, S., Lee, H., Kim, H., Kim, Y., Cho, J.E., Jin, H., Kim, D.Y., Ha, S.J., Kang, Y.A., Cho, S.N., and Lee, H. (2015). "Diagnostic performance of a cytokine and IFN-gamma-induced chemokine mRNA assay after Mycobacterium tuberculosis-specific antigen stimulation in whole blood from infected individuals." J Mol Diagn **17**(1): 90-99.

Kollman, P.A. (1996). "Advances and Continuing Challenges in Achieving Realistic and Predictive Simulations of the Properties of Organic and Biological Molecules." Accounts of Chemical Research **29**(10): 461-469.

Kortemme, T., and Baker, D. (2004). "Computational design of protein-protein interactions." Curr Opin Chem Biol **8**(1): 91-97.

Kotenko, S.V., Gallagher, G., Baurin, V.V., Lewis-Antes, A., Shen, M., Shah, N.K., Langer, J.A., Sheikh, F., Dickensheets, H., and Donnelly, R.P. (2003). "IFN-lambdas mediate antiviral protection through a distinct class II cytokine receptor complex." Nat Immunol **4**(1): 69-77.

Kotenko, S.V., Izotova, L.S., Pollack, B.P., Mariano, T.M., Donnelly, R.J., Muthukumaran, G., Cook, J.R., Garotta, G., Silvennoinen, O., Ihle, J.N., and et al. (1995). "Interaction between the components of the interferon gamma receptor complex." J Biol Chem **270**(36): 20915-20921.

Kotenko, S.V., and Pestka, S. (2000). "Jak-Stat signal transduction pathway through the eyes of cytokine class II receptor complexes." Oncogene **19**(21): 2557-2565.

Kraemer-Pecore, C.M., Wollacott, A.M., and Desjarlais, J.R. (2001). "Computational protein design." Curr Opin Chem Biol **5**(6): 690-695.

Krause, C.D., Mei, E., Xie, J., Jia, Y., Bopp, M.A., Hochstrasser, R.M., and Pestka, S. (2002). "Seeing the light: preassembly and ligand-induced changes of the interferon gamma receptor complex in cells." Mol Cell Proteomics **1**(10): 805-815.

Kuchar, M., Vankova, L., Petrokova, H., Cerny, J., Osicka, R., Pelak, O., Sipova, H., Schneider, B., Homola, J., Sebo, P., Kalina, T., and Maly, P. (2014). "Human interleukin-23 receptor antagonists derived from an albumin-binding domain scaffold inhibit IL-23-dependent ex vivo expansion of IL-17-producing T-cells." Proteins **82**(6): 975-989.

Kuchner, O., and Arnold, F.H. (1997). "Directed evolution of enzyme catalysts." Trends Biotechnol **15**(12): 523-530.

Lalvani, A. (2007). "Diagnosing tuberculosis infection in the 21st century: new tools to tackle an old enemy." Chest **131**(6): 1898-1906.

Lalvani, A., and Millington, K.A. (2007). "T cell-based diagnosis of childhood tuberculosis infection." Curr Opin Infect Dis **20**(3): 264-271.

Lalvani, A., and Millington, K.A. (2008a). "Screening for tuberculosis infection prior to initiation of anti-TNF therapy." Autoimmun Rev **8**(2): 147-152.

Lalvani, A., and Millington, K.A. (2008b). "T-cell interferon-gamma release assays: can we do better?" Eur Respir J **32**(6): 1428-1430.

Lalvani, A., and Pareek, M. (2010). "Interferon gamma release assays: principles and practice." Enferm Infecc Microbiol Clin **28**(4): 245-252.

Lalvani, A., Pathan, A.A., McShane, H., Wilkinson, R.J., Latif, M., Conlon, C.P., Pasvol, G., and Hill, A.V. (2001). "Rapid detection of Mycobacterium tuberculosis infection by enumeration of antigen-specific T cells." Am J Respir Crit Care Med **163**(4): 824-828.

Landar, A., Curry, B., Parker, M.H., DiGiacomo, R., Indelicato, S.R., Nagabhushan, T.L., Rizzi, G., and Walter, M.R. (2000). "Design, characterization, and structure of a biologically active single-chain mutant of human IFN-gamma." J Mol Biol **299**(1): 169-179.

Lassmann, T., Frings, O., and Sonnhammer, E.L. (2009). "Kalign2: high-performance multiple alignment of protein and nucleotide sequences allowing external features." Nucleic Acids Res **37**(3): 858-865.

Lazar, G.A., Dang, W., Karki, S., Vafa, O., Peng, J.S., Hyun, L., Chan, C., Chung, H.S., Eivazi, A., Yoder, S.C., Vielmetter, J., Carmichael, D.F., Hayes, R.J., and Dahiyat, B.I. (2006). "Engineered antibody Fc variants with enhanced effector function." Proc Natl Acad Sci U S A **103**(11): 4005-4010.

Lazaridis, T., and Karplus, M. (2000). "Effective energy functions for protein structure prediction." Curr Opin Struct Biol **10**(2): 139-145.

Le Coniat, M., Alcaide-Loridan, C., Fellous, M., and Berger, R. (1989). "Human interferon gamma receptor 1 (IFNGR1) gene maps to chromosome region 6q23-6q24." Hum Genet **84**(1): 92-94.

Lengyel, C.S., Willis, L.J., Mann, P., Baker, D., Kortemme, T., Strong, R.K., and McFarland, B.J. (2007). "Mutations designed to destabilize the receptor-bound conformation increase MICA-NKG2D association rate and affinity." J Biol Chem **282**(42): 30658-30666.

Lin, F.-C., and Young, H.A. (2013). "The talented interferon-gamma." Advances in Bioscience and Biotechnology **04**(07): 6-13.

Liongue, C., and Ward, A.C. (2007). "Evolution of Class I cytokine receptors." BMC Evol Biol **7**: 120.

Lippow, S.M., and Tidor, B. (2007). "Progress in computational protein design." Curr Opin Biotechnol **18**(4): 305-311.

Liu, S., Liu, S., Zhu, X., Liang, H., Cao, A., Chang, Z., and Lai, L. (2007). "Nonnatural protein-protein interaction-pair design by key residues grafting." Proc Natl Acad Sci U S A **104**(13): 5330-5335.

Liu, X., Ye, L., Bai, Y., Mojidi, H., Simister, N.E., and Zhu, X. (2008). "Activation of the JAK/STAT-1 signaling pathway by IFN-gamma can down-regulate functional expression of the MHC class I-related neonatal Fc receptor for IgG." J Immunol **181**(1): 449-463.

Liu, X.Q., Dosanjh, D., Varia, H., Ewer, K., Cockle, P., Pasvol, G., and Lalvani, A. (2004). "Evaluation of T-cell responses to novel RD1- and RD2-encoded Mycobacterium tuberculosis gene products for specific detection of human tuberculosis infection." Infect Immun **72**(5): 2574-2581.

Lofblom, J., Feldwisch, J., Tolmachev, V., Carlsson, J., Stahl, S., and Frejd, F.Y. (2010). "Affibody molecules: engineered proteins for therapeutic, diagnostic and biotechnological applications." FEBS Lett **584**(12): 2670-2680.

Lofblom, J., Frejd, F.Y., and Stahl, S. (2011). "Non-immunoglobulin based protein scaffolds." Curr Opin Biotechnol **22**(6): 843-848.

Luginbuhl, B., Kanyo, Z., Jones, R.M., Fletterick, R.J., Prusiner, S.B., Cohen, F.E., Williamson, R.A., Burton, D.R., and Pluckthun, A. (2006). "Directed evolution of an anti-prion protein scFv fragment to an affinity of 1 pM and its structural interpretation." J Mol Biol **363**(1): 75-97.

Lundell, D., Lunn, C., Dalgarno, D., Fossetta, J., Greenberg, R., Reim, R., Grace, M., and Narula, S. (1991). "The carboxyl-terminal region of human interferon gamma is important for biological activity: mutagenic and NMR analysis." Protein Eng **4**(3): 335-341.

Ma, B., Elkayam, T., Wolfson, H., and Nussinov, R. (2003). "Protein-protein interactions: structurally conserved residues distinguish between binding sites and exposed protein surfaces." Proc Natl Acad Sci U S A **100**(10): 5772-5777.

Mahairas, G.G., Sabo, P.J., Hickey, M.J., Singh, D.C., and Stover, C.K. (1996). "Molecular analysis of genetic differences between Mycobacterium bovis BCG and virulent M. bovis." J Bacteriol **178**(5): 1274-1282.

Mandalakas, A.M., Hesseling, A.C., Chegou, N.N., Kirchner, H.L., Zhu, X., Marais, B.J., Black, G.F., Beyers, N., and Walzl, G. (2008). "High level of discordant IGRA results in HIV-infected adults and children." Int J Tuberc Lung Dis **12**(4): 417-423.

Mandell, D.J., and Kortemme, T. (2009). "Computer-aided design of functional protein interactions." Nat Chem Biol **5**(11): 797-807.

Mao, C., Aguet, M., and Merlin, G. (1989). "Molecular characterization of the human interferon-gamma receptor: analysis of polymorphism and glycosylation." J Interferon Res **9**(6): 659-669.

Marcello, T., Grakoui, A., Barba-Spaeth, G., Machlin, E.S., Kotenko, S.V., MacDonald, M.R., and Rice, C.M. (2006). "Interferons alpha and lambda inhibit hepatitis C virus replication with distinct signal transduction and gene regulation kinetics." Gastroenterology **131**(6): 1887-1898.

Marlow, M.S., Dogan, J., Frederick, K.K., Valentine, K.G., and Wand, A.J. (2010). "The role of conformational entropy in molecular recognition by calmodulin." Nat Chem Biol **6**(5): 352-358.

Marsters, S.A., Pennica, D., Bach, E., Schreiber, R.D., and Ashkenazi, A. (1995). "Interferon gamma signals via a high-affinity multisubunit receptor complex that contains two types of polypeptide chain." Proc Natl Acad Sci U S A **92**(12): 5401-5405.

Marvin, J.S., and Lowman, H.B. (2003). "Redesigning an antibody fragment for faster association with its antigen." Biochemistry **42**(23): 7077-7083.

Matikainen, S., Sareneva, T., Ronni, T., Lehtonen, A., Koskinen, P.J., and Julkunen, I. (1999). "Interferon-alpha activates multiple STAT proteins and upregulates proliferation-associated IL-2Ralpha, c-myc, and pim-1 genes in human T cells." Blood **93**(6): 1980-1991.

Matsumoto, M., Tanaka, N., Harada, H., Kimura, T., Yokochi, T., Kitagawa, M., Schindler, C., and Taniguchi, T. (1999). "Activation of the transcription factor ISGF3 by interferon-gamma." Biol Chem **380**(6): 699-703.

Mendes, J., Guerois, R., and Serrano, L. (2002). "Energy estimation in protein design." Curr Opin Struct Biol **12**(4): 441-446.

Metcalfe, J.Z., Everett, C.K., Steingart, K.R., Cattamanchi, A., Huang, L., Hopewell, P.C., and Pai, M. (2011). "Interferon-gamma release assays for active pulmonary tuberculosis diagnosis in adults in low- and middle-income countries: systematic review and meta-analysis." J Infect Dis **204 Suppl 4**: S1120-1129.

Meyer, O. (2009). "Interferons and autoimmune disorders." Joint Bone Spine **76**(5): 464-473.

Miller, C.H., Maher, S.G., and Young, H.A. (2009). "Clinical Use of Interferon-gamma." Ann N Y Acad Sci **1182**: 69-79.

Moal, I.H., and Fernandez-Recio, J. (2012). "SKEMPI: a Structural Kinetic and Energetic database of Mutant Protein Interactions and its use in empirical models." Bioinformatics **28**(20): 2600-2607.

Mohammadian-Mosaabadi, J., Naderi-Manesh, H., Maghsoudi, N., Nassiri-Khalili, M.A., Masoumian, M.R., and Malek-Sabet, N. (2007). "Improving purification of recombinant human interferon gamma expressed in Escherichia coli; effect of removal of impurity on the process yield." Protein Expr Purif **51**(2): 147-156.

Moraga, I., Harari, D., Schreiber, G., Uze, G., and Pellegrini, S. (2009). "Receptor density is key to the alpha2/beta interferon differential activities." Mol Cell Biol **29**(17): 4778-4787.

Morellato-Castillo, L., Acharya, P., Combes, O., Michiels, J., Descours, A., Ramos, O.H., Yang, Y., Vanham, G., Arien, K.K., Kwong, P.D., Martin, L., and Kessler, P. (2013). "Interfacial cavity filling to optimize CD4-mimetic miniprotein interactions with HIV-1 surface glycoprotein." J Med Chem **56**(12): 5033-5047.

Mori, T., Sakatani, M., Yamagishi, F., Takashima, T., Kawabe, Y., Nagao, K., Shigeto, E., Harada, N., Mitarai, S., Okada, M., Suzuki, K., Inoue, Y., Tsuyuguchi, K., Sasaki, Y., Mazurek, G.H., and Tsuyuguchi, I. (2004). "Specific detection of tuberculosis infection: an interferon-gamma-based assay using new antigens." Am J Respir Crit Care Med **170**(1): 59-64.

Naylor, S.L., Sakaguchi, A.Y., Shows, T.B., Law, M.L., Goeddel, D.V., and Gray, P.W. (1983). "Human immune interferon gene is located on chromosome 12." J Exp Med **157**(3): 1020-1027.

Ng, E.W., Shima, D.T., Calias, P., Cunningham, E.T., Jr., Guyer, D.R., and Adamis, A.P. (2006). "Pegaptanib, a targeted anti-VEGF aptamer for ocular vascular disease." Nat Rev Drug Discov **5**(2): 123-132.

Northrup, S.H., and Erickson, H.P. (1992). "Kinetics of protein-protein association explained by Brownian dynamics computer simulation." Proc Natl Acad Sci U S A **89**(8): 3338-3342.

Nygren, P.A. (2008). "Alternative binding proteins: affibody binding proteins developed from a small three-helix bundle scaffold." FEBS J **275**(11): 2668-2676.

Ogata, K., Jaramillo, A., Cohen, W., Briand, J.P., Connan, F., Choppin, J., Muller, S., and Wodak, S.J. (2003). "Automatic sequence design of major histocompatibility complex class I binding peptides impairing CD8+ T cell recognition." J Biol Chem **278**(2): 1281-1290.

Okamoto, M., Kawabe, T., Iwasaki, Y., Hara, T., Hashimoto, N., Imaizumi, K., Hasegawa, Y., and Shimokata, K. (2005). "Evaluation of interferon-gamma, interferon-gamma-inducing cytokines, and interferon-gamma-inducible chemokines in tuberculous pleural effusions." J Lab Clin Med **145**(2): 88-93.

Okonechnikov, K., Golosova, O., Fursov, M., and team, U. (2012). "Unipro UGENE: a unified bioinformatics toolkit." Bioinformatics **28**(8): 1166-1167.

Pai, M., Denkinger, C.M., Kik, S.V., Rangaka, M.X., Zwerling, A., Oxlade, O., Metcalfe, J.Z., Cattamanchi, A., Dowdy, D.W., Dheda, K., and Banaei, N. (2014). "Gamma interferon release assays for detection of Mycobacterium tuberculosis infection." Clin Microbiol Rev **27**(1): 3-20.

Pai, M., Kalantri, S., and Dheda, K. (2006). "New tools and emerging technologies for the diagnosis of tuberculosis: part I. Latent tuberculosis." Expert Rev Mol Diagn **6**(3): 413-422.

Pai, M., Zwerling, A., and Menzies, D. (2008). "Systematic review: T-cell-based assays for the diagnosis of latent tuberculosis infection: an update." Ann Intern Med **149**(3): 177-184.

Paludan, S.R. (1998). "Interleukin-4 and interferon-gamma: the quintessence of a mutual antagonistic relationship." Scand J Immunol **48**(5): 459-468.

Pan, Y.C., Stern, A.S., Familletti, P.C., Khan, F.R., and Chizzonite, R. (1987). "Structural characterization of human interferon gamma. Heterogeneity of the carboxyl terminus." Eur J Biochem **166**(1): 145-149.

Pantazes, R.J., Grisewood, M.J., and Maranas, C.D. (2011). "Recent advances in computational protein design." Curr Opin Struct Biol **21**(4): 467-472.

Park, H., and Jeon, Y.H. (2011). "Free energy perturbation approach for the rational engineering of the antibody for human hepatitis B virus." J Mol Graph Model **29**(5): 643-649.

Peczuh, M.W., and Hamilton, A.D. (2000). "Peptide and protein recognition by designed molecules." Chem Rev **100**(7): 2479-2494.

Pestka, S. (2007). "The interferons: 50 years after their discovery, there is much more to learn." J Biol Chem **282**(28): 20047-20051.

Pestka, S., Kotenko, S.V., Muthukumaran, G., Izotova, L.S., Cook, J.R., and Garotta, G. (1997). "The interferon gamma (IFN-gamma) receptor: a paradigm for the multichain cytokine receptor." Cytokine Growth Factor Rev **8**(3): 189-206.

Pestka, S., Krause, C.D., and Walter, M.R. (2004). "Interferons, interferon-like cytokines, and their receptors." Immunol Rev **202**: 8-32.

Pestka, S., Langer, J.A., Zoon, K.C., and Samuel, C.E. (1987). "Interferons and their actions." Annu Rev Biochem **56**: 727-777.

Petrov, S., Ivanova, E., Chakarova, D., Posheva, V., Redzheb, M., Nacheva, G., and Ivanov, I. (2014). "A New Approach for Purification of Recombinant Human Interferon Gamma Expressed inEscherichia Coli." Biotechnology & Biotechnological Equipment **23**(1): 1101-1102.

Pierce, B.G., Haidar, J.N., Yu, Y., and Weng, Z. (2010). "Combinations of affinity-enhancing mutations in a T cell receptor reveal highly nonadditive effects within and between complementarity determining regions and chains." Biochemistry **49**(33): 7050-7059.

Pokkali, S., Das, S.D., and R, L. (2008). "Expression of CXC and CC type of chemokines and its receptors in tuberculous and non-tuberculous effusions." Cytokine **41**(3): 307-314.

Pollard, K.M., Cauvi, D.M., Toomey, C.B., Morris, K.V., and Kono, D.H. (2013). "Interferon-gamma and systemic autoimmunity." Discov Med **16**(87): 123-131.

Pommier, Y., and Marchand, C. (2012). "Interfacial inhibitors: targeting macromolecular complexes." Nat Rev Drug Discov **11**(1): 25-36.

Pouchot, J., Grasland, A., Collet, C., Coste, J., Esdaile, J.M., and Vinceneux, P. (1997). "Reliability of tuberculin skin test measurement." Ann Intern Med **126**(3): 210-214.

Prokunina-Olsson, L., Muchmore, B., Tang, W., Pfeiffer, R.M., Park, H., Dickensheets, H., Hergott, D., Porter-Gill, P., Mumy, A., Kohaar, I., Chen, S., Brand, N., Tarway, M., Liu, L., Sheikh, F., Astemborski, J., Bonkovsky, H.L., Edlin, B.R., Howell, C.D., Morgan, T.R., Thomas, D.L., Rehermann, B., Donnelly, R.P., and O'Brien, T.R. (2013). "A variant upstream of IFNL3 (IL28B) creating a new interferon gene IFNL4 is associated with impaired clearance of hepatitis C virus." Nat Genet **45**(2): 164-171.

Randal, M., and Kossiakoff, A.A. (2001). "The structure and activity of a monomeric interferon-gamma:alpha-chain receptor signaling complex." Structure **9**(2): 155-163.

Reichmann, D., Rahat, O., Cohen, M., Neuvirth, H., and Schreiber, G. (2007). "The molecular architecture of protein-protein binding sites." Curr Opin Struct Biol **17**(1): 67-76.

Rhee, S., Ebensperger, C., Dembic, Z., and Pestka, S. (1996). "The structure of the gene for the second chain of the human interferon-gamma receptor." J Biol Chem **271**(46): 28947-28952.

Richeldi, L. (2006). "An update on the diagnosis of tuberculosis infection." Am J Respir Crit Care Med **174**(7): 736-742.

Roberts, R.M., Liu, L., Guo, Q., Leaman, D., and Bixby, J. (1998). "The evolution of the type I interferons." J Interferon Cytokine Res **18**(10): 805-816.

Rosenzweig, S.D., and Holland, S.M. (2005). "Defects in the interferon-gamma and interleukin-12 pathways." Immunol Rev **203**: 38-47.

Ruhwald, M., Bjerregaard-Andersen, M., Rabna, P., Kofoed, K., Eugen-Olsen, J., and Ravn, P. (2007). "CXCL10/IP-10 release is induced by incubation of whole blood from tuberculosis patients with ESAT-6, CFP10 and TB7.7." Microbes Infect **9**(7): 806-812.

Ruhwald, M., Bodmer, T., Maier, C., Jepsen, M., Haaland, M.B., Eugen-Olsen, J., Ravn, P., and Tbnet (2008). "Evaluating the potential of IP-10 and MCP-2 as biomarkers for the diagnosis of tuberculosis." Eur Respir J **32**(6): 1607-1615.

Sadler, A.J., and Williams, B.R. (2008). "Interferon-inducible antiviral effectors." Nat Rev Immunol **8**(7): 559-568.

Sakatsume, M., and Finbloom, D.S. (1996). "Modulation of the expression of the IFN-gamma receptor beta-chain controls responsiveness to IFN-gamma in human peripheral blood T cells." J Immunol **156**(11): 4160-4166.

Sakatsume, M., Igarashi, K., Winestock, K.D., Garotta, G., Larner, A.C., and Finbloom, D.S. (1995). "The Jak kinases differentially associate with the alpha and beta (accessory factor) chains of the interferon gamma receptor to form a functional receptor unit capable of activating STAT transcription factors." J Biol Chem **270**(29): 17528-17534.

Schindler, C., and Brutsaert, S. (1999). "Interferons as a paradigm for cytokine signal transduction." Cell Mol Life Sci **55**(12): 1509-1522.

Schoenborn, J.R., and Wilson, C.B. (2007). "Regulation of interferon-gamma during innate and adaptive immune responses." Adv Immunol **96**: 41-101.

Schreiber, G., and Fersht, A.R. (1996). "Rapid, electrostatically assisted association of proteins." Nat Struct Biol **3**(5): 427-431.

Schreiber, G., Shaul, Y., and Gottschalk, K.E. (2006). "Electrostatic design of protein-protein association rates." Methods Mol Biol **340**: 235-249.

Schroder, K., Hertzog, P.J., Ravasi, T., and Hume, D.A. (2004). "Interferon-gamma: an overview of signals, mechanisms and functions." J Leukoc Biol **75**(2): 163-189.

Schymkowitz, J., Borg, J., Stricher, F., Nys, R., Rousseau, F., and Serrano, L. (2005). "The FoldX web server: an online force field." Nucleic Acids Res **33**(Web Server issue): W382-388.

Sefah, K., Phillips, J.A., Xiong, X., Meng, L., Van Simaeys, D., Chen, H., Martin, J., and Tan, W. (2009). "Nucleic acid aptamers for biosensors and bio-analytical applications." Analyst **134**(9): 1765-1775.

Selzer, T., Albeck, S., and Schreiber, G. (2000). "Rational design of faster associating and tighter binding protein complexes." Nat Struct Biol **7**(7): 537-541.

Sengupta, T., Tsutsui, Y., and Wintrode, P.L. (2009). "Local and global effects of a cavity filling mutation in a metastable serpin." Biochemistry **48**(34): 8233-8240.

Sester, M., Sotgiu, G., Lange, C., Giehl, C., Girardi, E., Migliori, G.B., Bossink, A., Dheda, K., Diel, R., Dominguez, J., Lipman, M., Nemeth, J., Ravn, P., Winkler, S., Huitric, E., Sandgren, A., and Manissero, D. (2011). "Interferon-gamma release assays for the diagnosis of active tuberculosis: a systematic review and meta-analysis." Eur Respir J **37**(1): 100-111.

Shah, M., DiPietro, D., Greenbaum, A., Ketemepi, S., Martins-Evora, M., Marsiglia, V., and Dorman, S.E. (2012). "Programmatic impact of QuantiFERON-TB Gold In-Tube implementation on latent tuberculosis diagnosis and treatment in a public health clinic." PLoS One **7**(5): e36551.

Sharabi, O., Dekel, A., and Shifman, J.M. (2011). "Triathlon for energy functions: who is the winner for design of protein-protein interactions?" Proteins **79**(5): 1487-1498.

Sharabi, O., Peleg, Y., Mashiach, E., Vardy, E., Ashani, Y., Silman, I., Sussman, J.L., and Shifman, J.M. (2009). "Design, expression and characterization of mutants of fasciculin optimized for interaction with its target, acetylcholinesterase." Protein Eng Des Sel **22**(10): 641-648.

Sheppard, P., Kindsvogel, W., Xu, W., Henderson, K., Schlutsmeyer, S., Whitmore, T.E., Kuestner, R., Garrigues, U., Birks, C., Roraback, J., Ostrander, C., Dong, D., Shin, J., Presnell, S., Fox, B., Haldeman, B., Cooper, E., Taft, D., Gilbert, T., Grant, F.J., Tackett, M., Krivan, W., McKnight, G., Clegg, C., Foster, D., and Klucher, K.M. (2003). "IL-28, IL-29 and their class II cytokine receptor IL-28R." Nat Immunol **4**(1): 63-68.

Sherry, S.T., Ward, M.H., Kholodov, M., Baker, J., Phan, L., Smigielski, E.M., and Sirotkin, K. (2001). "dbSNP: the NCBI database of genetic variation." Nucleic Acids Res **29**(1): 308-311.

Shifman, J.M., Choi, M.H., Mihalas, S., Mayo, S.L., and Kennedy, M.B. (2006). "Ca2+/calmodulin-dependent protein kinase II (CaMKII) is activated by calmodulin with two bound calciums." Proc Natl Acad Sci U S A **103**(38): 13968-13973.

Šípová, H., Ševců, V., Kuchař, M., Ahmad, J.N., Mikulecký, P., Osička, R., Malý, P., and Homola, J. (2012). "Surface plasmon resonance biosensor based on engineered proteins for direct detection of interferon-gamma in diluted blood plasma." Sensors and Actuators B: Chemical **174**: 306-311.

Skerra, A. (2000). "Engineered protein scaffolds for molecular recognition." J Mol Recognit **13**(4): 167-187.

Soh, J., Donnelly, R.J., Kotenko, S., Mariano, T.M., Cook, J.R., Wang, N., Emanuel, S., Schwartz, B., Miki, T., and Pestka, S. (1994). "Identification and sequence of an accessory factor required for activation of the human interferon gamma receptor." Cell **76**(5): 793-802.

Song, G., Lazar, G.A., Kortemme, T., Shimaoka, M., Desjarlais, J.R., Baker, D., and Springer, T.A. (2006). "Rational design of intercellular adhesion molecule-1 (ICAM-1) variants for antagonizing integrin lymphocyte function-associated antigen-1-dependent adhesion." J Biol Chem **281**(8): 5042-5049.

Stark, G.R., and Darnell, J.E., Jr. (2012). "The JAK-STAT pathway at twenty." Immunity **36**(4): 503-514.

Stark, G.R., Kerr, I.M., Williams, B.R., Silverman, R.H., and Schreiber, R.D. (1998). "How cells respond to interferons." Annu Rev Biochem **67**: 227-264.

Starke, J.R., and Committee On Infectious Diseases. (2014). "Interferon-gamma release assays for diagnosis of tuberculosis infection and disease in children." Pediatrics **134**(6): e1763-1773.

Stemmer, W.P. (1994). "DNA shuffling by random fragmentation and reassembly: in vitro recombination for molecular evolution." Proc Natl Acad Sci U S A **91**(22): 10747-10751.

Stigter, E.C., de Jong, G.J., and van Bennekom, W.P. (2005). "An improved coating for the isolation and quantitation of interferon-gamma in spiked plasma using surface plasmon resonance (SPR)." Biosens Bioelectron **21**(3): 474-482.

Stuber, D., Friedlein, A., Fountoulakis, M., Lahm, H.W., and Garotta, G. (1993). "Alignment of disulfide bonds of the extracellular domain of the interferon gamma receptor and investigation of their role in biological activity." Biochemistry **32**(9): 2423-2430.

Stumpp, M.T., Binz, H.K., and Amstutz, P. (2008). "DARPins: a new generation of protein therapeutics." Drug Discov Today **13**(15-16): 695-701.

Stybayeva, G., Kairova, M., Ramanculov, E., Simonian, A.L., and Revzin, A. (2010). "Detecting interferon-gamma release from human CD4 T-cells using surface plasmon resonance." Colloids Surf B Biointerfaces **80**(2): 251-255.

Subramaniam, P.S., Torres, B.A., and Johnson, H.M. (2001). "So many ligands, so few transcription factors: a new paradigm for signaling through the STAT transcription factors." Cytokine **15**(4): 175-187.

Supriya, P., Chandrasekaran, P., and Das, S.D. (2008). "Diagnostic utility of interferon-gamma-induced protein of 10 kDa (IP-10) in tuberculous pleurisy." Diagn Microbiol Infect Dis **62**(2): 186-192.

Sviridova, E., Bumba, L., Rezacova, P., Prochazkova, K., Kavan, D., Bezouska, K., Kuty, M., Sebo, P., and Kuta Smatanova, I. (2010). "Crystallization and preliminary crystallographic characterization of the iron-regulated outer membrane lipoprotein FrpD from Neisseria meningitidis." Acta Crystallogr Sect F Struct Biol Cryst Commun **66**(Pt 9): 1119-1123.

Takahashi, T.T., Austin, R.J., and Roberts, R.W. (2003). "mRNA display: ligand discovery, interaction analysis and beyond." Trends Biochem Sci **28**(3): 159-165.

Thiel, D.J., le Du, M.H., Walter, R.L., D'Arcy, A., Chene, C., Fountoulakis, M., Garotta, G., Winkler, F.K., and Ealick, S.E. (2000). "Observation of an unexpected third receptor molecule in the crystal structure of human interferon-gamma receptor complex." Structure **8**(9): 927-936.

Tsai, K.S., Chang, H.L., Chien, S.T., Chen, K.L., Chen, K.H., Mai, M.H., and Chen, K.T. (2013). "Childhood tuberculosis: epidemiology, diagnosis, treatment, and vaccination." Pediatr Neonatol **54**(5): 295-302.

Tuleuova, N., Jones, C.N., Yan, J., Ramanculov, E., Yokobayashi, Y., and Revzin, A. (2010). "Development of an aptamer beacon for detection of interferon-gamma." Anal Chem **82**(5): 1851-1857.

Tzeng, S.R., and Kalodimos, C.G. (2012). "Protein activity regulation by conformational entropy." Nature **488**(7410): 236-240.

Tzeng, S.R., and Kalodimos, C.G. (2013). "Allosteric inhibition through suppression of transient conformational states." Nat Chem Biol **9**(7): 462-465.

Ulrichs, T., Munk, M.E., Mollenkopf, H., Behr-Perst, S., Colangeli, R., Gennaro, M.L., and Kaufmann, S.H. (1998). "Differential T cell responses to Mycobacterium tuberculosis ESAT6 in tuberculosis patients and healthy donors." Eur J Immunol **28**(12): 3949-3958.

Valdar, W.S., and Thornton, J.M. (2001). "Protein-protein interfaces: analysis of amino acid conservation in homodimers." Proteins **42**(1): 108-124.

Valente, G., Ozmen, L., Novelli, F., Geuna, M., Palestro, G., Forni, G., and Garotta, G. (1992). "Distribution of interferon-gamma receptor in human tissues." Eur J Immunol **22**(9): 2403-2412.

Van Der Spoel, D., Lindahl, E., Hess, B., Groenhof, G., Mark, A.E., and Berendsen, H.J. (2005). "GROMACS: fast, flexible, and free." J Comput Chem **26**(16): 1701-1718.

Van Dorst, B., Mehta, J., Bekaert, K., Rouah-Martin, E., De Coen, W., Dubruel, P., Blust, R., and Robbens, J. (2010). "Recent advances in recognition elements of food and environmental biosensors: a review." Biosens Bioelectron **26**(4): 1178-1194.

van Zyl-Smit, R.N., Pai, M., Peprah, K., Meldau, R., Kieck, J., Juritz, J., Badri, M., Zumla, A., Sechi, L.A., Bateman, E.D., and Dheda, K. (2009). "Within-subject variability and boosting of T-cell interferon-gamma responses after tuberculin skin testing." Am J Respir Crit Care Med **180**(1): 49-58.

Voss, N.R., and Gerstein, M. (2010). "3V: cavity, channel and cleft volume calculator and extractor." Nucleic Acids Res **38**(Web Server issue): W555-562.

Walter, M.R., Windsor, W.T., Nagabhushan, T.L., Lundell, D.J., Lunn, C.A., Zauodny, P.J., and Narula, S.K. (1995). "Crystal structure of a complex between interferon-gamma and its soluble high-affinity receptor." Nature **376**(6537): 230-235.

Wand, A.J. (2013). "The dark energy of proteins comes to light: conformational entropy and its role in protein function revealed by NMR relaxation." Curr Opin Struct Biol **23**(1): 75-81.

Wang, L., Turner, M.O., Elwood, R.K., Schulzer, M., and FitzGerald, J.M. (2002). "A meta-analysis of the effect of Bacille Calmette Guerin vaccination on tuberculin skin test measurements." Thorax **57**(9): 804-809.

Weidle, U.H., Auer, J., Brinkmann, U., Georges, G., and Tiefenthaler, G. (2013). "The emerging role of new protein scaffold-based agents for treatment of cancer." Cancer Genomics Proteomics **10**(4): 155-168.

Whitehead, T.A., Baker, D., and Fleishman, S.J. (2013). "Computational design of novel protein binders and experimental affinity maturation." Methods Enzymol **523**: 1-19.

Wilson, C.J. (2015). "Rational protein design: developing next-generation biological therapeutics and nanobiotechnological tools." Wiley Interdiscip Rev Nanomed Nanobiotechnol **7**(3): 330-341.

Wu, B., Huang, C., Kato-Maeda, M., Hopewell, P.C., Daley, C.L., Krensky, A.M., and Clayberger, C. (2007). "Messenger RNA expression of IL-8, FOXP3, and IL-12beta differentiates latent tuberculosis infection from disease." J Immunol **178**(6): 3688-3694.

Young, H.A. (1996). "Regulation of interferon-gamma gene expression." J Interferon Cytokine Res **16**(8): 563-568.

Yu, Y., Zhang, Y., Hu, S., Jin, D., Chen, X., Jin, Q., and Liu, H. (2012). "Different patterns of cytokines and chemokines combined with IFN-gamma production reflect Mycobacterium tuberculosis infection and disease." PLoS One **7**(9): e44944.

11 Publications enclosed in full

Mikulecky, P., Cerny, J., Biedermannova, L., Petrokova, H., Kuchar, M., Vondrasek, J., Maly, P., Sebo, P., and Schneider, B. (2013). Increasing affinity of interferon-gamma receptor 1 to interferon-gamma by computer-aided design. *Biomed Res Int, 2013*, 752514. doi: 10.1155/2013/752514.

Černý, J., Biedermannová, L., Mikulecký, P., Zahradník, J., Charnavets, T., Šebo, P., and Schneider, B. (2015). Redesigning Protein Cavities as a Strategy for Increasing Affinity in Protein-Protein Interaction: Interferon-γReceptor 1 as a Model. *Biomed Res Int, 2015*, 1-12. doi: 10.1155/2015/716945.

Ahmad, J.N., Li, J., Biedermannova, L., Kuchar, M., Sipova, H., Semeradtova, A., Cerny, J., Petrokova, H., Mikulecky, P., Polinek, J., Stanek, O., Vondrasek, J., Homola, J., Maly, J., Osicka, R., Sebo, P., and Maly, P. (2012). Novel high-affinity binders of human interferon gamma derived from albumin-binding domain of protein G. *Proteins, 80*(3), 774-789. doi: 10.1002/prot.23234.

Šípová, H., Ševců, V., Kuchař, M., Ahmad, J.N., Mikulecký, P., Osička, R., Malý, P., and Homola, J. (2012). Surface plasmon resonance biosensor based on engineered proteins for direct detection of interferon-gamma in diluted blood plasma. *Sensors and Actuators B: Chemical, 174*, 306-311. doi: 10.1016/j.snb.2012.08.024.

Hindawi Publishing Corporation
BioMed Research International
Volume 2013, Article ID 752514, 12 pages
http://dx.doi.org/10.1155/2013/752514

Research Article

Increasing Affinity of Interferon-γ Receptor 1 to Interferon-γ by Computer-Aided Design

Pavel Mikulecký, Jiří Černý, Lada Biedermannová, Hana Petroková, Milan Kuchař, Jiří Vondrášek, Petr Malý, Peter Šebo, and Bohdan Schneider

Institute of Biotechnology AS CR, v. v. i., Vídeňská 1083, 142 20 Prague, Czech Republic

Correspondence should be addressed to Bohdan Schneider; bohdan@img.cas.cz

Received 29 April 2013; Revised 6 August 2013; Accepted 13 August 2013

Academic Editor: David Stammers

We describe a computer-based protocol to design protein mutations increasing binding affinity between ligand and its receptor. The method was applied to mutate interferon-γ receptor 1 (IFN-γ-Rx) to increase its affinity to natural ligand IFN-γ, protein important for innate immunity. We analyzed all four available crystal structures of the IFN-γ-Rx/IFN-γ complex to identify 40 receptor residues forming the interface with IFN-γ. For these 40 residues, we performed computational mutation analysis by substituting each of the interface receptor residues by the remaining standard amino acids. The corresponding changes of the free energy were calculated by a protocol consisting of FoldX and molecular dynamics calculations. Based on the computed changes of the free energy and on sequence conservation criteria obtained by the analysis of 32 receptor sequences from 19 different species, we selected 14 receptor variants predicted to increase the receptor affinity to IFN-γ. These variants were expressed as recombinant proteins in *Escherichia coli*, and their affinities to IFN-γ were determined experimentally by surface plasmon resonance (SPR). The SPR measurements showed that the simple computational protocol succeeded in finding two receptor variants with affinity to IFN-γ increased about fivefold compared to the wild-type receptor.

1. Introduction

Recent developments in structural biology greatly enhanced our understanding of structural and energetic aspects of protein-protein interactions, and design of proteins with targeted modifications by rational, computer-aided techniques is becoming a standard tool of protein engineering [1–5]. Yet, full comprehension of affinity and specificity of these interactions remains a challenge, and reliable explanation, let alone prediction, of the intermolecular affinity solely by computational tools remains a difficult task. Difficulties to predict the actual outcome of the interactions between large protein molecules at the atomic level arise mainly from a large number of small contributions that are compensatory in nature. Their rigorous description from the principles of quantum mechanics is conceptually possible, but computationally intractable and empirical models of interactions suffer from inadequate description of certain types of interactions, namely, electrostatic, and complex types of processes, namely, hydration. The large size of modeled biological systems leads to incomplete sampling of the conformational space of the interacting molecules. Molecular dynamics and even relatively inexpensive techniques [6] are able to consider more complex changes of the polypeptide backbone; typically, scanned are only conformations of amino acid side chains, and changes of the polypeptide backbone are limited or not allowed altogether so that larger rearrangements of the interacting molecules are hard to predict.

Despite all the limits in our understanding of the protein-protein interactions and technical obstacles related to their description, rational design of proteins with new or improved features is a promising alternative to experimental approaches for its speed and affordability [7]. The ingenious experimental techniques of directed evolution such as phage

display [8–10] and ribosome display [11, 12] are able to generate proteins with new affinities and/or activities ("functions"). These techniques may completely change protein affinity from one binding partner to another and speed up mutational processes occurring in nature randomly. On the other hand, these experimental techniques shed little light on the interaction itself and therefore have a limited use for explaining why binding has changed. In contrast, computational methods that take into account the structures and energetics of the interacting molecules can provide rational insight into physical nature of the process of intermolecular recognition. Recently, emerging complex approaches to protein design combine methods of computational rational design and directed evolution [13–15] to benefit from both these techniques [16].

The present work included computer modeling, tools of molecular biology, and biophysical measurements into an accessible protocol to predict and test mutations increasing affinity of a model protein, IFN-γ receptor 1, to its binding partner, IFN-γ. IFN-γ is an important molecule of innate and adaptive immune responses in vertebrates [20–23]. Receptor 1 of IFN-γ is a part of the signal pathway of IFN-γ that binds to cellular receptor 1 and formation of the complex induces subsequent aggregation with distinct receptor 2; the ternary complex between IFN-γ and its two receptors then activates the JAK/STAT signaling pathway leading to establishment of immune response. The role of IFN-γ in immune system is used in diagnosis of tuberculosis. Stimulated production of IFN-γ by antigens present exclusively in infectious *Mycobacterium tuberculosis* is used in the so-called interferon-gamma release assays (IGRAs) to diagnose latent tuberculosis infection (LTBI). Commercial kits such as QuantiFERON-TB Gold or T-SPOT.*TB* achieve sensitive detection of stimulated levels of IFN-γ by reaction with specific antibodies in ELISA-like arrangement. Current increase of latent TB and emergence of highly resistant strains of *M. tuberculosis* inspired investigation of alternative approaches to the testing that would be based on molecular systems more robust than currently used antibodies. Our previous work [24, 25] has indicated that a small protein scaffold albumin-binding domain (ABD) of protein G from *Streptococcus* G148 [26] trained against its target by ribosome display [12] is one possible alternative.

In this work, we decided to design high affinity IFN-γ binders based on a different protein molecule, the natural IFN-γ ligand, its receptor 1. Binding between IFN-γ and its receptor 1 occurring normally at the cellular membrane is also known to arise with the soluble extracellular portion of receptor 1 (hereafter labeled IFN-γ-Rx) [27, 28]. The existing crystal structures of the complexes [17, 29] and of the free human IFN-γ [30, 31] provided invaluable structural data to guide computational analysis. Mutations to modulate—increase as well as decrease—binding of IFN-γ-Rx to IFN-γ were searched for at the receptor residues forming the interface with IFN-γ and the interface receptor residues were subjected to computational mutational analysis by a modeling technique based on empirical force field. All 17 designed receptor mutants were then expressed, their affinities to IFN-γ were measured experimentally by surface plasmon resonance, and the predicted and the measured affinities were compared and discussed.

2. Materials and Methods

2.1. Selection of Amino Acid Mutations. The mutation analysis was based on analysis of the crystal structures of the complexes between the extracellular part of human interferon-γ receptor 1 (IFN-γ-Rx) and human IFN-γ, of PDB code 1fg9 [17] and 1fyh [29] contain five crystallographically independent molecules of IFN-γ-Rx in total; the asymmetric unit of 1fg9 contains three receptor molecules, but only two of them interact with IFN-γ; 1fyh has two receptor molecules interacting with IFN-γ. Therefore, there are four independent structures of the IFN-γ/IFN-γ-Rx complex. Potential mutations were searched for in the IFN-γ-Rx molecule, and the search was limited to its amino acid residues involved in direct interaction with IFN-γ. To make sure that all receptor residues potentially important for the interaction were included, we considered all residues within 6.0 Å from IFN-γ for mutations. A union of the four crystallographically unique interfaces consists of 40 receptor amino acid residues; they are depicted as wire models in Figure 1. The distances were calculated by the VMD program [32]. The variants potentially increasing the affinity of binding were selected by substituting the 40 residues of IFN-γ-Rx forming the interface with IFN-γ by the remaining 19 standard amino acid residues and calculating the changes of the interaction free energies, $\Delta\Delta G$. Mutations were calculated using the program FoldX (http://foldx.crg.es/) [33] independently for each of the four crystallographic interfaces, two from crystal structure 1fg9 and two from 1fyh. The crystal geometries were optimized and averaged by MD simulations independently for each interface. Two sets of calculations were run: the first set of $\Delta\Delta G$ values estimated the influence of mutations on the stability of the whole IFN-γ/IFN-γ-Rx complex, the second evaluated change of the interaction between the receptor molecule and the rest of the IFN-γ/IFN-γ-Rx complex. The protocol for these computations is summarized in the Supplementary Text 1 available online at http://dx.doi.org/10.1155/2013/752514.

2.2. Sequence Analysis. The alignment was performed on 32 IFN-γ receptor sequences from 19 species: 12 sequences of primates (six human sequences, six from other primates), 15 sequences from other mammals, three from birds, one amphibian, and one viral (the viral protein is not a cellular receptor but highly specific IFN-γ-binding protein). The list of their GenBank codes is in Supplementary Table S1. The global sequence alignment was calculated using the KAlign [18] algorithm as implemented in the program Ugene (http://ugene.unipro.ru/, [19]); the resulting consensus sequence is shown in Figure 2.

2.3. Molecular Dynamics (MD) of Wild-Type (WT) Complexes. MD simulations using the OpenMM [34] Zephyr [35] implementation of GPU accelerated version of GROMACS [36] suite of programs were used to test the stability, dynamic

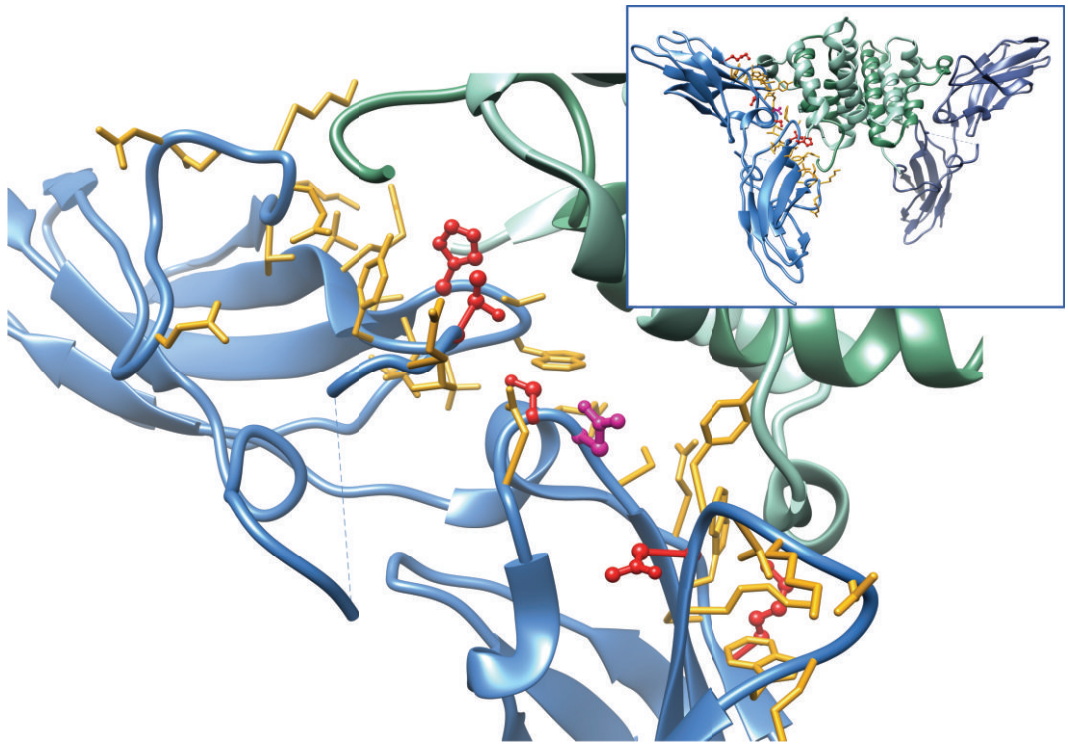

Figure 1: The interface between IFN-γ and the extracellular part of its receptor 1 (IFN-γ-Rx) from crystal structure 1fg9 [17]. Two IFN-γ-Rx molecules are drawn as blue cartoon and IFN-γ homodimer as green cartoon. The receptor residues forming the interface with IFN-γ are drawn as yellow sticks, the residues selected for mutations are highlighted in red, and the residue N96 in magenta. All the selected mutations are listed in Table 2.

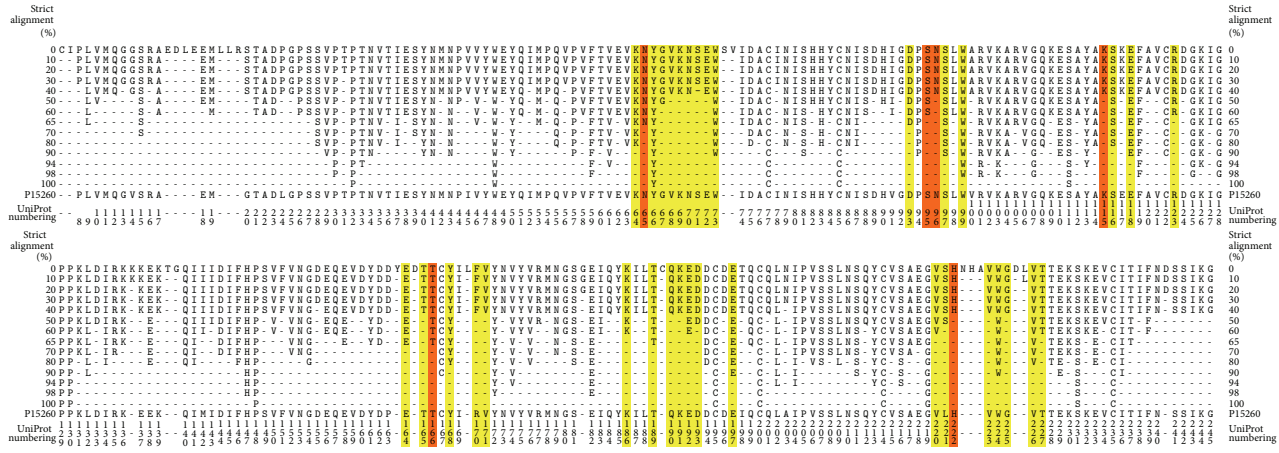

Figure 2: Conserved residues calculated by strict alignment of 32 sequences of the extracellular part of IFN-γ receptor 1 from 19 species. The receptor residues forming the interface with IFN-γ (i.e., residues no further than 6 Å from an IFN-γ atom) are highlighted in yellow; the residues selected for mutations are in red. All the selected mutations are listed in Table 2. Percentages of the conservation are shown on the left and right sides, sequence and numbering of UniProt P15260 on the bottom. Sequences used for the alignment are listed in Table S1. Numbering of the PDB entry 1fg9 can be derived from the UniProt one by subtracting 17. The alignment was computed by KAlign [18] as implemented in program Ugene [19].

properties, and interaction free energies (ΔG) of the IFN-γ/IFN-γ-Rx complexes. The chains A, B, C, and D of the PDB structure 1fg9 and chains A, B, D, and E of the PDB structure 1fyh were used in the simulations. Missing residues were added using the Modeller suite of programs [37]; the pdb2gmx program using parameters provided by the Zephyr program determined ionization state. All MD simulations were performed using the following setup. Implicit solvation (GBSA, $\varepsilon = 78.3$, with collision interval of 10.99 fs) was used in combination with parm96 force field [38]. The initial

IFN-γ/IFN-γ-Rx WT structure was optimized and the simulation was propagated at 300 K with time step of 2 fs. Snapshots of the geometry were saved every 10 ps throughout the simulation.

In order to test the stability of various structural predictions, we performed several MD simulations of the WT as well as mutated IFN-γ/IFN-γ-Rx complexes. Three simulations of the WT complex consisted of a 100 ns MD run of the chains A, B, C, and D from 1fg9, which contain two interfaces, and two 20 ns runs for structure 1fyh, one for chains A, B and the other for chains D, E. These simulations demonstrated the stability of geometries of the crystal structures during the simulation. In the course of 100 ns 1fg9 simulation, instantaneous $\Delta\Delta G$ values of one IFN-γ/IFN-γ-Rx interface switched to the value of the other interface and *vice versa*, suggesting sufficient sampling of the hypersurface of the free energy. For all the seventeen mutants, at least 10 ns MD simulations were run. They served as a reference for comparisons between calculated and measured affinities and to monitor the structural changes between the original crystal structures and the isolated solvated complexes.

To check the theoretical stability of the mutated receptor molecules, 20 ns MD simulations of their complexes with IFN-γ were performed; simulations were conducted according to the same protocol as for the WT complexes. The interaction ΔGs of the complexes were recalculated using FoldX on 1,000 snapshot structures from the converged second half of each MD simulation. The resulting values were used for comparison with the experimentally determined dissociation constants of the mutants.

2.4. Construction, Expression, and Purification of Recombinant Proteins. Codon-optimized synthetic open reading frame (ORF) encoding the residues 18 to 245 (P15260) of the extracellular domain of human IFN-γ-Rx was purchased from GenScript (Piscataway, NJ, USA). The ORF was cloned in frame as an *NcoI-XhoI* fragment into the pET-28b(+) vector (Novagen), resulting in the addition of N-terminal methionine (M*EMGT*) and C-terminal 6x His purification tag extension (*SIKG*LEHHHHHH). Residue mutations were introduced using the QuikChange II Site-Directed Mutagenesis Kit (Agilent Technologies) according to the manufacturer's protocol using the mutagenesis primers listed in Supplementary Table S2. All constructs were verified by DNA sequencing.

The recombinant receptor proteins were produced in *Escherichia coli* BL21(λDE3) (Novagen) at 37°C in LB medium containing 60 μg/mL of kanamycin for 4 hours after induction by 1 mM IPTG. Cells were harvested by centrifugation (8,000 g, 10 min, 4°C), disrupted by ultrasound in 50 mM Tris buffer pH 8, and the protein was extracted from inclusion bodies in buffer A and affinity-purified close to homogeneity on Ni-NTA agarose (Qiagen). The receptor domain was eluted with 250 mM imidazole in buffer A (pH 8), refolded from urea by dialysis against 100 mM Tris-Cl pH 8, 150 mM NaCl, 2.5 mM EDTA, 0.5 mM cystamine, and 2.5 mM cysteamine overnight at 4°C. Monomeric refolded receptor protein was separated from aggregates and purified to homogeneity on a Superdex 200 10/300 GL (GE Healthcare) column run in PBS buffer pH 7.4 at 4°C (Figure 3). Monodispersity of the purified receptor protein was verified by dynamic light scattering (DLS) using Malvern Zetasizer Nano ZS90.

Human natural IFN-γ is a homodimeric glycoprotein [39–41], but glycosylation is dispensable for its biological activity [42]. Interferon-γ used in all analyses here was produced as a recombinant protein in the so-called single-chain form (IFN-γ-SC). The variant with the sequence taken from the previous report [31] was cloned in frame as an *NdeI-XhoI* fragment containing the stop codon into the pET-26b(+) vector (Novagen) and produced in *Escherichia coli* BL21(λDE3). The cells were disrupted by ultrasound in buffer B (20 mM sodium phosphate buffer pH 7) and IFN-γ-SC was purified from the soluble cytoplasmic fraction on SP sepharose HP (GE Healthcare) equilibrated in buffer B using a linear gradient of NaCl.

2.5. Measurement of the Thermal Stabilities of the Mutants and WT. Protein melting temperature (Tm) was determined by fluorescence-based thermal shift assay (TSA) using fluoroprobe SYPRO Orange dye (Sigma Aldrich). The TSA was performed in "CFX96 Touch Real-Time PCR Detection System" (Bio-Rad) using FRET Scan Mode. The final volume of assay was 25 μL, concentrations of IFN-γ-R variants 3 μM, and dye at 8-fold dilution from 5000-fold stock. The reference was dye in assay buffer (PBS buffer pH 7.4) without protein. Samples in capped "Low Tube Strips, CLR" (Bio-Rad) were spun down immediately before the assay to remove possible air bubbles. For thermal denaturation, the samples were heated from 20°C to 75°C with stepwise increment of 0.5°C per minute and a 30 s hold step for every point, followed by the fluorescence reading. Reference subtracted data were normalized and used for first derivative calculation to estimate the melting temperature.

2.6. Measurement of the Interaction between IFN-γ and Its Receptor. Interactions between IFN-γ-Rx variants and IFN-γ-SC were measured by the technique of surface plasmon resonance (SPR) using the "ProteOn XPR36" instrument (Bio-Rad) on a HTG sensor chip with surface activated with Ni^{2+} cations (10 mM $NiSO_4$, 10 mM MES pH 6). His-tagged receptor molecules were diluted to concentration 10 μg/mL in PBST running buffer (PBS pH 7.4, 0.005% Tween20) and immobilized at a flow rate of 30 μL/min for 60 s. Purified IFN-γ-SC was diluted in PBST running buffer to concentrations ranging from 1.2 to 99 nM and passed over the sensor chip. Association of IFN-γ-SC with receptors was adjusted to 90 seconds at a flow rate of 100 μL/min and dissociation occurred in PBST running buffer for 10 min at the same flow rate. His-tagged Fe-regulated protein D (FrpD) from *Neisseria meningitidis* [43] was used as a negative control in the reference channel. The signal was corrected for nonspecific binding of the protein to the chip surface by subtraction of the response measured on uncoated interspots and in the reference channel. The doubly referenced data were analyzed and fitted to the 1 : 1 "Langmuir with drift" binding model using

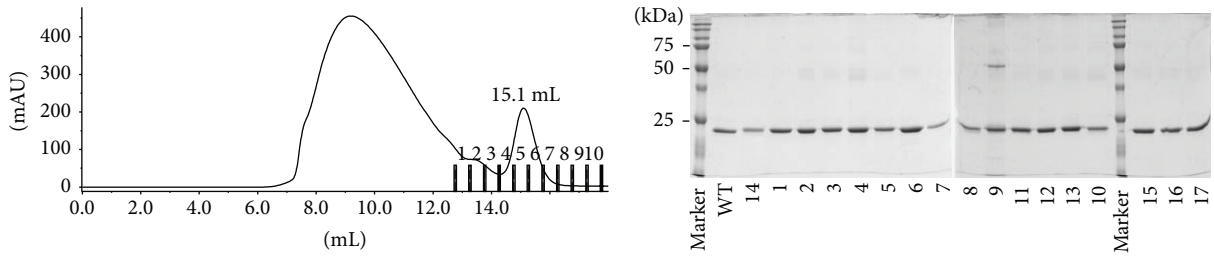

Figure 3: Purification of monomeric refolded recombinant 6xHis-tagged IFN-γ-Rx protein. (a) Typical chromatogram from separation of affinity-purified and refolded IFN-γ-Rx variants by gel permeation chromatography on Superdex 200 10/300 GL as described in Section 2. Fraction 6, containing the monomeric forms of refolded IFN-γ-Rx, was used for SPR measurements. (b) Analysis of purified soluble IFN-γ-Rx on 12.5% SDS-PAGE under nonreducing conditions. Proteins were extracted in 8 M urea from inclusion bodies and purified by metal affinity chromatography on Ni-NTA agarose as described in Section 2. Upon refolding by dialysis against urea-free buffer the monomeric fraction was separated as outlined above. IFN-γ-Rx with C-terminal His-Tag migrates at a molecular mass of 23 kDa when analyzed on non-reducing and at 27 kDa on reducing SDS-PAGE (not shown). Protein constructs are numbered as in Table 2.

ProteOn Manager version 3.1.0.6 software. Regeneration of the HTG sensor chip was accomplished using 300 mM EDTA pH 8.5. Reported SPR affinities were measured at 25°C.

3. Results and Discussion

3.1. Analysis of the Crystal Structures. The mutation analysis IFN-γ-Rx was limited to 40 amino acid residues that were identified as closer to 6.0 Å from IFN-γ in the crystal structures of IFN-γ/IFN-γ-R1 complexes (PDB codes 1fg9 [17] and 1fyh [29]). Table 1 compares root mean square deviations (rmsd) between the main chain atoms of these 40 residues at the interface and 40 randomly selected residues outside the interface and shows that all four IFN-γ-Rx molecules are quite similar: the residues involved in direct interaction with IFN-γ deviate from the reference chain D of 1fg9 by less than 0.5 Å, residues outside the interface by less than 2 Å. Notably, the structure of the receptor molecule, which is not in direct interaction with IFN-γ (chain E in 1fg9), differs from the other receptor molecules by more than 4 Å, significantly more than they differ from each other. Therefore, recognition between IFN-γ and its receptor 1 is likely to narrow conformational space available for the receptor molecule, a feature advantageous for the modeling effort.

Table 1: Structural similarity of the IFN-γ receptor molecules (IFN-γ-Rx) at and outside the interface with IFN-γ. Four receptor chains from crystal structures 1fg9 [17] and 1fyh [29] are compared to receptor chain D of 1fg9.

PDB	rmsd (Å)[a]	rmsd (Å)[b]
Code:chain	40 interface residues	40 random residues
1fg9:C	0.60	1.66
1fg9:E	4.16	4.32
1fyh:B	0.58	1.42
1fyh:E	0.59	1.06

[a]Root mean square deviations (rmsd) between the four IFN-γ-Rx molecules (labeled PDB_ID:chain) and the chain D of 1fg9. Deviations are calculated between the positions of the main chain atoms of the 40 residues forming the interface with IFN-γ.

[b]Root mean square deviations (rmsd) between the four IFN-γ-Rx molecules (labeled PDB_ID:chain) and the chain D of 1fg9. Deviations are calculated between the positions of the main chain atoms randomly selected outside the 40 residues forming the interface with IFN-γ.

3.2. In Silico Design of Mutants. To identify mutations increasing the affinity of IFN-γ-Rx to IFN-γ, we replaced each of the 40 receptor interface residues by the remaining 19 natural amino acids and calculated two types of changes of free energy ($\Delta\Delta G$) using the web-based program FoldX [33]. First, we estimated the stability of the mutated receptor by calculating $\Delta\Delta G$ in the complex. These $\Delta\Delta G$ values estimate the stability of the receptor molecules. Next, we tested how the receptor mutations change binding to IFN-γ and these $\Delta\Delta G$ gauge the change of affinity. Two example matrices of $\Delta\Delta G$ values are in Supplementary Table S3. Because the calculated $\Delta\Delta G$ values may differ between the four crystallographic interfaces, both types of the interacting matrices were independently calculated for all four interfaces. The differences between the corresponding $\Delta\Delta G$ values in the four stability and four affinity matrices are however not large because the four receptor molecules interacting with IFN-γ are structurally similar (Table 1).

Favorable (i.e., negative) stability and affinity $\Delta\Delta G$ values calculated for all four interfaces indicated promising mutations. This energy-based criterion for selection of mutants was supplemented by considering conservation of the receptor sequences in various species to avoid mutating the most preserved residues that may carry significant structural or functional role. Residues that were identified as conserved in more than 65% of 32 IFN-γ receptor sequences from 19 species (Figure 2, Supplementary Table S1) were not considered for mutations. By combining the criteria of energy stabilization and sequence variability, we selected nine most promising mutations (Table 2).

In addition to these nine single amino acid mutations, we decided to evaluate the additive effects of introduction of multiple mutants. Therefore, three mutations, N70G, S95R,

Table 2: Calculated and experimental values of the changes of free energy, $\Delta\Delta G$, of the interaction between IFN-γ-Rx mutants and IFN-γ-SC relative to the wild-type receptor.

Construct		The best $\Delta\Delta G$[c]	$\Delta\Delta G$ from MD[d]	Experimental $\Delta\Delta G$[e]	esd[f]
ID[a]	Mutation[b]	(kJ/mol)	(kJ/mol)	(kJ/mol)	(kJ/mol)
1	N65R	−5.4	17.3	2.1	—
2	N70G	−5.4	0.3	−0.6	—
3	S95R	−8.3	11.8	2.1	—
4	N96F	−13.0	−0.6	−0.2	—
5	N96W	−9.9	−6.1	−3.9	0.2
6	K115Y	−0.3	−9.6	0.7	—
7	T166M	−5.8	−5.4	2.0	—
8	T166Y	−9.8	0.9	2.5	—
9	H222R	−6.9	−15.8	−0.1	0.2
10	N96W + H222R	−7.1	−7.1	−5.0	0.2
11	N70G + S95R	−7.3	2.7	1.5	—
12	N70G + H222R	−4.6	−7.3	−0.3	—
13	S95R + H222R	−11.4	−10.8	1.5	—
14	N70G + S95R + H222R	−15.8	−5.6	0.5	0.1
15	Y66L	2.1	11.8	0.0	—
16	S71E	9.6	19.6	1.6	—
17	H222D	6.7	5.8	2.0	—

[a]Mutants 1–14 are single, double, and triple mutants designed to increase affinity to IFN-γ compared to WT. Mutants 15–17 were designed to lower the affinity between IFN-γ and IFN-γ-Rx but not to destabilize the unbound IFN-γ-Rx.

[b]Residues are numbered as in the UniProt entry P15260.

[c]For mutants 1–14, the most negative (most stabilizing) values obtained at the four crystal interfaces by FoldX [33]. For mutants 15–17, the $\Delta\Delta G$ listed are for the least positive (least destabilizing) interface.

[d]Averaged $\Delta\Delta G$ values calculated by FoldX on structures taken from snapshots of 10 to 20 ns MD runs by GROMACS [36].

[e]$\Delta\Delta G$ values determined from experimental SPR values of dissociation equilibrium constants K_d as $\Delta\Delta G = -RT \ln\{(K_d)_{WT}/(K_d)_{mut}\}$.

[f]Estimated standard deviations for the experimental values of $\Delta\Delta G$ with the number of independent SPR measurements $N > 2$ (Table 3).

and H222R, which were predicted to stabilize the interface significantly and are distant from each other, were combined into one triple and three double mutants so that all seven possible mutual combinations of the three mutations were studied. These selected mutants are schematically depicted in Figures 1 and 2 and listed in Table 2 under numbers 1–14.

All but one receptor constructs were designed prior to any experimental determination of their affinities. The only "second-generation" variant is the double mutant N96W + H222R (number 10 in Table 2) that was expressed because the single mutant N96W had a high experimental affinity and H222R showed neutral binding behavior, while these two single mutations are sequentially distant so that we assumed that they might influence each other the least.

3.3. Experimental Determination of the Affinities of the Mutants. All mutants proposed for construction (Table 2) were expressed, purified, and refolded making use of the protocol developed for the wild-type (WT) IFN-γ-Rx as described in Section 2. Affinities of WT and all mutants to a single-chain variant of IFN-γ (IFN-γ-SC, see Section 2 were measured by SPR. The SPR data are summarized in Table 3.

The mutants can be qualitatively divided into three groups. First, those that have higher affinity (lower K_d values) compared to the WT receptor, second, mutants with affinity close to that of WT, and third, mutants with affinity lower than WT (higher K_d values). A significant, about five-fold, increase of affinity compared to WT was observed for two mutants: N96W and N96W + H222R. A large group of mutants have their K_d values close to those of WT, for example, mutants N70G, N96F, and the triple mutant. From the formal statistical point of view, some of these K_d values may be significantly different from the values for WT, but the biological relevance of these changes is negligible. Finally, a few mutants, for example, N65R, S95R, or T166Y, have their affinities about two to three times lower than that of WT.

To test whether sequentially and spatially distant mutations affect the binding to IFN-γ-SC independently or in accord, three single mutations, N70G, S95R, and H222R, which were about 25 amino acids apart in sequence and more than 20 Å apart in 3D space, were combined to produce three double and one triple mutants. The cooperativity of mutations was checked by comparing the changes of experimental binding affinities ($\Delta\Delta G$) for the seven mutants in the series. Data in Table 2 show that experimental values of $\Delta\Delta G$ of the double mutants are approximately the sum of contributions from the single mutants and $\Delta\Delta G$ of the triple mutant is the sum of the values for the three single mutants. In general, the interplay of multiple mutations cannot be ruled out as nonadditive energetic effects have been observed for mutations at positions separated by more

Table 3: Affinity between IFN-γ-SC and IFN-γ-Rx mutants was predicted to increase affinity measured by surface plasmon resonance (SPR).

Construct		$k_a * 10^{-6}$	$k_d * 10^2$	K_d	N^e	esd (K_d)
ID	Mutation[a]	(1/Ms)[b]	(1/s)[c]	(nM)[d]		(nM)[f]
WT	—	1.24	3.78	30.8	14	1.5
1	N65R	0.882	6.28	71.2	1	na
2	N70G	1.12	2.64	23.6	1	na
3	S95R	0.650	4.54	69.8	2	na
4	N96F	1.01	2.83	28.0	1	na
5	N96W	1.43	0.909	6.34	4	0.49
6	K115Y	0.979	3.91	39.9	1	na
7	T166M	0.933	6.39	68.5	1	na
8	T166Y	0.940	7.82	83.1	1	na
9	H222R	1.19	3.49	29.4	6	1.9
10	N96W + H222R	2.40	1.00	4.16	3	0.37
11	N70G + S95R	0.889	4.94	55.9	2	na
12	N70G + H222R	1.46	3.91	26.9	2	na
13	S95R + H222R	1.05	5.90	56.3	2	na
14	N70G + S95R + H222R	1.09	4.01	37.0	5	2.1

[a]Residues are numbered as in UniProt P15260.
[b]Kinetic constant of association, k_a.
[c]Kinetic constant of dissociation, k_d.
[d]Dissociation equilibrium constants K_d calculated as k_d/k_a.
[e]Number of independent SPR measurements.
[f]Values of the estimated standard deviation (esd) of K_d are shown for mutants with three and more measurements (listed in column N).
Confidence limits calculated from the Students t-distribution at the 95% level are ±0.85, ±0.78, ±1.9, ±0.93, and ±2.6 nM for WT, N96W, H222R, N96W + H222R, and N70G + S95R + H222R, respectively.

than 9 Å [44]. In that study, association and dissociation rates have had the opposite effects on the overall nonadditivity of the mutants: association has been responsible for the cooperativity, while dissociation for the anticooperativity (less-than-additive energetics).

To monitor nonrandomness of predictions to *increase* the receptor affinity to IFN-γ, we selected a smaller set of variants that were predicted to *lower* the receptor affinity. To find these mutants, we searched for $\Delta\Delta G$ lowering the affinity but still increasing the stability of the receptor molecule itself. Three selected mutants are listed in Table 2 under numbers 15–17. The dissociation constants of mutants H222D and S71E are about two times lower than K_d of WT (2.2 and 2.0 times, resp.); the third mutant, Y66L, has about the same affinity as WT. These experimental K_d values thus support the general applicability of the computer predictions and the ability of our computer modeling protocol to suggest mutations that lead to the desired effects, be it affinity increase or decrease.

Our best single mutant (N96W) increases the binding free energy by about 5 kJ/mol; the corresponding decrease of K_d is about fivefold; binding improvement is generally comparable to other studies. A recent study has enhanced affinity of an antibody fragment to the I-domain of the integrin VLA1 [45] by about an order of magnitude by mutating four residues at the antibody part of the interface. Similarly, five amino acid substitutions increased affinity between integrin antigen LFA-1 and its ligand about twentyfold [46]. Single amino acid substitutions in decoy receptor TLR4 constructed of leucine-rich repeats increased affinity to myeloid differentiation protein 2 about tenfold [47]. Interestingly, this study reports high cooperativity among the single mutations as the affinity of double mutants has been reported up to a thousand-times higher compared to WT. Computer model of binding between acetylcholine esterase and its inhibitor fasciculin [48] has predicted that increase of affinity can be achieved by mutating five interface fasciculin residues. However, to achieve a better binding, at least one of the five mutations had to be scrapped and actually the tightest interaction (sevenfold increase) occurred with just one of the originally designed mutations. Using the same software, ORBIT, binding between peptides derived from myosin light chain kinase and calmodulin was modeled [49], and similarly to the previously mentioned study, some predicted mutations led to increase but others to decrease of affinity.

Despite the complicated nature of protein-protein interactions, a few general rules have been drawn from these and other studies: polar residues replacing hydrophobic ones destabilize complex formation and replacement of charged by hydrophobic residues increases binding [50].

Considering that the presented protocol was based on a straightforward geometric analysis of the crystal interface and the changes of the interaction free energy were estimated by an empirical force field containing many simplifications, a decrease of affinity in about a half of mutants designed to increase the affinity is not surprising, especially in the light of simplicity of the computational methods and complexity

of the system. In our opinion, a drawback of the computer-driven rational design based on energy calculations stems from a different fact than is the ratio between true and false positives: since many predictions of stabilizing mutations are incorrect, we should expect not only false positive but also the false negative error (type II error), $\Delta\Delta G$ values of stabilizing mutations calculated incorrectly as destabilizing. Because false negative predictions are never tested, computer predictions may miss mutations that would stabilize the complex more than any of the actually selected and tested mutants. This disadvantage does not exist in experimental protocols, such as ribosome display, that not only scan an incomparably larger portion of the overall sequence space, but also scan it without any prejudice. Regardless of its limits, *in silico* design of mutations increasing affinity between ligand and its receptor can be a useful tool because ligand-receptor interactions do not evolve for the maximal affinity but for affinity optimal to enable proper signalization. It is therefore likely that interfaces of most ligand-receptor complexes can be modified to increase their affinity.

3.4. Biochemical and Statistical Significance of the SPR Data. SPR measurements for WT and most receptor variants were repeated to test reproducibility (or rather repeatability) of the data. The data listed in Table 3 were measured on three different SPR chips and anchored receptor molecules originated from different batches but always using one batch of IFN-γ-SC. Measurements under these conditions are reliable and sufficiently accurate as is demonstrated by estimated standard deviations of the K_d values between 4 and 9%. The formal statistical significance of the differences between K_d values of the mutants and WT is given in Supplementary Text 2. The average value of K_d of WT receptor was determined as 30.8 ± 0.9 nM in our SPR experiments (Table 3). This value agrees well with the literary value 27 ± 9 nM determined by isothermal titration calorimetry for interaction between recombinant IFN-γ-SC and IFN-γ-Rx also at 25°C but in a different buffer (10 mM Pipes at pH 7.1, 150 mM NaCl) [31].

Dissociation constants of two variants can be used to calculate the changes of Gibbs energy of their interaction; for dissociation constants of WT $(K_d)_{\mathrm{WT}}$ and a mutant $(K_d)_{\mathrm{mut}}$:

$$\begin{aligned}\Delta\Delta G &= -\mathrm{RT}\,\ln\left(K_d\right)_{\mathrm{mut}} - \left\{-\mathrm{RT}\,\ln\left(K_d\right)_{\mathrm{WT}}\right\} \\ &= -\mathrm{RT}\,\ln\left\{\frac{\left(K_d\right)_{\mathrm{WT}}}{\left(K_d\right)_{\mathrm{mut}}}\right\}.\end{aligned} \tag{1}$$

The experimental $\Delta\Delta G$ values in Table 2 were calculated from K_d values measured using the same batch of IFN-γ-SC for each particular pair of WT and a mutant (see Supplementary Text 2). When the $\Delta\Delta G$ values were calculated from measurements using four different batches of IFN-γ-SC (but always the same batch for WT and a mutant), their mean values agreed with the values of the single-batch measurement but the uncertainty limits grew. Direct comparison of $\Delta\Delta G$ values obtained from measurements using different batches of IFN-γ-SC is thus less reliable. For two mutants N70G and N96W, the average $\Delta\Delta G$ and uncertainty limits were −0.7 ± 0.7 and −3.7 ± 1.0 kJ/mol, respectively.

3.5. Kinetics and Equilibrium of Binding. Table 3 shows that the mutants associate with IFN-γ-SC with similar kinetics (measured by association rate constant, k_a) but for most, the fast association is followed by fast dissociation (dissociation rate constant, k_d). However, the two mutants with significantly increased affinity to IFN-γ-SC, N96W, and N96W + H222R, dissociate much more slowly. Their kinetic behavior distinguishes them from the other mutants as illustrated in Figure 4, which compares the SPR interaction curves of two receptor mutants exhibiting fast release and one of the high-affinity mutants N96W with much slower release of IFN-γ-SC. Considering the formula to calculate dissociation equilibrium constant, $K_d = k_d/k_a$, the slower off-rates of mutants N96W and N96W + H222R, that is, smaller values of k_d, explain a large part of the increase of their higher affinity to IFN-γ-SC (lower values of K_d). The process of dissociation distinguishes these two mutants from the other receptor constructs and they are thus interesting not only for their thermodynamic properties, affinity, but also for the different kinetic characteristics of the interaction. In this context, the ability of SPR technique to determine kinetics of binding is crucial. The potential of this technique has been used to explain affinity between 14 mutations of an antibody and lysozyme [51] and to provide information about chemical aspects of this interaction.

Both alternate strategies for affinity increase, one based on faster binding, the other on a slower release of the complexed molecules, have been reported. Clark et al. [45] and this study reported increased affinity caused by a slower dissociation; other studies [52–55] have reported that the affinity increase of mutants is caused by higher rates of association rather than slower dissociation. Faster association has been attributed to increased electrostatic attraction between the binding partners, for example, for binding between TEM1 beta-lactamase and its protein inhibitor BLIP [53], but it can also originate from mutations of noninterfacial residues as in study [54]. Optimization of electrostatic contributions for protein-protein interactions has been recently reviewed [56].

The importance of kinetic effects in forming IFN-γ/IFN-γ-Rx complexes is indirectly supported by failure of PISA [57] to recognize the biologically "correct" complexes in both 1fg9 and 1fyh. PISA is a computer method estimating the stability of macromolecular interfaces from their crystal structures. It should be stressed that it is generally highly successful in discerning interactions stable in solution from "nonspecific" crystal-forming interfaces but in case of IFN-γ complexes, PISA recognizes correctly biological unit of only one, that formed with viral IFN-γ binding protein, PDB code 3bes [58]. In this case, rigidity of the receptor-like molecule and avidity of the interaction strengthen the binding. Stiffening of the interacting molecule(s) may be an alternative search strategy for high-affinity mutants as has been convincingly illustrated by the design of a "superkine" protein molecule [59].

3.6. Structure and Binding. Design of high-affinity mutants by computer-driven design relies on structural information. The knowledge of experimental structure even at a relatively low crystallographic resolution around 3 Å provides firm

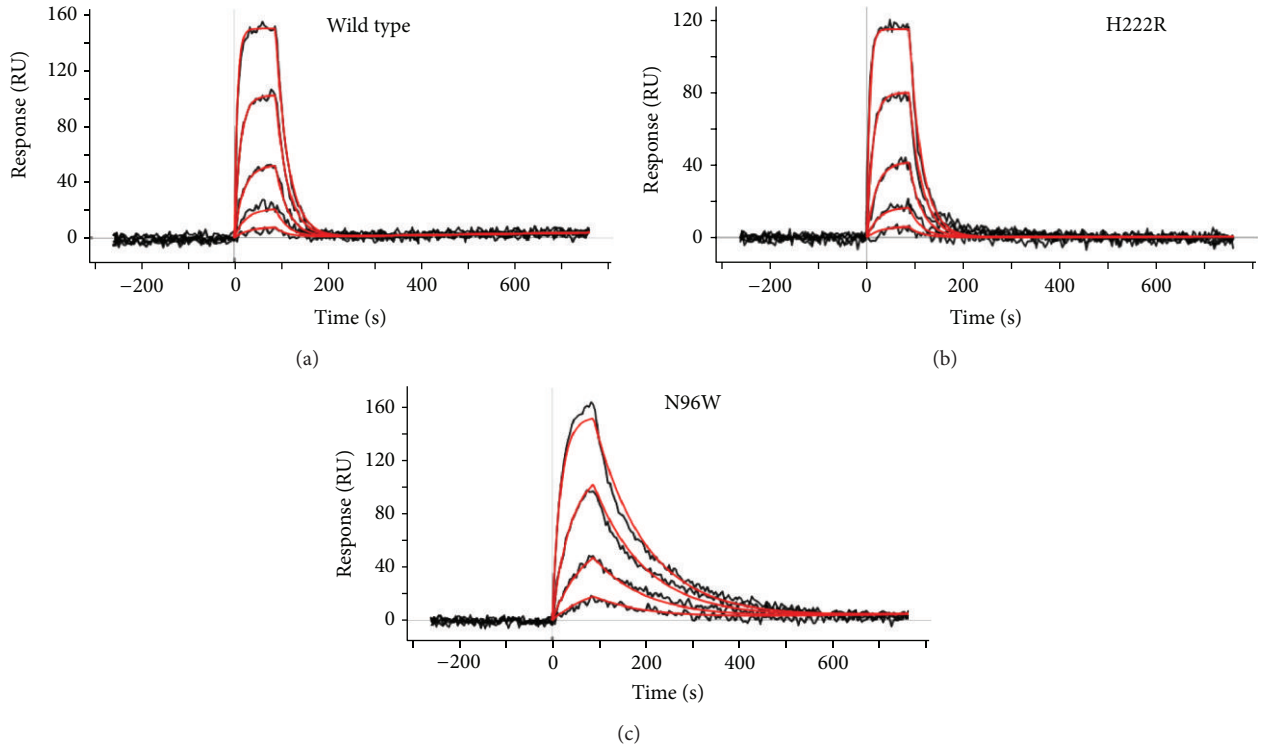

Figure 4: Association and dissociation curves of the SPR experiments. Most IFN-γ-Rx variants behave similarly as the wild-type (a) and mutant H222R (b): they bind IFN-γ-SC very fast but also release it fast. Two high-affinity binders, mutant N96W (c) and the double mutant N96W+H222R, bind the IFN-γ-SC molecules for a longer time, thus increasing the affinity to IFN-γ. The SPR experimental signal is in black; the fitted curves from which the association and dissociation kinetic constants are calculated are in red. The SPR data for all variants are in Table 3.

constraints for search of energetically favorable replacements and removes unavoidable uncertainty of computer-predicted structural models. Structural variations between crystal structures allow estimating the extent of flexibility of the molecules. The small differences between the four crystallographically independent structures of the IFN-γ/IFN-γ-Rx complex observed in structures 1fg9 [17] and 1fyh [29] (Table 1) indicate that the structural variations can be expected to be relatively small and that the energy computations, which are sensitive to structural variances, may be expected to provide reliable estimates. Structure of the third receptor molecule observed in structure 1fg9 that is not considered to be biologically relevant [17] differs from the structures of two complexed receptors.

The structural explanation of the increased affinity of the two high-affinity variants N96W and N96W + H222R is not straightforward. Based on snapshots from the MD simulations, the replacement of asparagine by tryptophan does not generate easily identifiable interactions such as hydrogen bonds or stacking between the tryptophan aromatic ring of its –N(H)– group and the rest of the receptor molecule or nearby atoms of IFN-γ-SC. On the contrary, one H-bond present in the WT complex is actually weakened. Surprisingly, instead of the expected stiffening of the nearby groups, the bulky tryptophan increased the mobility of several receptor residues, namely, N65 and Y66; values of their root mean square fluctuation grew by a factor of three. The only obvious stabilizing effect of a large tryptophan residue compared to a smaller asparagine is a larger number of van der Waals contacts it forms. We hypothesize that the higher stability of the complex, namely, its longer dissociation compared to WT, is driven by the entropic destabilization of a large tryptophan residue when it is exposed to the aqueous environment. The hydrophobic destabilization at the position 96 and the related increased flexibility of the receptor molecule suggested by the MD simulations for the N96W mutants help to rationalize their measured lower melting temperatures compared to WT. They were estimated to be 55°C for IFN-γ-Rx WT, 48°C for N96W, and 47°C for N96W + H222R (curves of thermal stabilities are in Supplementary Figure S1). The increase of flexibility at the interface of the complex suggests that ignoring entropic contribution to free energy [60] is not a generally acceptable approach. Better understanding of the stabilization effect of the tryptophan at the receptor position 96 clearly requires further study, at least reliably characterized temperature dependency of K_d values; our data acquired using receptor molecules anchored on the Ni^{2+}-coated HTG SPR chip (Supplementary Table S4) serve as initial estimates of the full thermodynamic description of the IFN-γ-SC/IFN-γ-Rx system.

3.7. Comparison between Computer-Predicted and Experimental Affinities. Table 2 summarizes the values of changes of

binding free energies, $\Delta\Delta G$ from the initial FoldX calculations (used to make predictions), averages from the FoldX calculations on a thousand MD snapshots, and from the SPR measurements. The most noticeable difference between the calculated and experimental values seems to be the scale: computer predictions clearly overestimated the magnitude of $\Delta\Delta G$s. Comparison between $\Delta\Delta G$ values calculated by FoldX for the initial structure and the values averaged over the MD snapshots indicated large differences; the values shifted for example, from −5 to +17 for N65R or from −13 to −0.6 for N96F.

After comparing FoldX calculated values of $\Delta\Delta G$ at the four crystallographic interfaces, we observed large fluctuations in several components of the FoldX force field, especially in the solvation and electrostatic contributions (data not shown). Considering relatively small structural variations between the individual crystal interfaces, we suggest that the Achilles heel of the predictions is a limited accuracy of modeling of solvation effects, the equilibrium between charged and uncharged states, and the contribution of polarizability of large ionized particles including amino acid residues. The computations are also likely underestimating (or systematically neglecting) possible mutation-induced rearrangements of the backbone. FoldX potential is likely to overestimate interaction energy of charged arginine as it repeatedly suggested to mutate different residues to R (N65R, S95R, and H222R). All these suggested mutations to arginine are incorrect in the light of the experimental results regardless whether they were predicted as stabilizing or destabilizing by the MD calculations. However, the overall performance of the FoldX force field was satisfactory especially in the light of a recent report that no empirical potential predicts correctly all types of interaction [61].

Perhaps surprisingly, $\Delta\Delta G$ values based on the 10–20 ns MD simulations, which are sufficient to rearrange the backbone, did not offer any systematic improvement of the agreement with the experimental $\Delta\Delta G$ values over the FoldX predictions on either the crystal structure or on the averaged MD structures. Computationally more demanding MD data shifted the $\Delta\Delta G$ values in both directions, closer to the experimental values as in the case of N65R, S95R, and N96F, but also off them, as for mutants of K115Y and H222R. Despite the currently prevailing opinion that long MD simulations are indispensible for reliable description of molecular systems and prediction of affinity modulation [62], we conclude that for the purpose of mutant design, predictions based on simply relaxed crystal structure can be as reliable as predictions based on much more laborious and expensive calculations. Also other authors [60] have observed that full MD simulation is not more successful in prediction of mutants than simpler approaches, and that the inclusion of nonlocal flexibility of the to-be mutated protein structure led to a higher number of false positive predictions [45].

4. Conclusions

In the present work, we used a generally applicable computer protocol to identify mutations increasing binding of two proteins and applied it to increase affinity of the extracellular domain of human interferon-γ receptor 1 (IFN-γ-Rx) to its natural ligand IFN-γ. The best mutant had affinity five times larger than the wild-type receptor. The computer-aided protocol was based on analysis of available crystal structures 1fg9 [17] and 1fyh [29], consideration of sequence conservation among 32 receptor sequences from 19 species, and free energy calculations by a web-based empirical force field FoldX [33]. We designed nine single-site mutants, five double, and one triple mutant. All these mutants were expressed as recombinant proteins in *Escherichia coli*, purified, and refolded, and their affinities to recombinant IFN-γ were measured by surface plasmon resonance (SPR) with IFN-γ as analyte and IFN-γ-Rx anchored to the surface of the chip. Table 3 shows that of nine single mutants selected for the analysis, one, N96W, exhibits about fivefold increase of affinity to IFN-γ compared to WT receptor (the corresponding $\Delta\Delta G$ is −5 kJ/mol). In addition, one double mutant combining two single mutations (N96W + H222R) showed a similar increase of affinity, likely brought about also by the N96W mutation. The higher affinity of the variants containing the N96W mutation was a consequence of their slower rate of dissociation (off-rates) than that observed for WT, the association rates (on-rates) of WT and all mutants were about the same.

The results demonstrate that computer-aided design of single-site amino acid mutations is an applicable strategy to increase binding between two complex proteins with already highly optimized interface and affinity in the nanomolar range.

Acknowledgments

Support from the Czech Science Foundation (Grant P305/10/2184) and the institutional Grant AV0Z50520701 are greatly acknowledged.

References

[1] C. M. Kraemer-Pecore, A. M. Wollacott, and J. R. Desjarlais, "Computational protein design," *Current Opinion in Chemical Biology*, vol. 5, no. 6, pp. 690–695, 2001.

[2] T. Kortemme and D. Baker, "Computational design of protein-protein interactions," *Current Opinion in Chemical Biology*, vol. 8, no. 1, pp. 91–97, 2004.

[3] D. Reichmann, O. Rahat, M. Cohen, H. Neuvirth, and G. Schreiber, "The molecular architecture of protein-protein binding sites," *Current Opinion in Structural Biology*, vol. 17, no. 1, pp. 67–76, 2007.

[4] D. J. Mandell and T. Kortemme, "Computer-aided design of functional protein interactions," *Nature Chemical Biology*, vol. 5, no. 11, pp. 797–807, 2009.

[5] J. Karanicolas and B. Kuhlman, "Computational design of affinity and specificity at protein-protein interfaces," *Current Opinion in Structural Biology*, vol. 19, no. 4, pp. 458–463, 2009.

[6] C. A. Smith and T. Kortemme, "Predicting the tolerated sequences for proteins and protein interfaces using rosettabackrub flexible backbone design," *PLoS ONE*, vol. 6, no. 7, Article ID e20451, 2011.

[7] S. J. Fleishman, T. A. Whitehead, E. M. Strauch, J. E. Corn, S. B. Qin et al., "Community-wide assessment of protein-interface modeling suggests improvements to design methodology," *Journal of Molecular Biology*, vol. 414, pp. 289–302, 2011.

[8] G. P. Smith, "Filamentous fusion phage: novel expression vectors that display cloned antigens on the virion surface," *Science*, vol. 228, no. 4705, pp. 1315–1317, 1985.

[9] G. P. Smith and V. A. Petrenko, "Phage display," *Chemical Reviews*, vol. 97, no. 2, pp. 391–410, 1997.

[10] J. W. Kehoe and B. K. Kay, "Filamentous phage display in the new millennium," *Chemical Reviews*, vol. 105, no. 11, pp. 4056–4072, 2005.

[11] J. Hanes and A. Plückthun, "In vitro selection and evolution of functional proteins by using ribosome display," *Proceedings of the National Academy of Sciences of the United States of America*, vol. 94, no. 10, pp. 4937–4942, 1997.

[12] D. Lipovsek and A. Plückthun, "In-vitro protein evolution by ribosome display and mRNA display," *Journal of Immunological Methods*, vol. 290, no. 1-2, pp. 51–67, 2004.

[13] S. J. Fleishman, T. A. Whitehead, D. C. Ekiert et al., "Computational design of proteins targeting the conserved stem region of influenza hemagglutinin," *Science*, vol. 332, no. 6031, pp. 816–821, 2011.

[14] J. Karanicolas, J. E. Corn, I. Chen et al., "A De Novo protein binding pair by computational design and directed evolution," *Molecular Cell*, vol. 42, no. 2, pp. 250–260, 2011.

[15] T. A. Whitehead, A. Chevalier, Y. Song, C. Dreyfus, S. J. Fleishman et al., "Optimization of affinity, specificity and function of designed influenza inhibitors using deep sequencing," *Nature Biotechnology*, vol. 30, pp. 543–548, 2012.

[16] T. S. Chen and A. E. Keating, "Designing specific protein-protein interactions using computation, experimental library screening, or integrated methods," *Protein Science*, vol. 21, pp. 949–963, 2012.

[17] D. J. Thiel, M.-H. Le Du, R. L. Walter et al., "Observation of an unexpected third receptor-molecule in the crystal structure of human interferon-γ receptor complex," *Structure*, vol. 8, no. 9, pp. 927–936, 2000.

[18] T. Lassmann, O. Frings, and E. L. L. Sonnhammer, "Kalign2: high-performance multiple alignment of protein and nucleotide sequences allowing external features," *Nucleic Acids Research*, vol. 37, no. 3, pp. 858–865, 2009.

[19] I. E. Efremov, M. Y. Fursov, and Y. E. Danilova, *Ugene: High Performance Genome Analysis Suite*, Moscow, Russia, 2009.

[20] U. Müller, U. Steinhoff, L. F. L. Reis et al., "Functional role of type I and type II interferons in antiviral defense," *Science*, vol. 264, no. 5167, pp. 1918–1921, 1994.

[21] E. C. Borden, G. C. Sen, G. Uze et al., "Interferons at age 50: past, current and future impact on biomedicine," *Nature Reviews Drug Discovery*, vol. 6, no. 12, pp. 975–990, 2007.

[22] K. Schroder, P. J. Hertzog, T. Ravasi, and D. A. Hume, "Interferon-γ: an overview of signals, mechanisms and functions," *Journal of Leukocyte Biology*, vol. 75, no. 2, pp. 163–189, 2004.

[23] P. W. Gray and D. V. Goeddel, "Structure of the human immune interferon gene," *Nature*, vol. 298, no. 5877, pp. 859–863, 1982.

[24] J. N. Ahmad, J. Li, L. Biedermannova, M. Kuchar, H. Sipova et al., "Novel high-affinity binders of human interferon gamma derived from albumin-binding domain of protein g," *Proteins*, vol. 80, pp. 774–789, 2012.

[25] H. Sipova, V. Sevcu, M. Kuchar, J. N. Ahmad, P. Mikulecky et al., "Surface plasmon resonance biosensor based on engineered proteins for direct detection of interferon-gamma in diluted blood plasma," *Sensors and Actuators B*, vol. 174, pp. 306–311, 2012.

[26] M. U. Johansson, I.-M. Frick, H. Nilsson et al., "Structure, specificity, and mode of interaction for bacterial albumin-binding modules," *Journal of Biological Chemistry*, vol. 277, no. 10, pp. 8114–8120, 2002.

[27] W. T. Windsor, L. J. Walter, R. Syto, J. Fossetta, W. J. Cook et al., "Purification and crystallization of a complex between human interferon gamma receptor (extracellular domain) and human interferon gamma," *Proteins*, vol. 26, pp. 108–114, 1996.

[28] L. Michiels, J. Haelewyn, P. Proost, and M. De Ley, "The soluble extracellular portion of the human interferon-γ receptor is a valid substitute for evaluating binding characteristics and for neutralizing the biological activity of this cytokine," *International Journal of Biochemistry and Cell Biology*, vol. 30, no. 4, pp. 505–516, 1998.

[29] M. Randal and A. A. Kossiakoff, "The structure and activity of a monomeric interferon-γ:α-chain receptor signaling complex," *Structure*, vol. 9, no. 2, pp. 155–163, 2001.

[30] S. E. Ealick, W. J. Cook, S. Vijay-Kumar et al., "Three-dimensional structure of recombinant human interferon-γ," *Science*, vol. 252, no. 5006, pp. 698–702, 1991.

[31] A. Landar, B. Curry, M. H. Parker et al., "Design, characterization, and structure of a biologically active single-chain mutant of human IFN-γ," *Journal of Molecular Biology*, vol. 299, no. 1, pp. 169–179, 2000.

[32] W. Humphrey, A. Dalke, and K. Schulten, "VMD: visual molecular dynamics," *Journal of Molecular Graphics*, vol. 14, no. 1, pp. 33–38, 1996.

[33] J. Schymkowitz, J. Borg, F. Stricher, R. Nys, F. Rousseau, and L. Serrano, "The FoldX web server: an online force field," *Nucleic Acids Research*, vol. 33, no. 2, pp. W382–W388, 2005.

[34] P. Eastman and V. S. Pande, "Openmm: a hardware-independent framework for molecular simulations," *Computing in Science and Engineering*, vol. 12, pp. 34–39, 2010.

[35] M. S. Friedrichs, P. Eastman, V. Vaidyanathan et al., "Accelerating molecular dynamic simulation on graphics processing units," *Journal of Computational Chemistry*, vol. 30, no. 6, pp. 864–872, 2009.

[36] D. Van Der Spoel, E. Lindahl, B. Hess, G. Groenhof, A. E. Mark, and H. J. C. Berendsen, "GROMACS: fast, flexible, and free," *Journal of Computational Chemistry*, vol. 26, no. 16, pp. 1701–1718, 2005.

[37] N. Eswar, B. John, N. Mirkovic et al., "Tools for comparative protein structure modeling and analysis," *Nucleic Acids Research*, vol. 31, no. 13, pp. 3375–3380, 2003.

[38] P. A. Kollman, "Advances and continuing challenges in achieving realistic and predictive simulations of the properties of organic and biological molecules," *Accounts of Chemical Research*, vol. 29, no. 10, pp. 461–469, 1996.

[39] W. F. DeGrado, Z. R. Wasserman, and V. Chowdry, "Sequence and structural homologies among type I and type II interferons," *Nature*, vol. 300, no. 5890, pp. 379–381, 1982.

[40] T. Arakawa, Y.-R. Hsu, and D. Chang, "Structure and activity of glycosylated human interferon-γ," *Journal of Interferon Research*, vol. 6, no. 6, pp. 687–695, 1986.

[41] S. Pestka, J. A. Langer, K. C. Zoon, and C. E. Samuel, "Interferons and their actions," *Annual Review of Biochemistry*, vol. 56, pp. 727–777, 1987.

[42] H. C. Kelker, Y. K. Yip, P. Anderson, and J. Vilcek, "Effects of glycosidase treatment on the physicochemical properties and biological activity of human interferon-γ," *Journal of Biological Chemistry*, vol. 258, no. 13, pp. 8010–8013, 1983.

[43] E. Sviridova, L. Bumba, P. Rezacova et al., "Crystallization and preliminary crystallographic characterization of the iron-regulated outer membrane lipoprotein FrpD from Neisseria meningitidis," *Acta Crystallographica Section F*, vol. 66, no. 9, pp. 1119–1123, 2010.

[44] B. G. Pierce, J. N. Haidar, Y. Yu, and Z. Weng, "Combinations of affinity-enhancing mutations in a T cell receptor reveal highly nonadditive effects within and between complementarity determining regions and chains," *Biochemistry*, vol. 49, no. 33, pp. 7050–7059, 2010.

[45] L. A. Clark, P. A. Boriack-Sjodin, J. Eldredge et al., "Affinity enhancement of an *in vivo* matured therapeutic antibody using structure-based computational design," *Protein Science*, vol. 15, no. 5, pp. 949–960, 2006.

[46] G. Song, G. A. Lazar, T. Kortemme et al., "Rational design of intercellular adhesion molecule-1 (ICAM-1) variants for antagonizing integrin lymphocyte function-associated antigen-1-dependent adhesion," *Journal of Biological Chemistry*, vol. 281, no. 8, pp. 5042–5049, 2006.

[47] J. Han, H. J. Kim, S.-C. Lee et al., "Structure-based rational design of a Toll-like receptor 4 (TLR4) decoy receptor with high binding affinity for a target protein," *PLoS ONE*, vol. 7, no. 2, Article ID e30929, 2012.

[48] O. Sharabi, Y. Peleg, E. Mashiach et al., "Design, expression and characterization of mutants of fasciculin optimized for interaction with its target, acetylcholinesterase," *Protein Engineering, Design and Selection*, vol. 22, no. 10, pp. 641–648, 2009.

[49] J. M. Shifman and S. L. Mayo, "Modulating calmodulin binding specificity through computational protein design," *Journal of Molecular Biology*, vol. 323, no. 3, pp. 417–423, 2002.

[50] D. W. Sammond, Z. M. Eletr, C. Purbeck, and B. Kuhlman, "Computational design of second-site suppressor mutations at protein-protein interfaces," *Proteins*, vol. 78, no. 4, pp. 1055–1065, 2010.

[51] E. De Genst, D. Areskoug, K. Decanniere, S. Muyldermans, and K. Andersson, "Kinetic and affinity predictions of a protein-protein interaction using multivariate experimental design," *Journal of Biological Chemistry*, vol. 277, no. 33, pp. 29897–29907, 2002.

[52] J. S. Marvin and H. B. Lowman, "Redesigning an antibody fragment for faster association with its antigen," *Biochemistry*, vol. 42, no. 23, pp. 7077–7083, 2003.

[53] T. Selzer, S. Albeck, and G. Schreiber, "Rational design of faster associating and tighter binding protein complexes," *Nature Structural Biology*, vol. 7, no. 7, pp. 537–541, 2000.

[54] C. S. E. Lengyel, L. J. Willis, P. Mann et al., "Mutations designed to destabilize the receptor-bound conformation increase MICA-NKG2D association rate and affinity," *Journal of Biological Chemistry*, vol. 282, no. 42, pp. 30658–30666, 2007.

[55] G. Schreiber, Y. Shaul, and K. E. Gottschalk, "Electrostatic design of protein-protein association rates," *Methods in Molecular Biology*, vol. 340, pp. 235–249, 2006.

[56] R. D. Gorham Jr., C. A. Kieslich, and D. Morikis, "Electrostatic clustering and free energy calculations provide a foundation for protein design and optimization," *Annals of Biomedical Engineering*, vol. 39, no. 4, pp. 1252–1263, 2011.

[57] E. Krissinel and K. Henrick, "Inference of macromolecular assemblies from crystalline state," *Journal of Molecular Biology*, vol. 372, no. 3, pp. 774–797, 2007.

[58] A. A. Nuara, L. J. Walter, N. J. Logsdon et al., "Structure and mechanism of IFN-γ antagonism by an orthopoxvirus IFN-γ-binding protein," *Proceedings of the National Academy of Sciences of the United States of America*, vol. 105, no. 6, pp. 1861–1866, 2008.

[59] A. M. Levin, D. L. Bates, A. M. Ring et al., "Exploiting a natural conformational switch to engineer an interleukin-2 'superkine'," *Nature*, vol. 484, no. 7395, pp. 529–533, 2012.

[60] R. T. Bradshaw, B. H. Patel, E. W. Tate, R. J. Leatherbarrow, and I. R. Gould, "Comparing experimental and computational alanine scanning techniques for probing a prototypical protein-protein interaction," *Protein Engineering, Design and Selection*, vol. 24, no. 1-2, pp. 197–207, 2011.

[61] O. Sharabi, A. Dekel, and J. M. Shifman, "Triathlon for energy functions: who is the winner for design of protein-protein interactions?" *Proteins*, vol. 79, no. 5, pp. 1487–1498, 2011.

[62] R. T. Bradshaw, P. G. A. Aronica, E. W. Tate, R. J. Leatherbarrow, and I. R. Gould, "Mutational Locally Enhanced Sampling (MULES) for quantitative prediction of the effects of mutations at protein-protein interfaces," *Chemical Science*, vol. 3, no. 5, pp. 1503–1511, 2012.

Supplementary material

Increasing affinity of interferon-γ receptor 1 to interferon-γ by computer-aided design

Pavel Mikulecký, Jiří Černý, Lada Biedermannová, Hana Petroková, Milan Kuchař, Jiří Vondrášek, Petr Malý, Peter Šebo, and Bohdan Schneider (*)

Institute of Biotechnology AS CR, v. v. i., Vídeňská 1083, CZ-142 20 Prague, Czech Republic

(*) Corresponding author:
phone: +420 241 063 624 ; fax: +420 296 443 610
email: bohdan@img.cas.cz ; http: http://www.structbio.eu/BS/

Supplementary text 1. Methods

Protocol of the computations.

The necessary software was obtained free of charge from following web addresses:

1. Modeller 9.12, http://salilab.org/modeller
2. FoldX 3.0 Beta 4, http://foldx.crg.es
3. OpenMM Zephyr 2.0.3, https://simtk.org/home/zephyr (contains GPU accelerated version of GROMACS)

1. Modeller suite of programs version 9.12 was used to model residues missing ("not visible in the electron density") from the 1fg9 crystal structure.

The following loop and C-terminal residues were added (residue numbers according to the PDB):

VAL C 142, ASP C 143, TYR C 144, VAL D 142, ASP D 143, TYR D 144, ASP D 145, PRO D 146, GLU D 147

PHE D 222, ASN D 223, SER D 224

The missing residues were constructed employing the "loopmodel" routine and fast MD refinement (by "`refine.fast`"). The lowest energy structure was chosen from ten models and used for the subsequent mutation analysis. All missing residues were outside the interface area.

2. The *in silico* mutation of selected interface residues was performed using locally installed binary of the FoldX program.

The analyzed coordinates included four chains from each crystal structure – ABCD from 1fg9, and ABDE from 1fyh, respectively. The structures of 20 mutants at all forty mutated positions (see Figure 2) in PDB format were generated using the

```
<PositionScan>#,ONELETCHAINRESNR
```

keyword, where the `ONELET`, `CHAIN`, and `RESNR` were replaced for each interface residue by its one letter code, PDB chain, and the residue number.

The FoldX program calculated simultaneously also the ΔΔG values of these mutations. These ΔΔG values measured the effect of mutations to the overall stability of the IFN-γ/IFN-γ-Rx complex.

To address the (de)stabilizing effect of interface mutations on the receptor binding, the FoldX keyword

```
<AnalyseComplex>#,CHAIN
```

was used, with the CHAIN representing the IFN-γ-Rx chain. This keyword performs analysis of the interaction of the selected chain with the rest of the structure, for instance interaction between chain C and the remaining chains ABD in 1fg9.

3. The graphical interface OpenMM Zephyr was used for preparation and execution of the MD simulations.

This graphical user interface (GUI) is shielding a potential user from the detailed setup of MD simulation. The preparation of successful simulation contains choosing the starting PDB structure from within the GUI, selecting the desired combination of force field, other conditions, e.g. solvation model and temperature, and clicking the Simulate button. We used the default

parameters, parm96 force field, implicit solvation (GBSA, ε = 78.3, with collision interval of 10.99 fs), temperature of 300 K, and time step of 2 fs. OpenMM Zephyr automatically runs the GROMACS (sub)programs with the proper parameters. The protocol includes:

Transformation of PDB file PROTEIN.pdb to PROTEIN_processed.pdb with `ffamber` naming conventions.

Running `pdb2gmx` to protonate and set the force field parameters:

```
pdb2gmx -f PROTEIN_processed.pdb -o PROTEIN_processed.gro -p
PROTEIN_processed.top -ter -ignh
```

Running `editconf` to define periodic solvation box:

```
editconf -bt cubic -d 0.7 -f PROTEIN_processed.gro -o
PROTEIN_processed.box.gro
```

Running `grompp` and `mdrun_openmm`: run first for restrained optimization of hydrogen atoms:

```
grompp -f em.mdp -c PROTEIN_processed.box.gro -p PROTEIN_processed.top -
o PROTEIN_processed.box.em.tpr -po em.out.mdp

mdrun_openmm -c PROTEIN_processed.box.em.gro -s
PROTEIN_processed.box.em.tpr
```

and finally followed by `grompp` and `mdrun_openmm` for the production MD run:

```
grompp -f PROTEIN_processed.box.em.md.mdp -c
PROTEIN_processed.box.em.gro -p PROTEIN_processed.top -o
PROTEIN_processed.box.em.md.tpr -po md.out.mdp

mdrun_openmm -s PROTEIN_processed.box.em.md.tpr -o
PROTEIN_processed.box.em.md.trr -c PROTEIN_processed.box.em.md.gro -cpo
PROTEIN_processed.box.em.md.cpt
```

Supplementary text 2. Results

Statistical significance of the K_d values.

The formal statistical significance of the differences between K_d values of the mutants and WT can only be tested for a few mutants, namely for those for which more than three measurements of K_d were performed using the same batch of IFN-γ-SC. We used the two-sample *t*-test comparing two normally distributed means [1]. The null hypothesis (H0) of the test is the identity of K_d values of the mutant and WT: $K_{d(mut)} - K_{d(WT)} = 0$, the alternative hypothesis (H1) is a higher affinity of the mutant, i.e. $K_{d(mut)} - K_d(WT) < 0$. The values of *t* are -38.1 for N96W, -1.6 for H222R, and +8.3 for the triple mutant, respectively. Because one-tailed value of the parameter *t* for ~15 degrees of freedom is ±1.75, the higher affinity of N96W is highly significant (-38.1 < -1.75) while the improvement of binding for H222R is insignificant (-1.6 > -1.75); H222R can indeed be called a neutral binder. The degrees of freedom were calculated as $N_{(mut)} + N_{(WT)} - 2$; the numbers of measurements, N, are in Table 3.

Variability of SPR data measured for different batches of IFN-γ-SC.

Table 3 reports SPR data determined with one batch of IFN-γ-SC. When the measurements were carried out with four different batches of IFN-γ-SC, the averages of K_d values remained in general agreement but the error margins of the latter measurements were much higher: K_d values for WT, N70G and N96W are 21±9 (13), 19±17 (8), and 5.3±3.5 (7) nM, respectively (confidence limits calculated at the 95% level, number of measurements in parentheses). Therefore, individual values of K_d from measurements with different batches of IFN-γ-SC, which do not allow statistical treatment, should not be directly compared. All IFN-γ-SC batches were prepared by the same protocol; large error margins are likely caused by hard-to-control proteolysis of the C-terminus during purification process that has been reported previously [2].

Dissociation constants of two variants can be used to calculate the relative changes of Gibbs energy of their interaction; for dissociation constants of WT $(K_d)_{WT}$ and a mutant $(K_d)_{mut}$:

$$\Delta\Delta G = -RT\ln(K_d)_{mut} - \{-RT\ln(K_d)_{WT}\} = -RT\ln\{(K_d)_{WT}/(K_d)_{mut}\}$$

Because of stability issues with IFN-γ-SC described above, these ΔΔG values need to be calculated from K_d measurements using the same batch of IFN-γ-SC.

Table 3 does not list k_{on}, k_{off}, and K_d of the "negative" mutants 15, 16, and 17 because their K_d values were measured only once using batch of IFN-γ-SC different from what was used for the other variants.

Table S1. Sequences used for the global alignment of the IFN-γ-Rx sequences from 19 various species. The alignment is shown in Figure 2. Listed are GenBank GI codes of all 32 sequences and names of the proteins.

1. gi|145975948 truncated interferon-gamma receptor 1 [Homo sapiens] human.
2. gi|4557880 interferon gamma receptor 1 precursor [Homo sapiens] human
3. gi|189069218 unnamed protein product [Homo sapiens] human
4. gi|62897165 interferon gamma receptor 1 variant [Homo sapiens] human.
5. gi|13562049 interferon-gamma receptor [Homo sapiens] human
6. gi|632543 interferon-gamma receptor alpha chain [Homo sapiens] human.
7. gi|90083401 unnamed protein product [Macaca fascicularis] crab-eating macaque, species, primates.
8. gi|297291656 PREDICTED: interferon gamma receptor 1-like isoform 1 [Macacamulatta] crab-eating macaque, species, primates.
9. gi|297291658 PREDICTED: interferon gamma receptor 1-like isoform 2 [Macacamulatta] crab-eating macaque, species, primates.
10. gi|197100085 interferon gamma receptor 1 [Pongo abelii] Sumatran orangutan, species, primates.
11. gi|332213427 PREDICTED: interferon gamma receptor 1 isoform 1 [Nomascus leucogenys] Northern white-cheeked gibbon, species, primates.
12. gi|114609481 PREDICTED: interferon gamma receptor 1 isoform 5 [Pan troglodytes] chimpanzee, species, primates.
13. gi|296483981 interferon gamma receptor 1 [Bos taurus] cattle, species, even-toed ungulates
14. gi|78050063 interferon gamma receptor 1 [Bos taurus] cattle, species, even-toed ungulates.
15. gi|45385782 interferon gamma receptor 1 [Bos taurus] cattle, species, even-toed ungulates.
16. gi|45385784 interferon gamma receptor 1 [Cervus elaphus] red deer, species, even-toed ungulates.
17. gi|295444941 interferon gamma receptor 1 [Sus scrofa] pig, species, even-toed ungulates.
18. gi|194216473 PREDICTED: similar to interferon gamma receptor 1 [Equus caballus] horse, species, odd-toed ungulates.
19. gi|74198189 unnamed protein product [Mus musculus] house mouse, species, rodents.
20. gi|6754306 interferon gamma receptor 1 precursor [Mus musculus] house mouse, species, rodents.
21. gi|309329 interferon-gamma receptor precursor [Mus musculus] house mouse, species, rodents.
22. gi|149039622 interferon gamma receptor 1 [Rattus norvegicus] Norway rat, species, rodents.
23. gi|38541396 Interferon gamma receptor 1 [Rattus norvegicus] Norway rat, species, rodents.
24. gi|16758624 interferon gamma receptor 1 [Rattus norvegicus] Norway rat, species, rodents.
25. gi|334324216 PREDICTED: interferon gamma receptor 1-like [Monodelphis domestica] gray short-tailed opossum, species, marsupials.
26. gi|57031680 PREDICTED: similar to Interferon-gamma receptor alpha chain precursor (IFN-gamma-R1) (CD119 antigen) (CDw119) [Canis familiaris] dog, subspecies, carnivores.
27. gi|281354680 hypothetical protein PANDA_003082 [Ailuropoda melanoleuca] giant panda, species, carnivores.
28. gi|224047948 PREDICTED: similar to interferon gamma receptor 1 [Taeniopygia guttata] zebra finch, species, birds.
29. gi|194332850 interferon gamma receptor 1 [Gallus gallus] chicken, species, birds.
30. gi|326915840 PREDICTED: interferon gamma receptor 1-like [Meleagris gallopavo] turkey, species, birds.
31. gi|118404146 interferon gamma receptor 1 [Xenopus (Silurana) tropicalis] western clawed frog, species, frogs & toads
32. gi|211956284 soluble IFN-g receptor [Deerpox virus W-1170-84] Deerpox virus.

Table S2. Mutagenesis primers designed for the introduction of single residue substitution into IFN-γ-Rx WT. Mutated nucleotides are underlined.

Mutant	Primers	Length
N65R	GTTTTTACCGTCGAAGTGAAACGTTATGGCGTGAAAAATAGCGA TCGCTATTTTTCACGCCATAACGTTTCACTTCGACGGTAAAAAC	44 bp
N70G	GAAAAACTATGGCGTGAAAGGCAGCGAATGGATCGATGCG CGCATCGATCCATTCGCTGCCTTTCACGCCATAGTTTTTC	40 bp
S95R	ATCATGTGGGCGACCCGCGTAACTCCCTGTGGGTT AACCCACAGGGAGTTACGCGGGTCGCCCACATGAT	35 bp
N96F	CATGTGGGCGACCCGAGTTTCTCCCTGTGGGTTCGTGTC GACACGAACCCACAGGGAGAAACTCGGGTCGCCCACATG	39 bp
N96W	GATCATGTGGGCGACCCGAGTTGGTCCCTGTGGGTTCGTGTCAA TTGACACGAACCCACAGGGACCAACTCGGGTCGCCCACATGATC	44 bp
K115Y	GAAAGAATCAGCGTATGCCTACTCGGAAGAATTCGCCGTG CACGGCGAATTCTTCCGAGTAGGCATACGCTGATTCTTTC	40 bp
T166M	ATGACCCGGAAACCATGTGTTACATTCGTG CACGAATGTAACACATGGTTTCCGGGTCAT	30 bp
T166Y	GTCGATTATGACCCGGAAACCTATTGTTACATTCGTGTTTATAACG CGTTATAAACACGAATGTAACAATAGGTTTCCGGGTCATAATCGAC	46 bp
H222R	TGAAGGCGTTCTGCGTGTCTGGGGTGTCA TGACACCCCAGACACGCAGAACGCCTTCA	29 bp
Y66L	CCGTCGAAGTGAAAAACCTGGGCGTGAAAAATAGCG CGCTATTTTTCACGCCCAGGTTTTTCACTTCGACGG	36 bp
S71E	GAAAAACTATGGCGTGAAAAATGAAGAATGGATCGATGCGTGCATC GATGCACGCATCGATCCATTCTTCATTTTTCACGCCATAGTTTTTC	46 bp
H222D	CTGAAGGCGTTCTGGATGTCTGGGGTGTC GACACCCCAGACATCCAGAACGCCTTCAG	29 bp

Table S3. Color-coded values of ΔΔG calculated using FoldX for chains C/ABD of the PDB structure 1fg9. Red indicates stabilization, blue destabilization. The first set of ΔΔG values estimates the influence of mutations on stability of the whole IFN-γ/IFN-γ-Rx complex (a), the second set of ΔΔG values estimates (de)stabilization of the interaction between the receptor molecule and the rest of the IFN-γ/IFN-γ-Rx complex (b).

a)

res	G	A	V	L	I	S	T	C	M	N	Q	K	R	H	P	D	E	F	Y	W
K_64	3.33	1.7	0.32	-	0.2	2.85	2.47	1.2	0.6	2.12	0.59	0.0	-	24.2	8.1	4.91	5.72	9.7	14.4	9.97
N_65	0.38	-	-	-	-	-	-	-	-	0.0	-	-	-	-0.44	-	0.76	0.84	-	-1.57	-
Y_66	2.90	1.6	1.77	1.12	1.6	2.41	3.13	1.5	-	1.83	2.54	0.22	0.24	1.37	3.4	3.41	4.56	-	0.00	-
G_67	0.0	3.0	4.22	1.51	3.0	4.25	5.46	3.4	3.2	3.32	2.66	2.65	5.04	3.61	9.5	2.46	3.74	2.7	3.10	4.23
V_68	2.22	0.6	0.0	-	-	1.66	1.31	0.8	1.0	0.38	1.15	1.59	1.20	3.73	6.0	2.54	1.14	4.1	5.38	5.19
K_69	0.08	-	0.17	0.02	0.1	-	-	0.0	0.3	0.36	0.15	0.0	-	0.35	-	-	0.05	0.0	0.05	0.13
N_70	-	-	0.19	-	-	-	0.29	-	-	0.0	-	-	-	-0.64	-	-	-	-	-0.62	-
S_71	0.47	1.1	1.51	0.54	1.8	0.0	0.98	0.5	0.9	0.07	0.61	0.38	0.73	1.07	0.8	0.98	0.94	0.2	0.32	0.21
E_72	-	-	0.31	0.24	0.1	-	-	0.0	0.6	0.40	0.19	0.05	0.26	0.32	-	0.25	0.0	-	-0.77	0.26
W_73	2.37	2.3	1.99	1.36	1.9	3.06	2.73	2.3	0.9	3.14	3.31	3.58	4.01	2.83	1.1	2.76	2.87	1.8	1.29	0.0
D_93	0.53	-	2.66	-	-	0.39	-	-	-	1.00	-	-	0.15	0.61	-	0.0	-	-	0.10	-
S_95	1.32	0.7	-	-	-	0.0	-	0.3	0.2	0.84	-	0.05	-	4.37	1.0	1.82	2.57	2.3	2.53	4.05
N_96	0.89	0.4	0.34	-	-	0.96	0.41	0.5	-	0.0	0.42	0.47	-	0.18	3.8	0.35	1.61	-	-0.21	-
S_97	-	-	-	-	-	0.0	-	-	-	-	-	-	1.68	-1.42	-	-	-	-	-2.84	-
W_99	2.90	1.7	0.00	0.63	-	2.15	1.07	1.4	0.5	2.54	1.52	2.06	3.52	2.24	3.0	3.35	3.24	0.3	1.21	0.0
K_115	0.94	0.6	0.15	-	-	0.65	0.35	0.3	-	0.73	0.23	0.0	1.05	0.86	0.3	0.83	0.39	-	-1.50	0.43
S_116	0.18	-	2.04	-	0.1	0.0	0.42	0.5	-	-	1.89	1.92	2.26	7.47	3.2	2.27	2.01	7.8	10.3	7.19
E_118	-	-	0.35	-	1.0	-	0.22	-	-	-	-	-	-	0.12	-	0.03	0.0	-	-0.90	-
R_123	2.44	1.3	2.30	0.92	2.5	2.39	2.46	1.6	1.6	1.62	2.27	1.11	0.0	2.01	0.7	4.48	4.24	1.2	0.97	2.46
E_164	-	0.2	2.00	0.26	2.1	0.38	1.42	0.0	0.2	-	-	-	0.12	-0.17	2.6	0.09	0.0	-	-0.11	0.08
T_165	0.85	0.1	0.35	-	-	0.00	0.0	0.3	-	1.22	0.56	-	-	1.00	2.5	3.63	2.40	2.2	1.71	6.09
T_166	-	-	-	-	-	-	0.0	-	-	-	-	-	0.26	0.17	-	0.88	1.15	-	-0.94	-
Y_168	-	-	-	0.34	0.2	-	-	-	0.4	-	0.71	-	0.29	0.11	2.0	2.67	2.49	-	0.00	0.17
R/F_17	-	-	-	-	-	0.29	-	-	-	0.45	-	-	0.0	-1.28	2.0	-	-	-	-2.47	-
V_171	2.42	1.1	0.0	0.69	0.0	1.76	1.33	0.8	1.2	1.18	0.57	0.71	1.17	1.67	0.8	1.65	1.13	0.7	1.89	1.20
K_186	0.29	0.3	0.64	-	0.3	0.04	0.58	-	-	0.02	0.20	0.0	0.45	0.64	-	-	-	-	0.21	0.07
T_189	0.92	-	-	-	0.4	0.33	0.0	0.6	-	0.84	0.00	0.47	0.44	1.78	1.7	2.07	1.51	0.4	0.71	0.90
Q_190	-	-	-	-	-	-	-	-	-	-	0.0	0.40	0.92	0.23	0.3	-	0.49	-	-0.60	-
K_191	0.60	0.0	0.73	-	0.3	0.49	0.73	0.6	-	0.00	-	0.0	0.33	0.52	-	0.00	-	0.5	0.39	0.02
E_192	-	-	0.02	-	0.6	-	-	-	0.6	-	0.35	0.76	1.41	0.56	5.8	-	0.0	0.2	2.37	2.60
D_193	-	-	0.28	-	0.2	-	0.09	-	0.0	-	-	-	-	-0.39	-	0.0	-	-	-0.45	-
E_197	-	-	0.02	-	-	-	0.17	0.1	-	0.12	-	-	-	0.40	-	0.33	0.0	-	-0.45	0.12
V_220	2.56	1.4	0.0	0.10	-	2.26	1.61	1.4	1.0	2.49	1.66	1.86	2.10	1.92	4.0	2.22	1.11	0.5	0.94	1.09
L_221	3.13	2.6	2.70	0.0	2.6	2.13	2.02	2.2	1.7	3.20	3.15	2.47	2.90	1.68	3.5	4.78	4.11	2.2	8.35	3.80
H_222	-	-	0.22	-	0.1	-	0.13	-	-	-	-	-	-	0.00	-	-	-	-	-1.69	-
V_223	1.29	2.0	0.0	-	-	2.42	1.21	0.8	-	1.55	0.83	0.14	2.10	34.5	3.4	2.30	2.27	3.8	5.30	5.32
W_224	3.33	3.0	2.90	1.91	2.9	3.81	4.23	3.0	2.2	4.20	3.54	2.82	3.10	2.42	2.2	4.52	4.45	1.0	1.53	0.0
G_225	0.0	1.8	6.50	4.89	8.0	2.78	5.98	3.0	4.1	2.94	5.28	3.55	4.48	5.09	7.4	4.21	5.79	4.4	5.26	5.03
V_226	1.26	0.4	0.0	-	-	0.65	0.98	0.3	0.0	0.79	0.80	0.42	0.49	1.94	-	1.48	0.94	0.0	0.41	1.34
T_227	0.13	-	-	-	-	-	0.0	-	-	-	-	-	-	-0.12	-	0.70	-	-	-0.94	-

Table S3 b)

res	G	A	V	L	I	S	T	C	M	N	Q	K	R	H	P	D	E	F	Y	W
K_64	1.68	1.7	1.22	1.15	1.3	1.66	1.93	1.2	1.2	1.76	0.53	0.0	-	0.96	1.6	3.31	3.75	3.0	3.80	2.79
N_65	0.29	0.2	-	-	-	0.20	-	0.0	-	0.0	-	-	-	0.00	0.1	0.11	0.09	0.0	0.01	0.03
Y_66	4.20	3.5	2.86	2.85	4.1	4.30	4.20	3.5	1.1	4.46	3.61	1.83	1.16	2.52	3.5	4.73	4.24	-	0.0	1.16
G_67	0.0	0.9	0.14	-	-	1.24	1.22	0.7	-	0.96	-	0.31	1.20	0.74	2.0	-	0.41	0.1	0.23	0.90
V_68	1.92	0.7	0.0	1.97	0.5	0.91	1.68	0.3	2.0	-	-	1.11	0.97	1.86	5.2	0.50	0.04	0.3	2.04	2.18
K_69	1.40	1.4	1.45	1.39	1.4	1.42	1.44	1.4	1.4	1.45	1.41	0.0	1.46	1.43	1.1	1.19	1.44	1.3	1.37	1.37
N_70	0.02	-	0.21	0.18	0.2	-	0.15	0.0	0.1	0.0	0.11	0.08	0.03	0.04	-	0.29	0.17	0.0	0.07	0.14
S_71	2.21	2.2	1.96	1.49	1.5	0.0	0.18	1.8	1.5	1.62	1.70	1.30	1.17	1.99	1.8	2.19	2.09	1.4	1.69	1.52
E_72	-	-	-	-	-	-	-	-	-	-	-	-	-	-	-	-	0.0	-	-	-
W_73	0.25	0.1	-	0.18	0.0	0.10	-	0.1	0.1	-	0.29	-	0.01	-	-	0.08	0.07	-	0.40	0.0
D_93	0.05	-	-	-	-	0.09	0.07	-	-	0.10	0.06	0.07	0.27	0.35	-	0.0	-	0.2	0.29	0.19
S_95	0.51	0.2	0.10	-	-	0.0	0.22	0.2	-	0.19	0.12	-	-	0.33	0.4	0.39	0.98	0.1	0.29	-
N_96	-	-	-	-	-	-	-	-	-	0.0	-	-	-	-	-	0.04	0.22	-	-	-
S_97	-	0.2	-	0.04	-	0.00	0.32	-	-	-	0.20	-	0.0	-	-	-	-	-	-	-
W_99	0.63	0.4	0.29	0.24	-	0.62	0.50	0.2	-	0.74	1.09	-	1.89	0.72	0.3	-	0.97	0.6	-	0.0
K_115	0.04	0.1	0.17	0.21	0.1	0.23	0.10	0.2	0.2	0.48	0.01	0.0	-	0.15	0.0	0.18	0.40	0.2	0.22	0.23
S_116	-	-	-	-	0.0	0.0	-	-	-	-	-	-	-	-	-	-	-	-	-	-
E_118	-	-	-	-	-	-	-	-	-	-	-	-	-	-	-	-	0.0	-	-	-
R_123	1.40	1.1	1.32	1.60	1.5	1.26	1.27	1.2	1.9	1.58	2.20	0.94	0.0	1.29	0.9	2.20	2.47	1.1	0.93	1.41
E_164	0.30	0.3	0.62	0.47	0.4	0.35	0.39	0.3	0.2	0.26	0.26	0.29	0.34	0.33	0.3	0.16	0.0	0.4	0.45	0.46
T_165	0.03	0.0	0.15	0.07	0.1	0.02	0.0	0.0	0.0	0.11	0.06	0.05	0.13	0.19	0.0	0.29	0.10	0.3	0.28	0.02
T_166	0.43	0.5	-	-	-	0.01	0.0	-	-	-	-	0.22	0.09	0.67	0.1	1.98	1.43	0.1	-	-
Y_168	0.14	0.0	-	-	-	0.09	-	0.0	-	0.12	-	-	-	-	-	0.07	-	0.1	0.0	-
R/F_17	0.30	0.2	0.30	0.29	0.3	0.29	0.30	0.3	0.2	-	0.56	0.13	0.0	0.29	0.3	0.41	0.50	0.2	0.27	0.27
V_171	-	-	0.0	0.00	0.0	-	-	-	-	-	0.31	-	-	-	-	-	-	-	-	0.08
K_186	-	-	-	-	-	-	-	-	-	-	-	0.0	0.04	-	-	-	-	0.0	0.04	0.10
T_189	0.00	-	0.00	0.00	0.0	0.00	0.0	0.0	0.0	0.00	0.00	0.02	0.08	0.01	0.0	-	-	0.0	0.10	-
Q_190	-	-	-	-	-	-	-	-	-	-	0.0	-	-	-	-	-	-	0.1	0.09	0.45
K_191	-	-	0.11	0.17	0.0	-	0.13	-	-	-	0.06	0.0	0.01	-	0.0	-	0.05	0.1	-	0.46
E_192	0.04	0.0	0.04	0.04	0.0	0.04	0.04	0.0	0.0	0.04	0.04	0.04	0.04	0.04	0.1	-	0.0	0.0	0.07	0.03
D_193	0.06	0.0	0.06	0.06	0.0	0.06	0.06	0.0	0.0	0.06	0.06	0.08	0.12	0.10	0.0	0.0	0.01	0.0	0.06	0.06
E_197	0.10	0.0	0.10	0.10	0.1	0.10	0.13	0.1	0.1	0.09	0.10	0.11	0.14	0.09	0.1	-	0.0	0.0	0.09	0.09
V_220	-	-	0.0	0.01	0.0	-	0.03	-	0.1	0.39	0.12	0.46	0.76	0.19	-	-	-	0.3	0.37	-
L_221	-	0.0	0.12	0.0	0.0	0.05	0.04	-	-	-	-	-	-	-	0.3	-	-	-	-	-
H_222	-	0.0	-	-	-	0.00	-	-	-	-	-	-	-	0.0	-	0.04	-	-	-	-
V_223	1.62	1.2	0.0	0.49	0.0	0.76	1.05	0.3	-	1.58	1.03	0.42	0.58	2.89	1.7	2.88	2.34	4.6	6.32	5.13
W_224	1.61	1.8	1.82	1.15	1.5	1.99	1.86	1.8	0.7	2.53	2.04	1.66	1.60	1.11	1.7	2.02	2.84	1.0	1.27	0.0
G_225	0.0	0.1	2.31	2.00	4.7	0.58	2.48	1.3	1.5	0.94	2.42	1.10	0.35	2.60	1.3	1.54	2.60	2.2	2.45	2.21
V_226	0.00	0.0	0.0	-	-	0.00	0.00	0.0	0.0	-	-	-	-	0.00	0.1	0.02	-	-	-	-
T_227	0.00	0.0	0.01	0.12	0.0	0.00	0.0	0.0	0.1	0.01	-	0.04	0.06	0.10	0.0	-	-	0.2	0.42	0.17

Table S4. Preliminary data of temperature dependency of affinities between IFN-γ-Rx and IFN-γ-SC for selected mutants measured by SPR at 15 °C, 20 °C, 25 °C, 30 °C, and 35 °C.

Mutant		K_d [nM]					ΔH (*)	ΔS (*)	R^2
ID	mutant	15 °C	20 °C	25 °C	30 °C	35 °C	[kJ/mol]	[J/molK]	(**)
2	N70G	14.7	17.3	23.6	49.2	77.0	0.93	-1.03	0.94
3	S95R	38.6	44.4	69.4	107.	153.	0.78	-0.62	0.97
5	N96W	5.55	5.28	6.1	12.2	24.3	0.80	-0.46	0.81
9	H222R	16.4	19.4	30.1	56.0	103.	1.01	-1.32	0.95
WT	--	16.8	21.7	30.5	59.9	92.8	0.94	-1.11	0.97

(*) Enthalpic and entropic contributions to free energy (values of ΔH and ΔS, respectively) were calculated from equation $\Delta G = \Delta H - T\Delta S$ by fitting the linear equation $\ln K_d = \{-\Delta H/R\}/T + \Delta S/R$ for coefficients $-\Delta H/R$ and $\Delta S/R$ assuming that ΔH and ΔS are temperature independent. Values at 35 °C were not considered for the determination of the temperature dependencies of ΔH and ΔS.

(**) Correlation coefficient of the least square fit of the regression equation mention above.

Figure S1. Melting temperatures of the WT and selected mutants. Curves obtained from fluorescence-based thermal shift assay of IFN-γ-Rx WT (blue, melting temperature 55 °C), N96W (red, melting temperature 48 °C) and N96W+H222R (green, melting temperature 47 °C). a) Normalized data of PBS buffer subtracted data of IFN-γ-R WT, N96W and N96W+H222R. b) First derivative of the data represented in (a). The lowest value of each curve represents melting temperature (Tm) of IFN-γ-R variants.

a)

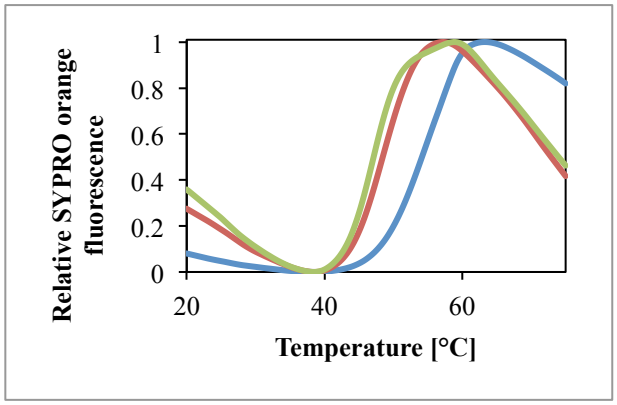

b)

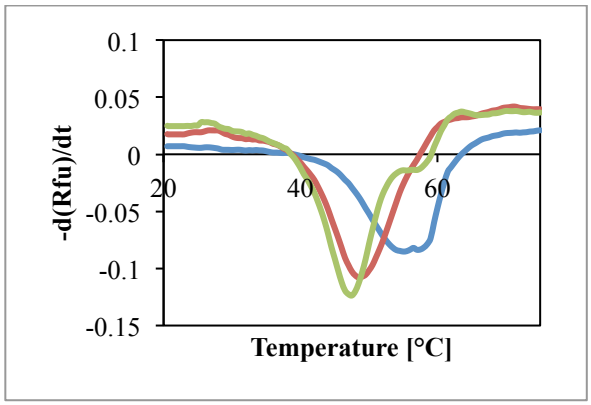

Supplement References

1. Freund JE & Williams FJ (1966) Dictionary/outline of basic statistics. New York: McGraw-Hill.

2. Landar A, Curry B, Parker MH, DiGiacomo R, Indelicato SR, *et al.* (2000) Design, characterization, and structure of a biologically active single-chain mutant of human ifn-gamma. ***J Mol Biol* 299**: 169-179.

Hindawi Publishing Corporation
BioMed Research International
Volume 2015, Article ID 716945, 12 pages
http://dx.doi.org/10.1155/2015/716945

Research Article

Redesigning Protein Cavities as a Strategy for Increasing Affinity in Protein-Protein Interaction: Interferon-γ Receptor 1 as a Model

Jiří Černý, Lada Biedermannová, Pavel Mikulecký, Jiří Zahradník, Tatsiana Charnavets, Peter Šebo, and Bohdan Schneider

Laboratory of Biomolecular Recognition, Institute of Biotechnology, Academy of Sciences of the Czech Republic, Vídeňská 1083, 142 20 Prague, Czech Republic

Correspondence should be addressed to Bohdan Schneider; bohdan.schneider@gmail.com

Received 2 October 2014; Revised 22 December 2014; Accepted 28 December 2014

Academic Editor: Yuedong Yang

Combining computational and experimental tools, we present a new strategy for designing high affinity variants of a binding protein. The affinity is increased by mutating residues not at the interface, but at positions lining internal cavities of one of the interacting molecules. Filling the cavities lowers flexibility of the binding protein, possibly reducing entropic penalty of binding. The approach was tested using the interferon-γ receptor 1 (IFNγR1) complex with IFNγ as a model. Mutations were selected from 52 amino acid positions lining the IFNγR1 internal cavities by using a protocol based on FoldX prediction of free energy changes. The final four mutations filling the IFNγR1 cavities and potentially improving the affinity to IFNγ were expressed, purified, and refolded, and their affinity towards IFNγ was measured by SPR. While individual cavity mutations yielded receptor constructs exhibiting only slight increase of affinity compared to WT, combinations of these mutations with previously characterized variant N96W led to a significant sevenfold increase. The affinity increase in the high affinity receptor variant N96W+V35L is linked to the restriction of its molecular fluctuations in the unbound state. The results demonstrate that mutating cavity residues is a viable strategy for designing protein variants with increased affinity.

1. Introduction

In studying specificity and affinity of protein-protein interactions, the main focus is traditionally on the structural properties of the interface, for example, complementarity of the residue composition, hydrogen-bonding networks, and the role of hydration [1]. However, there is also a significant contribution of the conformational dynamics to the binding affinity. Analysis of molecular dynamics simulations of 17 protein-protein complexes and their unbound components with quasi-harmonic analysis [2] concluded that the protein flexibility has an important influence on the thermodynamics of binding. Moreover, changes in the protein conformational dynamics may lead to substantial changes in affinity to binding partners without an apparent structural change of the complex. For example, reorganization of the hydrogen bonding networks and solvent bridges of the interacting molecules upon mutation, which was accompanied only by subtle structural changes, leads to radically different binding free energy [3, 4]. A recent work [5] shows that the apparent change in the amino acid dynamics determined by NMR spectroscopy is linearly related to the change in the overall binding entropy and also that changes in side-chain dynamics determined from NMR data can be used as a quantitative estimate of changes in conformational entropy [6, 7]. Also, an analysis of crystallographic B-factors has revealed a significant decrease of flexibility of residues exposed to solvent compared to flexibility of residues interacting with another biomolecule and further compared to their flexibility in the protein core [8]. This "freezing" of atoms upon complexation and in the protein core is only slightly larger for the side chain atoms than for the main chain atoms. Entropic cost specific for side-chain freezing has been computationally evaluated as a small, but important contribution to the thermodynamics

of binding [9, 10]. These results indicate that changes in amino acid conformational entropy upon binding contribute significantly to the free energy of protein-protein association.

However important the interaction interface is for the affinity, the interaction is influenced by the whole composition of the cognate molecules, so that modulation of affinity can be achieved by changing other residues than residues at the interface. One such possible alternative approach would be filling cavities in one of the binding partners, thus influencing the stability and dynamics of the interacting proteins [11–14]. Thermodynamic consequences of introducing cavity-filling mutations have been discussed for residues at the interaction interface [15–17] showing that filling the interfacial cavity increases affinity due to both gain in binding enthalpy and a loss in binding entropy, the latter being attributed to a loss of conformational degrees of freedom. It has been shown that interactions between the internal "core" residues is responsible for the folding and thermal stability of a protein [18]. Here, we decided to test whether the protein-protein affinity could be increased by mutations not on the interface, but in cavities inside one of the cognate protein molecules.

This study follows our previous article [21] in which we designed mutations increasing the affinity of human interferon-γ receptor 1 (IFNγR1) towards its natural cognate molecule interferon-γ (IFNγ), an important protein of innate immunity [22, 23]. Here, we retain this model system and the main contours of the protocol but replace the search for interface mutations by searching for mutations in the receptor cavities in order to further increase its interaction affinity to IFNγ and our computer analysis revealed four such cavity mutants. Combining one of these cavity mutations with the best variant designed in our previous study led to a sevenfold increase in affinity compared to the wild-type receptor. We show that the affinity increase in this mutant is related to the restricted flexibility of amino acids in the unbound state of IFNγR1.

2. Materials and Methods

2.1. Outline of the Protocol. Our computational predictions are based on the analysis of crystal structures of complexes between IFNγ and the extracellular part of IFNγR1, namely, the structures of PDB codes 1fg9 [19] and 1fyh [20] that contain four crystallographically independent IFNγ/IFNγR1 complexes. Throughout the paper, IFNγR1 residues are numbered as in UniProt entry P15260. We used the empirical force field implemented in the software FoldX [24] to search for mutations within the positions lining the internal cavities of IFNγR1 molecule that would increase its stability and/or its affinity to IFNγ. All designed mutants of IFNγR1 were subsequently expressed and purified and their affinity to a "single-chain" form of IFNγ (IFNγSC, [25]) was measured. Individual steps of the computational protocol as well as experimental procedures are described below.

2.2. In Silico Design of Variants. The program 3V [26] was used to identify internal cavities in all four available structures of IFNγR1 molecules complexed with IFNγ. In total, 52 cavity-lining residues, which were identified as encapsulating the cavities in at least one of the four structures, were extracted using the VMD program [27]. Each of 52 amino acid residues identified as lining the internal receptor cavities was mutated in all four crystal IFNγ/IFNγR1 complexes to 20 amino acid residues using the "`positionscan`" and "`analyzecomplex`" FoldX keywords. This represented $52 \times 4 \times 20$ mutations (including self-mutations leading to $\Delta\Delta G = 0$). Three types of changes of free energy ($\Delta\Delta G$) were calculated using the program FoldX:

(1) "$\Delta\Delta G$ of folding of IFNγR1 in complex" gauged the influence of mutations on the stability of the whole IFNγ/IFNγR1 complex;

(2) "$\Delta\Delta G$ of folding of free IFNγR1" estimated the effect of mutations on the stability of the isolated receptor;

(3) "$\Delta\Delta G$ of binding" of complex between IFNγR1 and IFNγ estimated the change of the interaction between the receptor molecule and the rest of the complex.

2.3. Modeling. IFNγR1 models are based on PDB structures 1fg9 [19] and 1fyh [20]. Missing residues in both structures were added using Modeller suite of programs [28]. The lowest energy loop models were used for further calculations.

2.4. Molecular Dynamics (MD) Simulations. MD simulations were run using GROMACS suite of programs to test the stability and dynamic properties, including analysis of values of root means square fluctuations (RMSF) [29] and the effect of variable geometry on prediction of changes of interaction free energy ($\Delta\Delta$Gs), of the IFNγ/IFNγR1 complexes (PDB codes 1fyh and 1fg9). More detailed protocol of MD and FoldX calculations follows.

2.5. Protocol of Molecular Dynamics (MD) Calculations. For the MD simulations the following setup was used: protonation state was determined by `pdb2gmx` program using parameters provided by the OpenMM [30] Zephyr [31] program. Implicit solvation (GBSA, $\varepsilon = 78.3$, with collision interval of 10.99 fs) was used in combination with parm96 force field [32]. OpenMM Zephyr implementation of GPU accelerated version of GROMACS [29] suite of programs was used to simulate the systems. The initial crystal structures were optimized and the simulation was propagated at 300 K with the time step of 2 fs. RMSF (root-mean square fluctuations) of atoms in the analyzed proteins were calculated from the 100 ns trajectory to estimate flexibility of residues; they were calculated by `g_rmsf` program in 5 ns windows.

2.6. Construction, Expression, and Purification of Recombinant IFNγR1 Variants. We followed the protocols from our previous study [21] for all proteins produced in this study. All selected IFNγR1 variants were prepared, expressed, and successfully purified to homogeneity by the following protocol.

Codon-optimized synthetic gene (GenScript) encoding extracellular domain of human IFNgR1 (residues 18–245) was cloned into the pET-28b(+) vector (Novagen) using

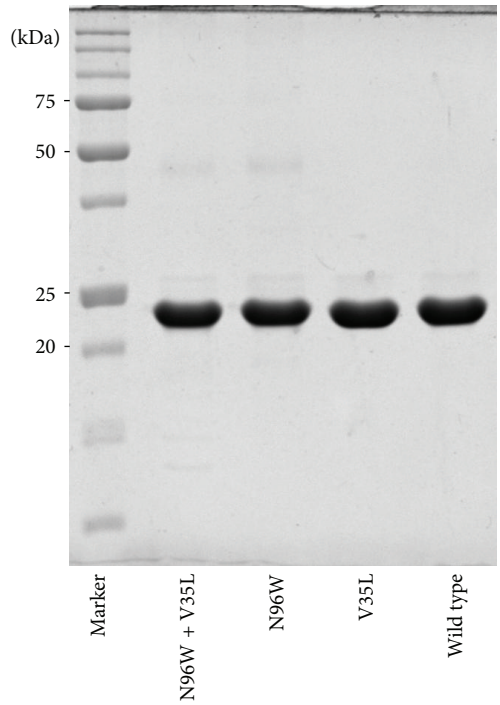

Figure 1: Nonreducing 12.5% SDS-PAGE gel of selected monomeric refolded recombinant His-tagged IFNγR1 variants. Proteins were extracted from inclusion bodies by 8 M urea, further purified on Ni-NTA agarose, and dialyzed, and monomeric fraction was separated on gel filtration column (see above). IFNγR1 with C-terminal His-Tag migrates at a molecular mass of 23 kDa when analyzed on nonreducing SDS-PAGE gel.

NcoI and *XhoI* restriction enzymes in frame with N-terminal start codon and C-terminal HisTag. The QuikChange II Site-Directed Mutagenesis Kit (Agilent Technologies) was used for mutating the IFNγR1 gene according to manufacturer's manual using primers listed below. Primers were designed by web-based PrimerX program (http://www.bioinformatics.org/primerx/).

The recombinant IFNγR1 variants were expressed in *Escherichia coli* BL21 (λDE3) in LB medium containing 60 μg/mL of kanamycin at 37°C for 4 hours after induction by 1 mM IPTG. Harvested cells by centrifugation (8,000 g, 10 min, 4°C) were disrupted by ultrasound in 50 mM Tris buffer pH 8 and centrifuged at 40,000 g, 30 min, 4°C, and inclusion bodies were dissolved in 50 mM Tris buffer pH 8 containing 8 M urea and 300 mM NaCl to extract protein that was further affinity-purified on Ni-NTA agarose (Qiagen) in the same buffer. Protein was eluted from resin by 250 mM Imidazole pH 8 in previous buffer and refolded by dialysis against 100 mM Tris-HCl pH 8, 150 mM NaCl, 2.5 mM EDTA, 0.5 mM Cystamine, and 2.5 mM Cysteamine overnight at 4°C. Final purification of monomeric receptor variants was performed at 4°C on a HiLoad 16/600 Superdex 200 pg (GE Healthcare) equilibrated by PBS buffer pH 7.4 (Figure 1). Monodispersity of the purified receptor protein was verified by dynamic light scattering (DLS) using Malvern Zetasizer Nano ZS90 instrument (data not shown).

2.7. Primers. Mutagenesis primers are designed for the introduction of single residue substitution into IFNγR1 WT. Mutated nucleotides are underlined. We have the following:

V35L

Forward: 5′-GTCCCGACCCCGACCAACTTGACGATT-GAAAGTTACAAC-3′

Reverse: 5′-GTTGTAACTTTCAATCGTCAAGTTGGT-CGGGGTCGGGAC-3′

A114E

Forward: 5′-GAAAGAATCAGCGTATGAAAAATCGGA-AGAATTCGCC-3′

Reverse: 5′-GGCGAATTCTTCCGATTTTTCATACGC-TGATTCTTTC-3′

D124N

Forward: 5′-CGCCGTGTGCCGTAATGGCAAAATCG-3′

Reverse: 5′-CGATTTTGCCATTACGGCACACGGCG-3′

H222Y

Forward: 5′-CTGAAGGCGTTCTGTATGTCTGGGGTG-TC-3′

Reverse: 5′-GACACCCCAGACATACAGAACGCCTTC-AG-3′

2.8. Construction, Expression, and Purification of IFNγSC. Recombinant interferon gamma in so-called single chain form (IFNγSC) described by [25] was cloned into pET-26b(+) vector (Novagen) using *NdeI* and *XhoI* restriction enzymes in frame with N-terminal start codon not to have no peptide leader nor tag.

The recombinant IFNγSC was expressed in *E. coli* BL21 (λDE3) in LB medium containing 60 μg/mL of kanamycin at 30°C for 4 hours after induction by 1 mM IPTG. Harvested cells by centrifugation (8,000 g, 10 min, 4°C) were disrupted by ultrasound in 20 mM Na-Phosphate buffer pH 7.3 and centrifuged at 40,000 g, 30 min, 4°C, and soluble fraction was further purified on SP Sepharose HP (GE Healthcare) using linear gradient of NaCl and further purified to homogeneity by gel filtration in same procedure as IFNγR1 receptor (see above).

2.9. Biophysical Characterization of the Studied Proteins. Melting temperatures of the receptor variants were measured using fluorescence-based thermal shift assay and for selected mutants by CD melting experiments. Interactions between IFNγR1 variants and IFNγSC were measured by the technique of surface plasmon resonance (SPR) as discussed in our previous study [21]. Experimental procedures are detailed below.

Table 1: Cavities in the four molecules of the IFNγR1 receptor in crystal structures 1fg9 [19] and 1fyh [20]. The receptor molecules are labeled by chain ID (chains C and D from 1fg9 and chains B and E from 1fyh). Figure 2 shows cavities 1–8 as they project into the chain C of 1fg9.

	Surface [Å^2]*	Number of residues lining the cavity†	Residues selected for mutation	Cavity observed in IFNγR1 chain of	
				1fg9	1fyh
1	134	7	V35, A114	C D	—
2	133	5	—	—	B E
3	470	14	D124	C D	—
4	262	9	H222	C D	B E
5	120	6	—	C D	E
6	165	7	—	C D	E
7	177	7	—	D	B E
8	138	5	—	C	B

*Surface calculated with a probe radius of 0.25 Å for cavities combined from all relevant receptor chains.
†Some residues are shared by neighboring cavities.

2.10. CD Measurements. CD spectra were recorded using "Chirascan-plus" (Applied Photophysics) spectrometer in steps of 1 nm over the wavelength range of 190–260 nm. Samples at a concentration of 0.2 mg/mL were placed into 0.05 cm path-length quartz cell to the thermostated holder and individual spectra were recorded at the temperature of 25°C. The CD signal was expressed as the difference between the molar absorption of the right- and left-handed circularly polarized light and the resulting spectra were buffer subtracted. To analyze the ratio of the secondary structures we used the CDNN program provided with Chirascan CD spectrometer [33]. For CD melting measurements, samples at a concentration of 1.5 mg/mL were placed into 10 mm path-length quartz cell to the thermostated holder and CD signal at 280 nm was recorded at 1°C increment at rate of 1.0°C/min over the temperature range of 25 to 65°C with an averaging time of 10 seconds. CD melting curves were normalized to relative values between 1.0 and 0.0.

2.11. Thermostability of the IFNγR1 Variants by Thermal-Based Shift Assay. Melting temperature (T_m) curves of the WT and selected variants were obtained from fluorescence-based thermal shift assay (TSA) using fluoroprobe. Experiment was performed in "CFX96 Touch Real-Time PCR Detection System" (Bio-Rad) using FRET Scan Mode. The concentration of fluorescent SYPRO Orange dye (Sigma Aldrich) was 8-fold dilution from 5000-fold stock and protein concentration was 2 μL in final volume of 25 μL. As a reference we used only buffer (PBS buffer pH 7.4) without protein. Thermal denaturation of proteins was performed in capped "Low Tube Strips, CLR" (Bio-Rad) and possible air bubbles in samples were removed by centrifugation immediately before the assay. The samples were heated from 20°C to 75°C with stepwise increment of 0.5°C per minute and a 30 s hold step for every point, followed by the fluorescence reading. Data subtraction by reference sample was normalized and used for first derivative calculation to estimate the melting temperature.

2.12. SPR Measurements. His-tagged receptor molecules were diluted to concentration of 10 μg/mL in PBST running buffer (PBS pH 7.4, 0.005% Tween 20) and immobilized on a HTG sensor chip activated with Ni^{2+} cations at a flow rate 30 μL/min for 60 s to gain similar surface protein density. Purified IFNγSC was diluted in running buffer to concentrations ranging from 0.1 to 9 nM and passed over the sensor chip for 90 seconds at a flow rate 100 μL/min (association phase). Dissociation was measured in the running buffer for 10 min at the same flow rate. Correction for nonspecific binding of IFNγSC to the chip surface was done by subtraction of the response measured on uncoated interspots and reference channel coated with His-tagged Fe-regulated protein D (FrpD) from Neisseria meningitides [34]. Data were processed in the ProteOn Manager software (version 3.1.0.6) and the doubly referenced data were fitted to the 1 : 1 "Langmuir with drift" binding model.

3. Results and Discussion

3.1. Internal Cavities Identified in IFNγR1. The cavity analysis revealed generally different number and size of cavities for each IFNγR1 crystal structure; their characteristics are listed in Table 1; their location in a representative receptor molecule (PDB entry 1fg9, chain C [19]) is highlighted in Figures 2(a) and 2(b). All amino acid residues lining cavities in all four IFNγR1 proteins complexed with IFNγ were combined, resulting in 52 residues used in subsequent *in silico* analysis.

3.2. In Silico Design of Variants. All 52 amino acids lining the cavities of the receptor molecule were subject to the mutation analysis by FoldX. The resulting $\Delta\Delta G$ values indicated potential for mutation leading to increasing the receptor affinity to IFNγ. The mutations were ordered by their $\Delta\Delta G$ values and the first 50 best mutations from each crystal structure (200 mutations in total) were further analyzed. Of these 200 mutations, twelve positions were predicted in all four or at least three crystal structures. The twelve promising positions are highlighted in orange and yellow in Figure 2(c). Following the previous study [21], where we observed significant differences between $\Delta\Delta G$ predicted directly from the crystal structures and from structures after molecular dynamics (MD) relaxation, we performed short

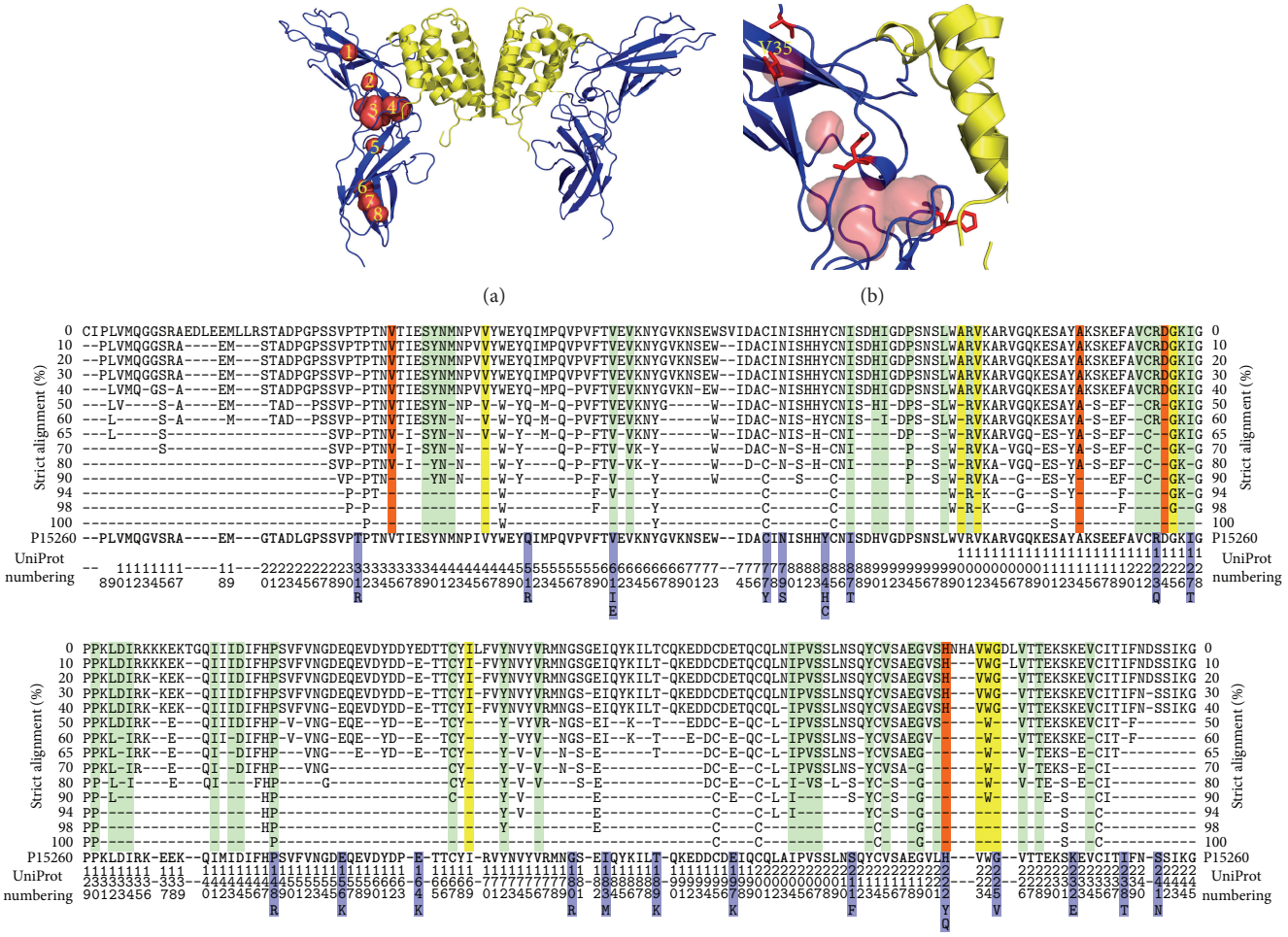

Figure 2: (a) The complex between IFNγ and the extracellular part of its receptor 1 (IFNγR1) from crystal structure of PDB code 1fg9 [19]. The two IFNγR1 molecules are drawn as blue cartoon and IFNγ homodimer as yellow cartoon. The eight identified cavities in the receptor molecule are shown as numbered red surfaces. (b) A close-up of the mutated cavities. The receptor cavities are drawn as red surface and residues selected for mutations as red sticks; valine 35 is labeled. (c) Residue conservancy calculated by strict alignment of 32 sequences of the extracellular part of IFNγR1 from 19 species. The residues lining the cavities and not suitable for mutation are highlighted in green, those selected by FoldX as mutable in yellow, and the residues selected for mutations after MD simulations are in red (they are also listed in Table 1). Blue highlights show IFNγR1 mutants occurring naturally in humans. Percentages of the conservation are shown on the left and right sides; analyzed sequence (residues 6–245 of the UniProt entry P15260) is shown at the bottom of the alignment.

(10 ns) MD simulations of the four crystal structures of complexes between wild type IFNγR1 and IFNγ, and repeated the FoldX mutation analysis on 500 snapshots extracted from these MD trajectories. After averaging of the predicted $\Delta\Delta G$ values for the twelve selected positions, we made the final selection of the four candidate mutations. The averaged $\Delta\Delta G$ values resulting from these calculations for structure 1fg9, receptor chain C, are summarized in Figure 3. The final selection of the four variants is listed in Table 2 together with the changes of their binding free energies averaged over 500 MD snapshots from each of the four IFNγ/IFNγR1 complexes in crystal structures 1fg9 and 1fyh.

Finally, the four consensus candidate mutations, which resulted as the best replacements of the WT sequence, were expressed, and characterized by SPR, CD, and thermal-based shift assay. The relative affinities of these four cavity-filling single mutants are shown in Figure 4(a) together with relative affinities of the double mutants combining the four cavity-filling mutations with mutation N96W.

As Table 2 and in detail Figure 3 show, the $\Delta\Delta G$ calculations revealed only modest potential gains in interaction affinity, probably because of small cavity volumes as well as the fact that they are often lined by evolutionary highly conserved residues. As opposed to the interface mutations, where the predicted $\Delta\Delta G$s of IFNγR1 stability and binding to IFNγ served as a sufficient criterion for the selection of affinity increasing mutations, there was no clear-cut rule for selecting internal cavity mutations that would result in improved interaction energy. We thus decided to test experimental consequences of combination of three types of $\Delta\Delta G$ values

Table 2: Predicted changes of free energy changes ($\Delta\Delta G$) of the four selected IFNγR1 variants with cavity-lining mutations relative to the wild type receptor. All energy values are in kcal/mol.

Variant	$\Delta\Delta G$ of folding of IFNγR1 in complex*	$\Delta\Delta G$ of folding of free IFNγR1†	$\Delta\Delta G$ of binding of IFNγR1/IFNγ complex‡	Sequence conservation¶
V35L	−0.88	−0.85	−0.02	80%
A114E	0.28	0.46	−0.20	60%
D124N	0.65	0.88	−0.21	40%
H222Y	−0.72	−0.69	0.15	40%

*$\Delta\Delta G$ of folding of IFNγR1 bound to IFNγ measures the influence of mutations on the stability of the whole complex.
†$\Delta\Delta G$ of folding of IFNγR1 alone represents changes of the stability of the isolated receptor.
‡$\Delta\Delta G$ of binding of the whole complex between IFNγR1 and IFNγ estimates the change of the affinity between the receptor molecule and the rest of the complex.
¶Sequence conservation of amino acid residues at positions 35, 114, 124, and 222. It was based on the global alignment of 32 sequences of the extracellular part of IFNγR1 (Figure 2(c)).

[1]		GLY	ALA	VAL	LEU	ILE	SER	THR	CYS	MET	ASN	GLN	LYS	ARG	HIS	PRO	ASP	GLU	PHE	TYR	TRP
VAL	35	2.8	2.0	0.0	−0.9	−0.4	2.9	1.6	1.3	0.1	2.0	2.5	3.5	5.1	4.7	1.2	3.4	3.5	4.3	7.3	10.6
VAL	46	3.8	2.2	0.0	−0.1	−0.3	3.1	1.8	1.8	0.6	2.4	3.0	4.1	6.4	6.4	2.0	3.6	3.7	4.0	6.6	9.1
VAL	100	5.6	3.7	0.0	0.3	−0.3	4.2	2.4	2.7	0.8	3.6	3.9	5.4	7.6	6.2	5.0	5.5	5.1	4.0	6.8	9.8
VAL	102	5.2	3.3	0.0	1.2	−0.4	4.0	2.2	2.5	1.8	3.6	4.1	7.1	11.9	9.4	4.8	4.9	4.9	7.5	11.2	15.6
ALA	114	1.0	0.0	−0.2	0.1	0.1	0.3	0.2	0.1	0.3	0.6	0.2	0.2	0.7	3.3	2.3	1.1	0.3	0.7	1.0	1.9
ASP	124	3.0	2.2	2.5	1.4	2.5	2.3	2.7	2.0	1.7	0.7	1.4	1.8	2.1	2.3	5.7	0.0	1.5	1.4	1.6	2.5
GLY	125	0.0	2.0	6.0	6.4	7.7	2.9	5.6	3.0	4.7	5.7	6.8	8.1	10.1	31.3	6.2	7.1	7.1	12.0	14.1	21.8
ILE	169	5.1	3.7	1.1	0.1	0.0	4.7	3.2	2.9	0.3	3.0	3.2	4.1	5.5	3.9	1.8	4.2	3.6	1.9	4.7	7.0
HIS	222	0.7	0.1	0.8	−0.3	1.1	−0.3	0.6	0.4	−0.3	−0.6	0.5	−0.1	0.3	0.0	2.9	−0.1	0.5	−1.1	−0.7	1.1
VAL	223	2.5	2.0	0.0	0.7	0.3	3.7	1.4	2.3	0.9	3.0	3.2	3.8	6.3	14.2	7.3	4.6	4.9	7.6	11.5	15.6
TRP	224	5.5	4.7	3.5	2.8	3.1	5.5	4.9	4.5	2.4	4.8	4.2	4.2	4.0	3.3	4.6	5.9	5.2	1.1	1.5	0.0
GLY	225	0.0	1.5	3.3	2.0	3.4	2.0	3.3	1.8	1.6	2.1	2.5	2.6	2.9	4.7	4.3	2.9	3.0	2.4	2.6	2.9

[2]		GLY	ALA	VAL	LEU	ILE	SER	THR	CYS	MET	ASN	GLN	LYS	ARG	HIS	PRO	ASP	GLU	PHE	TYR	TRP
VAL	35	2.8	2.0	0.0	−0.9	−0.4	2.9	1.6	1.3	0.1	2.0	2.5	3.6	5.3	4.5	1.2	3.4	3.5	4.3	7.3	10.7
VAL	46	5.0	3.0	0.0	−0.2	−0.5	4.1	2.4	2.4	0.5	3.2	3.8	5.1	8.1	7.6	2.9	4.8	4.8	4.4	7.9	11.5
VAL	100	5.7	3.8	0.0	0.3	−0.3	4.2	2.4	2.7	0.8	3.7	4.0	5.5	7.7	5.9	5.0	5.5	5.1	4.1	6.8	9.7
VAL	102	5.2	3.3	0.0	1.2	−0.4	4.0	2.2	2.5	1.8	3.6	4.1	7.1	11.9	9.5	4.8	4.9	4.9	7.5	11.2	15.7
ALA	114	1.0	0.0	−0.2	0.2	0.2	0.3	0.2	0.1	0.4	0.7	0.3	0.3	0.7	3.4	2.3	1.2	0.5	0.8	1.1	2.0
ASP	124	2.4	1.6	2.0	0.7	1.7	1.8	2.1	1.6	0.9	0.9	1.3	1.0	1.4	1.5	4.8	0.0	1.4	1.0	1.2	1.8
GLY	125	0.0	2.0	6.0	6.4	7.8	2.9	5.6	3.0	4.8	5.8	6.8	8.2	10.2	32.2	6.2	7.1	7.2	12.1	14.2	21.9
ILE	169	5.1	3.7	1.1	0.1	0.0	4.7	3.2	2.9	0.3	3.0	3.2	4.2	5.6	3.8	1.8	4.2	3.7	1.9	4.7	7.0
HIS	222	−0.1	−0.6	0.5	−0.4	0.6	−1.0	0.2	−0.1	−0.4	−0.7	0.2	−0.5	0.0	0.0	2.3	−0.3	−0.2	−0.9	−0.7	0.6
VAL	223	0.9	0.6	0.0	0.2	−0.2	1.7	0.4	1.2	0.1	1.2	1.1	0.5	0.9	1.0	5.6	1.6	1.2	0.1	0.3	0.6
TRP	224	2.7	2.1	1.3	1.2	1.1	2.5	2.1	1.9	0.9	2.2	1.9	1.6	2.0	2.0	2.2	2.4	2.0	0.3	0.6	0.0
GLY	225	0.0	1.2	1.9	0.8	1.7	1.2	1.7	1.1	0.6	0.9	0.9	0.8	1.0	1.0	2.8	1.0	1.0	0.4	0.5	0.3

[3]		GLY	ALA	VAL	LEU	ILE	SER	THR	CYS	MET	ASN	GLN	LYS	ARG	HIS	PRO	ASP	GLU	PHE	TYR	TRP
VAL	35	0.0	0.0	0.0	0.0	0.0	0.0	0.0	0.0	0.0	0.0	0.0	−0.1	−0.2	0.0	0.0	0.0	0.0	0.0	0.0	−0.1
VAL	46	0.0	0.0	0.0	0.0	0.0	0.0	0.0	0.0	0.0	0.0	0.0	0.0	0.0	0.0	0.0	0.0	0.0	0.0	0.0	0.0
VAL	100	0.0	0.0	0.0	0.0	0.0	0.0	0.0	0.0	0.0	0.0	0.0	0.0	0.0	0.0	0.0	0.0	0.0	0.0	0.0	0.0
VAL	102	0.0	0.0	0.0	0.0	0.0	0.0	0.0	0.0	0.0	0.0	0.0	0.0	0.0	0.0	0.0	0.0	0.0	0.0	0.0	0.0
ALA	114	0.0	0.0	0.0	−0.1	−0.1	0.0	0.0	0.0	−0.1	−0.1	−0.1	−0.1	0.0	−0.1	0.0	−0.1	−0.2	−0.1	−0.1	−0.1
ASP	124	0.2	0.1	0.0	−0.1	0.1	0.1	0.0	−0.1	−0.1	−0.2	−0.2	−0.1	−0.1	0.1	0.2	0.0	−0.1	−0.1	−0.1	0.1
GLY	125	0.0	0.0	0.0	0.0	−0.1	0.0	0.0	0.0	0.0	0.0	0.0	−0.1	−0.1	−0.1	−0.1	0.0	0.0	−0.1	−0.1	−0.1
ILE	169	0.0	0.0	0.0	0.0	0.0	0.0	0.0	0.0	0.0	0.0	0.0	0.0	0.0	0.0	0.0	0.0	0.0	0.0	0.0	0.0
HIS	222	1.3	1.2	0.9	0.7	0.8	1.1	0.9	0.7	0.4	0.3	0.5	0.4	0.2	0.0	1.2	0.5	0.6	0.1	0.2	0.8
VAL	223	1.7	1.4	0.0	0.1	0.4	2.0	0.8	1.2	0.3	1.5	1.6	2.0	3.2	6.1	2.2	2.7	2.9	5.7	8.2	10.4
TRP	224	3.3	3.1	2.6	1.8	2.2	3.3	3.0	3.0	1.4	2.9	2.3	2.4	2.0	1.3	2.8	3.6	3.1	0.9	0.8	0.0
GLY	225	0.0	0.3	1.1	0.6	1.2	0.6	1.2	0.4	0.3	0.8	0.9	0.9	0.9	2.9	1.3	1.4	1.3	1.1	1.1	1.4

Figure 3: Color-coded values of free energy changes ($\Delta\Delta G$) of mutating the twelve cavity-lining residues of IFNγR1. $\Delta\Delta G$ values were calculated using the program FoldX for 500 MD snapshots and averaged. Red colored matrix fields indicate stabilization, blue ones destabilization. Shown are $\Delta\Delta G$ values calculated for PDB 1fg9 [19]; receptor chain C. analogical matrices are calculated for 1fg9 receptor chain D, and for receptor chains B and E from the structure 1fyh [20]. (1) "$\Delta\Delta G$ of folding of IFNγR1 in complex" gauged the influence of mutations on the stability of the whole IFNγ/IFNγR1 complex. (2) "$\Delta\Delta G$ of folding of free IFNγR1" estimated the effect of mutations on the stability of the isolated receptor. (3) "$\Delta\Delta G$ of binding" of complex between IFNγR1 and IFNγ made an estimate of change of the interaction between the receptor molecule and the rest of the complex.

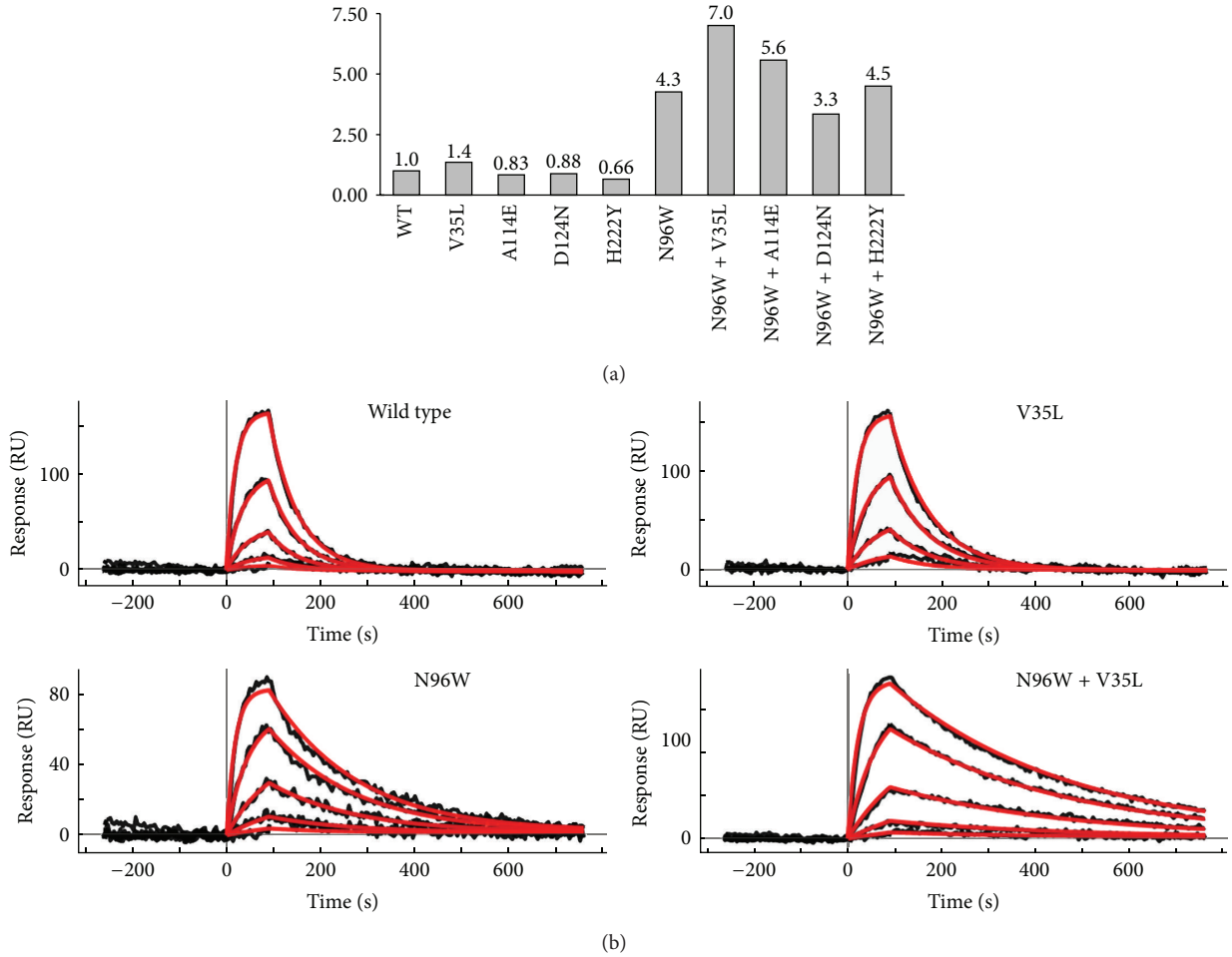

Figure 4: Affinities of the IFNγR1 wild type (WT) and mutants to IFNγSC obtained from SPR measurements. (a) Graph represents relative affinities of IFNγR1 variants compared to WT. All selected "cavity" single amino acid mutation variants bind to the IFNγSC with similar affinity as WT, but the V35L variant has slightly higher affinity itself and further increases the affinity of the "interface" mutant N96W if combined together. (b) SPR sensorgrams showing the interaction between IFNγSC and selected IFNγR1 variants. The V35L variant behaves similarly as WT displaying fast association and dissociation phases. Two variants (N96W and N96W + V35L) with higher affinities compared to WT bind IFNγSC with slower dissociation phase, thus increasing the affinity. Measured SPR signal is in black and calculated fitted curves are in red; concentrations of IFNγSC used for SPR measurements were as follows: 0.1, 0.3, 1.0, 3.0, and 9.0 nM.

calculated from the MD snapshots. To identify potentially favorable mutations, we combined $\Delta\Delta G$ values of folding ($\Delta\Delta G$ types (1) and (2) in the *in silico* protocol described in Materials and Methods) and of binding (type (3)). The first two mutations, V35L and H222Y, were predicted to increase $\Delta\Delta G$ of folding to a similar extent for both the complexed and free IFNγR1 ($\Delta\Delta G$ (1) and (2)), while calculated values of their $\Delta\Delta G$ of binding were virtually zero. The other two selected mutations, A114E and D124N, were predicted to slightly improve $\Delta\Delta G$ of binding while both types of their $\Delta\Delta G$ of folding were destabilizing. In the latter case, $\Delta\Delta G$ of folding of free IFNγR1 (type 2) was more unfavorable than $\Delta\Delta G$ of folding of complexed IFNγR1 (type 1). This means that the complex is predicted to be relatively more stable compared to the free IFNγR1.

3.3. Experimental Determination of the Affinities between IFNγR1 Variants and IFNγSC. Computer-designed IFNγR1 variants were expressed and purified and their affinities to IFNγSC were determined by SPR measurements; relative affinities are plotted in Figure 4(a); SPR sensograms are depicted in Figure 4(b). The calculated K_d values showed that the four selected "cavity" single amino acid mutation variants bind to the IFNγSC with similar affinity as WT; a modest increase was observed for the V35L variant. In line with our previous work, we decided to test to what extent the effect of two distant point mutations is additive. To this end, we combined the four cavity mutants designed here with the variant with the highest affinity designed previously, N96W. The results were quite encouraging: while affinity of one double mutant (N96W + H222Y) is neutral and one (N96W + D124) affinity actually decreased, two double mutants, N96W with A114E and V35L, had affinity increased compared to WT. The affinity increase of one of the double mutants, N96W + V35L, is significant, seven times higher than affinity of WT.

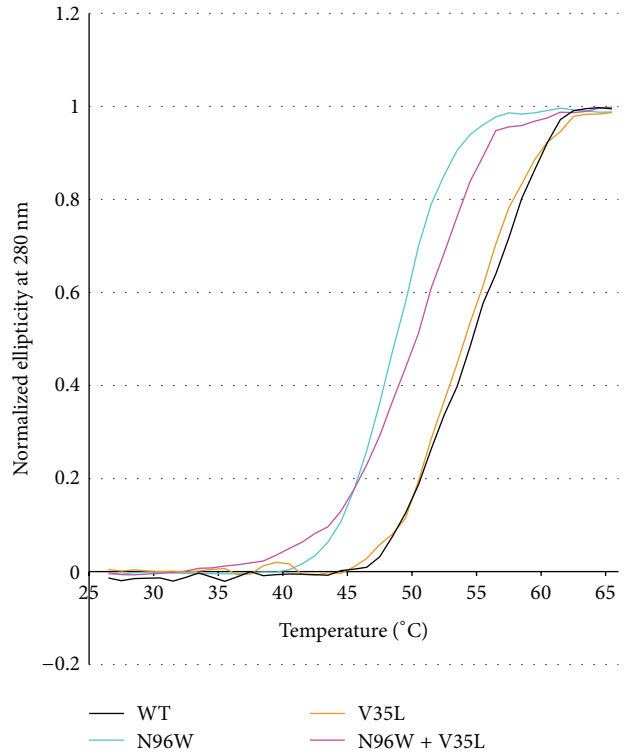

Figure 5: Normalized melting curves of IFNγR1 variants measured by temperature-dependent near ultraviolet circular dichroism (CD) spectra. Each data point is from the intensity measured at 280 nm. IFNγR1 WT, V35L, N96W, and N96W + V35L variants were measured in PBS buffer between 25 and 65°C at steps 1°C/minute. The melting temperature (T_m) of IFNγR1 variants was determined as 54°C for WT, 53°C for V35L, 50°C for N96W + V35L, and 48°C for N96W, respectively.

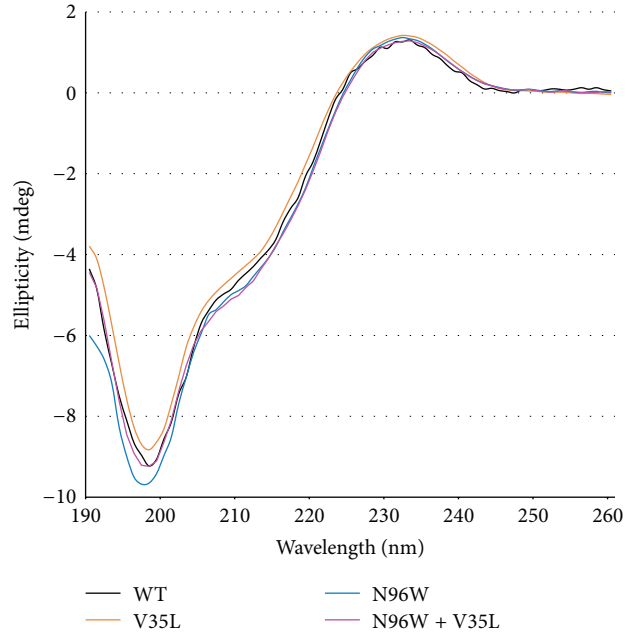

Figure 6: Circular dichroism (CD) spectra of IFNγR1 variants (WT, N96W, V35L, and N96W + V35L) measured in water at 25°C. CD melting curves for the same variants are shown in Figure 5.

The thermal stability (Figure 5) and secondary structure (Figure 6) of four IFNγR1 variants, V35L, N96W, N96W + V35L, and WT, were studied by CD and their melting temperatures were confirmed by thermal-based shift assay (Figure 7); the CD-measured melting temperatures are 53, 48, 50, and 54°C, respectively. Both variants with the highest affinity, N96W and N96W + V35L, have melting temperatures lower than WT, so that mutation from asparagine to tryptophan at the position 96 apparently causes a decrease of IFNγR1 thermal stability. However, the CD spectra of all four proteins are highly similar (Figure 6); their analysis provided virtually identical composition of the secondary structure elements dominated by the beta-sheet fractions indicating that no global structural rearrangements were caused by the mutations and the fold of these four variants is most likely the same. Moreover, the spectra are in agreement with the spectrum measured previously [35] for WT of IFNγR1.

3.4. Analysis of Internal Dynamics of the IFNγR1 Variants. To test how a cavity-filling mutation changes the flexibility of the receptor molecule in unbound and complexed states we analyzed root-mean square fluctuations (RMSF) of the selected variants. Comparison of RMSF sorted by their

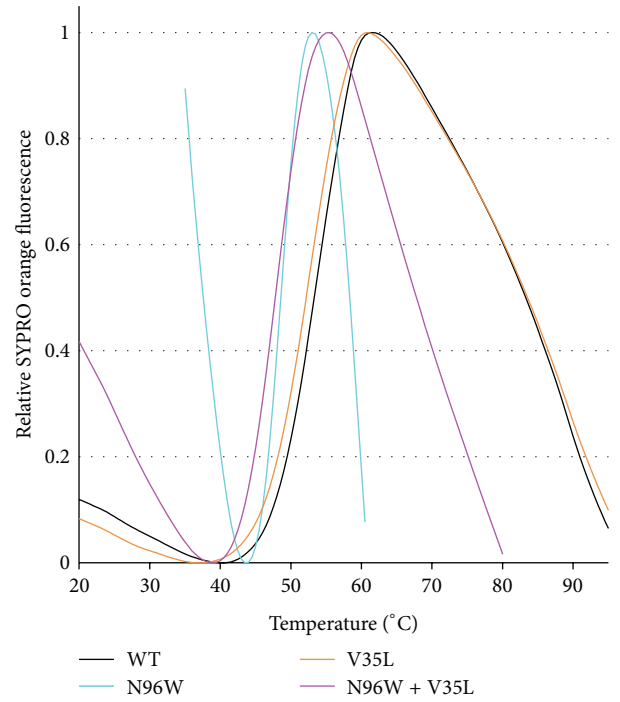

Figure 7: Melting temperatures of selected IFNγR1 variants determined by thermal-based shift assay. Plotted are normalized data of reference-subtracted fluorescence intensities of IFNγR1 WT, V35L, N96W, and N96W + V35L. The melting temperatures (T_m) of IFNγR1 variants were determined from the first derivatives of the curves plotted in the figure: 55°C for WT, 53°C for V35L, 49°C for N96W, and 48°C for N96W + V35L. The T_m values determined by temperature-dependent CD spectra and thermal-based shift assay are within 1°C the same.

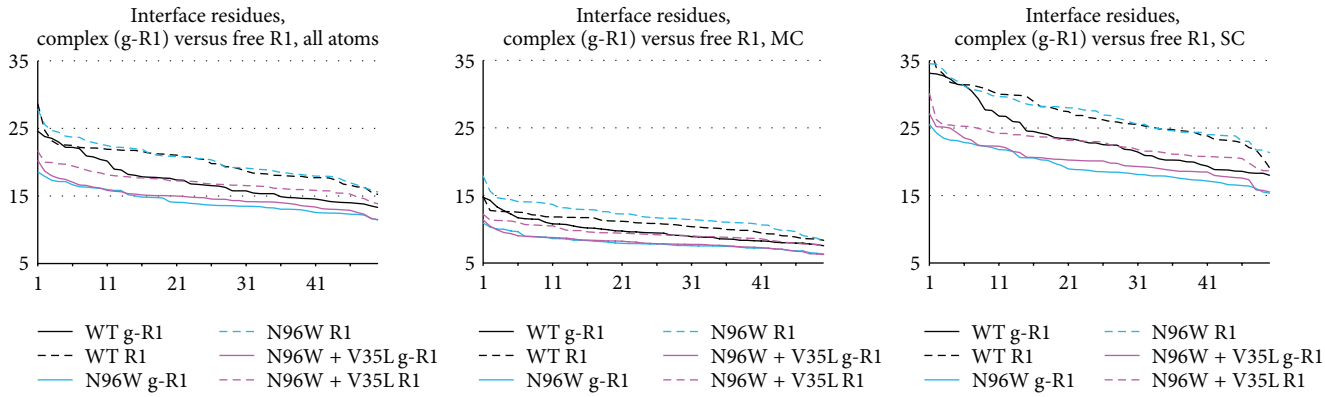

(a)

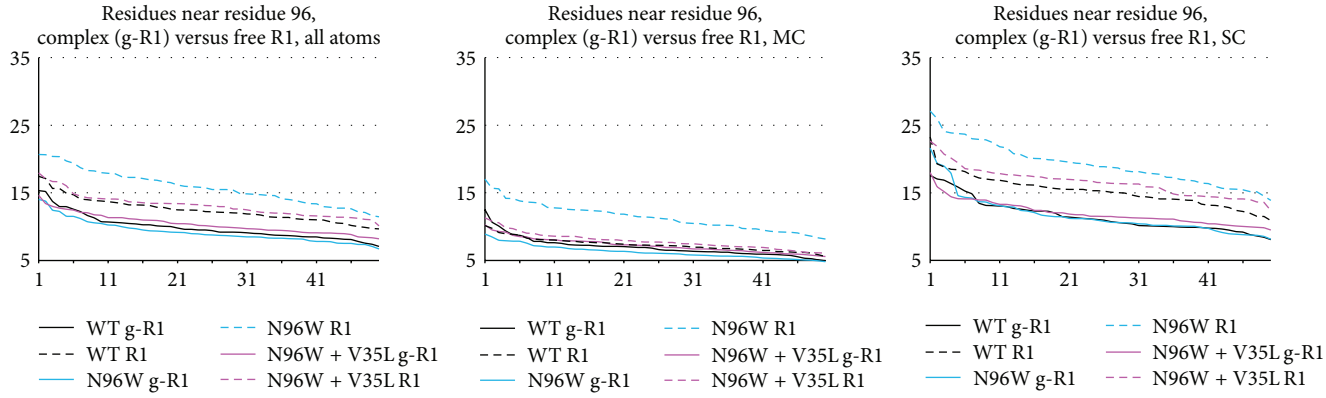

(b)

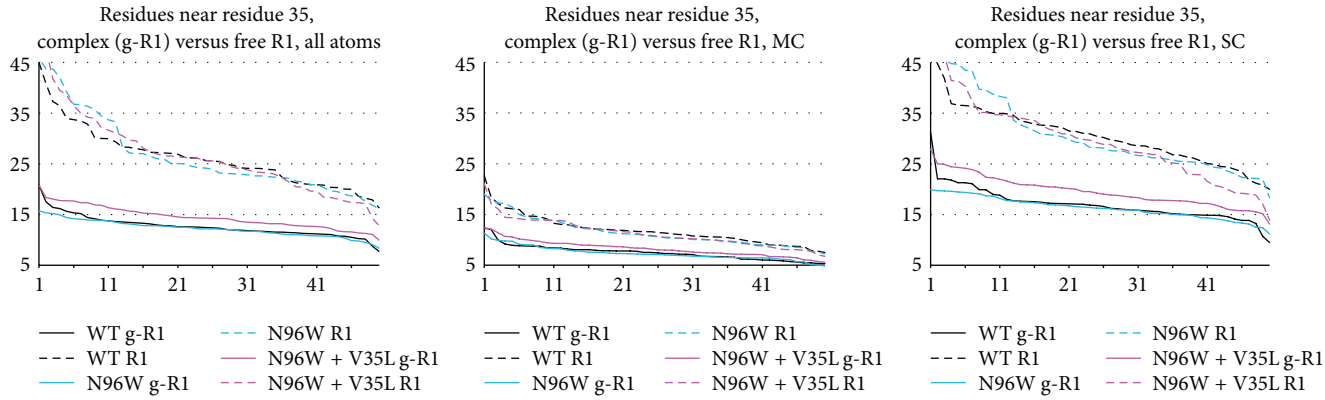

(c)

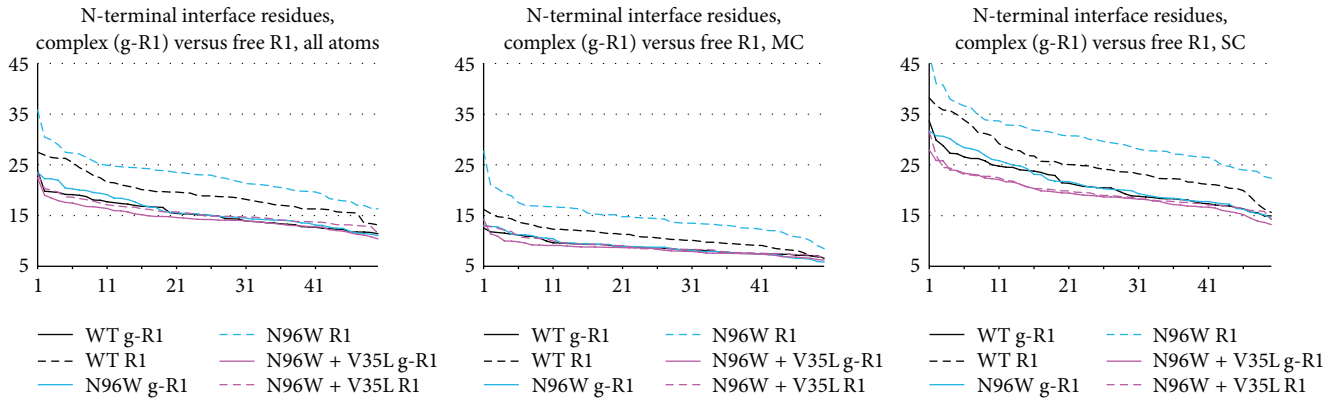

(d)

Figure 8: Continued.

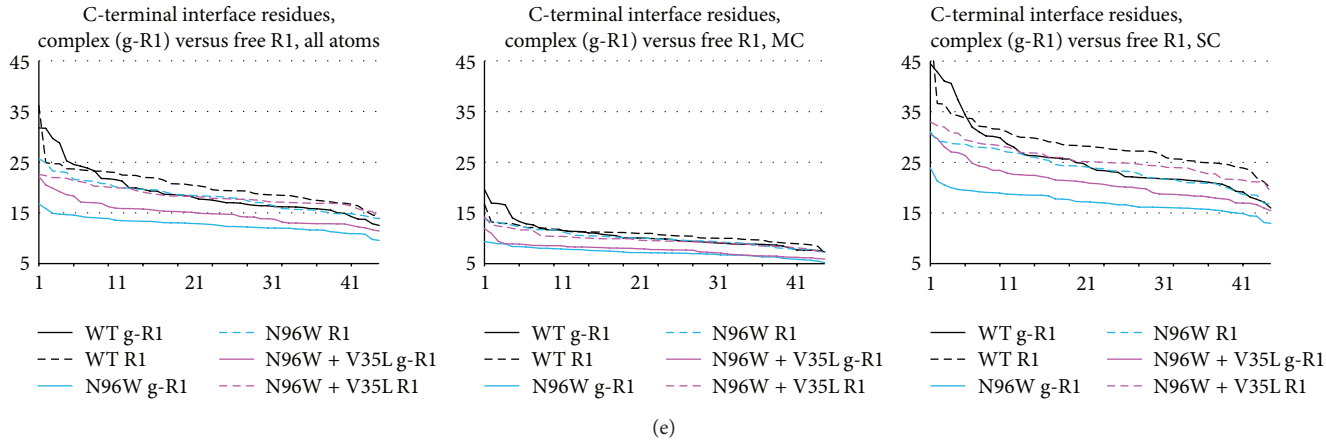

(e)

Figure 8: Ranked RMSF values collected at the last 50 ns of the 100 ns MD simulations of WT, N96W, and N96W + V35L variants of IFNγR1. Solid lines labeled g-R1 denote RMSF values of the IFNγ/IFNγR1 complex; dashed lines labeled R1 denote values of IFNγR1 alone. The RMSF values are on the y-axis; the rank of the values (1–50) is on the x-axis. Shown are RMSF values of all atoms, main chain atoms (MC), and side chain atoms (SC) for the following residues: (a) all 40 interface residues (i.e., residue numbers 64, 65, 66, 67, 68, 69, 70, 71, 72, 73, 93, 95, 96, 97, 99, 115, 116, 118, 123, 164, 165, 166, 168, 170, 171, 186, 189, 190, 191, 192, 193, 197, 220, 221, 222, 223, 224, 225, 226, and 227); (b) residues within 6 Å of residue 96 (i.e., residue numbers 65, 66, 67, 91, 92, 93, 94, 95, 96, 97, 98, 119, 120, 121, and 224); (c) residues within 6 Å of residue 35 (i.e., residue numbers 32, 33, 34, 35, 36, 37, 46, 47, 48, 49, 100, 101, 102, 114, 115, 116, and 117); (d) the interface residues from the N-terminal domain (i.e., residues 64 to 123); (e) the interface residues from the C-terminal domain (i.e., residues 164 to 227).

values, "ranked RMSF," for WT, N96W, and N96W + V35L, are plotted in Figure 8 (solid lines for IFNγ/IFNγR1 complexes, dashed lines for IFNγR1 alone). These plots revealed significant differences between dynamics of the variants as is detailed below.

(1) The interface residues of N96W and WT are more flexible in the free receptor than in the complex, while the flexibility of the interface residues of N96W + V35L is similar for the free and complexed receptor (Figures 8(a) and 8(d)). This indicates entropically more favorable binding of the N96W + V35L variant compared to the other two variants.

(2) Interestingly, the origin of this behavior is different in the N-terminal and C-terminal domains of the IFNγR1 molecule: in the N-terminal domain (Figure 8(d)), the flexibility of the interface residues of all variants is similar in the bound state, while being different in unbound state; they are most flexible in N96W and the least in N96W + V35L. In the C-terminal domain (Figure 8(e)), the flexibility of the three variants is similar in their free states, but it differs in the bound state between N96W, which has the lowest flexibility, and WT with the highest flexibility.

(3) The V35L mutation stiffens the receptor nonlocally and makes especially the C-terminal interface residues more flexible in the bound state compared to the N96W mutant (Figure 8(e)).

(4) To sum up, the V35L mutation brought flexibility of the free and complexed receptor closer together, indicating reduced entropy penalty of binding and resulting in the higher affinity of the N96W + V35L double mutant compared to N96W mutant.

Filling the cavity by hydrophobic groups as in the V35L mutation is stabilizing but not as much as would be implied by $\Delta\Delta G$ of the removal of the corresponding hydrophobic group to water. A compensatory effect lowering a potential increase of the protein and/or complex stability has been observed previously [13] and a comparable decrease of stabilization was also predicted here by FoldX. Filling of a cavity may stabilize the interaction by several mechanisms, for example, by reducing the entropic penalty of complexation by stiffening interacting molecules in the free state, or indirectly by destabilization of the intermediate molten globule state rather than by stabilization of the folded protein [36]. These compensatory effects further illustrate complexity of protein-protein interactions (and/or folding) and the known limits of computational approaches to increasing protein-protein affinity [37].

An important issue potentially affecting reliability of FoldX predictions is the flexibility of the receptor molecule. The first round of FoldX $\Delta\Delta G$ calculations based on the static crystal structures suggested one additional mutation, G225Y, as potentially increasing receptor affinity to IFNγ. Although further calculations using structures of snapshots from the MD simulations did not confirm this prediction, we expressed and characterized this mutation. The experimental data were in agreement with the MD-based prediction showing much lower binding affinity compared to the WT (the ratio of the respective K_d values was 0.4), and also the N96W + G225Y double mutant had a fairly low binding affinity (compared to WT, the ratio of the respective K_d values was 3.1, which is lower than for the N96W mutant). This observation can be explained by the structural properties of the receptor molecule. The loop region of IFNγR1 containing the G225 residue is flexible and any residue at the position 225 is thus only a fraction of time in the geometry, in which it may

increase the binding affinity. An important role of flexibility at the C-terminal part of the interacting IFNγ and IFNγR1 is well illustrated by a study of IFNγ modified at its C-terminal side [38].

3.5. Sequence Conservation of Mutable Residues. We checked sequence conservation for the 12 positions selected by the FoldX calculations for potential cavity-filling mutations. Global alignment of 32 sequences of the extracellular part of IFNγR1 from various organisms by Kalign as implemented in program Ugene [39] (Figure 2(c)) shows conservation between 40 and 98% for these positions; the position V35 is well conserved (80%). The independence of sequence conservation and its potential for stabilizing mutation filling-up protein cavity ("mutability") contrasts with previously observed tight correlation between conservation and mutability for receptor residues interacting with IFNγ [21]: we tested several mutations of the interface residues S97 and E118, which were conserved at the 90% level (Figure 2(c)), namely, S97X (X = L, N, W) and E118X (X = M, F, Y, W), and they did not bind IFNγSC at all (unpublished SPR data) despite the fact that binding of these mutants to IFNγ was predicted to be stronger than that of WT.

3.6. Relationship Between FoldX $\Delta\Delta G$ Values and Naturally Occurring IFNγR1 Variants. Interesting, albeit indirect, validation of the present FoldX predictions of $\Delta\Delta G$ of mutations can be found among naturally occurring IFNγR1 single-point mutations collected in the database of single nucleotide polymorphism (dbSNP) [40]. The database contains 25 nucleotide mutations at 22 unique positions of the extracellular part of the IFNγ receptor, which is studied here; these 22 positions are marked blue in Figure 2(c). Most of the $\Delta\Delta G$ predictions for these natural mutants show neutral effect on the stability of free IFNγR1 and on its complex with IFNγ. This is in agreement with the fact that only two of the natural mutants exhibit deleterious effects or are represented by a pathological phenotype.

4. Conclusions

We present a new computational strategy for designing higher affinity variants of a binding protein and show that it is possible to increase the affinity of a protein-protein interaction by mutations not at the interface, but in the interior cavities of a binding partner. The mutations were selected at positions lining internal cavities of one binding partner, and an *in silico* protocol identified mutations that would fill the protein cavities and increase the stability of the complex. We showed that the selection of such cavity mutations in interferon-γ receptor 1 (IFNγR1) could be performed based on a combination of simple empirical force-field calculations and MD simulations. The mechanism by which the cavity mutations cause affinity increase is shown to be restriction of molecular fluctuations, which can be related to reduced entropy penalty upon binding [6, 7]. IFNγR1 WT and all computationally designed receptor mutants were expressed, purified, and refolded, and the affinity towards the cognate protein, IFNγSC, was measured by SPR. While single mutants showed roughly the same affinity as WT, double mutants combining cavity mutations with the best interface mutation obtained previously [21] were successful in further increasing the binding affinity.

The results demonstrate that mutating cavity residues is a viable strategy for designing protein variants with increased binding affinity. The comparison of computational data and experiments helped to further improve our understanding of forces governing protein-protein interactions. The newly obtained high-affinity binders of IFNγ could be developed into a new diagnostic tool. The significance of the present work can be seen in the fact that small $\Delta\Delta G$ gains of cavity mutants led to significant increase of affinity when combined with more conventional mutations influencing the interface.

Conflict of Interests

The authors declare that there is no conflict of interests regarding the publication of this paper.

Acknowledgments

Support from Grant P305/10/2184 from the Czech Science Foundation is greatly acknowledged. This study was supported by BIOCEV CZ.1.05/1.1.00/02.0109 from the ERDF, Biotechnological expert CZ.1.07/2.3.00/30.0020, and by institutional Grant RVO 86 652 036.

References

[1] P. L. Kastritis and A. M. J. J. Bonvin, "Molecular origins of binding affinity: seeking the Archimedean point," *Current Opinion in Structural Biology*, vol. 23, no. 6, pp. 868–877, 2013.

[2] R. Grünberg, M. Nilges, and J. Leckner, "Flexibility and conformational entropy in protein-protein binding," *Structure*, vol. 14, no. 4, pp. 683–693, 2006.

[3] T. N. Bhat, G. A. Bentley, G. Boulot et al., "Bound water molecules and conformational stabilization help mediate an antigen-antibody association," *Proceedings of the National Academy of Sciences of the United States of America*, vol. 91, no. 3, pp. 1089–1093, 1994.

[4] Y. Urakubo, T. Ikura, and N. Ito, "Crystal structural analysis of protein-protein interactions drastically destabilized by a single mutation," *Protein Science*, vol. 17, no. 6, pp. 1055–1065, 2008.

[5] K. K. Frederick, M. S. Marlow, K. G. Valentine, and A. J. Wand, "Conformational entropy in molecular recognition by proteins," *Nature*, vol. 448, no. 7151, pp. 325–329, 2007.

[6] M. S. Marlow, J. Dogan, K. K. Frederick, K. G. Valentine, and A. J. Wand, "The role of conformational entropy in molecular recognition by calmodulin," *Nature Chemical Biology*, vol. 6, no. 5, pp. 352–358, 2010.

[7] A. J. Wand, "The dark energy of proteins comes to light: conformational entropy and its role in protein function revealed by NMR relaxation," *Current Opinion in Structural Biology*, vol. 23, no. 1, pp. 75–81, 2013.

[8] B. Schneider, J. C. Gelly, A. G. de Brevern, and J. Cerny, "Local dynamics of proteins and DNA evaluated from crystallographic B factors," *Acta Crystallographica D: Biological Crystallography*, vol. 70, part 9, pp. 2413–2419, 2014.

[9] C. Wang, O. Schueler-Furman, and D. Baker, "Improved side-chain modeling for protein-protein docking," *Protein Science*, vol. 14, no. 5, pp. 1328–1339, 2005.

[10] C. Cole and J. Warwicker, "Side-chain conformational entropy at protein-protein interfaces," *Protein Science*, vol. 11, no. 12, pp. 2860–2870, 2002.

[11] M. Bueno, N. Cremades, J. L. Neira, and J. Sancho, "Filling small, empty protein cavities: structural and energetic consequences," *Journal of Molecular Biology*, vol. 358, no. 3, pp. 701–712, 2006.

[12] T. Ohmura, T. Ueda, K. Ootsuka, M. Saito, and T. Imoto, "Stabilization of hen egg white lysozyme by a cavity-filling mutation," *Protein Science*, vol. 10, no. 2, pp. 313–320, 2001.

[13] M. Tanaka, H. Chon, C. Angkawidjaja, Y. Koga, K. Takano, and S. Kanaya, "Protein core adaptability: crystal structures of the cavity-filling variants of *Escherichia coli* rnase HI," *Protein and Peptide Letters*, vol. 17, no. 9, pp. 1163–1169, 2010.

[14] T. Koudelakova, R. Chaloupkova, J. Brezovsky et al., "Engineering enzyme stability and resistance to an organic cosolvent by modification of residues in the access tunnel," *Angewandte Chemie—International Edition*, vol. 52, no. 7, pp. 1959–1963, 2013.

[15] S. Atwell, M. Ultsch, A. M. de Vos, and J. A. Wells, "Structural plasticity in a remodeled protein-protein interface," *Science*, vol. 278, no. 5340, pp. 1125–1128, 1997.

[16] Y. Kawasaki, E. E. Chufan, V. Lafont et al., "How much binding affinity can be gained by filling a cavity?" *Chemical Biology and Drug Design*, vol. 75, no. 2, pp. 143–151, 2010.

[17] L. Morellato-Castillo, P. Acharya, O. Combes et al., "Interfacial cavity filling to optimize CD4-mimetic miniprotein interactions with HIV-1 surface glycoprotein," *Journal of Medicinal Chemistry*, vol. 56, no. 12, pp. 5033–5047, 2013.

[18] J. Černý, J. Vondrášek, and P. Hobza, "Loss of dispersion energy changes the stability and folding/unfolding equilibrium of the trp-cage protein," *The Journal of Physical Chemistry B*, vol. 113, no. 16, pp. 5657–5660, 2009.

[19] D. J. Thiel, M.-H. Le Du, R. L. Walter et al., "Observation of an unexpected third receptor-molecule in the crystal structure of human interferon-γ receptor complex," *Structure*, vol. 8, no. 9, pp. 927–936, 2000.

[20] M. Randal and A. A. Kossiakoff, "Crystallization and preliminary X-ray analysis of a 1:1 complex between a designed monomeric interferon-gamma and its soluble receptor," *Protein Science*, vol. 7, no. 4, pp. 1057–1060, 1998.

[21] P. Mikulecký, J. Černý, L. Biedermannová et al., "Increasing affinity of interferon-γ receptor 1 to interferon-γ by computer-aided design," *BioMed Research International*, vol. 2013, Article ID 752514, 12 pages, 2013.

[22] K. Schroder, P. J. Hertzog, T. Ravasi, and D. A. Hume, "Interferon-gamma: an overview of signals, mechanisms and functions," *Journal of Leukocyte Biology*, vol. 75, no. 2, pp. 163–189, 2004.

[23] E. C. Borden, G. C. Sen, G. Uze et al., "Interferons at age 50: past, current and future impact on biomedicine," *Nature Reviews Drug Discovery*, vol. 6, no. 12, pp. 975–990, 2007.

[24] J. Schymkowitz, J. Borg, F. Stricher, R. Nys, F. Rousseau, and L. Serrano, "The FoldX web server: an online force field," *Nucleic Acids Research*, vol. 33, no. 2, pp. W382–W388, 2005.

[25] A. Landar, B. Curry, M. H. Parker et al., "Design, characterization, and structure of a biologically active single-chain mutant of human IFN-γ," *Journal of Molecular Biology*, vol. 299, no. 1, pp. 169–179, 2000.

[26] N. R. Voss and M. Gerstein, "3V: cavity, channel and cleft volume calculator and extractor," *Nucleic Acids Research*, vol. 38, no. 2, pp. W555–W562, 2010.

[27] W. Humphrey, A. Dalke, and K. Schulten, "VMD: visual molecular dynamics," *Journal of Molecular Graphics*, vol. 14, no. 1, pp. 33–38, 1996.

[28] B. Webb and A. Sali, "Protein structure modeling with MODELLER," *Methods in Molecular Biology*, vol. 1137, pp. 1–15, 2014.

[29] B. Hess, C. Kutzner, D. van der Spoel, and E. Lindahl, "GROMACS 4: algorithms for highly efficient, load-balanced, and scalable molecular simulation," *Journal of Chemical Theory and Computation*, vol. 4, no. 3, pp. 435–447, 2008.

[30] P. Eastman and V. S. Pande, "OpenMM: a hardware-independent framework for molecular simulations," *Computing in Science & Engineering*, vol. 12, no. 4, pp. 34–39, 2010.

[31] M. S. Friedrichs, P. Eastman, V. Vaidyanathan et al., "Accelerating molecular dynamic simulation on graphics processing units," *Journal of Computational Chemistry*, vol. 30, no. 6, pp. 864–872, 2009.

[32] P. A. Kollman, "Advances and continuing challenges in achieving realistic and predictive simulations of the properties of organic and biological molecules," *Accounts of Chemical Research*, vol. 29, no. 10, pp. 461–469, 1996.

[33] G. Bohm, R. Muhr, and R. Jaenicke, "Quantitative analysis of protein far UV circular dichroism spectra by neural networks," *Protein Engineering*, vol. 5, no. 3, pp. 191–195, 1992.

[34] E. Sviridova, L. Bumba, P. Rezacova et al., "Crystallization and preliminary crystallographic characterization of the iron-regulated outer membrane lipoprotein FrpD from *Neisseria meningitidis*," *Acta Crystallographica Section F: Structural Biology and Crystallization Communications*, vol. 66, part 9, pp. 1119–1123, 2010.

[35] M. Fountoulakis and R. Gentz, "Effect of glycosylation on properties of soluble interferon gamma receptors produced in prokaryotic and eukaryotic expression systems," *Nature Biotechnology*, vol. 10, no. 10, pp. 1143–1147, 1992.

[36] T. Sengupta, Y. Tsutsui, and P. L. Wintrode, "Local and global effects of a cavity filling mutation in a metastable serpin," *Biochemistry*, vol. 48, no. 34, pp. 8233–8240, 2009.

[37] T. S. Chen and A. E. Keating, "Designing specific protein-protein interactions using computation, experimental library screening, or integrated methods," *Protein Science*, vol. 21, no. 7, pp. 949–963, 2012.

[38] E. Saesen, S. Sarrazin, C. Laguri et al., "Insights into the mechanism by which interferon-γ basic amino acid clusters mediate protein binding to heparan sulfate," *Journal of the American Chemical Society*, vol. 135, no. 25, pp. 9384–9390, 2013.

[39] K. Okonechnikov, O. Golosova, M. Fursov, and UGENE Team, "Unipro ugene: a unified bioinformatics toolkit," *Bioinformatics*, vol. 28, no. 8, pp. 1166–1167, 2012.

[40] S. T. Sherry, M.-H. Ward, M. Kholodov et al., "DbSNP: the NCBI database of genetic variation," *Nucleic Acids Research*, vol. 29, no. 1, pp. 308–311, 2001.

PROTEINS
STRUCTURE ■ FUNCTION ■ BIOINFORMATICS

Novel high-affinity binders of human interferon gamma derived from albumin-binding domain of protein G

Jawid N. Ahmad,[1†] Jingjing Li,[2†] Lada Biedermannová,[2] Milan Kuchař,[2] Hana Šípová,[3] Alena Semerádtová,[4] Jiří Černý,[2] Hana Petroková,[2] Pavel Mikulecký,[2] Jiří Polínek,[2] Ondřej Staněk,[1] Jiří Vondrášek,[2] Jiří Homola,[3] Jan Malý,[4] Radim Osička,[1] Peter Šebo,[1,2] and Petr Malý[2*]

[1] Institute of Microbiology of the ASCR, v. v. i., Vídeňská 1083, 142 20 Prague, Czech Republic
[2] Institute of Biotechnology of the ASCR, v. v. i., Vídeňská 1083, 142 20 Prague, Czech Republic
[3] Institute of Photonics and Electronics of the ASCR, v. v. i., Chaberská 57, 182 51 Prague, Czech Republic
[4] Faculty of Science, Jan Evangelista Purkyně University, České Mládeže 8, 400 96 Ústí nad Labem, Czech Republic

ABSTRACT

Recombinant ligands derived from small protein scaffolds show promise as robust research and diagnostic reagents and next generation protein therapeutics. Here, we derived high-affinity binders of human interferon gamma (hIFNγ) from the three helix bundle scaffold of the albumin-binding domain (ABD) of protein G from *Streptococcus* G148. Computational interaction energy mapping, solvent accessibility assessment, and *in silico* alanine scanning identified 11 residues from the albumin-binding surface of ABD as suitable for randomization. A corresponding combinatorial ABD scaffold library was synthesized and screened for hIFNγ binders using *in vitro* ribosome display selection, to yield recombinant ligands that exhibited K_d values for hIFNγ from 0.2 to 10 n*M*. Molecular modeling, computational docking onto hIFNγ, and *in vitro* competition for hIFNγ binding revealed that four of the best ABD-derived ligands shared a common binding surface on hIFNγ, which differed from the site of human IFNγ receptor 1 binding. Thus, these hIFNγ ligands provide a proof of concept for design of novel recombinant binding proteins derived from the ABD scaffold.

Proteins 2011; 00:000–000.

Key words: recombinant ligand; protein scaffold; computational design; combinatorial library; ribosome display.

INTRODUCTION

Interferon gamma is a pro-inflammatory cytokine that plays a key role in innate immune response.[1–3] It consists of a 143 residue-long all-alpha glycoprotein forming a head-to-tail dimer[4,5] in which four of the six helices of one subunit are interlocked with two of the helices of the other subunit. This yields a globular homodimer structure with a noncrystallographic twofold axis.[6]

Currently, specific antibodies are used for determination of levels of human interferon gamma (hIFNγ) released by activated antigen-specific memory T cells, such as in the commercial enzyme-linked immunosorbent assay (ELISA) or ELISPOT assays for detection of latent tuberculosis infection. In turn, development of microfluidic biosensors for hIFNγ, or other bioanalytes, often requires the use of alternative and more robust reagents that can resist reducing conditions, hydrodynamic shearing forces and/or refold quantitatively upon denaturation. These are typically small engineered binding proteins (recombinant ligands), which are nowadays intensely explored as an alternative to antibodies for many applications.[7–9]

Because of the complexity of the folding problem, however, de novo design of proteins with desirable properties remains difficult. Therefore, engineering of protein scaffolds with robustly organized structure has been used to generate recombinant ligands.[8,10–13] Protein domains that are stable enough to tolerate amino acid substitutions without losing the original fold have, indeed, successfully been used for generation of highly complex libraries of randomized scaffold variants.[7,12,14,15] These were subsequently screened for binders of numerous targets, using high-

[†]Jawid N. Ahmad and Jingjing Li contributed equally to this work.

Grant sponsor: Grant Agency of The Academy of Sciences of the Czech Republic; Grant number: KAN200520702; Grant sponsor: Grant Agency of the Czech Republic; Grant number: P305/10/2184; Grant sponsor: Academy of Sciences of the Czech Republic, Institutional Research Concept; Grant numbers: AV0Z50200510 and AV0Z50520701.
*Correspondence to: Petr Malý, Institute of Biotechnology of the ASCR, v. v. i., Vídeňská 1083, 142 20 Praha 4, Czech Republic. E-mail: petr.maly@img.cas.cz.
Received 16 August 2011; Revised 5 October 2011; Accepted 17 October 2011
Published online 29 October 2011 in Wiley Online Library (wileyonlinelibrary.com). DOI: 10.1002/prot.23234

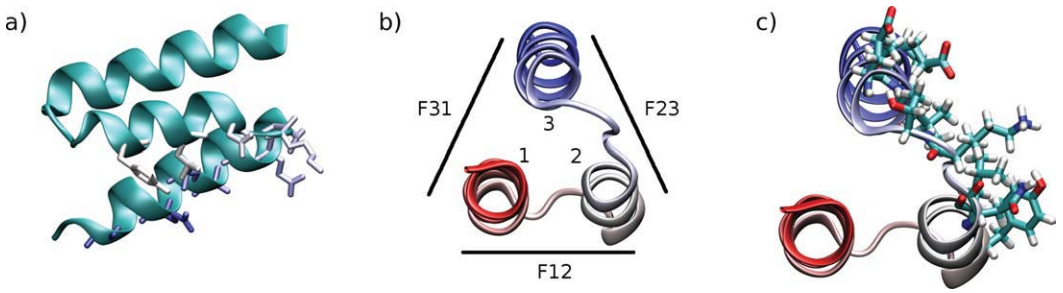

Figure 1

The ABD scaffold. (**a**) ABD protein structure in ribbon representation, with the 11 residues selected for randomization shown as sticks. (**b**) Definition of the three faces of the ABD molecule. (**c**) ABD protein structure with indicated randomized residues in the same orientation as in (b).

throughput selection technologies, such as phage or cell surface display *in vivo*,[16] or display of nascent proteins on ribosomes *in vitro*.[17] Typically, the diversification of a scaffold sequence involves combinatorial randomization at certain positions[8] and affinity maturation of selected binders by a combination of semirational and random mutagenesis procedures.[18] The bottleneck of these approaches, however, is the choice of residues for randomization, so as to preserve the stability and folding of the scaffold.[15] Toward this aim, empirical,[7] structure-instructed,[8] and "consensus design" approaches have been used,[19] with the latter allowing successful construction of combinatorial DARPin libraries.[20,21] In these approaches, however, some of the positions suitable for randomization may be missed, as conservation of function and structure are particularly hard to distinguish in globular proteins and mutations of surface residues can affect protein stability. On the other hand, the surface of most protein scaffolds appears to contain residue patches where extensive sequence variation does not affect the overall structure.[22]

In this study, we analyzed the potential to serve as a binder scaffold for a 46 residue-long segment from the third albumin-binding domain (ABD) of protein G from *Streptococcus* G148 (SpG), also called the GA module (PDB ID: 1GJT, residues 20–65). This left-handed three-helix bundle domain binds human serum albumin (HSA) with nanomolar affinity[23–25] and exhibits a 3D structure that resembles a trigonal prism, with edges formed by the three helices [Fig. 1(a–c)]. Previous alanine scanning experiments revealed that residues contributing the affinity for HSA were located on the face F23.[26] Indeed, structural analysis of the HSA complex with the ALB8_GA protein of *Finegoldia magna* (PDB ID: 1TF0) confirmed that residues from the second ABD helix and the loops surrounding it are involved in HSA binding together with residues from helix 3.[27]

In a recent study, ABD library was constructed by randomization of 15 surface residues, based on structural and sequence conservation analysis, resulting in HSA-binders with 50–500 femtomolar affinities.[28] Moreover, a high thermal ($T_m \approx 70^\circ C$) and chemical stability was reported for ABD, which further qualified it as a candidate for construction of scaffold libraries. Recently, a dual affinity binder was constructed using randomization of ABD scaffold and phage display selection.[29]

In this work, we explored the potential of the ABD scaffold to yield binders of other targets than HSA. Toward this aim, rational selection of ABD residues amenable for randomization was complemented by computational analysis of structural stability of ABD upon *in silico* mutagenesis, so as to instruct the construction of a combinatorial library of ABD scaffolds. A highly mutable contiguous residue patch on the ABD surface was identified, which upon randomization and ribosome display selection yielded ligands that bind hIFNγ with nanomolar affinities.

MATERIALS AND METHODS

Interaction energy map

The structure of the third ABD of protein G from *Streptococcus* strain G148 was obtained from Protein Data Bank under accession code 1GJT. Its residues 20–65, marked here as ABD sequence, were used for structure modeling, with the numbering of residues 1–46 corresponding to the truncated sequence throughout this article.

For identification of the key stabilizing residues in the ABD structure, we used the interaction energy map (IEM) method, which evaluates the importance of each residue in protein structure based on the amount of stabilization energy the residue brings to the stability of the fold.[30] Standard parm94 force field[31] was applied as implemented in Amber 8 package,[32] together with the generalized Born solvent model,[33] using the standard value of dielectric constant of $\varepsilon_r = 78.5$ for water.

To calculate the individual residue–residue interactions in Amber, the polypeptide chain was split into fragments, cutting the peptide bond, and capping the fragments

with acetyl group ($H_3C—C=O—$) at the N terminus and with N-methyl group ($—NH—CH_3$) at the C terminus. The stabilization energy of *n*th residue was then calculated as the sum of all its pair-wise interaction energies in pairs of *n*th and *m*th residue, such as $|n - m| > 2$ (i.e., non-neighboring residues). Amber 8 package[32] and our own script were used for the calculations.

Calculation of solvent accessibility

The solvent-accessible surface area (SASA) of each residue in the ABD structure was calculated using the Parameter OPtimized Surfaces (POPS) web server[34,35] with atomic-level resolution algorithm and parameters.

In silico alanine scanning using Eris

The Eris protein stability estimator was used to predict the thermodynamic stability of the ABD fold following *in silico* mutation at certain positions.[36] This enables to accurately compute stability changes of proteins upon mutations using the protein-modeling force field Medusa, based on physical descriptions of atomic interactions and not relying on parameter training with available experimental protein stability data. The freely available Eris web server was used for calculations[37] with backbone prerelaxation option and backbone flexibility allowed.

Generation of DNA library

HPLC-purified synthetic oligonucleotides were used. The forward primer ABDLIB-setB1c (5′-TTAGC TGAAG CTAAA GTCTT AGCTA ACAGA GAACT TGACA AATAT GGAGT AAGTG AC-3′) and the reverse primer setB-rev (5′-ACCGCGGATC CAGGTAA-3′) were used for PCR in 10 times higher molar concentration than the connecting ABDLIB-setB2c template oligonucleotide. The latter had distinct codons randomized at defined positions (5′-ACCGCGGATCCAGGTAAMNNAGCTAAAATM NNATCTATMNNMNNTTTTACMNNMNNAACMNNM NNGGCMNNGTTGATMNNGTTCTTGTAMNNGTCAC TTACTCCATATTTGTC-3′), in which M represents C/A, N any nucleotides out of A, G, C or T. In order to prepare the DNA template for ribosome display, a published protocol[38] was used with slight modifications. To serve as a protein spacer for ribosome display, the *tolA* gene (GENE ID: 946625 tolA) coding for a membrane anchored protein from the TolA-TolQ-TolR complex was amplified from *Escherichia coli* K12 strain genomic DNA, using the primer pairs ABDLIB-tolA-link (5′-TTACCTGGATCCGCGGTCGGTTCGAGCTC-CAAGCTTGGATCTGGT GGCCAGAAGCAA-3′) and tolArev (5′-TTTCCGCTCGAGCTACGGTTT GAAGTC-CAATGGCGC-3′). The obtained products were linked to the randomized ABD sequences using amplification with primer pairs EWT5-ABDfor1 (5′-TTCCTCCATGG GTATGAGAGGATCGCATCACCATCACCATCACTTAGC TGAAGCTAAAGTCTTA-3′) and tolArev. The primer EWT5-ABDfor1 contains a sequence encoding a tetrapeptide MetArgGlySer and a six histidine tag fused to the N-terminus of the ABD. To add the T7 promoter and ribosome binding site sequences, the obtained DNA fragment was subjected to further consecutive PCR amplifications with the set of primers T7B (5′-ATACGAAATTAATACGACTCACTATAGGGAGACCACA ACGG-3′), SD-EW (5′-GGGAG ACCACAACGGTTTCC CTCTAGAAAT AATTTTGTTTAACTTTAAGAAGGAG A TATACCATGGGTATGAGAGGATCG-3′) and *tolA*k (5′-CCGCACACCAGTAAGGTGTG CGGTTTCAGTTGCCG CTTTCTTTCT-3′), generating a DNA library of ABD variants lacking the downstream stop codon.

Ribosome display selection

An aliquot of the generated DNA library with an estimated complexity of 10^{13} ABD allele variants was used for *in vitro* transcription reaction and the resulting mRNA was translated using *E. coli* S30 extract as described.[38] The translated products were loaded into microtiter plate wells precoated with 3% bovine serum albumin (BSA) for a preselecting subtraction of BSA-binding ligands at 4°C for 1 h, before transfer into Maxisorp (NUNC, Denmark) microtiter plate wells coated with recombinant hIFNγ and blocked with BSA. After incubation at 4°C for 1 h, the plate wells were washed three times with TBS (50 m*M* Tris-HCl pH 7.4, 150 m*M* NaCl), followed by washing with ice-cold WBT (50 m*M* Tris-acetate, pH 7.0, 150 m*M* NaCl, 50 m*M* MgAc) with increasing concentrations of Tween-20. To release mRNA from the bound ribosome complex, elution with elution buffer (50 m*M* Tris-acetate, pH 7.5, 150 m*M* NaCl, 50 m*M* ethylenediaminetetraacetic acid (EDTA)) containing 50 μg/mL of *Saccharomyces cerevisiae* RNA as carrier was performed. Purified RNA was transcribed into cDNA using a specific reverse transcription with setB-rev reverse primer, annealing to the 3′ end of the ABD cDNA. Double-strand DNA was next obtained by PCR using EWT5-ABDfor1 and setB-rev primers. The final amplified DNA encoding selected ABD variants contained T7 promoter and RBS sequences and a truncated *tolA* fragment. To isolate high affinity binders, the stringency of binding and washing conditions was increased after each round of selection (Table I).

ELISA screening for hIFNγ binders

DNA encoding ABD variants isolated after the final round of selection was fused with full-length *tolA* sequence using PCR amplification with the EWT5-ABD-for1 and tolArev primer pair. The resulting DNA product was digested with *Nco*I and *Xho*I enzymes, ligated into the pET28b plasmid, and transformed into *E. coli* DH5α. For production of the 6×His-ABD-tolA fusion products,

Table I
Stringency of Washing Conditions Used in Each Cycle of Ribosome Display

Cycle number	1	2	3	4	5[a]	6	7[b]
Immobilized hIFNγ (μg/mL)	25	25	10	4	1	0.2	0.02
Wash times	5	10	10	10	10	10	10
Tween-20 in Wash buffer (%)	0.05	0.05	0.25	0.5	1	1	1

[a]Clones obtained after five rounds of selection are called PM series in clone list (Fig. 3).
[b]Clones obtained after seven rounds of selection are called JA series in clone list (Fig. 3).

plasmids with cloned DNA were transformed into *E. coli* BL21 (DE3). Individual clones producing various ABD-TolA proteins were grown from colonies randomly picked from an agar plate in 96 deep-well plates in 1 mL of Luria-Bertani (LB) medium with 60 μg/mL of kanamycin and 0.2 m*M* isopropyl-beta-D-thiogalactopyranoside (IPTG). After cultivation for 18 h at 37°C, the bacteria were pelleted by centrifugation at 3000*g* for 30 min, and the supernatant was discarded. A total of 250 μL of PBS containing 0.1% Tween-20 (PBST) and 200 μg/mL lysozyme was used to resuspend the pellet, and cells were lysed by three cycles of freezing at −80°C for 30 min followed by thawing in a water bath at 37°C for 30 min. The resulting suspensions were centrifuged at 3000*g* for 30 min, and 50 μL of supernatant from each well was applied to a PolySorp microtiter plate (NUNC) coated with hIFNγ at the concentration 5 μg/mL. Upon 1 h incubation at room temperature, the plate was washed with PBST five times, anti-His-tag antibody diluted (1:5000) in PBS with 3% BSA (PBSB) was added for 45 min, and the plate wells were washed repeatedly and developed in 0.1*M* citrate buffer, pH 5.0 containing 0.5 mg/mL *o*-phenylenediamine (OPD) and 0.01% H_2O_2 for 5 min. The colorimetric reaction was stopped by adding 100 μL 2*M* H_2SO_4 and absorbance at 492 nm was determined. Lysate containing wild-type (WT) version of ABD, ABD-WT-TolA fusion protein, was applied to HSA-coated wells to serve as positive control, whereas negative control background was determined in wells coated with 3% BSA. Identity of constructs yielding ABD variants binding to hIFNγ was determined by DNA sequencing.

Sequence analysis, clustering, and modeling of selected ABD variants

Multiple sequence alignment and construction of the similarity tree was performed using the ClustalW program.[39] The tree is presented as a phenogram rendered by the Phylodendron online service (http://iubio.bio.indiana.edu/treeapp). The homology modeling of selected ABD variants was performed using the Modeller program[40] based on the ABD_WT as a template. Resulting three-dimensional structures were refined by the FoldX program[41] and Stricher et al., (in preparation) and subjected to flexible side chain docking to the hIFNγ (3D structure taken from the PDB code 1FG9). The docking was performed using the ClusPro server.[42] For each selected ABD variant, we ran a short (2 ns) molecular dynamics (MD) simulation of the top 10 predicted structures of the complex using the Gromacs version 4 suite of programs.[43] The solute was put inside a periodic box of water and charge neutralizing ions with dimensions exceeding the size of the solute by 10 Å in each direction and simulated at constant 300 K and 1 atm conditions with cutoffs of 10 Å and 2 fs time step, using the FF03 force field[44] with the TIP3P explicit water solvation model. The snapshots of geometry (nonminimized, saved each 1 ps) from last 500 ps of each trajectory were used to calculate the averaged ΔG of binding within the FoldX force field approximation.

Production of ABD-TolA proteins

Two milliliters of overnight cultures of clones producing interferon binders were inoculated into 200 mL of LB medium containing 60 μg/mL kanamycin and grown for 4 h at 37°C, before 1 m*M* IPTG was added for additional 4 h. Cells were harvested by centrifugation at 4000*g*, pellets were resuspended in 25 mL of lysis buffer (50 m*M* NaH_2PO_4, 300 m*M* NaCl, 10 m*M* imidazole, pH 8.0), and cells were disrupted by ten 10 s ultrasound pulses at 27 W power output (Misonix S3000). The lysates were centrifuged for 20 min at 23,700*g*, applied to 1 mL Ni-NTA columns (Qiagen) equilibrated with lysis buffer, and the columns were washed with 20 mL of wash buffer (lysis buffer containing 20 m*M* imidazole). ABD-TolA fusion proteins were eluted with 5 mL of lysis buffer containing 250 m*M* imidazole. Typical yield of purified ABD-TolA protein produced by *E. coli* BL21 host cells in LB broth medium is more than 20 mg/L.

ELISA assay for binding to hIFNγ

Serially diluted purified ABD-TolA variants were applied to the Polysorp microtiter plate coated with 5 μg/mL hIFNγ, and the plate was incubated at RT for 1 h. The plate was washed five times with ice-cold PBST and monoclonal Anti-His_6-tag-horse radish peroxidase (HRP) conjugate solution in PBSB (dilution 1:5000) and OPD substrate were used to detect bound ABD-TolA proteins as above. The plots of absorbance at 492 nm versus ABD concentration were subjected to sigmoidal fitting using Origin software (OriginLab Corporation, USA) and apparent dissociation constants (K_d) were calculated.

Competition ELISA with synthetic ABD35

Polysorp 96-well plate (NUNC, Denmark) was coated with 100 μL coating buffer containing 10 μg/mL hIFNγ

(produced by Proteix, s.r.o., Czech Republic) and kept at 4°C overnight. The plate was washed with PBST (PBS with 0.05% Tween-20) pH 7.4, and blocking step was done using 300 µL 1% BSA in PBST followed by 2 h incubation at 37°C. The plate was then washed with PBST three times. Serially diluted synthetic ABD35 protein variant (46 residues, Institute of Organic Chemistry and Biochemistry ASCR, v.v.i., Prague, Czech Republic) was added into wells containing 100 n*M* solutions of individual ABD-TolA variants in 1% BSA/PBST. Following 2 h of co-incubation at room temperature, the plate was washed five times with PBST and 100 µL of 5000-fold diluted monoclonal anti-polyhistidine peroxidase conjugate was added into each well for 1 h, before the plate was washed three times with PBST and OPD solution was added. Reaction was stopped by 2*M* sulfuric acid and absorbance at 492 nm was measured.

Preparation of *in vivo* biotinylated hIFNγ

A DNA fragment encoding a 143 residue-long variant of hIFNγ with an N-terminal methionine residue and a C-terminal AviTag consensus sequence (GLNDIFEAQKIEWHE) was PCR-amplified using appropriate primers, cloned in the pET-28b vector, and used to transform *E. coli* BL21 (DE3) BirA cells. C-terminally biotinylated hIFNγ-AviTag protein was produced in *E. coli* cultures upon induction with 1 m*M* IPTG in the presence of 50 µ*M* D-biotin (Sigma-Aldrich), extracted from inclusion bodies with 8*M* urea in 50 m*M* Tris buffer (pH 7.4) and purified by chromatography on SP Sepharose pH 7.4 followed by Phenyl Sepharose CL-4B (Pharmacia) at pH 7.4. The eluted hIFNγ-AviTag protein was dialyzed into 50 m*M* ammonium acetate solution pH 5.0.

Preparation of *in vivo* biotinylated ABD variants

To express and produce ABD variants without TolA moiety, a 19 residue-long N-terminal *trp* leader sequence (MKAIFVLNAQHDEAVDAMD) was fused to the ABD scaffold sequence and a C-terminal AviTag biotinylation consensus sequence (GLNDIFEAQKIEWHE) was added. This yielded 82 amino acid residue-long ABD-AviTag constructs. These ABD-AviTag binders were produced as biotinylated proteins in *E. coli* BL21 (DE3) BirA strain, expressing the biotin ligase (BirA), as above and were extracted from inclusion bodies with solution of 50 m*M* Tris, 150 m*M* NaCl, 8*M* urea, pH = 8.0.

Production of soluble recombinant hIFNγ receptor 1 (hIFNγR1)

A codon-optimized synthetic gene encoding the mature 228 residue-long extracellular domain of hIFNγR1 with an N-terminal methionine residue and a C-terminal LEHHHHHH polyhistidine tag (237 residues in total, 27 kDa) was purchased from GenScript (USA). The soluble form of the receptor was produced in IPTG-induced *E. coli* SHuffle T7 Express cells (New England Biolabs, USA) at 16°C, and the protein was purified from cytoplasmic extracts using metallo-affinity chromatography on Ni-NTA agarose (Qiagen).

Binding specificity testing

Polysorp 96-well plate (NUNC, Denmark) was coated at 4°C overnight with 10 µg/mL of different target proteins (hIFNγ, Culture Filtrate Protein-10/Early Secreted Antigenic Target 6 complex, lysozyme, BSA, HSA) and human serum (1:10 dilution in coating buffer). The plate was washed with PBST (PBS + 0.05% Tween-20) pH 7.4, and blocked with 2% BSA in PBST for 1 h at 30°C. After washing, His_6-ABD-TolA proteins at indicated concentrations in PBST with 2% BSA were added. Binding of His_6-ABD-TolA variants was detected by Anti-His-tag monoclonal antibody conjugated with HRP at 1:4000.

Chemical biotinylation of ABD-TolA proteins

Before immobilization on the biosensor chip for surface plasmon resonance (SPR) measurements, C-terminal carboxyl groups of ABD-TolA proteins were labeled with biotin hydrazide. Purified ABD-TolA proteins were dialyzed against the reaction buffer (10 m*M* 2-(N-morpholino)ethanesulfonic acid (MES) pH 4.8). Then, 2.5 µL of 5 m*M* biotin hydrazide (Sigma-Aldrich) in dry dimethyl sulphoxide and 1.25 µL 50 m*M* 1-ethyl-3-(3-dimethylaminopropyl)carbodiimide hydrochloride (EDC) (Sigma-Aldrich) in reaction buffer were added per mg of the protein, mixed, and incubated for 2 h. To remove nonreacted biotin hydrazide, EDC, and the precipitate occasionally forming during the reaction (cross-linked proteins), the solution was centrifuged for 2 min at 5000 RPM and the supernatant was dialyzed against SPR running buffer (10 m*M* HEPES 7.4).

Preparation of the SPR biosensor

All modification steps were performed sequentially on an SPR chip inserted in the microfluidic block of a SensiQ instrument (ICX Nomadics, USA) with on-line control of the degree of modification [resonance unit (RU)]. The temperature was set to 25°C and flow rate to 10 µL/min. After thermal equilibration of the chip (2 h), the carboxyl groups of the chip (COOH-2, ICX Nomadics) were activated in both reference and measurement channels with injection of 200 µL of freshly prepared mixture of 0.4*M* EDC and 0.1*M* N-hydroxysuccinimide (NHS) (MES buffer pH 6.0). Biotin hydrazide was next covalently coupled to surface of the working channel in 1.25 m*M* MES pH 4.8 (200 µL injection). Free NHS-ester groups were deactivated by injecting 200 µL of 1*M* ethanolamine-hydrochloride pH 8.5 into both channels.

Then, the flow rate was reduced to 5 μL/min, and the working channel surface was coated with avidin (50 μL injection, 100 n*M* in running buffer). Finally, 100 μL of biotinylated ABD-TolA variants (2.5 μg/mL, running buffer) was injected and bound to the surface (∼ 100 RU) due to the avidin-biotin interaction.

SPR analysis with immobilized ABD-TolA

The flow rate (25 μL/min) and temperature (25°C) were held constant during the SPR experiments. hIFNγ stock solution (8.2 μ*M* in running buffer) was prepared from a frozen aliquot in 50 m*M* acetate buffer pH 5.0. Serial dilutions (25–200 n*M*) of hIFNγ as analyte were prepared and sampled into both working and reference channels. The assay template was set as follows: association of the hIFNγ with the immobilized ABD-TolA (180 s, 75 μL of the hIFNγ), intermission time for observing the dissociation (running buffer flow, 360 s), and finally, the regeneration of the sensor surface (25 μL solution of 0.05% SDS and 0.15 m*M* HCl, 600 s running buffer flow). The last step allowed to recover the initial baseline and to start another assay cycle. Reference channel was used for real-time reference curve subtraction. Blank buffer injections were used to allow double referencing of the data set. Data processing and kinetic model fitting were performed using Qdat, derived from Scrubber2 and developed by BioLogic Software (Australia). A 1:1 fitting model without mass transport limitations was chosen for calculation of K_d using a set of 5 SPR binding curves. All parameters (k_{on}, k_{off}) except for R_{max} were fitted globally. The obtained residual standard deviations were lower than 5% of the maximum experimental response. For the validation of the curves and parameter values, the residual plot was inspected for nonrandom distribution.

SPR analysis with free ABD-TolA

SPR measurements of free ABD-TolA proteins were carried out using custom SPR biosensors (Institute of Photonics and Electronics AS CR, v.v.i., Prague, Czech Republic) with four independent sensing spots.[45] The SPR sensor output is stated in nanometers (nm) and describes the spectral shift of SPR. The response in nm can be easily transformed to units used by BIACORE instruments using the calibration equation: 1 nm = 150 RU. Briefly, recombinant streptavidin was covalently linked to sensor chip surface as described[46] and used to capture the biotinylated hIFNγ target. To suppress nonspecific adsorption, the chip surface was blocked for 10 min with a solution of 500 μg/mL BSA in SA buffer. Attachment of biotinylated hIFNγ was performed in SA buffer (10 m*M* sodium acetate, pH 5 at 25°C). Once a stable baseline was reached, solution of hIFNγ was flowed across the sensing surface for 10 min. This step was followed by washing of the sensor surface with SA buffer. Running buffer (10 m*M* HEPES, 150 m*M* NaCl, 50 μ*M* EDTA, 0.005% Surfactant P20, pH 7.4, 25°C) was injected into the flow-cell until the baseline became stable. The solution of particular ABD-TolA variants at concentrations ranging from 20 to 500 nM were injected into the measuring (+hIFNγ) and reference (−hIFNγ) channels. After 5 min incubation, ABD-TolA solution was replaced with running buffer, and the dissociation was monitored for at least 15 min. Each concentration was measured on at least two different SPR chips. Reference-compensated sensor responses to at least three concentrations were fitted with Langmuir model implemented in BiaEvaluation software, taking mass transport into account. All the measurements were performed at 25°C and flow-rate of 30 μL/min.

RESULTS

Computational analysis of mutability of the GA module

To generate a library of the ABD scaffolds, we identified ABD residues suitable for randomization, the substitution of which was unlikely to affect the structure and stability of ABD. Inspection of the structure of the HSA complex with ALB8-GA protein revealed that residues from the conserved consensus sequence of the GA module family (helices 2 and 3 with residues 19–27 and 31–44, respectively) are in contact (i.e., within less than 4 Å) with the HSA chain.[27] It was, hence, plausible to assume that the conserved residues not participating in HSA binding (i.e., residues L1, A4, K5, A8, E11, L12, D19, I25, N26, V31, and L42) were structurally important and must not be mutated to preserve scaffold stability. The consensus analysis, however, did not allow assessing the structural importance of residues that were in contact with HSA. These, in turn, needed to be randomized to eliminate HSA binding and generate novel binding specificities to unrelated targets.

To this end, the solved NMR structure of ABD (ABD-WT) was analyzed using the IEM method,[30] to computationally assess the overall stability changes of the scaffold following substitution of individual amino acid residues. Contribution of each residue to stabilization of the ABD structure was calculated as the sum of its pair-wise interaction energies (E_{int}) with all other ABD residues except sequence neighbors. Residues with the lowest (most negative) value of total interaction energy were then taken as key stabilizing residues of the structure. At the same time, the key residues were also characterized by a high number of stabilizing interactions ($E_{int} < -0.5$ kcal/mol).

As shown in Figure 2(a), the residues revealed by IEM as bringing the largest stabilization to the structure were, in the order of decreasing contribution, L12 (−17.7 kcal/mol), K5 (−17.0 kcal/mol), I25 (−16.7 kcal/mol), R10 (−15.3 kcal/mol), N9 (−15.2 kcal/mol), A8 (−14.5 kcal/

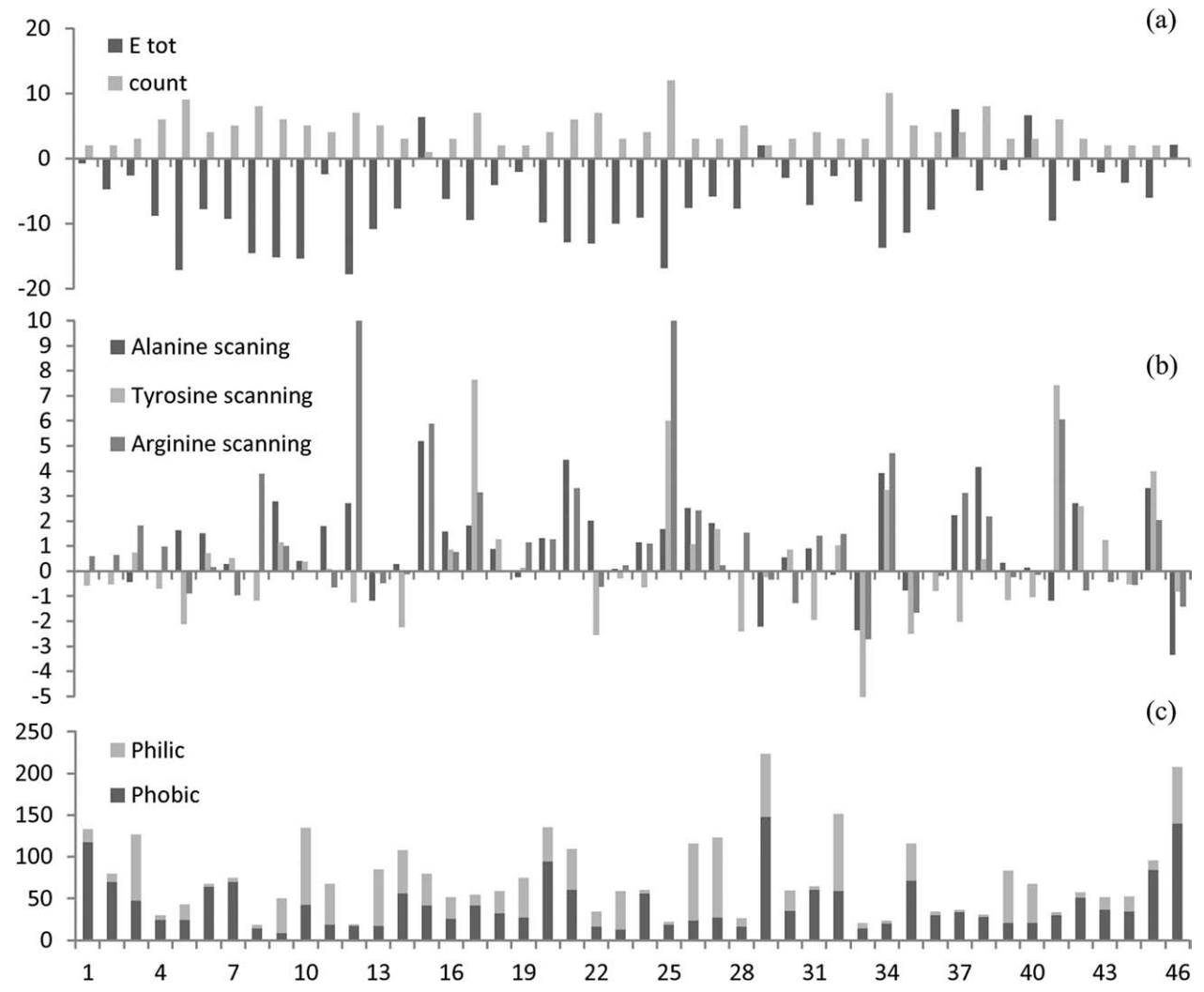

Figure 2

Computational analysis of ABD mutability. (**a**) Total interaction energies (E_{tot} in kcal/mol) for individual amino acid residues of the ABD structure (black) and the number of stabilizing interactions ($E_{int} < -0.5$ kcal/mol) for each residue (gray). (**b**) ABD stability change ($\Delta\Delta G$, in kcal/mol) upon *in silico* alanine, tyrosine and arginine scanning. (**c**) SASA of individual ABD residues. The size of the bar denotes the total SASA of the residue, the proportion of hydrophilic SASA and hydrophobic SASA denoted in gray and black color, respectively. Calculation was done using POPS server.[34,35]

mol), V34 (−13.6 kcal/mol), respectively (E_{tot} in parenthesis). Interestingly, not all of these key residues were nonpolar residues forming the hydrophobic core, for example, with small SASA. Despite their large SASA [c.f. Fig. 2(c)], three out of seven of the key residues found to substantially contribute to ABD stability were, indeed, the polar and charged residues K5, N9, and R10. Importantly, these were all located at the surface of helix 1, and none of the residues predicted to form the stabilizing framework was located in helices 2 and 3, which are involved in binding of HSA. These results suggested that randomization of helices 2 and 3 would not only yield loss of HSA binding but may also have little or no impact on stability of the ABD scaffold.

Destabilization effects caused by residue substitutions were first assessed by *in silico* scanning mutagenesis of the ABD surface formed by helices 2 and 3 [Fig. 2(b)]. Besides alanine scanning, also tyrosine and arginine residue scanning was performed to assess the impact of insertion of the bulkier residues that are frequently found at protein–protein interfaces.[47,48] The predicted changes in protein stability induced by individual substitutions ($\Delta\Delta G$) were calculated using the Eris server[36] and advantage was taken of the capacity of Eris to model backbone flexibility and mutation-induced backbone conformational changes. This approach was previously shown to be particularly important for $\Delta\Delta G$ estimation of small-to-large mutations, thus allowing to increase the accuracy of prediction and yield-

ing significant correlation with the experimental data.[49] As shown in Figure 2(b), in the 26 residue-long segment comprising helices 2 and 3 (positions 16–45), the Eris scanning protocol identified the residues V17, Y21, I25, V34, and I41 as nonmutable. With the exception of residue Y21, these residues mostly appear to be nonpolar and buried in the hydrophobic core of ABD. In combination with the assessment of SASA [Fig. 2(c)], this computational analysis allowed to chose 11 surface residues of ABD, the randomization of which was predicted to have the least impact on stability of the ABD scaffold (e.g., Y20, L24, N27, K29, T30, E32, G33, A36, L37, E40, and A44).

Ribosome display selection of hIFNγ binders

To screen for hIFNγ binders, a synthetic oligonucleotide library was designed in NNK code with 11 codon positions randomized, yielding a theoretical complexity of 32^{11} codons ($= 3.6 \times 10^{16}$). Taking into account, the redundancy of the genetic code, where the same amino acid residue can be encoded by up to six synonymous codons, randomization of 11 codons of the the ABD encoding sequence was expected to give rise to $\sim 2 \times 10^{14}$ (i.e., 20^{11}) ABD variants. A library of 10^{14} oligonucleotide molecules was synthesized, bearing randomized codons at selected position of the ABD gene and $\sim 10^{13}$ annealed double stranded oligonucleotide molecules (25 pmol) were used per reaction to assemble a library of genes encoding randomized ABD-*tolA* fusion constructs by successive rounds of PCR-mediated assembly. The obtained DNA template pool was subjected to *in vitro* transcription and used for *in vitro* translation, yielding formation of ternary complexes of ribosomes with attached nascent ABD-TolA fusions proteins. These were selected for binding to immobilized hIFNγ in hIFNγ-coated microtiter plates, with successively decreasing the coated target protein (hIFNγ) concentration and increasing the stringency of washing after each selection cycle (increasing the number of wash cycles and the detergent concentration).

In the first selection campaign, consisting of five rounds of ribosome display, a collection of total 32 of clones [Petr Maly (PM) series] was retained for sequencing (Fig. 3) and 13 of them were selected for more detailed characterization.

To increase the probability of finding strong hIFNγ binders, the selection campaign was repeated, increasing the number of ribosome display selection rounds to seven and starting from an independently constructed library. Here, 321 clones were picked in total and analyzed by ELISA for production of hIFNγ binders (data not shown). In this collection [Jawid Ahmad (JA) series], 15 of ABD-TolA fusion constructs exhibiting the best binding properties were selected for sequencing (Fig. 3) and further characterization.

Sequence analysis and clustering

Sequences of 47 construct (32 from PM series and 15 from JA series), exhibiting hIFNγ binding in ELISA screening, were determined and compared. Only about 1.3% of all detected changes were PCR-introduced errors, with only five codon-changing base substitutions (5 of 47 × 19 positions, 0.56%) found in the first 19 codon segment excluded from randomization. In turn, a total of 17 unintended mutations (3 deletions and 14 substitutions) were found within the 16 nonrandomized codons encoding helices 2 and 3 of ABD (Fig. 3). This corresponded to an average error frequency of 2.26% (17 of 47 × 16 positions). As these mutations were mostly adjacent to randomized codons, such bias (4.03-fold) may indicate a positive selection during ribosome display for unintended mutations that contributed to hIFNγ binding capacity of the selected ligands.

Further, the relative average occurrence of individual amino acid residues at the 11 randomized positions was compared for the PM and JA clone series. For most of the amino acid residues, a roughly equal frequency of occurrence at the randomized positions was observed in both clone series. However, a noteworthy increase of arginine (3.0×), tryptophane (2.4×), and phenylalanine (2.4×) occurrence at randomized positions was observed within clones of the PM series, as compared with clones of the JA series. In turn, the JA series clones were statistically enriched for proline (3.7×), glutamine (6.4×), and aspartate (10.6×) residues at the randomized positions. Further sequence differences between clones from the two series could also be documented by the increased occurrence of frequently represented residues, where the overall content of arginine + tryptophane residues in the PM series was 22.3%, compared with 10.3% in the JA series. In the case of proline + serine residues, the values of 8.5% and 22.4% were, respectively, found for proteins selected in the two series. This suggests that sequence characteristics can be derived for clones originating from either of the two series. This indicates that enhanced stringency during selection of the JA clone series (see Table I) may have biased the preference for certain amino acid residues in the ligands that were retrieved by the ribosome display.

To further investigate the sequence similarity among all analyzed ABD variants, clustering using ClustalW program was performed. On the basis of a similarity tree, subgroups of ABD variants with highest similarity were identified (Fig. 3). Although the overall similarity calculated for all 47 clones was found to be on average at an 80.22% level, it varied between 81.52 and 86.74% between group members. Nevertheless, a general sequence consensus representing a shared hIFNγ-binding motif in the obtained ABD variants and their subgroups could not be identified. This suggests that the characterized ABD variants may bind hIFNγ in several modes.

Affinity and specificity of ABD-derived ligands

Whole cell lysates, controlled for ABD content by Western blots, were used to define an initial set of 28

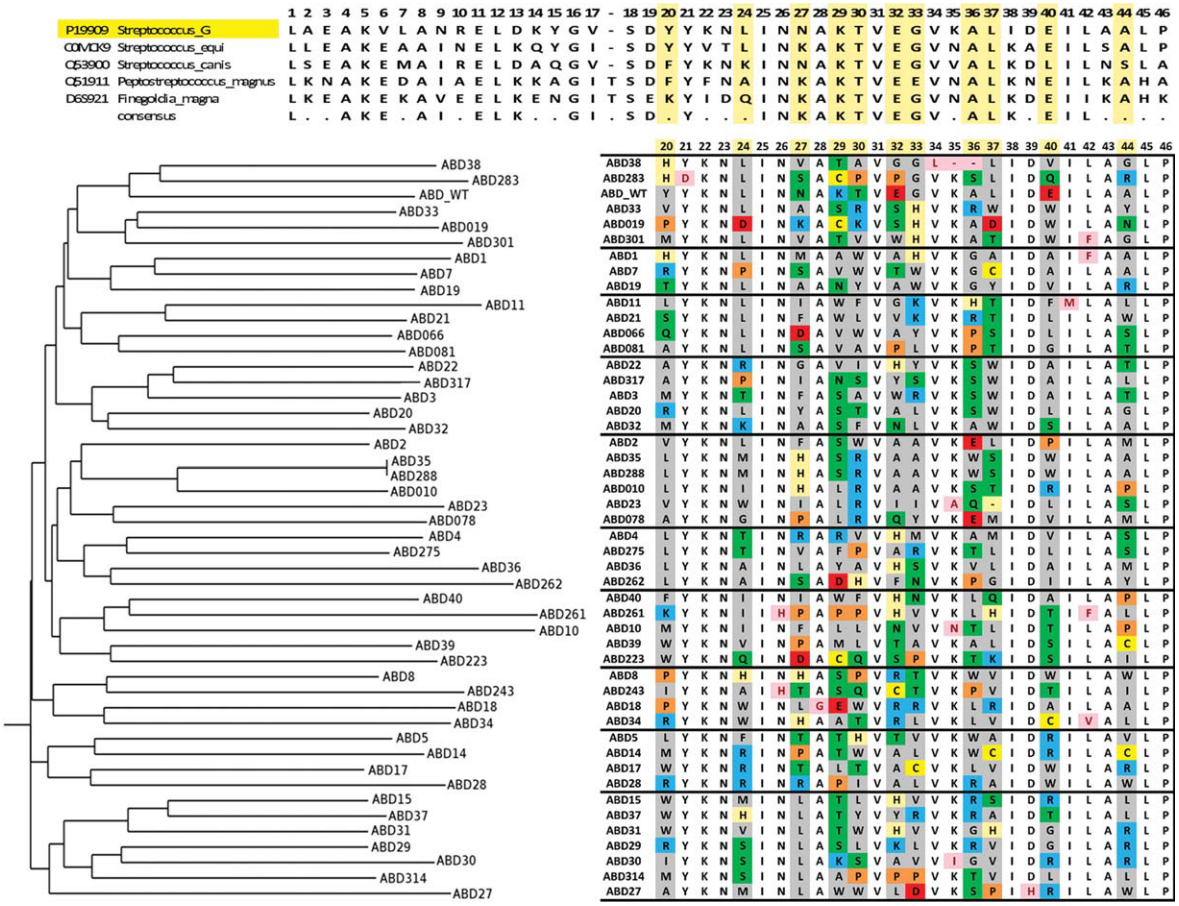

Figure 3

Similarity tree of ABD variants binding hIFNγ. ABD of streptococcal protein G (highlighted in yellow, G148_GA3) was aligned with homologous protein sequences available in the UniProt database (top) and the randomized portions of sequenced ABD variants selected in ribosome display for hIFNγ binding (lower part). Positions of 11 randomized residues are indicated using a color code, according to residue type. Pink boxes indicate unintended mutations within the randomized ABD segment corresponding to residues 20–46. In the nonrandomized N-terminal part of ABD (residues 1–19, not shown), 5 unintended substitutions were present (E3G, L1S, R10K, K5E, and N9K in ABD10, 14, 28, 36, and 262, respectively). Multiple alignment and similarity tree construction was performed in ClustalW.[39] Clones numbered ABD010, ABD019, ABD066, ABD078, ABD081, ABD223, ABD243, ABD261, ABD262, ABD275, ABD283, ABD288, ABD301, ABD314, and ABD317 represent JA series, all other clones belong to PM series, ABD_WT indicates sequence of parental nonmutated ABD.

best binders within the PM and JA clone series. Constructs yielding the highest apparent affinity for hIFNγ in ELISA were chosen for purification of the corresponding His_6-ABD-TolA fusion proteins, as documented in Figure 4. These 363 residues-long fusion proteins consisted of a twelve residue-long N-terminal 6×His tag fused to a 46 residue-long ABD scaffold moiety and a 305 residue-long TolA tail, making for a calculated molecular mass of 36.3 kDa on average. ELISA was used for preliminary assessment of binding properties of 11 purified His_6-ABD-TolA constructs and the affinity of best binders for hIFNγ was determined by SPR biosensor measurements for six best binders.

In the first setup, ABD-TolA variants were biotinylated *in vitro*, immobilized onto avidin-coated SPR sensors and hIFNγ was circulated at different concentrations over the chip surface. In the reversed setup, *in vivo* biotinylated hIFNγ was immobilized and binding of circulating His_6-ABD-TolA proteins was measured. As documented by representative binding curves for the ABD29-TolA and ABD35-TolA variants in Figure 5(a,b) and summarized in Table II, the six characterized ABD-TolA variants exhibited a K_d value for hIFNγ in the nanomolar range.

To verify that presence of the C-terminal TolA spacer in the His_6-ABD-TolA proteins did not interfere with binding of the ligand to hIFNγ, SPR measurements were performed with a chemically synthesized ABD35 binder variant comprising only the 46 residues of the scaffold. A slightly lower affinity of the synthetic ABD35 toward immobilized biotinylated hIFNγ ($K_d \sim 19$ n*M*) was found than that observed for the His_6-ABD35-TolA-fusion protein ($K_d \sim 10$ n*M*). This may suggest that fusion to the

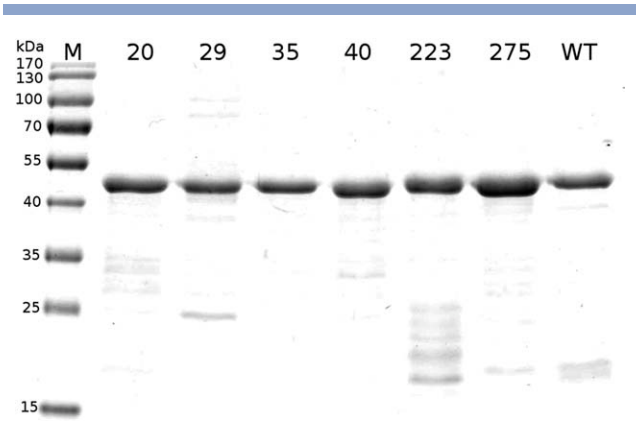

Figure 4

SDS-PAGE electrophoresis of ABD-TolA variants. The ABD-TolA fusion proteins with N-terminal polyhistidine tag were purified from *E. coli* cell lysates on Ni-NTA and separated on 12.5% polyacrylamide gel stained by Coomassie blue.

Table II

Affinity of Selected ABD-TolA Variants Binding to Recombinant hIFNγ Measured Using SPR

ABD variant	K_d (n*M*) Immobilized biotinylated ABD clones	K_d (n*M*) Immobilized biotinylated hIFNγ
35	0.2	10.0 ± 0.2
275	0.8	8.4 ± 0.6
29	1.5	1.8 ± 0.2
223	2.4	4.6 ± 0.4
20	3.5	2.7 ± 0.3
40	6.5	9.2 ± 0.7

TolA spacer may stabilize the structure of ABD. Alternatively, the orientation of surface-bound His_6-ABD35-TolA-fusion protein and bound hIFNγ may allow for avidity effects, that is, the hIFNγ dimer can bind more than one ABD protein. These effects, however, cannot occur in the reverse setting, where the ABD proteins are in solution and hIFNγ molecules are immobilized on the surface. Moreover, the affinities of the best His_6-ABD-TolA constructs for hIFNγ compared well to the affinity of recombinant version of the extracellular domain of hIFNγ receptor 1. This exhibited a K_d value of ∼ 1.7 n*M*, in good agreement with published values ranging from of 1.4 to 2.0 n*M*.[50] It can, hence, be concluded that the recombinant ligands derived from the engineered ABD scaffolds exhibited a similar affinity for hIFNγ as its natural receptor.

To investigate the selectivity of hIFNγ binding, ELISA experiments were performed on microplates coated with HSA, complete human serum or with several unrelated purified proteins (hen egg lysozyme or *Mycobacterium tuberculosis* ESAT-6 and CFP-10 antigens). As documented in Figure 6(a), the tested ABD-TolA constructs bound hIFNγ with a high selectivity and exhibited a minimal binding to HSA or BSA, in contrast to wild type His_6-ABD-TolA that bound HSA with high affinity [Fig. 6(b)]. The randomization of residues from the F23 surface of ABD [cf. Fig. 1(b)], hence, lead to a sharp loss of binding capacity for HSA and generated a new binding specificity for hIFNγ. The WT ABD-TolA construct, used as control, exhibited some background binding to

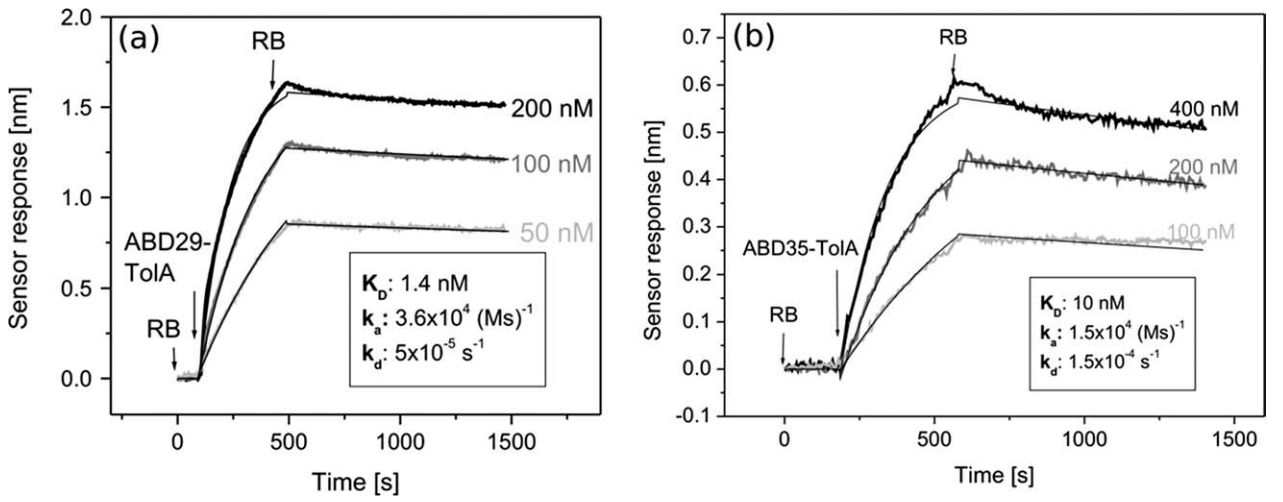

Figure 5

SPR analysis of binding of two ABD variants to immobilized hIFNγ target. C-terminally biotinylated hIFNγ was immobilized on streptavidin-coated biosensor chip and (**a**) ABD29-TolA or (**b**) ABD35-TolA proteins were flowed over chip surface in running buffer (RB). The recorded biosensor response was fitted with a 1:1 model considering mass transport limitations.

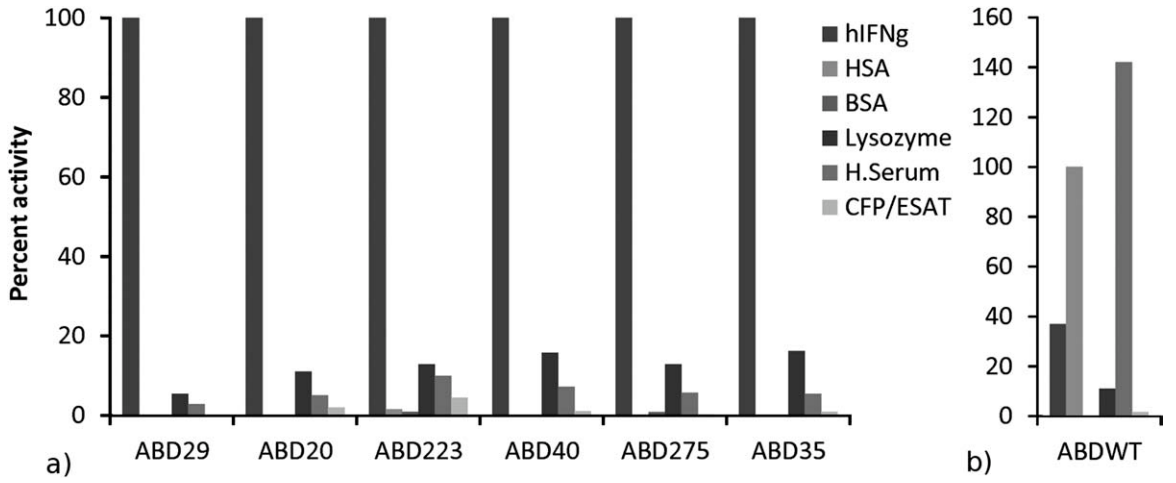

Figure 6

Binding specificity of ABD variants. Binding of purified ABD-TolA proteins to indicate target proteins coated on microplate wells was determined by ELISA. Average values from three independent experiments are shown. (**a**) Percentage of binding of indicated ABD-TolA proteins to various targets. Binding to hIFNγ was taken as 100%. HSA, human serum albumin; CFP/ESAT, culture filtrate protein-10/early secreted antigenic target 6 complex. (**b**) Binding of the initial (WT) ABD-TolA construct molecule to the coated proteins. Binding to purified human serum albumin (natural ABD target) was taken as 100%.

the IFNγ target. This might reflect an unspecific interaction of the TolA moiety with IFNγ as well as some initial capacity of intact WT ABD to bind IFNγ with a low affinity, which upon randomization and selection was enhanced by several orders of magnitude.

ABD variants all bind the same hIFNγ surface

We used molecular modeling approaches to explore the binding regions possibly recognized on the surface of hIFNγ by the engineered ABD scaffolds. To obtain predicted structures of the selected ABD variants, homology modeling with ABD was performed using wild type structure as a template, followed by a side-chain relaxation. Binding positions were predicted based on docking of the modeled ABD variant structures onto the known hIFNγ structure and a set of 10 most probable arrangements of the complex with each variant was identified. This was subjected to prediction of binding affinity (ΔG). Analysis of the best scoring binding modes of the different ABD variant predicted that all of them are likely to occupy a common binding region on hIFNγ that was different from the binding site recognized by the hIFNγR1 (Fig. 7). To investigate whether the individual ABD variants recognized identical or overlapping epitopes on the surface of the hIFNγ, their competition for hIFNγ binding was examined. WT-ABD-TolA protein was used as a noncompeting control, the competition for hIFNγ binding between synthetic ABD35 and its His_6ABD35-TolA variant was used as a positive control. As indeed documented in Figure 8, at increased concentrations, the synthetic ABD35 protein out-competed all tested His_6-ABD-TolA variants from binding to hIFNγ.

To further investigate whether individual ABD-TolA proteins competed with each other for hIFNγ binding, competition of pairs of unlabeled and biotinylated His_6-

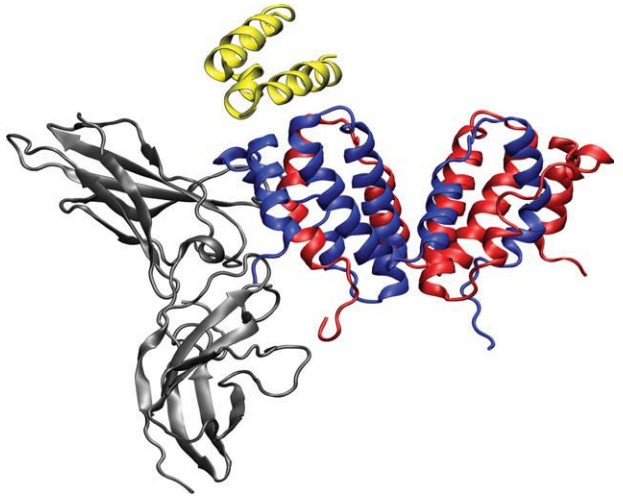

Figure 7

Model of ABD scaffold interaction with hIFNγ. Visualization of the predicted ABD binding site on hIFNγ. Individual ABD variant sequences were modeled on the template of the known ABD structure (PDB code 1GJT, residues 20–65) and docked onto the hIFNγ homodimer (PDB 1FG9) using ClusPro. The structure of hIFNγR1 (PDB 1FG9) was included into the model of the ABD-hIFNγ complex to highlight its different binding site.

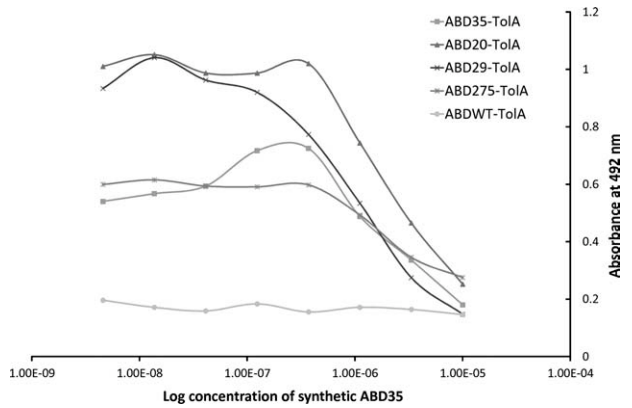

Figure 8

Different ABD-TolA proteins compete for binding to the same surface on hIFNγ. Synthetic ABD35 protein was serially diluted into microplate wells and allowed to compete for binding to coated hIFNγ in the presence of indicated His_6-ABD–TolA proteins (100 n*M*). The level of binding in the absence of competitor differs for individual ABD variants according to differences in affinity for hIFNγ (c.f. Table II).

ABD-TolA ligands was assessed. Here again, the results suggested that all tested ABD-derived ligands competed for binding to the same or overlapping binding site(s) on hIFNγ (data not shown).

To corroborate these results, SPR biosensor experiments were performed in which binding of synthetic ABD35 protein to immobilized hIFNγ-biotin was assessed following loading to 75% of maximal saturation and incomplete dissociation of the ABD35-TolA protein. A clear decrease of the sensor response to subsequent loading of synthetic ABD35 was observed, as compared with control channel to which only synthetic ABD35 was loaded (data not shown here). Moreover, competition for the binding to hIFNγ-biotin between the His_6-ABD20-TolA and His_6-ABD35-TolA proteins was also observed, as documented in Figure 9(a). In this experiment, the sensor with the immobilized hIFNγ molecules was preincubated with ABD35-TolA. At the end of the injection, the amount of bound ABD35-TolA reached ~ 80% of the saturation level (the saturation value was estimated from the fit of the data with Langmuir model using BiaEvaluation software). Because of the gradual dissociation of the ABD35-TolA, the saturation was about 65% of the maximum, just before the injection of the second ABD-TolA. A notable decrease in ABD20-TolA binding to the immobilized hIFNγ, compared with the binding to immobilized hIFNγ without the ABD35-TolA, was then observed.

To rule out the influence of steric hindrance due to the 305 residue-long TolA tail, competition experiments were also performed with ABD-AviTag proteins, which contained ABD extended only by a short 17-amino-acid long tail. As shown in Figure 9(b), significantly lower binding of ABD275-AviTag to immobilized hIFNγ was observed when the sensor was preincubated with ABD20-AviTag. This further supported the conclusion that the best hIFNγ binders derived from ABD recognize the same binding region on hIFNγ.

ABD variants bind to a different site than hIFNγ receptor 1

To examine the computational prediction that ABD scaffolds bind to a different site than the hIFNγ receptor

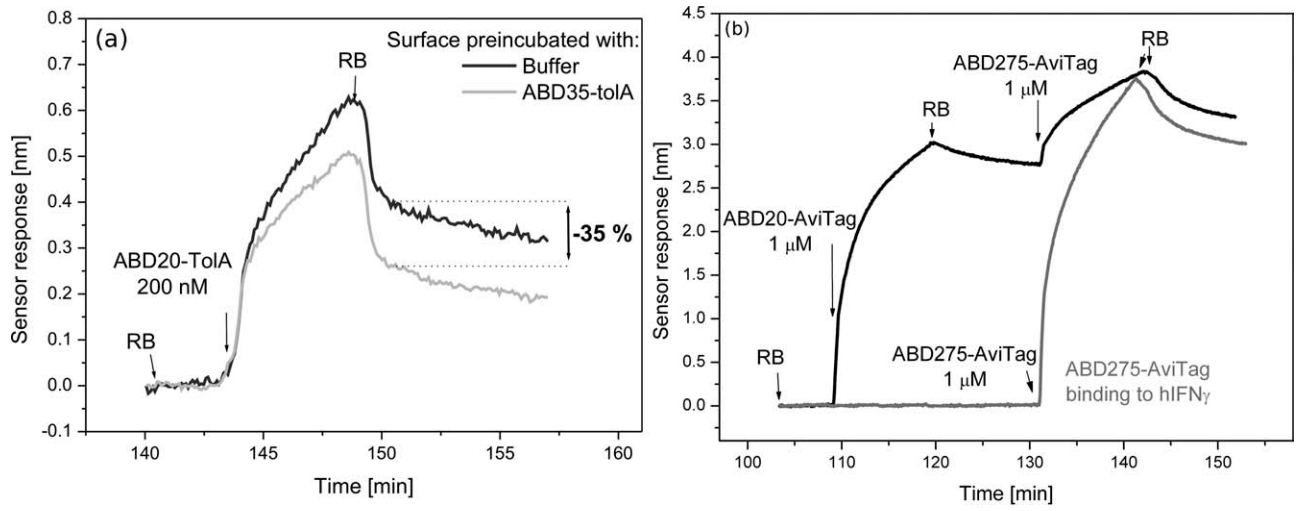

Figure 9

SPR analysis of competition for hIFNγ binding between selected ABD variants. (**a**) Sensor response to 200 n*M* ABD20-TolA binding to the immobilized hIFNγ that was preincubated with 800 n*M* ABD35-TolA and washed for 5 min. (**b**) Comparison of the kinetic curves for ABD275-AviTag binding to the immobilized hIFNγ upon preincubation with ABD20-AviTag (black line) and without the preincubation (gray line).

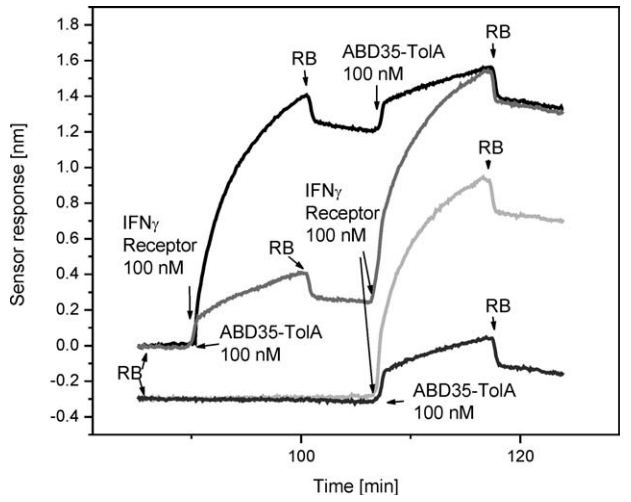

Figure 10

IFNγ receptor 1 and ABD35 ligand do not compete for binding to immobilized hIFNγ. Response of hIFNγ-coated SPR sensor to sequential binding of 100 n*M* ABD35-TolA and hIFNγ receptor 1 proteins (upper two lines), as compared with binding of the 100 n*M* proteins alone (lower two lines with lower offset). Arrows indicate the point at which indicated solutions were injected.

1 (hIFNγR1), competition between ABD35-TolA and the extracellular domain of hIFNγR1 was assessed. The SPR sensor was functionalized with biotinylated hIFNγ (as above), loaded for 10 min with 100 n*M* solution of hIFNγR1 protein, washed with running buffer, and exposed for 10 min to circulating ABD35-TolA protein at 100 n*M* concentration. The surface coverage with the hIFNγR1 reached about 90% of accessible binding sites, as estimated from the fit of the sensor response with Langmuir model. In the second channel, the order of interaction steps was reversed, starting with ABD35-TolA binding, followed by hIFNγR1 injection. Binding of hIFNγR1 and ABD35-TolA individually to immobilized hIFNγ was monitored in two other control channels. As shown in Figure 10, indeed, the order of the incubation steps had no influence on the final level of sensor response. Furthermore, no difference in the levels of response to subsequent binding of ABD35-TolA, or of hIFNγR1 was observed on sensors preloaded with the other protein. It can, hence, be concluded that hIFNγR1 and ABD35-TolA proteins bind to different sites on hIFNγ.

DISCUSSION

Construction of novel binders using a three-helix bundle scaffold has been already well documented in affibody molecules,[12,51] where randomization of 13 of total 58 amino acids immunoglobulin-binding domain of *Staphylococcus aureus* Protein A served as a powerful approach for the selection of high-affinity binders to several proteins, such as protein human factor VIII,[52] or recently ErbB3.[53] These novel binders lacking disulphide bonds exhibit several beneficial properties such as efficient refolding ability and high protein stability. Thus, the ABD scaffold represents another smaller three-helical alternative to affibodies.

Besides using hIFNγ as a model target for testing of the potential of the ABD scaffold to yield high affinity ligand, there was also a practical motivation to the present work. Selecting small scaffold binders for hIFNγ was aimed to generate high affinity ligands for applications in which antibodies fail, such as biosensors, where high shearing forces, pH changes, and reducing or denaturing conditions during sensor stripping, lead to loss of antibody functionality, whereas small scaffolds can easily refold to a functional state. In particular, the ABD ligands are aimed for use in biosensor detection of hIFNγ released upon specific antigenic stimulation of T lymphocytes in whole blood for detection of latent tuberculosis.

The results presented here document the usefulness of a semirational approach to design of artificial binding proteins (recombinant ligands) for a given target. Starting from a stable protein scaffold of only 46 residues, we performed the computational analysis of its structure and binding properties, in order to identify residues suitable for randomization for the purpose of generating a combinatorial library of protein scaffolds. This approach enabled us to restrict the need for randomization to only 11 positions of the ABD scaffold, where permutation of amino acid residues at 11 positions within a protein still yields $\sim 2 \times 10^{14}$ possible protein variants.

Moreover, attention was paid to pick for randomization the residues that were known to be involved in HSA binding. This allowed to ablate the natural binding affinity of ABD for HSA and to replace it with a newly engineered binding capacity for hIFNγ. Subsequent selection of binders using ribosome display allowed retrieving of ABD scaffolds that bound hIFNγ with a nanomolar affinity. This raises a question whether selection conditions can be optimized for any chosen target and how many selection rounds are sufficient for obtaining of ABD-derived binders with highest possible affinity from within a combinatorial scaffold library. Theoretically, the more selection steps during ribosome display are used, the higher the probability of enriching and selecting the best binders. With this assumption in mind, we performed two screening protocols with five or seven rounds of selection, respectively. The only difference between steps 5 and 7 was the concentration of the hIFNγ target that was decreased by a factor of 50 (Table I). Yet, changes in the statistical representation of certain residues selected at randomized positions in the two binder collections were observed, with no clear correlation to the experimentally determined levels of binding affinity for hIFNγ

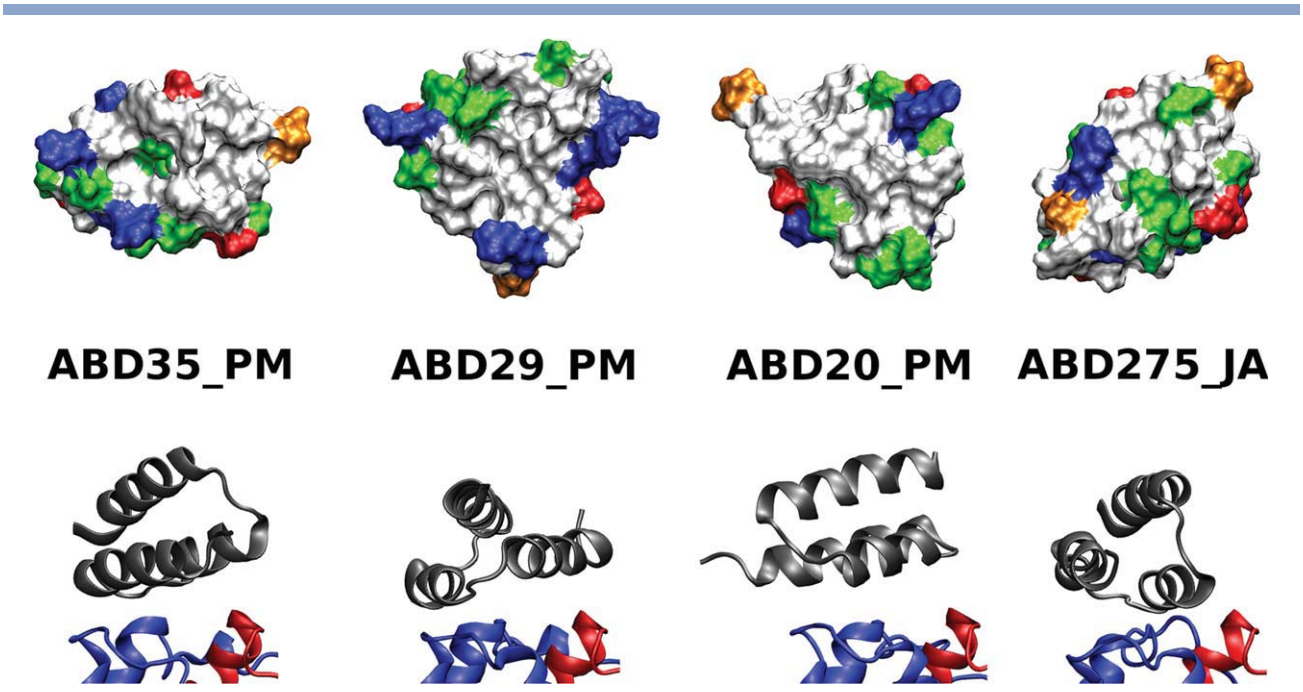

Figure 11

Predicted binding surfaces of indicated ABD variants (top) and their predicted modes of interaction with hIFNγ (bottom). Amino acid residues are color-coded as in Figure 3: gray, hydrophobic; green, polar; red, anionic; blue, cationic. Proline residue is given in orange. Orientation of a particular ABD binder is depicted with respect to the same hIFNγ reference position (blue-red cartoon representation).

being noticeable. In both selection series, the best obtained constructs exhibited binding affinities in the nanomolar range. In each round of ribosome display selection, however, the composition of the ligand pool and the complexity of retained binder library appeared to evolve according to increasingly stringent conditions. These appeared to result in changes in statistical representation of types of ABD variants in the pool. In the first rounds of *in vitro* selection, the ABD variants were likely sorted according to their affinity for the target. In contrast, the hIFNγ binders retained after the final rounds of ribosome display exhibited a similar level of binding affinity. These were likely selected in an affinity-independent manner. Nevertheless, two clones of identical sequence (ABD35 vs. ABD288) were found among the best hIFNγ binders obtained in two independent selection campaigns. This indicates that under the used conditions the function-directed statistical enrichment was sufficient and reached a plateau.

The affinity constants determined by SPR for ABD variants obtained in the two experimental setups revealed that the best hIFNγ binders derived from ABD exhibited K_d values in the nanomolar range. Most clones exhibited, indeed, rather similar binding affinities to immobilized or free hIFNγ target. However, the ABD35 and ABD275 variants demonstrated a substantial difference in target binding in the two SPR setups. Sub-nanomolar K_d values for binding of free hIFNγ from solution were observed with the biotinylated ABD35-TolA and ABD275-TolA variants immobilized on avidin-coated sensor surface. In turn, an order of magnitude lower binding constant was observed in the reversed setup, when C-terminally biotinylated hIFNγ was immobilized in an oriented manner on the avidin-coated sensor and the ABD35-TolA and ABD275-TolA proteins bound from solution. It is plausible to assume that for these two particular ABD variants their binding modes may allow pairs of avidin-immobilized ABD-TolA molecules to bind a single hIFNγ homodimer, thus exhibiting an increased avidity for the target. In turn, no "avidity effect" would be observed with free ABD-TolA molecules binding from a solution to immobilizied hIFNγ homodimers independently of each other. Furthermore, all described ABD variants competed with each other for hIFNγ binding. It appears, therefore, unlikely that only the ABD35 and ABD275 scaffolds are selectively binding to site(s) on hIFNγ that would become less accessible upon oriented immobilization on the avidin-coated chip.

Computational comparison of the surfaces predicted to interact with hIFNγ in various ABDs (Fig. 11) indicated that the core area of their binding surface would be formed by hydrophobic residues and the surrounding area would contain polar and charged residues. The distribution of the latter would, however, vary significantly and a common feature underlying hIFNγ binding could not be clearly identified. This would suggest that the

high affinity of the best binders for hIFNγ may result from a combinatorial interaction of more types of residues, rather than from a major binding motif formed by a structurally predefined consensus. This interpretation would also be supported by the different calculated sizes of the predicted interacting surfaces of ABD variants (Fig. 11), obtained upon structure relaxation of the ABD scaffolds in MD simulations of ABD-hIFNγ complexes. The observed average RMSD values of ABD backbone atoms with respect to the ABD-WT crystal structure reference are 1.61, 1.52, 1.34, and 1.29 Å for ABD35, ABD29, ABD20, and ABD 275, respectively. These values represent the extent of induced geometry change of the ABD structure upon binding to the hIFNγ.

In the case of the ABD29 construct, the binding surface would be enlarged due to increased distance between helices 2 and 3, which may result in location of the helix 1 in closer proximity to the hIFNγ surface (a "flattened" binding mode). Contrary to that, the ABD275 variant is predicted to interact with hIFNγ preferentially through the randomized residues of helix 2, with a minimum interacting contribution of helix 3 (an "oblique" binding mode). This would mean that randomization-mediated sequence changes may control also the orientation of the ligand relative to its target, as suggested in Figure 11. These predictions, however, await experimental testing by determination of the structures of above discussed selected ligands that is currently attempted.

Collectively, the presented results demonstrate the potential of the ABD scaffold to be used for design and selection of novel recombinant ligands of diagnostic or therapeutic targets.

ACKNOWLEDGMENTS

We thank Alena Lehovcová and Petra Kadlčáková for excellent technical assistance.

REFERENCES

1. Muller U, Steinhoff U, Reis LFL, Hemmi S, Pavlovic J, Zinkernagel RM, Aguet M. Functional-role of type-I and type-II interferons in antiviral defense. Science 1994;264:1918–1921.
2. Goodbourn S, Didcock L, Randall RE. Interferons: cell signalling, immune modulation, antiviral response and virus countermeasures. J Gen Virol 2000;81 (Part 10):2341–2364.
3. Randall RE, Goodbourn S. Interferons and viruses: an interplay between induction, signalling, antiviral responses and virus countermeasures. J Gen Virol 2008;89 (Part 1):1–47.
4. Ealick SE, Cook WJ, Vijaykumar S, Carson M, Nagabhushan TL, Trotta PP, Bugg CE. 3-Dimensional structure of recombinant human interferon-gamma. Science 1991;252:698–702.
5. Lunn CA, Davies L, Dalgarno D, Narula SK, Zavodny PJ, Lundell D. An active covalently linked dimer of human interferon-gamma—subunit orientation in the native protein. J Biol Chem 1992;267:17920–17924.
6. Thiel DJ, le Du MH, Walter RL, D'Arcy A, Chene C, Fountoulakis M, Garotta G, Winkler FK, Ealick SE. Observation of an unexpected third receptor molecule in the crystal structure of human interferon-gamma receptor complex. Structure 2000;8:927–936.
7. Binz HK, Pluckthun A. Engineered proteins as specific binding reagents. Curr Opin Biotechnol 2005;16:459–469.
8. Nygren PA, Skerra A. Binding proteins from alternative scaffolds. J Immunol Methods 2004;290:3–28.
9. Skerra A. Alternative non-antibody scaffolds for molecular recognition. Curr Opin Biotechnol 2007;18:295–304.
10. Dennis MS, Lazarus RA. Kunitz domain inhibitors of tissue factor-factor Viia. 1. Potent inhibitors selected from libraries by phage display. J Biol Chem 1994;269:22129–22136.
11. Koide A, Bailey CW, Huang XL, Koide S. The fibronectin type III domain as a scaffold for novel binding proteins. J Mol Biol 1998;284:1141–1151.
12. Nord K, Gunneriusson E, Ringdahl J, Stahl S, Uhlen M, Nygren PA. Binding proteins selected from combinatorial libraries of an alpha-helical bacterial receptor domain. Nat Biotechnol 1997;15:772–777.
13. Nygren PA, Uhlen M. Scaffolds for engineering novel binding sites in proteins. Curr Opin Struct Biol 1997;7:463–469.
14. Hey T, Fiedler E, Rudolph R, Fiedler M. Artificial, non-antibody binding proteins for pharmaceutical and industrial applications. Trends Biotechnol 2005;23:514–522.
15. Hosse RJ, Rothe A, Power BE. A new generation of protein display scaffolds for molecular recognition. Protein Sci 2006;15:14–27.
16. Smith GP. Filamentous fusion phage—novel expression vectors that display cloned antigens on the virion surface. Science 1985;228:1315–1317.
17. Mattheakis LC, Bhatt RR, Dower WJ. An in-vitro polysome display system for identifying ligands from very large peptide libraries. Proc Natl Acad Sci USA 1994;91:9022–9026.
18. Leung DW, Chen E, Goeddel DV. A method for random mutagenesis of a defined DNA segment using a modified polymerase chain reaction. Technique 1989;1:11–15.
19. Forrer P, Binz HK, Stumpp MT, Pluckthun A. Consensus design of repeat proteins. Chembiochem 2004;5:183–189.
20. Binz HK, Stumpp MT, Forrer P, Amstutz P, Pluckthun A. Designing repeat proteins: well-expressed, soluble and stable proteins from combinatorial libraries of consensus ankyrin repeat proteins. J Mol Biol 2003;332:489–503.
21. Stumpp MT, Forrer P, Binz HK, Pluckthun A. Designing repeat proteins: modular leucine-rich repeat protein libraries based on the mammalian ribonuclease inhibitor family. J Mol Biol 2003;332:471–487.
22. Wiederstein M, Sippl MJ. Protein sequence randomization: efficient estimation of protein stability using knowledge-based potentials. J Mol Biol 2005;345:1199–1212.
23. Johansson MU, Frick IM, Nilsson H, Kraulis PJ, Hober S, Jonasson P, Linhult M, Nygren PA, Uhlen M, Bjorck L, Drakenberg T, Forsen S, Wikstrom M. Structure, specificity, and mode of interaction for bacterial albumin-binding modules. J Biol Chem 2002;277:8114–8120.
24. Kraulis PJ, Jonasson P, Nygren PA, Uhlen M, Jendeberg L, Nilsson B, Kordel J. The serum albumin-binding domain of streptococcal protein G is a three-helical bundle: a heteronuclear NMR study. FEBS Lett 1996;378:190–194.
25. Nygren PA, Ljungquist C, Tromborg H, Nustad K, Uhlen M. Species-dependent binding of serum albumins to the streptococcal receptor protein-G. Eur J Biochem 1990;193:143–148.
26. Linhult M, Binz HK, Uhlen M, Hober S. Mutational analysis of the interaction between albumin-binding domain from streptococcal protein G and human serum albumin. Protein Sci 2002;11:206–213.
27. Lejon S, Frick IM, Bjorck L, Wikstrom M, Svensson S. Crystal structure and biological implications of a bacterial albumin binding module in complex with human serum albumin. J Biol Chem 2004;279:42924–42928.
28. Jonsson A, Dogan J, Herne N, Abrahmsen L, Nygren PA. Engineering of a femtomolar affinity binding protein to human serum albumin. Protein Eng Des Sel 2008;21:515–527.

29. Alm T, Yderland L, Nilvebrant J, Halldin A, Hober S. A small bispecific protein selected for orthogonal affinity purification. Biotechnol J 2010;5:605–617.
30. Bendova-Biedermannova L, Hobza P, Vondrasek J. Identifying stabilizing key residues in proteins using interresidue interaction energy matrix. Proteins: Struct Funct Bioinform 2008;72:402–413.
31. Cornell WD, Cieplak P, Bayly CI, Gould IR, Merz KM, Ferguson DM, Spellmeyer DC, Fox T, Caldwell JW, Kollman PA. A second generation force field for the simulation of proteins, nucleic acids, and organic molecules. J Am Chem Soc 1995;117:5179–5197.
32. Case DA, Darden TA, Cheatham TEI, Simmerling CL, Wang J, Duke RE, Luo R, Merz KM, Wang B, Pearlman DA, Crowley M, Brozell S, Tsui V, Gohlke H, Mongan J, Hornak V, Cui G, Beroza P, Schafmeister C, Caldwell JW, Ross WS, Kollman PA. AMBER 8. San Francisco: University of California; 2004.
33. Tsui V, Case DA. Theory and applications of the generalized Born solvation model in macromolecular simulations. Biopolymers 2000;56:275–291.
34. Cavallo L, Kleinjung J, Fraternali F. POPS: a fast algorithm for solvent accessible surface areas at atomic and residue level. Nucleic Acids Res 2003;31:3364–3366.
35. Fraternali F. POPS server, Vol. 2008. Available at: http://mathbio.nimr.mrc.ac.uk/wiki/POPS. Accessed on November 2, 2011.
36. Yin SY, Ding F, Dokholyan NV. Eris: an automated estimator of protein stability. Nat Methods 2007;4:466–467.
37. Yin S, Ding F, Dokholyan NV. Eris protein stability. 2007; Available at: http://eris.dokhlab.org. Accessed on November 2, 2011.
38. Zahnd C, Amstutz P, Pluckthun A. Ribosome display: selecting and evolving proteins in vitro that specifically bind to a target. Nat Methods 2007;4:269–279.
39. Larkin MA, Blackshields G, Brown NP, Chenna R, McGettigan PA, McWilliam H, Valentin F, Wallace IM, Wilm A, Lopez R, Thompson JD, Gibson TJ, Higgins DG. Clustal W and clustal X version 2.0. Bioinformatics 2007;23:2947–2948.
40. Eswar N, John B, Mirkovic N, Fiser A, Ilyin VA, Pieper U, Stuart AC, Marti-Renom MA, Madhusudhan MS, Yerkovich B, Sali A. Tools for comparative protein structure modeling and analysis. Nucleic Acids Res 2003;31:3375–3380.
41. Schymkowitz J, Borg J, Stricher F, Nys R, Rousseau F, Serrano L. The FoldX web server: an online force field. Nucleic Acids Res 2005;33:W382–W388.
42. Comeau SR, Kozakov D, Brenke R, Shen Y, Beglov D, Vajda S. ClusPro: performance in CAPRI rounds 6-11 and the new server. Proteins: Struct Funct Bioinform 2007;69:781–785.
43. Hess B, Kutzner C, van der Spoel D, Lindahl E. GROMACS 4: algorithms for highly efficient, load-balanced, and scalable molecular simulation. J Chem Theory Comput 2008;4:435–447.
44. Duan Y, Wu C, Chowdhury S, Lee MC, Xiong GM, Zhang W, Yang R, Cieplak P, Luo R, Lee T, Caldwell J, Wang JM, Kollman P. A point-charge force field for molecular mechanics simulations of proteins based on condensed-phase quantum mechanical calculations. J Comput Chem 2003;24:1999–2012.
45. Vaisocherová H, Zítová A, Lachmanová M, Štěpánek J, Králíková S, Liboska R, Rejman D, Rosenberg I, Homola J. Investigating oligonucleotide hybridization at subnanomolar level by surface plasmon resonance biosensor method. Biopolymers 2006;82:394–398.
46. Vaisocherová H, Snášel J, Špringer T, Šípová H, Rosenberg I, Štěpánek J, Homola J. Surface plasmon resonance study on HIV-1 integrase strand transfer activity. Anal Bioanal Chem 2009;393:1165–1172.
47. Ansari S, Helms V. Statistical analysis of predominantly transient protein-protein interfaces. Proteins: Struct Funct Bioinform 2005;61:344–355.
48. Glaser F, Steinberg DM, Vakser IA, Ben-Tal N. Residue frequencies and pairing preferences at protein-protein interfaces. Proteins: Struct Funct Genet 2001;43:89–102.
49. Yin S, Ding F, Dokholyan NV. Modeling backbone flexibility improves protein stability estimation. Structure 2007;15:1567–1576.
50. Fountoulakis M, Juranville JF, Stuber D, Weibel EK, Garotta G. Purification and biochemical-characterization of a soluble human interferon-gamma receptor expressed in *Escherichia coli*. J Biol Chem 1990;265:13268–13275.
51. Nord K, Nilsson J, Nilsson B, Uhlen M, Nygren PA. A combinatorial library of an alpha-helical bacterial receptor domain. Protein Eng 1995;8:601–608.
52. Nord K, Nord O, Uhlen M, Kelley B, Ljungqvist C, Nygren PA. Recombinant human factor VIII-specific affinity ligands selected from phage-displayed combinatorial libraries of protein A. Eur J Biochem 2001;268:4269–4277.
53. Kronqvist N, Malm M, Gostring L, Gunneriusson E, Nilsson M, Guthenberg IH, Gedda L, Frejd FY, Stahl S, Lofblom J. Combining phage and staphylococcal surface display for generation of ErbB3-specific affibody molecules. Protein Eng Des Sel 2011;24:385–396.

Sensors and Actuators B 174 (2012) 306–311

Contents lists available at SciVerse ScienceDirect

Sensors and Actuators B: Chemical

journal homepage: www.elsevier.com/locate/snb

Surface plasmon resonance biosensor based on engineered proteins for direct detection of interferon-gamma in diluted blood plasma

H. Šípová[a], V. Ševců[a], M. Kuchař[b], J.N. Ahmad[c], P. Mikulecký[b], R. Osička[c], P. Malý[b], J. Homola[a,*]

[a] Institute of Photonics and Electronics of the ASCR, v. v. i., Prague, Czech Republic
[b] Institute of Biotechnology of the ASCR, v. v. i., Prague, Czech Republic
[c] Institute of Microbiology of the ASCR, v. v. i., Prague, Czech Republic

ARTICLE INFO

Article history:
Received 8 April 2012
Received in revised form 10 August 2012
Accepted 13 August 2012
Available online 30 August 2012

Keywords:
Surface plasmon resonance
Biosensor
Engineered binders
ABD scaffold

ABSTRACT

Human interferon gamma (hIFNγ) is an important inflammatory cytokine, which is extensively expressed by immune system in response to various pathogens. In this work we present a biosensor for the direct detection of hIFNγ based on surface plasmon resonance (SPR) and engineered proteins derived from albumin binding domain (ABD) of protein G. We compare two methods for the immobilization of ABD: covalent coupling and immobilization via streptavidin–biotin interaction. It is shown that both the methods fail to preserve the activity of short ABD binders to hIFNγ due to either low accessibility of the binding site of the scaffold, or disruption of its tertiary structure. We, therefore, employed ABD proteins fused with a helical TolA spacer protein. We demonstrated that concentrations of hIFNγ as low as 0.2 nM can be detected in both buffer and albumin-depleted 2% human plasma using the reported SPR biosensor.

1. Introduction

Interferon gamma (hIFNγ) is a cytokine that is critical for innate and adaptive immunity against viral and intracellular bacterial infections and for control of tumor growth [1,2]. High hIFNγ expression is also associated with a number of autoimmune diseases. The active form of this cytokine is a homodimer consisting of two 143-amino acid polypeptides. Traditionally, secreted cytokines such as hIFNγ are detected using antibody-based sandwich immunoassays [3]. While physiological levels of hIFNγ are ~pg/mL, in case of *Mycobacterium tuberculosis* infection, hIFNγ levels in stimulated heparinized blood samples can be elevated to hundreds of pg/mL [4]. The levels of hIFNγ in cultured blood samples induced by specific tuberculous antigens can be elevated up to ~ng/mL [5]. While robust and well-established, the traditional strategies are time-consuming, and provide little information concerning the kinetics of interaction between antigen and antibody.

Biosensors, such as those based on surface plasmon resonance (SPR), enable rapid, sensitive, and real-time analysis and thus present an attractive alternative to conventional techniques [6]. Biosensors have been used for the detection of a wide variety of biomolecules (proteins, peptides, nucleic acids, etc.) and intact micro-organisms (bacteria, viruses) [7]. Biosensor-based detection of cytokines have been reported [8,9], including an SPR biosensor for the detection of hIFNγ [10,11]. Specifically, Stigter et al. detected hIFNγ in 100× diluted blood plasma and achieved a limit of detection (LOD) of 16 nM (250 ng/mL) [10].

An overwhelming majority of biosensors for detection of cytokines utilize antibodies as biorecognition elements, primarily due to their high specificity and wide availability. Recently, strategies based on new recognition elements with improved specificity, stability and cost-efficiency have emerged as viable alternatives to antibody-based assays [12]. One of these alternatives are aptamers – single stranded DNA or RNA oligonucleotides designed and selected *in vitro* to provide high affinity to an analyte of choice [13]. For instance, aptamers have been used in a FRET-based assay for IFN-γ with a limit of detection of 5 nM [14].

Considerable attention has also recently focused on the use of protein scaffolds for biorecognition elements. These scaffolds are polypeptide folds of intrinsic stability of conformation, which can be adapted to bind a variety of analytes using protein engineering methods [15–17]. Due to their small size and ease of production, they are ideal for use in affinity biosensors [18]. In our recent work, we used ribosome display for selection of engineered binders for hIFNγ derived from albumin binding domain (ABD) of protein G from *Streptococcus* G148. A large protein library was reduced to 6 selected binders, which were shown to bind hIFNγ with nanomolar to subnanomolar affinity [19]. Furthermore, we have used one of those binders (ABD20) to develop an SPR biosensor-based competition assay for hIFNγ detection and reached a LOD of 2 nM [20].

In this study, we immobilized the ABD binders directly to the SPR sensor surface in order to develop an SPR biosensor for direct

* Corresponding author. Tel.: +420 266 773 404; fax: +420 284 680 222.
E-mail address: homola@ufe.cz (J. Homola).

0925-4005/$ – see front matter © 2012 Elsevier B.V. All rights reserved.
http://dx.doi.org/10.1016/j.snb.2012.08.024

detection of hIFNγ. We have evaluated two of the most common protein immobilization methods (direct covalent coupling and streptavidin–biotin interaction) in terms of their ability to assure efficient immobilization of the engineered ligands and to preserve their affinity to hIFNγ. The new biosensor was tested for detection of hIFNγ in diluted human plasma, where we also evaluated the fouling properties of the sensor surface. Finally, we have calibrated the biosensor for detection of hIFNγ in both buffer and diluted human plasma and demonstrated a 10-fold improvement of LOD compared to the detection using competition assay format for detection in both buffer and in diluted blood plasma.

2. Materials and methods

2.1. SPR sensor

In this work we utilized a four-channel SPR based on wavelength spectroscopy of surface plasmons. The sensor was developed at the Institute of Photonics and Electronics (Prague, Czech Republic), and consists of a halogen lamp, a sensor head and a four-channel spectrograph [21]. In the sensor head, the incident light is collimated, polarized and then introduced into the SPR coupling prism. The reflected light from four sensing spots is collected into four optical fibers and coupled to a four-channel spectrograph. The sensor chip is interfaced with the coupling prism, and consists of a glass slide coated with an adhesion-promoting titanium layer (thickness – 2 nm) and a gold film (thickness – 50 nm). Upon the incidence of light on the gold film, surface plasmons are excited on the surface of gold. A change in the refractive index at the surface of the gold film results in a change in the wavelength at which the excitation of surface plasmons occurs (resonant wavelength). A flow-cell with four separate flow chambers facing each sensing spot is interfaced with the chip to confine the liquid sample during the experiment. The depth of each flow chamber is approximately 50 μm and the volume of each flow-cell chamber is about 1 μL. A peristaltic pump is used to deliver liquid samples to the flow-cell. The four-channel sensor is equipped with a temperature control system employing a thermoelectric cooler and a thermistor embedded in the SPR setup and a temperature controller with a feedback loop, which can maintain the temperature of the flow-cell chamber with a precision of 0.01 °C. The sensor response is represented by the change of the resonant wavelength and can be calibrated to the change in the surface coverage of bound molecules. The calibration coefficient is proportional to their molar weight and depends on the resonant wavelength. For the SPR sensors used in this study (resonant wavelength around 750 nm), a 1 nm resonant wavelength shift represents a change in the protein surface coverage of 18 ng/cm^2.

2.2. Reagents

Carboxylic (HS—C_{11}—EG_3—OCH_2—COOH) and hydroxylic (HS—C_{11}EG—OH) alkanethiols were obtained from Prochimia, Poland. Ethanolamine hydrochloride (EA), N-hydroxysuccinimide (NHS) and 1-ethyl-3-(3-dimethylaminopropyl) carbodiimide hydrochloride (EDC) were purchased from Biacore (Uppsala, Sweden). Streptavidin from *Streptomyces avidinii* and bovine serum albumin (BSA) were purchased from Sigma–Aldrich (St. Luis, USA). Recombinant human interferon gamma (hIFNγ) was purchased from Proteix s.r.o. (Prague, Czech Republic). Blood plasma samples were kindly provided by the Institute of Hematology and Blood Transfusion, Czech Republic. Plasma was centrifuged from whole blood of healthy donors with anticoagulant citrate dextrose solution (ACD) and stored at −80 °C until use. Plasma depletion was performed using Hu-6 Multiple Affinity Removal System purchased from Agilent (St. Clara, USA). Repeated freeze/thaw cycles were avoided. All other chemicals used were of analytical reagent grade.

2.3. Preparation of ABD proteins

The ABD_{WT}-AviTag, ABD20-AviTag and ABD275-AviTag proteins were constructed from the corresponding TolA fusion variants [6], in which the 305-amino acid helical TolA moiety was replaced by the AviTag sequence. The resulting 9.1 kD proteins were produced in *E. coli* BL21 (DE3) BirA cells, extracted from inclusion bodies with 8 M urea, 150 mM NaCl in 50 mM Tris buffer (pH 8), purified by size exclusion chromatography and refolded by >100-fold dilution into the SPR running buffer.

3 Experimental

3.1 Functionalization of the SPR chip

The ABD proteins were immobilized on the surface of an SPR sensor chip by either covalent attachment to a ω−carboxyalkylthiol-self-assembled monolayer (SAM) via amide-bond-forming chemistry or by attachment of the biotinylated proteins to the streptavidin covalently attached to the SAM. The procedure for the preparation of the mixed self-assembled monolayer of $HSC_{11}(EG)_2$—OH and $HSC_{11}(EG)_3OCH_2COOH$ alkenthiols and activation of carboxylic groups is described in detail in Ref. [22]. The functionalized SPR chip was mounted to the SPR sensor and all the subsequent molecular interactions were monitored in real-time. The temperature was set to 25 °C and a flow rate was kept at 20 μL/min. The carboxylic groups were activated with 5 min injection of 1:1 solution of 0.2 M NHS and EDC. After a baseline was established in SA buffer (10 mM sodium acetate, pH 5 at 25 °C), solution of streptavidin or ABD in the concentration of 50 or 5 μg/mL, respectively, in SA buffer was pumped into the flow-cell chamber for 10 min. After a short injection of the SA buffer, a 500 μg/mL solution of BSA was pumped into the chamber for 5 min. The non-covalently bound proteins were then washed away with a buffer of high ionic strength (PBS_{Na}; 1.4 mM KH_2PO_4, 8 mM Na_2HPO_4, 2.7 mM KCl, 0.75 M NaCl, pH 7.4 at 25 °C). The remaining carboxylic groups were deactivated with 5 min injection of 1 M ethanolamine–hydrochloride (pH 8.5). The immobilization of biotinylated proteins (ABD-AviTag) to the streptavidin-coated surface and the detection steps were performed in the running buffer (RB: 10 mM HEPES, 150 mM NaCl, 50 μM EDTA, 0.005% Surfactant P20, pH 7.4 at 25 °C), where a solution of 5 μg/mL ABD-AviTag in RB was pumped through the sensor chamber for 10 min until a stable baseline was reached. This step was followed by washing the sensor surface with RB to remove any unbound proteins.

3.2. Detection of hIFNγ with SPR biosensor

The detection of hIFNγ was performed in RB at a temperature of 25 °C and a flow rate of 20 μL/min. 10 min continuous injections of hIFNγ in RB, RB + BSA (10 mM HEPES, 150 mM NaCl, 50 μM EDTA, 0.005% Surfactant P20, 500 μg/mL BSA pH 7.4 at 25 °C) or in plasma diluted with RB to both reference and measuring channels were performed. After 10 min, the sample solution was replaced with running buffer and the dissociation phase was monitored. The absolute sensor response after 2 min of dissociation was used as the sensor response to the given concentration. Each concentration was measured using at least 3 different SPR chips. Calibration curves were established using sensor responses obtained for different concentrations of hIFNγ-AviTag (prepared as in the Ref. [19]) using a four-parameter logistic function.

4 Results and discussion

4.1 Immobilization of ABD binders

The immobilization methods for SPR chip functionalization were evaluated in terms of surface concentration of immobilized ABD binders and their activity towards the hIFNγ. Two ABD variants were used in this study – ABD20 and ABD275, which was shown in our previous work to bind the hIFNγ with nM affinity [19]. The ABD wild type (ABD_{WT}) was used to determine the influence of the immobilization method on the structure of the ABD proteins and their ability to bind the analyte.

The ABD proteins containing AviTag consensus sequence for *in vivo* biotinylation were immobilized using the streptavidin–biotin interaction (Fig. 1A). The amine-coupling chemistry produced a surface concentration of streptavidin of approximately 2×10^{12} molecules/cm^2. In the subsequent step, biotinylated ABD20-AviTag, ABD275-AviTag and ABD_{WT}-AviTag were immobilized reaching the surface concentration of $4–6 \times 10^{12}$ ABD molecules/cm^2. This corresponds to 2–3 molecules of ABD per one streptavidin molecule, which is a very dense surface coverage for ABD and is comparable to surface concentrations achieved for small and flexible short DNA and RNA oligonucleotides with a molecular weight of 7,5 kDa [23]. Fig. 2A shows the reference-compensated sensor response to a solution of 100 nM hIFNγ on the sensor surface coated with ABD20-AviTag. It can be seen that the ABD20-AviTag showed no ability to bind the hIFNγ. The same experiments were performed with ABD275–AviTag immobilized via streptavidin–biotin interaction with the same negative results. Interestingly, the ABD_{WT}-AviTag preserved the ability to bind the human serum albumin (HSA) even after immobilization (Fig. 2B). That indicates that both the ABD20-AviTag and ABD275-AviTag (9.1 kDa) failed to bind the hIFNγ (35 kDa), even though the immobilized ABD_{WT}-AviTag was able to interact with the twice larger HSA (67 kDa). It suggests that the immobilization of the ABD-AviTag via streptavidin–biotin interaction makes the binding site of ABD completely inaccessible for hIFNγ. The interaction of the HSA with the ABD20-AviTag and ABD275-AviTag immobilized via streptavidin–biotin surface chemistry generated sensor response equal to the sensor response in the reference channel functionalized with streptavidin only (data not shown).

The second immobilization method under study was the direct covalent immobilization of ABD-AviTag to the self-assembled monolayer (Fig. 1B). The covalent immobilization ABD_{WT}-AviTag resulted in inferior binding of HSA decreasing both (i) the initial binding rate by a factor of more than 2 and (ii) the sensor response to HSA (150 nM) by a factor of 4 (Fig. 2B). This suggests that a significant portion of the immobilized ABD_{WT}-AviTag molecules was damaged by the covalent coupling, where the fraction that remained active after the immobilization was disrupted, and/or

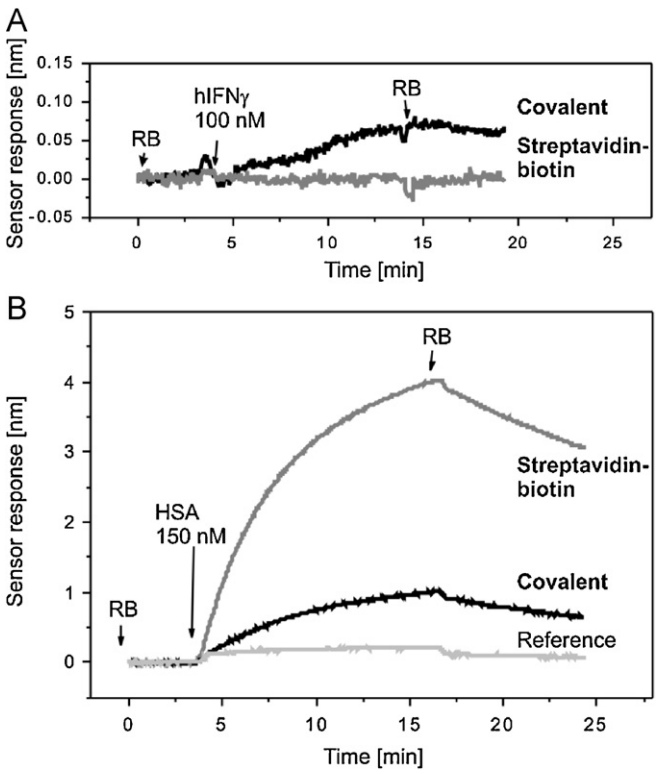

Fig. 2. Direct detection of hIFNγ and HSA in running buffer using the ABD-AviTag binders immobilized via covalent coupling and streptavidin–biotin interaction. (A) Binding of hIFNγ on the SPR chip surface coated with ABD20-AviTag. Shown sensor responses were reference-compensated. (B) Binding of HSA to ABD_{WT}-AviTag immobilized using two different approaches. Arrows indicate injection of the respective solutions.

in bad orientation for HSA capture. The reference-compensated sensor response to binding of hIFNγ on the SPR chip with covalently immobilized ABD20-AviTag is shown in Fig. 2A. The sensor response is higher than the one obtained with ABD20-AviTag immobilized via streptavidin–biotin, but still very low considering the nanomolar affinity between ABD20-AviTag and hIFNγ that had been measured in the reversed setting with hIFNγ immobilized to the sensor surface. The covalent coupling of ABD, therefore, provides better accessibility for hIFNγ binding, but is likely to cause damage to the structure of the three-helix bundle of the protein.

To increase the distance between surface of the SPR chip and ABD proteins we used ABD-TolA fusion proteins, which contain the ABD scaffold and long consensus sequence of amino acids [19]. The TolA spacer adds a considerable mass to the whole protein reaching

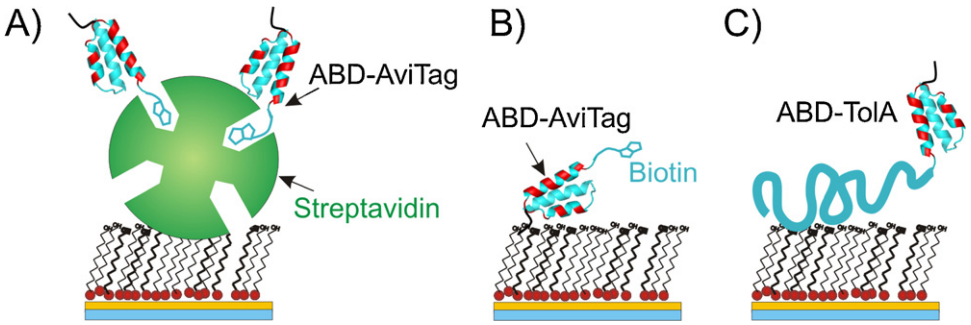

Fig. 1. Tested methods for ABD immobilization on the SPR chip coated with self-assembled monolayer of alkanethiols: (A) immobilization of ABD-AviTag via the streptavidin–biotin interaction; (B) covalent immobilization of ABD-AviTag; (C) covalent immobilization of ABD-TolA.

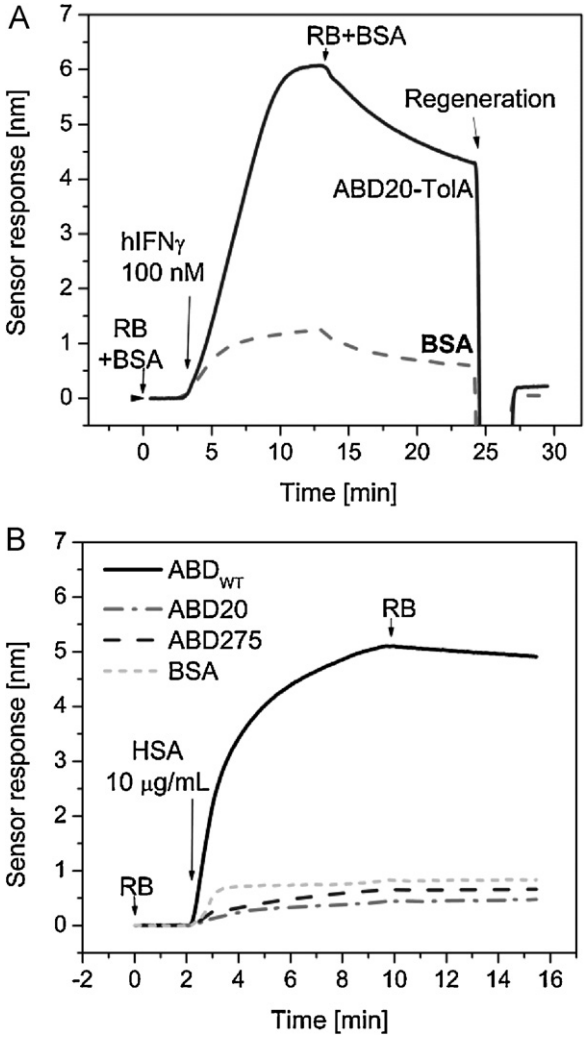

Fig. 3. Detection of hIFNγ and HSA using the ABD-TolA fusion proteins immobilized with covalent coupling. (A) Binding of hIFNγ to the surface coated with ABD20-TolA and to the reference surface with BSA. (B) Interaction of HSA with surface coated with various ABD-TolA variants. Arrows indicate injection of the respective solutions.

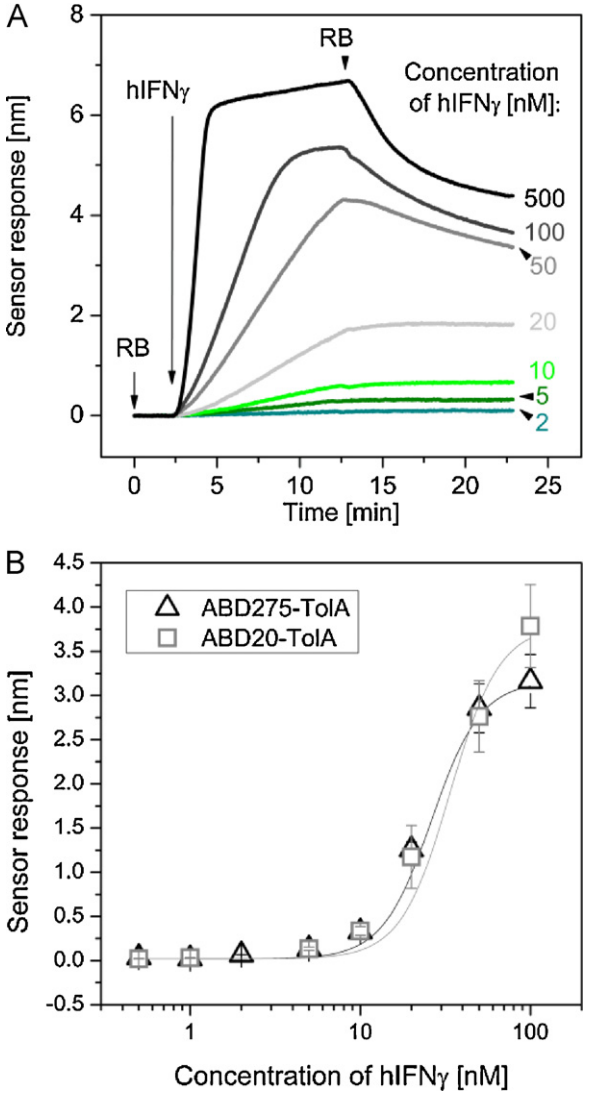

Fig. 4. Direct detection of hIFNγ in RB buffer: (A) Sensor responses to various concentrations of hIFNγ binding to ABD20-TolA immobilized using covalent chemistry. (B) Calibration curve for hIFNγ detection in semi-log scale.

36,5 kDa as opposed to 9.1 kDa of ABD-AviTag. The lysines present in the TolA moiety were expected to diminish the probability of distortion of ABD scaffold after covalent immobilization to the sensor surface (Fig. 1C). Fig. 3A demonstrates the sensor response to binding of 100 nM hIFNγ using covalently immobilized ABD20-TolA. It can be seen that the sensor response has significantly increased when compared to rates of hIFNγ binding to the surface coated with ABD-AviTag, suggesting that the accessibility of ABD-TolA for hIFNγ binding has been improved significantly. Fig. 3A also demonstrates the non-specific binding of the hIFNγ to the reference sensor surface coated with BSA. We assign it to partial misfolding of the recombinant hIFNγ, which is then more prone to non-specific adsorption, as no such behavior was observed when hIFNγ-AviTag (ref. [19]) was used (data not shown). The interaction of HSA (concentration – 10 μg/mL) with various ABD-TolA ligands immobilized on the sensor is shown in Fig. 3B. Stability of the complex of HSA with ABD_{WT}-TolA is higher than the stability of its complex with immobilized ABD_{WT}-AviTag as reflected by both the faster association and slower dissociation of HSA. At this concentration of HSA (10 μg/mL), its interaction with ABD20-TolA and ABD275-TolA was close to the level of its non-specific adsorption to the reference surface.

4.2. Detection of hIFNγ in buffer

For direct detection of hIFNγ, the ABD20-TolA and ABD275-TolA fusion proteins were covalently attached to the sensor surface via the methods discussed above. To establish a calibration curve, solutions of hIFNγ were flowed through both the detection and reference chamber of the flow-cell for 10 min. Fig. 4A shows the reference-compensated sensor response to binding of hIFNγ for a concentration range of 2–500 nM (ABD20-TolA). For construction of a calibration curve, the sensor response was read after 2 min in buffer. Fig. 4B shows the calibration curves of the SPR biosensor utilizing ABD20-TolA and ABD275-TolA as biorecognition elements. Fig. 4B was created using sensor responses to a minimum of 3 chips, with two replicas per chip. A limit of detection of 200 pM for both ABD20 and ABD275 was determined from the concentration of hIFNγ that resulted in a sensor response equal to three standard deviations of the baseline noise (5×10^{-4} nm). It was found that the sensor surface can be regenerated with 4 mM Glycine (pH 1.5) which allows for at least 10 detection/regeneration cycles with only minor decrease in the activity of ABD20-TolA or ABD275-TolA.

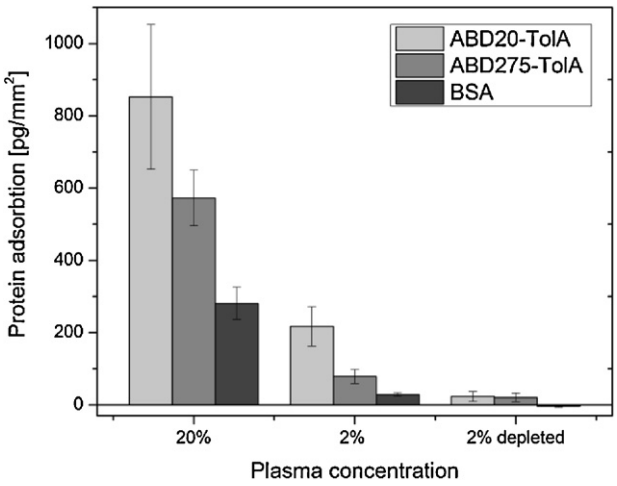

Fig. 5. Non-specific adsorption of proteins to the sensor surface coated with ABD-TolA (grey) and BSA (black) from diluted human plasma. Incubation time with the diluted plasma was 10 min.

4.3. Non-specific adsorption in blood plasma

The sensor surfaces coated with both ABD20-TolA and ABD275-TolA were evaluated for non-specific adsorption from diluted human plasma. Human blood plasma was diluted with running buffer with BSA to 20% and 2% concentration and was pumped to reference and measuring channels for 10 min. The levels of non-specific adsorption were read 2 min after the end of the incubation. Fig. 5 shows the level of non-specific adsorption for SPR chips using ABD20-TolA, ABD275-TolA, and the BSA reference, where data were taken from a minimum of three chips. It should be noted that the surface concentration of residual proteins adsorbed non-specifically on the BSA surface from 20% human plasma is lower than that observed for the non-fouling surfaces consisting of modified dextran reported by Stigter et al. [10], who reported adsorption of 0.6 ng/mm^2 of proteins on the dextran modified with 11-mercaptoundecanoic acid in 25% plasma. This suggests that BSA is efficient at blocking the residual negative charges on the SAM surface and improves the non-fouling properties of the surface. However, as follows from Fig. 5, the non-specific adsorption of proteins from human plasma was approximately 2 and 3 times higher on surfaces functionalized with ABD275-TolA and ABD20-TolA, respectively. This may be partially attributed to the TolA spacer protein being attached to the surface in more than one place, therefore decreasing the amount of covalently bound BSA in the blocking step when compared to the sensor surfaces coated with ABD-AviTag proteins. Another significant contribution to this non-specific adsorption of proteins from human plasma is most likely caused by the residual affinity of ABD20 and ABD275 to HSA, which seem to differ by almost factor of two for those two variants. Although the affinity of the engineered proteins to HSA is reduced by several orders of magnitude when compared to ABD_{WT}, it may be observed when HSA is present at high concentrations. To investigate this issue, we performed the same assay using protein-depleted plasma prepared using a commercial kit. As follows from Fig. 5, the amount of non-specifically bound proteins from 2% protein-depleted human plasma is significantly reduced on both the reference and measuring channels.

4.4 Detection of hIFNγ in depleted human plasma

To calibrate the SPR biosensor for detection of hIFNγ in depleted plasma, the 2% depleted plasma was spiked with various concentrations of hIFNγ and analyzed with the SPR biosensor. The temporal

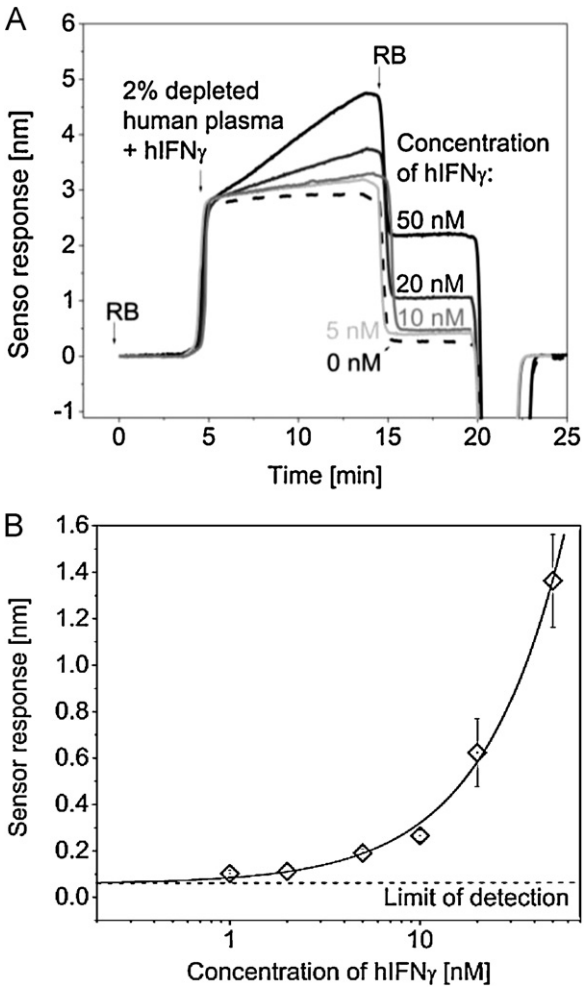

Fig. 6. Direct detection of hIFNγ in 2% depleted plasma. (A) Sensor responses to various concentrations of hIFNγ binding to ABD20-TolA immobilized using covalent chemistry. (B) Reference-compensated calibration curve for hIFNγ detection in semi-log scale.

sensor response to the binding of hIFNγ to the ABD20-TolA coated sensor surface is shown in Fig. 6A. The transition observed during the exchange of depleted human plasma and the buffer is due to the different composition of the two solutions. To establish a calibration curve and limit of hIFNγ detection, each concentration was measured at least 2 times on 2 different chips. The calibration curve of the developed sensor is shown in Fig. 6B. The limit of detection in 2% depleted human plasma was determined to be 0.2 nM, which agrees with the LOD achieved in buffer. This LOD is superior by an order of magnitude to that achieved in our previous work, where the ABD20-TolA was used in competition assay and the LOD of 2 nM was achieved [20]. Moreover, this LOD is almost 2 orders of magnitude below the limit of detection reported by Stigter et al., who detected hIFNγ in 2% plasma using an SPR biosensor with antibodies and carboxyl-modified dextran [10].

4 Conclusions

In this work, we have employed engineered binders derived from albumin binding domain (ABD) to develop an SPR biosensor for detection of human interferon gamma (hIFNγ). Two immobilization methods have been evaluated in terms of their ability to provide high surface density of the ABD binders and to preserve their affinity to hIFNγ. Immobilization of short ABD-AviTag variants via streptavidin–biotin interaction or direct covalent

immobilization to the self-assembled monolayer was found to hamper binding of hIFNγ, likely due to either steric hindrance, or disruption of the ABD structure. The covalent immobilization of ABD fused with TolA protein was demonstrated to preserve the ability of ABD to bind hIFNγ with high affinity. The sensor functionalized with ABD-TolA showed higher non-specific adsorption of proteins from diluted plasma compared to the reference surface, which was attributed mainly to minor residual affinity of the engineered proteins to human serum albumin. Using the SPR biosensor functionalized with ABD-TolA, the limit of detection for hIFNγ was established at 0.2 nM both for the detection in buffer and 2% depleted human blood plasma.

Acknowledgements

This research was supported by the Academy of Sciences of the Czech Republic (Praemium Academiae, institutional research concepts AV0Z50520701 and AV0Z20670512 and research grant KAN200520702) and by the Czech Science Foundation (research grants P303/10/1849 and P205/12/G118).

References

[1] K. Schroder, P.J. Hertzog, T. Ravasi, D.A. Hume, Interferon-gamma: an overview of signals, mechanisms and functions, Journal of Leukocyte Biology 75 (2004) 163–189.
[2] X.Y. Hu, L.B. Ivashkiv, Cross-regulation of signaling pathways by interferon-gamma: implications for immune responses and autoimmune diseases, Immunity 31 (2009) 539–550.
[3] K. Dheda, R.V. Smit, M. Badri, M. Pai, T-cell interferon-gamma release assays for the rapid immunodiagnosis of tuberculosis: clinical utility in high-burden vs. low-burden settings, Current Opinion in Pulmonary Medicine 15 (2009) 188–200.
[4] F. Bartalesi, S. Vicidomini, D. Goletti, C. Fiorelli, G. Fiori, D. Melchiorre, et al., QuantiFERON-TB Gold and the TST are both useful for latent tuberculosis infection screening in autoimmune diseases, European Respiratory Journal 33 (2009) 586–593.
[5] A. Veerapathran, R. Joshi, K. Goswami, S. Dogra, E.E. Moodie, M.V. Reddy, et al., T-cell assays for tuberculosis infection: deriving cut-offs for conversions using reproducibility data, PLoS ONE 3 (2008) e1850.
[6] X.D. Fan, I.M. White, S.I. Shopova, H.Y. Zhu, J.D. Suter, Y.Z. Sun, Sensitive optical biosensors for unlabeled targets: a review, Analytica Chimica Acta 620 (2008) 8–26.
[7] J. Homola, Surface plasmon resonance sensors for detection of chemical and biological species, Chemical Reviews 108 (2008) 462–493.
[8] T.M. Battaglia, J.F. Masson, M.R. Sierks, S.P. Beaudoin, J. Rogers, K.N. Foster, et al., Quantification of cytokines involved in wound healing using surface plasmon resonance, Analytical Chemistry 77 (2005) 7016–7023.
[9] T.H. Chou, C.Y. Chuang, C.M. Wu, Quantification of Interleukin-6 in cell culture medium using surface plasmon resonance biosensors, Cytokine 51 (2010) 107–111.
[10] E.C.A Stigter, G.J. de Jong, W.P. van Bennekom, An improved coating for the isolation and quantitation of interferon-gamma in spiked plasma using surface plasmon resonance (SPR), Biosensors and Bioelectronics 21 (2005) 474–482.
[11] G. Stybayeva, M. Kairova, E. Ramanculov, A.L. Simonian, A. Revzin, Detecting interferon-gamma release from human CD4 T-cells using surface plasmon resonance, Colloid Surface B 80 (2010) 251–255.
[12] B. Van Dorst, J. Mehta, K. Bekaert, E. Rouah-Martin, W. De Coen, P. Dubruel, et al., Recent advances in recognition elements of food and environmental biosensors: a review, Biosensors and Bioelectronics 26 (2010) 1178–1194.
[13] K. Sefah, J.A. Phillips, X.L. Xiong, L. Meng, D. Van Simaeys, H. Chen, et al., Nucleic acid aptamers for biosensors and bio-analytical applications, Analyst 134 (2009) 1765–1775.
[14] N. Tuleuova, C.N. Jones, J. Yan, E. Ramanculov, Y. Yokobayashi, A. Revzin, Development of an aptamer beacon for detection of interferon-gamma, Analytical Chemistry 82 (2010) 1851–1857.
[15] C. Gronwall, S. Stahl, Engineered affinity proteins–generation and applications, Journal of Biotechnology 140 (2009) 254–269.
[16] P. Holliger, P.J. Hudson, Engineered antibody fragments and the rise of single domains, Nature Biotechnology 23 (2005) 1126–1136.
[17] A. Skerra, Engineered protein scaffolds for molecular recognition, Journal of Molecular Recognition 13 (2000) 167–187.
[18] L. Torrance, A. Ziegler, H. Pittman, M. Paterson, R. Toth, I. Eggleston, Oriented immobilisation of engineered single-chain antibodies to develop biosensors for virus detection, Journal of Virological Methods 134 (2006) 164–170.
[19] J.N. Ahmad, J. Li, L. Biedermannová, M. Kuchař, H. Šípová, A. Semerádtová, et al., Novel high-affinity binders of human interferon gamma derived from albumin-binding domain of protein G, Proteins: Structure, Function and Bioinformatics 80 (2012) 774–789.
[20] H. Šípová, V. Ševců, M. Kuchař, J.N. Ahmad, P. Mikulecký, P. Šebo, et al., Sensitive detection of interferon-gamma with engineered proteins and surface plasmon resonance biosensor, Procedia Engineering 25 (2011) 940–943.
[21] H. Vaisocherová, K. Mrkvová, M. Piliarik, P. Jinoch, M. Steinbachová, J. Homola, Surface plasmon resonance biosensor for direct detection of antibody against *Epstein-Barr* virus, Biosensors and Bioelectronics 22 (2007) 1020–1026.
[22] H. Vaisocherová, J. Snášel, T. Špringer, H. Šípová, I. Rosenberg, J. Štěpánek, et al., Surface plasmon resonance study on HIV-1 integrase strand transfer activity, Analytical and Bioanalytical Chemistry 393 (2009) 1165–1172.
[23] H. Vaisocherová, A. Zitová, M. Lachmanová, J. Štěpánek, S. Králíková, R. Liboska, et al., Investigating oligonucleotide hybridization at subnanomolar level by surface plasmon resonance biosensor method, Biopolymers 82 (2006) 394–398.

Biographies

Hana Šípová (MSc) obtained her MSc degree from Charles University in Prague in 2008. Currently she is a graduate student at the Institute of Photonics and Electronics AS CR in Prague. Her research interests are in biosensors and bioassays for detection of biomolecular targets and biosensor-based investigation of interactions of nucleic acids and proteins.

Veronika Ševců (MSc) obtained her MSc degree from Charles University in Prague in 2009. Since then she has been Research Assistant at the Institute of Photonics and Electronics AS CR in Prague. Her research interests are in sensors based on surface plasmon resonance and their bioanalytical applications.

Milan Kuchař (MSc, PhD) graduated from the Faculty of Biological Science, University of South Bohemia in Ceske Budejovice, Czech Republic. He finished his PhD studies in molecular and cell biology at the Faculty of Sciences, Masaryk University in Brno, Czech Republic. Then he spent postdoctoral fellowship at the Department of Functional Genomics and Proteomics, Institute of Experimental Biology, Faculty of Science, Masaryk University, Brno. Currently he works as Research Assistant in the Laboratory of Ligand Engineering, Institute of Biotechnology AS CR, Prague.

Jawid N. Ahmad (MSc) graduated from the Science College of Swami Ramanand Teerth Maratwada University in Nanded, India, in 2007 and since then has been a PhD student at the Laboratory of Molecular Biology of Bacterial Pathogens at the Institute of Microbiology AS CR, Prague.

Pavel Mikulecký (MSc.) graduated from the Department of Cell Biology and Genetics, Faculty of Science, Charles University in Prague in 2009 and since then has been a PhD student. At present he works at the Laboratory of Molecular Recognition, Institute of Biotechnology AS CR, Prague.

Radim Osička (MSc., PhD) graduated from the Institute of Chemical Technology in Prague in 2004 and now works as Senior Scientist at the Laboratory of Molecular Biology of Bacterial Pathogens at the Institute of Microbiology AS CR, Prague.

Petr Malý (PhD 1992) is head of Laboratory of Ligand Engineering at the Institute of Biotechnology AS CR, Prague, Czech Republic. He spent postdoctoral fellowship at the Department of Pathology and Howard Hughes Medical Institute, The University of Michigan Medical School, Ann Arbor, USA. Since 1998 to 2005 he was group leader at the Institute of Molecular Genetics in Prague. As visiting scientist he also worked at the Department of Biochemistry and Mol. Biology, Oklahoma Center for Medical Glycobiology, College of Medicine, the University of Oklahoma, USA. He also was participating investigator of Consortium for Functional Glycomics (USA, 2001–2008).

Jiří Homola (PhD 1993, DSc 2009) is Director of the Institute of Photonics and Electronics AS CR, Prague (Czech Republic). He also is Affiliate Professor at the University of Washington, Seattle (USA) and Adjunct Professor at the University of Oulu (Finland). His research interests are in photonics and biophotonics with emphasis on optical sensors and biosensors. He is a member of Editorial Board of *Sensors and Actuators B* and *Journal of Sensors*, and a member of International Advisory Board of *Analytical and Bioanalytical Chemistry*. He also is Fellow of SPIE and Senior Member of IEEE.